STUDY ON SOME ASPECTS OF DISSIMILAR WELDING OF FERRITIC STAINLESS STEEL TO MILD STEEL BY SUBMERGED ARC WELDING AND PROCESS OPTIMIZATION

By

RANJEET KUMAR

EXAMINATION ROLL No. M4MEC1613

CLASS ROLL No. 001411202017

REGISTRATION No. 129390 of 2014-2015

THESIS

SUBMITTED IN PARTIAL FULFILMENT OF THE

REQUIREMENTS FOR THE DEGREE OF

MASTER OF ENGINEERING IN MECHANICAL ENGINEERING

IN THE FACULTY OF ENGINEERING & TECHNOLOGY

JADAVPUR UNIVERSITY

BLUE EARTH MACHINE SHOP AND

G.C SEN MEMORIAL MACHINE TOOLS RESEARCH LABORATORY

Mechanical Engineering Department

Jadavpur University

Kolkata – 700032

2016

JADAVPUR UNIVERSITY

Raja S.C. Mallick Road, Kolkata 700032, West Bengal

FACULTY OF ENGINEERING AND TECHNOLOGY

CERTIFICATE OF RECOMMENDATION

Date: May , 2016

We hereby recommend that the thesis prepared under our supervision by Ranjeet Kumar, examination roll number – M4MEC1613, entitled "**STUDY ON SOME ASPECTS OF DISSIMILAR WELDING OF FERRITIC STAINLESS STEEL TO MILD STEEL BY SUBMERGED ARC WELDING AND PROCESS OPTIMIZATION"** be accepted in partial fulfilment of the requirements for the degree of Master of Engineering in Mechanical Engineering.

To the best of our knowledge, the matter embodied in the thesis has not been submitted to any other University/Institute for the award of any degree or diploma.

Countersigned

_____ Dr. Gautam Nandi

Dr. Dipankar Sanyal

Head, Mechanical Engineering Department

_____

Dr. Pradip Kumar Pal

_____

Dr. Siviji Bandyopadhyay

Dean, Faculty of Engineering and Technology

(Thesis Supervisors)

Faculty of Engineering and Technology

Mechanical Engineering Department

Jadavpur University

Kolkata-700032

CERTIFICATE OF APPROVAL

The foregoing thesis entitled **"STUDY ON SOME ASPECTS OF DISSIMILAE WELDING OF FERRITIC STAINLESS STEEL TO MILD STEEL BY SUBMERGED ARC WELDING AND PROCESS OPTIMIZATION"** is hereby approved as credible study of an Engineering subject and presented in a manner satisfactory to warrant its acceptance as a pre-requisite to the degree for which it has been submitted. It is understood that by this approval, the undersigned, do not endorse or approve any statement made, opinion expressed or conclusion drawn therein, but approve the thesis only for the purpose for which it has been submitted.

Committee of final examination for evaluation of the thesis

_____

_____

_____

Signature (s) of the examiners

DECLARATION OF ORIGINALITY AND COMPLIANCE OF ACADEMIC ETHICS

I hereby declare that this thesis contains literature survey and original research work by the undersigned candidate, as part of his Master of Mechanical Engineering studies.

All information in this document have been obtained and presented in accordance with academic rules and ethical conduct.

I also declare that, as required by the rules of conduct, I have fully cited and referenced all material and results that are not original to this work.

Name : Ranjeet Kumar

Examination roll number : M4MEC1613

Class roll number : 001411202017

Thesis Title : "Study on some aspects of dissimilar welding of ferritic stainless steel to mild steel by submerged arc welding and process optimization"

Signature :

Date :

ACKNOWLEDGEMENT

The author gratefully expresses his sincere gratitude to the thesis supervisors Dr. Gautam Nandi and Dr. Pradip Kumar Pal, Mechanical Engineering Department, Jadavpur University for their invaluable guidance, suggestions and encouragement in the course of the present work. From the beginning of this work, they gave their valuable instructions and guided him properly in the right path to complete the work and this thesis. It would really not have been possible for him to complete this thesis without their assistance, proper guidance and motivation. It was really a pleasure to work under their supervision. They also helped him to find all the resources that were needed for completing his thesis work.

The author is also thankful to Prof. Dipankar Sanyal, Head, Mechanical Engineering Department, Jadavpur University, for his constant help in different academic and administrative matters.

The author is indebted to Dr. Sanjib Acharya and Prof. Avijit Mukherjee, faculty members of Mechanical Engineering Department, Jadavpur University, for their invaluable help and advice to this thesis work from time to time. The author acknowledges the help rendered by Prof. Gautam Mazumdar, In-charge, Machine Tools Research Laboratory, Mechanical Engineering Department, Jadavpur University. The author feels very much grateful to Prof. Titas Nandi, Workshop Superintendent Mechanical Engineering Department, Jadavpur University, for his immense help for this work. He is also grateful to Dr. Ashish Bandyopadhyay, professor of the same department of the university for his constant encouragement.

The author is thankful to shri Ranjit Kangsabanik and Shri Sashadhar Rang, staff members of Mechanical Engineering Department for their help. The author is very much thankful to all other staff members of Blue Earth Workshop and G.C Sen Memorial Machine Tools Research Laboratory for their immense co-operation during the thesis work.

The author also feels indebted is to Mr. Bignesh Das at Materials and Metallurgical Engineering Department of Jadavpur University, for his invaluable support.

The author would like to convey thanks to Ramesh Rudrapati, Assistant Professor, Mechanical Engineering Department, JSPM's Imperial College of Engineering & research, Pune, Maharashtra for his constant support and help. The author desires to convey thanks to

Arindam Sarkar, Ph.D student of Mechanical Engineering Department who helped in learning process optimization, at certain stages.

The author will fail in his duty if he does not offer thanks to all his friends, seniors and class mates for presenting the thesis in the present form.

The author's family has been very helpful and supportive during his Post Graduate study. The author wishes to thank them for their support and encouragement.

At last, the author is thankful to all others who have assisted him directly or indirectly to accomplish this work.

RANJEET KUMAR

Examination Roll No. M4MEC1613

Registration No. 129390 of 2014-2015

SUMMARY

Submerged arc welding (SAW) is an arc welding process in which the arc is concealed by a blanket of granular and fusible flux. Heat for SAW is generated by an arc between a bare, solid metal (or cored) consumable-wire or strip electrode and the work-piece. Selection of welding parameters plays a significant role on the quality of the welded joints. The quality of the joint can be evaluated in terms of weld-bead geometry, mechanical properties, distortion, microstructural characteristics etc. Dissimilar welding is a challenging area, demand of research in this area is increasing. In the present work dissimilar welding of AISI 409 ferretic stainless steel to mild steel has been performed by submerged arc welding using mild steel as filler wire. Thickness of both the base materials is 8 mm each. Experiments are designed according to Taguchi method (L9 orthogonal array) considering three factors and three levels. The input parameters considered are current, stickout length and traverse speed. The responses are ultimate tensile strength (UTS), percentage elongation (PE), HAZ widths at stainless steel side and mild steel side and weld hardness. The effect of input parameters on the responses is studied. Mathematical model has also been developed by RSM. Response surface plots and contour plots are generated as well. Multi-objective optimization is carried out to identify the optimal parametric combination. Adequacy of the models has been tested using ANOVA. Further, microstructural study of the welded samples has been done in an elaborative manner. Based on the results and analyses some conclusions are finally drawn.

CONTENTS

CHAPTER 1

1. INTRODUCTION

Manufacturing is involved in turning raw materials to finished products to be used for some purpose. The manufacturing technology primarily involves sizing, shaping and imparting desired combination of the properties to the material so that component or engineering system being produced can perform the intended function in its expected life. Manufacturing processes have been developed in a wide range, in order to produce the engineering components of very simple to complex geometrics of different physical, chemical, mechanical and dimensional properties. In industry most of the materials are fabricated into the desired shapes mainly by one of the four methods viz., casting, forming, machining and welding. The selection of a particular technique depends upon different factors which may include shape and size of the component, precision/accuracy required, cost, material and its availability, complexity of geometry of the component and the number of units to be produced, properties of the materials etc. In manufacturing, different components are joined (or assembled) together to get the desired shape and size. Three major joining techniques namely mechanical joint (nuts, bolts, and rivets), adhesive joint (epoxy resin) and welding are commonly used for manufacturing. Welding is one of the most commonly used fabrication techniques for manufacturing engineering components for different sectors.

Welding is a metallurgical fusion process of permanently joining two or more similar or dissimilar metals or nonmetals. It is the process of joining similar or dissimilar metals with or without application of heat, with or without application of pressure and with or without addition of filler metal. However, there are some non-fusion welding techniques as well. Welding is fast and is one of the most economical ways to join metal together permanently. Though there are a number of well observed welding processes but arc welding with uncoated/coated electrodes is still the most popular welding process. These processes are mainly shielded metal arc welding (SMAW), flux cored arc welding (FCAW), carbon arc welding (CAW), tungsten inert gas welding (TIGW), metal inert gas welding (MIGW), plasma arc welding (PAW) and submerged arc welding (SAW). Among the arc welding techniques shielded metal arc welding (SMAW) was invented first and it is a manual welding process, followed by submerged arc welding (SAW) and gas tungsten arc welding (GTAW). Gas metal arc welding (GMAW) was invented later around 1940’s. Submerged arc welding

(SAW) is used for thick materials, high deposition rate with butt joint and flat welding position, whereas gas tungsten arc welding (GTAW) provides best quality weld with low productivity for thinner joints. Gas metal arc welding (GMAW) is a versatile welding process to weld a wide range of materials with high quality and productivity. The selection of the welding process depends upon the types of materials, thickness of the materials to be joined, type of joint, welding position, deposition rate, shape and size required by the joint etc.

Most materials can be welded by more than one process but some are easier to weld than others. For comparing required welding process of a material in welding 'weldability' term is defined. Weldability is the capable of being welded into inseparable joints having specific properties such as definite weld strength, proper structure etc. with minimum requirements of special considerations or precautions. It depends upon the melting point, thermal conductivity, thermal expansion, surface conduction, change in microstructure etc. These characteristics can be controlled by proper shielding atmosphere, proper fluxing material, proper welding procedure, proper heat treatment before and after deposition. Low carbon steels have the best weldability amongst metals [1].

Joining dissimilar materials is often more difficult than joining the same material or alloys with minor differences in composition; however, many dissimilar materials can be joined successfully with the appropriate joining process and specialized procedures. Improving the ability to join dissimilar materials with engineered properties are enabling new approaches to light-weighting automotive structures, improving methods for energy production, creating next generation medical products and consumer devices, and many other manufacturing and industrial uses. Joints of dissimilar metals are used to achieve special combination of properties as well as to save cost incurred towards costly and scarce materials. The properties of dissimilar welding joints and even the feasibility of welding processes are influenced by many factors, for example, carbon migration from the low alloy side, microstructure gradient and different residual stress situations across different regions of weld metal. Some weld defects, such as dilutions and cracks, may generate in weld metal and lead to the great decrease of weld metal properties, if the welding process is not well controlled. Many researchers are doing extensive research on the properties of dissimilar weld joints and its effect on the welding behavior and mechanical properties of the joints.

There are many numbers of statistical techniques available for engineering and scientific studies. Taguchi method has become most popular among them. This is used for the model fitting of physical experiments, and also for numerical experiments. The objective of design of experiment (DOE) is the selection of the points where the response should be

evaluated. It minimizes the variation in product response while keeping the mean response on target. The product can be made robust to changes in operating and environmental conditions. Since the method is applied in a systematic way at a pre-production stage (off line), it can greatly reduce the number of time consuming tests, thus saving in costs and wasted product.

In the present research work, dissimilar welding of ferritic stainless steel AISI 409 to mild steel AISI 1018 by submerged arc welding (SAW) has been studied. Emphasis has been given to identify the effect of some selected input parameters (current, stick-out length and traverse speed) on the quality of butt-welded joints. Quality of the welded joints has been judged by visual inspection, tensile test, measurement of hardness at different zones, scanning electron microscope (SEM); also microstructural studies have been considered important. Process optimization has been carried out as well.

1.1 WELDING AND ALLIED PROCESSES

Welding is a dependable, efficient and economic method for permanently joining similar or dissimilar metals. Welding is one of the most commonly used fabrication or sculptural techniques for manufacturing engineering components, that joins materials, usually metals or thermoplastics, by causing fusion in most of the cases, which is distinct from lower temperature metal joining techniques such as brazing and soldering, which do not melt the base metal for power, fertilizer, petro-chemical, automotive, food processing, and many other sectors. Welding generally uses localized heating during common fusion welding processes (like: shielded metal arc, submerged arc, gas metal arc welding etc.) for melting the faying surfaces and filler metal. However, localized and differential heating & cooling experienced by the metal during welding makes it significantly different from other manufacturing techniques. During fusion welding, the pieces to be joined (the work pieces) are melted at the joining interface and usually a filler material is added to form a pool of molten material (the weld pool) which solidifies to become a strong joint. In contrast, soldering and brazing do not involve melting the workpiece but rather a lower melting point material is melted between the workpieces to bond them together.

1.1.1 DEVELOPMENT AND AUTOMATION IN WELDING

The submerged arc process is a well established and extremely versatile method of welding. It is the first successful method of automatic arc welding. Submerged arc welding is very often either semi-automatic or automatic.

The earliest evidence of welding can be traced back to the Bronze Age and is still being perfected today. In the 19th century, major breakthroughs in welding were made where in 1836 Englishman Edmund Davy discovered acetylene and acetylene was soon utilized by the welding industry. Arc welding and oxy-fuel welding were among the first processes to develop late in the 19^{th} century and electric resistance welding followed soon after. Electrical arc was first described by Davy in England, in the year 1809, but the beginning of arc welding could become possible only with the improvement in the electric dynamos or generators between 1877 and 1880. August de Meritens established arc welding process in 1881 which was applied to join certain component of electrical storage batteries. After this in 1890, C.L. Coffin of Detroit was awarded the first U.S. patent for an arc welding process using a metal electrode. In 1892, N.G. Slavianoff from Germany proposed the use of bare wire metallic electrode for joining metals and in this case, the arc being unshielded, satisfactory welds could not be produced. Strohmenger first developed coated electrode in 1900 due to which a coating of lime helped the arc to be much more stable. A number of other welding processes were developed during this period. Some of them included seam welding, spot welding, flash butt welding, and projection welding. Stick electrodes became a popular welding tool around this time as well. Welding technology advanced quickly during the early 20th century as World War I and World War II drove the demand for reliable and inexpensive joining methods.

Automatic welding was first introduced in 1920 by P. O. Nobel. Automatic welding technique integrated the use of arc voltage and bare electrode wires. It was used for repairing and molding metals. Several types of electrodes were also developed during this decade. The patent for TIG welding was obtained by Hobart and Devers in 1930 in USA and first gas tungsten arc spot welding torch based upon TIG welding was introduced around 1946. The credit for submerged arc welding (SAW) goes to Kennedyy, Rodermundand Jones (1935) of USA. Metal Inert Gas (MIG) welding came out in 1948 as a result of further researches and development carried out on covered electrode metal arc and tungsten inert welding process. Lyubavskii and Novoshilov in 1953 invented popularized CO_2 welding process which became a welding process of choice for welding steels, as it was comparatively economical. Soon, electrode wires of smaller diameter were launched. This made welding of thin materials more convenient. After many/several researches and improvement in the field of welding during the 1960-80's, dualshield welding, innershield, and electroslag welding were developed. Plasma arc welding was also invented by Gage during this time which was used for metal spraying.

Electron beam welding was developed by the French, which is still used by the aircraft manufacturing industries of the United States.

Some of the recent developments in the welding industry include the friction welding process developed in Russia, and laser welding. Several references [2 - 4] have been found useful in making the above summary of development of welding and its automation.

1.1.2 CLASSIFICATION OF WELDING PROCESSES

Today many different welding processes are in use, each with their own advantages and limitations. The basic task is to choose the appropriate process for a particular application which satisfies the technological requirements and the most cost effective. The principal governing factors are: type of materials, type of joints, productivity requirements, quality standard, cost of welding etc.

Welding methods can roughly be classified into pressure processes, fusion processes, brazing and soldering by the mechanism of joining metals. In the pressure processes, the joint is made by applying pressure to the area of contact of the two components, which may or may not be heated to a molten state and this process can be carried out both at room temperature and at an elevated temperature. In fusion processes, two components are joined by heating the area of contact to a molten state and no pressure is applied, a molten filler material is also added if necessary. Soldering, brazing, adhesive bonding, thermal spraying etc are the allied processes in which a filler metal having a lower melting point than that of the base metal is melted with a gas torch or in a furnace and is applied to the area of contact. The molten filler metal wets the surfaces of the base metal and is drawn into or held in the joint by the capillary action without fusing the base metals. There are about 35 different welding techniques, brazing and soldering processes in use by industry today.

American welding society bas classified the welding process in a manner which is shown, in a modified form, in Figure 1.1. Various welding processes differ in manner in which temperature and pressure are combined and achieved **[**5**]**.

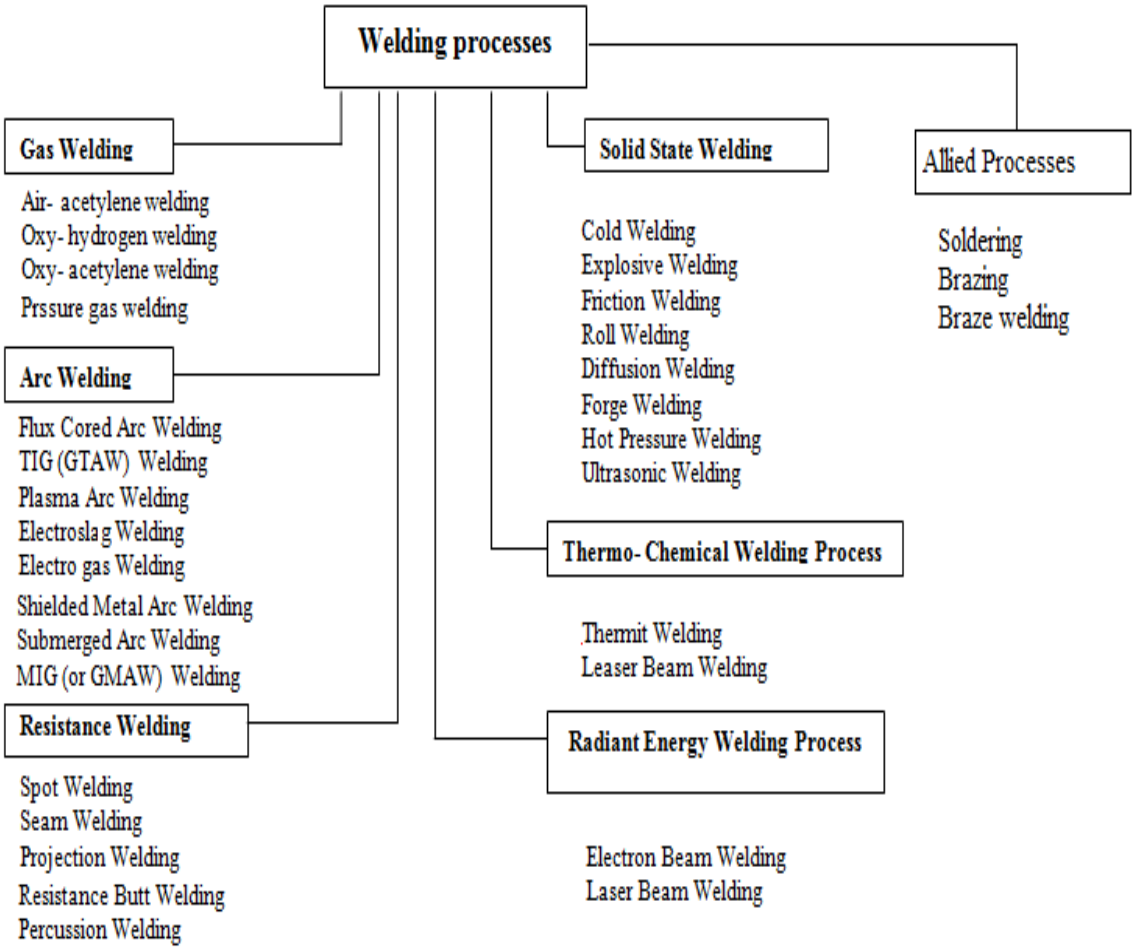

Figure 1.1 Classification of welding and allied processes

In the present work SAW has been used. It is a special type of arc welding. Some fundamentals of arc welding are discussed next.

Table 1.1 gives an idea about suitability of the respective processes to weld different materials.

Table 1.1 Different welding processes for different materials

Metal	Welding process	Cutting process
Mild steel	All welding processes	Oxyfuel, Plasma
Aluminium	Gas tungsten arc, gas metal arc	Plasma
Stainless steel	Gas tungsten arc, gas metal arc, shielded metal arc	Plasma
Chrome moly steel	Gas tungsten arc, oxyfuel	Plasma
Titanium	Gas tungsten arc	Plasma
Cast iron	Shielded metal arc, brazing	Plasma
Brass	Braze welding	Plasma

1.1.3 WELDING TERMINOLOGY

There is some special technical vocabulary (or language) that is used in welding. The basic terms of the welding language include:

Filler Material:- When welding two pieces of metal together, one often has to leave a space between the joint. The material that is added to fill this space during the welding process is known as the filler material (or filler metal). Two types of filler metals commonly used in welding are welding rods and welding electrodes.

- Welding Rod:- The term welding rod refers to a form of filler metal that does not conduct an electric current during the welding process. The only purpose of a welding rod is to supply filler metal to the joint. This type of filler metal is often used for gas welding.
- Electrode:- In electric arc welding, the term electrode refers to the component that conducts the current from the electrode holder to the metal being welded. Electrodes are classified into two groups: consumable and non-consumable.
  - Consumable electrodes not only provide a path for the current but they also supply filler metal to the joint. An example is the electrode used in shielded metal-arc welding.
  - Non-consumable electrodes are only used as a conductor for the electrical current, such as in gas tungsten arc welding. The filler metal for gas tungsten arc welding is a hand fed consumable welding rod.

Flux:- Before performing any welding process, the base metal must be cleaned form impurities such as oxides (rust). Unless these oxides are removed by using a proper flux, a faulty weld may result. The term flux refers to a material used to dissolve oxides and release trapped gases and slag (impurities) from the base metal such that the filler metal and the base metal can be fused together. Fluxes come in the form of a paste, powder, or liquid. Different types of fluxes are available and the selection of appropriate flux is usually based on the type of welding and the type of the base metal.

1.1.4 WELDING POWER SOURCES

Arc welding is the most popular welding process today. In arc welding, the heat required is obtained from electrical energy. An arc is produced between the tip of the electrode and the workpiece to be welded, by the use of an AC or DC power supply. A welding arc is a high current low voltage electric discharge operating generally in the range of 10–50 volts. All arc welding processes require a continuous supply of electric current of

sufficient and appropriate amperage and voltage to maintain a stable arc. This current may be either alternating (AC) or direct (DC), and it must be supplied to a welding electrode through a device that enables precise control of the current. This controlling device is called a power source. The current is supplied to the power source from utility power lines, or developed by generators or alternators driven by close-coupled gasoline or diesel engines. For efficient welding, a power source must be able to control the arc characteristics needed for a specific job. In one job, a forceful, deeply penetrating arc may be required, while, in another job, a soft, less penetrating arc may be necessary to avoid burn through. Therefore, the type, capacity and output characteristics of a power source must be thoroughly examined, taking account of the welding procedure to be taken.

Arc welding power sources are classified according to the type of current (AC or DC), and according to their voltage output, which can either be variable (variable-voltage type) or constant (constant-voltage type). A further classification designates the method by which energy is supplied to the power source from a power line directly or through an electric motor (motor-generator type) or from a gasoline or diesel engine (engine-driven type). Alternating current (AC), obtained directly from the power line, goes through a transformer in the AC power source that allows for the control of the current. Direct current (DC) is produced from the AC line power by either using the line power to run an electric motor that turns a DC generator (motor-generator type) or using the line power through a transformer and then a rectifier (rectifier type). Combination power sources, producing both AC and DC, are basically transformer-rectifier type. The welding process dictates the type of power source needed. Tables 1.2 - 1.3 list some features relating in welding power sources. Table 1.2 describes the requirement of the power sources for different arc welding processes and Table 1.3 shows the comparison between AC and DC power sources.

Table 1.2 Power source requirements for arc welding processes

Welding process	Output characteristic	Types of current
Shielded metal arc welding TIG welding Submerged arc welding	Variable voltage	AC or DC
Gas metal arc welding Electrogas arc welding	Constant voltage	DC
Self shielded arc welding	Variable voltage	AC
	Constant voltage	DC

Table 1.3 Comparison between AC and DC power sources

Comparison item	DC power source	AC power source
Arc stability	Excellent	Less stable
Polarity	Variable	Constant
Arc blow	Yes	Almost none
Open circuit voltage	Lower (50-60 V)	Higher (65-95 V)
Possibility of electric shock	Lower	Higher
Machine construction	Complicated	Simple
Machine price	Higher	Lower
Maintaince	Not easy	Easy
Noise	Rotary type:- noisy Rectifier type:- quiet	Quiet

1.1.5 PRINCIPLE OF ARC WELDING

In the work reported here, submerged arc welding (SAW) is used. SAW can be considered as special case of arc welding. And as such, some fundamentals of arc welding are discussed below.

An arc is a sustained electric discharge through the ionized gas column called plasma β between the two electrodes. Initially a good contact is made between the electrode and the work. Thereafter the electrode is withdrawn. As a result, the metallic bridges start breaking, thus increasing the current density per bridge. Finally the current density rises to such a value that the bridges start boiling. Under such condition, the electrons come out of both the surfaces by process known as thermionic emission. Obviously, the electrons (having negative charge) coming out of the anode are pulled back, where those coming out of the cathode are also attracted towards the anode.

The rate at which the electrons are emitted from a hot surface is given by

$$\mathbf{I = C\theta^2 exp(-\beta/\theta),} \qquad (1.1)$$

where 'I' is in ampere/cm^2; 'θ' is the absolute temperature, 'C' is a constant, and 'β' is given by

$$\mathbf{\beta = \phi e/k\theta} \qquad (1.1a)$$

With e = charge of an electron, k = Boltzmann's constant, and ϕ (when measured in electron volts) is the thermionic work function. ϕ, in fact represents the kinetic energy necessary to boil out an electron. It is obvious from the eq. (1.1) that a low value of ϕ**,** together with a high value of θ, makes the emission of electron easier. Once started, the arc itself becomes a source of ions through a process of ionization. These ions are attracted by the cathode, called the primary electrons and the second set, known as secondary electron, and is

produced as result of the ionization of the arc gap. With tungsten and carbon electrodes, the primary electrons carry most of the current, whereas with copper or aluminium electrodes, the secondary electrons carry most of the current.

An electron of charge 'e', moving in an electric field of gradient 'E' (volt/distance), experiences a force of magnitude 'eE'. In other words, it accelerates at a rate of 'Ee/m', where 'm' is its mass. So if it travels through a distance 'd' before colliding with another particle (a neutral atom or another electron), it has a kinetic energy 'eEd'. This kinetic energy is heat and manifests itself through increased temperature .The interparticle collision taking place in the gap between the electrodes, gives rise to a process called thermal ionization. Normally these collisions are elastic and both momentum and kinetic energy are conserved. However, occasionally a collision is such that an electron may be completely knocked out from a neutral atom, producing a free electron and a positively ion; such a collision is not elastic in nature .A definite amount of energy is required to produce ionization in a given atom or molecule. This energy (in electron volts) is numerically equal to the ionization potential (in volt or voltage) and is to be supplied continuously between two electrodes.

1.1.6 FORCES AFFECTING THE ARC

Arc welding processes which use consumable electrodes, the electrode is melted continuously and the metal is transferred to the work-piece through the arc. This transferred metal combines with the molten metal in the weld pool to give a particular shape to the weld bead. The depth of penetration, the stability of the weld pool, amount of spatter and other factors depend on the mode of metal transfer from the consumable electrodes. This mode of metal transfer largely depends on some dominant factors which include the forces acting on the droplet. The major forces taking part in this process are

a) Gravitational force (F_g):- It is a detaching or helping force for down hand welding and a retaining force for overhead welding. Magnitude of this force is equal to the weight of the molten metal droplet and is expressed as,

$$\mathbf{F_g = mg} \qquad (1.2)$$

where, m = mass of the droplet, g = gravitational force.

b) Surface tension force (F_s):- Surface tension tends to retain the molten droplet at the tip of the electrode. The magnitude of the force at the time of droplet detachment under its own weight is given by the expression,

$$\mathbf{F_s = 2\pi\gamma r\, f(r/c)} \qquad (1.3)$$

where, γ = surface tension, r = radius of electrode, c = constant of capillarity.

c) Electromechanical pinch force (F_p):- When electric current is passed through a conical conductor like the welding arc, axial forces are acting on it which is directed from the small cross-section to the large one. This results in the setting up of a plasma jet provided the current is of sufficient magnitude. Also, when a current carrying conductor is under the influence of its own magnetic field, radial contracting forces are developed which produce pressure within the conductor. The combined effect is a detaching force acing on the molten droplet at the tip and is known as pinch effect.

If an electrode is considered as consisting of a number of concentrating cylinders of varying diameters with one inside the other then on the basis of current flow in parallel conductors, a contracting force is experienced by the electrode. This force is hardly of any consequence on the solid electrode but results in considerable influence on the detachment of the molten droplet from the tip of the electrode, and is referred to as Lorentz force or electromagnetic pinch force. This force at a distance 'r' from the axis of the electrode is given by the expression,

$$\mathbf{f = 100\mu I^2/8\pi^2 R^2(2 - r^2/R^2)}\ \text{N/cm}^2 \qquad (1.4)$$

where, I = current, R = diameter of the electrode, μ = magnetic permeability

The net electromagnetic pinch force on the droplet, tending to detach it from the electrode tip is determined by,

$$\mathbf{F_p = {}_0\int^R 2\pi rf.dr} \qquad (1.5)$$

and it is approximately equal to $I^2/200$.

d) Drag force (F_d):- A drag force is produced due to the flow of gas around the drop which helps in detaching the droplet from the electrode tip. The magnitude of this force may be affected by the amount of gas flow in GMAW or to a limited extent by the amount of gases produced from the coatings in SMAW [6].

1.1.7 DEFECTS IN WELDING

A flaw or flaws that by nature or accumulated effect render a pile or product unable to meet minimum acceptance standards or specifications is called defect. A welding defect is any flaw that compromises the usefulness of a weldment in the welding. There are various welding difficulties which arise frequently in the welding processes. The main aim is to minimize these difficulties and produce quality weld. The major defects of welding are classified as follows: some of these are shown in Figure 1.2 (a - f).

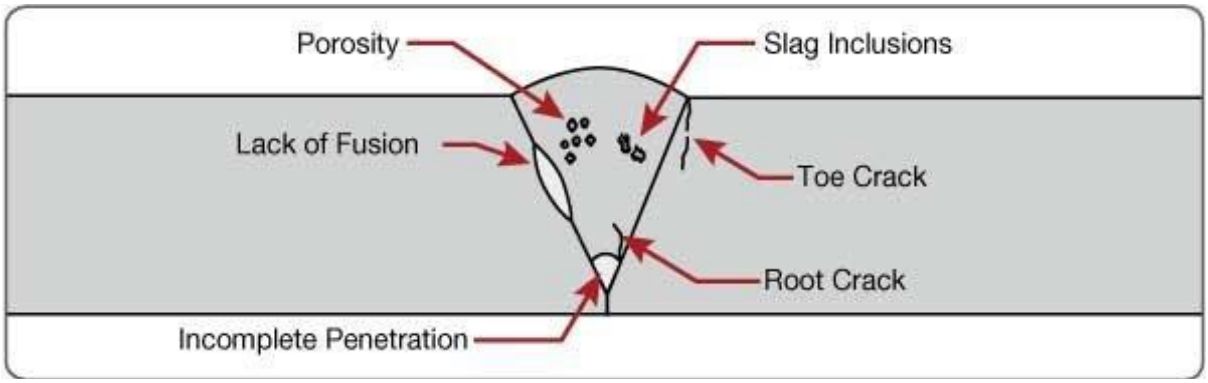

Figure 1.2(a) Different welding defects [7]

a) Poor fusion:- Poor fusion or lack of fusion is defined as the unfused area between weld metal and base material or previously welded layer. This happens when the base metal or the previous layer is not completely or insufficiently molten. This causes lack of complete union between deposited metal and parent metal. It appears as discontinuity in the weld zone. It can be resulted from failure to raise proper melting temperature, improper surface cleaning, improper welding current and wrong size of electrode etc. Details of lack of fusion are shown in figure 1.2(b).

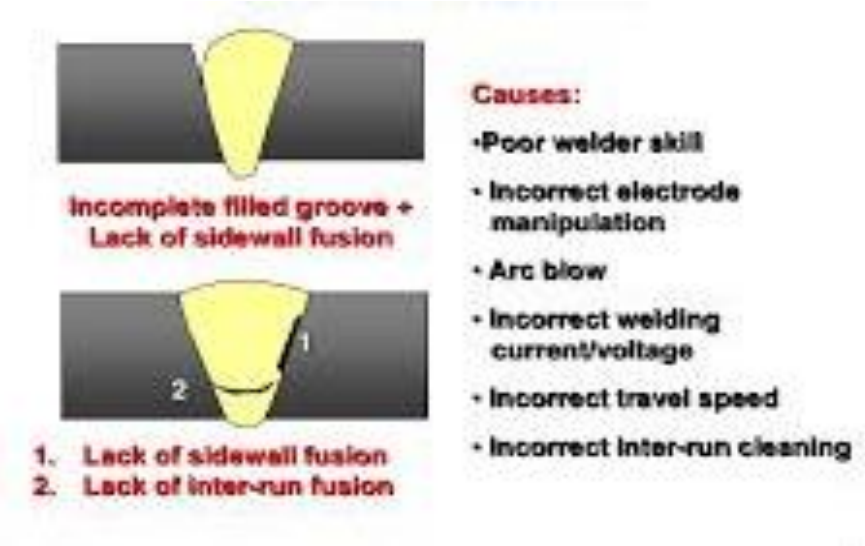

Figure 1.2(b) Lack of fusion [8]

b) Undercut:- It appears as a small notch at the weld interface. Undercut is a groove cut along the toe of the weld and left unfilled. This type of welding defect occurs due to high amperage current, electrode angle, long arc length, rust, fast travel speed etc. Undercutting can be avoided with careful attention during preparation of the edge, cleaning metal before welding, setting machine on scrap metal to correct parameters and by improving the welding process. Figure 1.2(c) contains undercut defect of welding and slag inclusion.

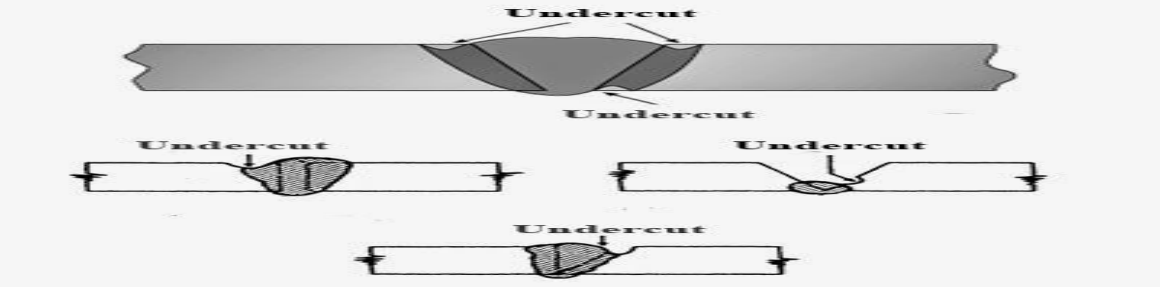

Figure 1.2(c) Welding defect: undrcut and slag inclusion [8]

c) Slag inclusion:- Slag particles getting traped in the fusion zone causes slag inclusion. These can occur when several runs are made along a V join when joining thick plate using flux cored or flux coated rods and the slag covering a run is not totally removed after every run before the following run. It can be due to high viscosity of molten metal, low temperature, rapid cooling, improper removal of previous layer. Figure 1.2(d) shows porosity and slag inclusions in the weld.

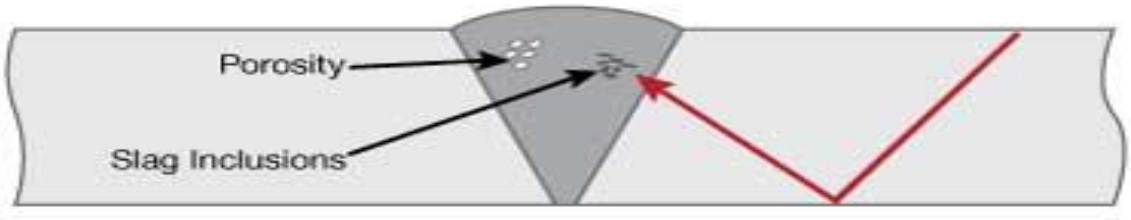

Figure 1.2(d) Porosity and slag inclusions in weld [8]

d) Cracks:- This may occur due just to thermal shrinkage or due to a combination of strain accompanying phase change and thermal shrinkage. In the case of welded stiff frames, a combination of poor design and inappropriate procedure may result in high residual stresses and cracking. Where alloy steels or steels with a carbon content greater than about 0.2% are being welded, self cooling may be rapid enough to cause some(brittle) martensite to form. This will easily develop cracks. To prevent these problems a process of pre-heating in stages may be needed and after welding a slow controlled post cooling in stages will be required. Different types of crack are shown in Figure 1.2(e).

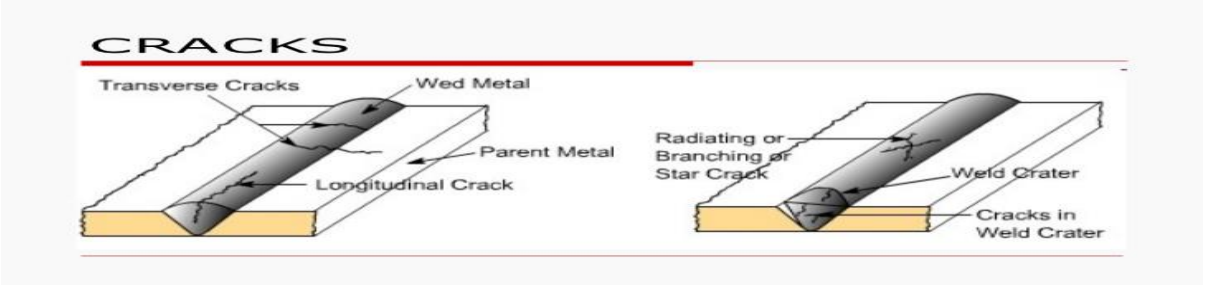

Figure 1.2(e) Different cracks in weld [9]

e) Porosity:- This occurs when gases are trapped during the solidification of weld metal (Figure 1.2(d)). These may arise from damp consumables or metal or, from dirt, particularly oil or grease, on the metal in the vicinity of the weld. This can be avoided by ensuring that all consumables are stored in dry condition and work is carefully cleaned and degreased prior to welding.

f) Spatter:- Spatter occurs from metal drops expelled from the weld that stick to the surrounding surfaces. Spatter is usually caused by operating outside acceptable parameters for the desired metal transfer mode. Reducing the wire feed speed will reduce the current and produce spatter. Too low a voltage will also cause spatter. Figure 1.2(f) represents spatter in the weld.

Figure 1.2(f) Spatter in welding [9]

1.2 SUBMERGED ARC WELDING (SAW)

This is an automated/semi-automated process developed for high quality butt welds in thick plates like container fabrication, bridge construction etc. Submerged arc welding (SAW) is considered to be the workhorse of the fabrication industry and a common arc welding process due to its reliability and capability of producing good quality weld. This process is used to fabricate large thick sections; with thickness ranging from 10 mm to 500 mm. Submerged arc welding is an arc welding process in which the arc is concealed by a blanket of granular and fusible flux. Heat required for SAW is generated by an arc between a bare solid metal (or cored) consumable wire or strip electrode and the work-piece. The arc is maintained in a cavity of molten flux or slag which refines the weld metal and also protects it from atmospheric contamination. Fluxes used in SAW is a fundamental granular fusible minerals ingredient containing oxides of manganese, silicon, titanium, aluminium, calcium, zirconium, magnesium and other compounds such as calcium fluoride on which the stability of the arc depends. The flux is specially formulated to be compatible with a given electrode wire type so that the combination of flux and wire yields desired mechanical properties. All fluxes react with the weld pool to produce the weld metal chemical composition and the mechanical, chemical properties, crack resistance and other qualities of the final weld deposit

can be controlled by the flux. SAW is usually operated as a fully mechanized or automatic process, but it can be semi-automatic, as well. Important welding parameters are current, stick-out length, arc voltage and travel speed- all influence bead shape, depth of penetration and chemical composition of the deposited weld metal. Because the operator cannot see the weld pool, greater reliance must be placed on parameter settings. As the degree of automation in the SAW process increases, the direct influence of the operator decreases and the precise setting of the parameters become much more important as compared to the manual welding process. According to material thickness, joint type and size of component, proper choice of the parameters can increase deposition rate and improve bead shape. Currents ranging from 300A to 3000A are commonly used and main source power supply should be 440 volts. Currents up to 5000A can also be used in multiple arcs welding and velocity may be 5 m/min. The SAW process provides very high welding productivity, depositing 4–10 times the amount of weld metal per hour as compared to ordinary metal arc welding process. DC or AC powers as well as a combination of both are common sources of power on multiple electrode systems. Constant voltage power supply is a most commonly used source. In the present investigation of dissimilar welding of ferritic stainless steel to mild steel submerged arc welding is used.

1.2.1 OPERATION OF SUBMERGED ARC WELDING

The diagram shown in Figure 1.3 indicates, in schematic form, the principle of submerged arc welding. The filler material is an uncoated, continuous wire electrode, applied to the joint together with a flow of fine-grained flux, which is supplied from a flux hopper via a tube. The electrical resistance of the electrode should be as low as possible to facilitate welding at a high current, and so the welding current is supplied to the electrode through contacts very close to the arc and immediately above it. The arc burns in a cavity which, apart from the arc itself, is filled with gas and metal vapour. The size of the cavity in front of the arc is delineated by unmelted basic material and behind it by the molten weld. The top of the cavity is formed by molten flux. The diagram also shows the solidified weld and the solidified flux, which covers the weld in a thin layer and which must subsequently be removed. Not all of the flux supplied is used up: the excess flux can be sucked up and used again.

The flux also has a thermal insulating effect, and thus reduces heat losses from the arc. As a result, more of the input energy is available for the actual welding processes itself than is the case with processes involving an exposed arc. The thermal efficiency is greater and the rate of welding is faster. It has been found that submerged arc welding has a thermal efficiency of about 90%, as against an approximate value of about 75% for MMA welding. Electric current,

which produces the arc, is supplied to electrode through the contact tube. Submerged arc welding can be performed using either DC or AC. The current can be direct current (DC) with electrode positive (reverse polarity), with electrode negative (straight polarity) or alternating current. In the SAW process, electric current flows though the arc and the weld pool, which consists of molten flux and molten weld metal. Figure 1.3 indicates the schematic diagram of principle of operation of submerged arc welding process. Figure 1.4 shows the block diagram of a submerged arc welding machine.

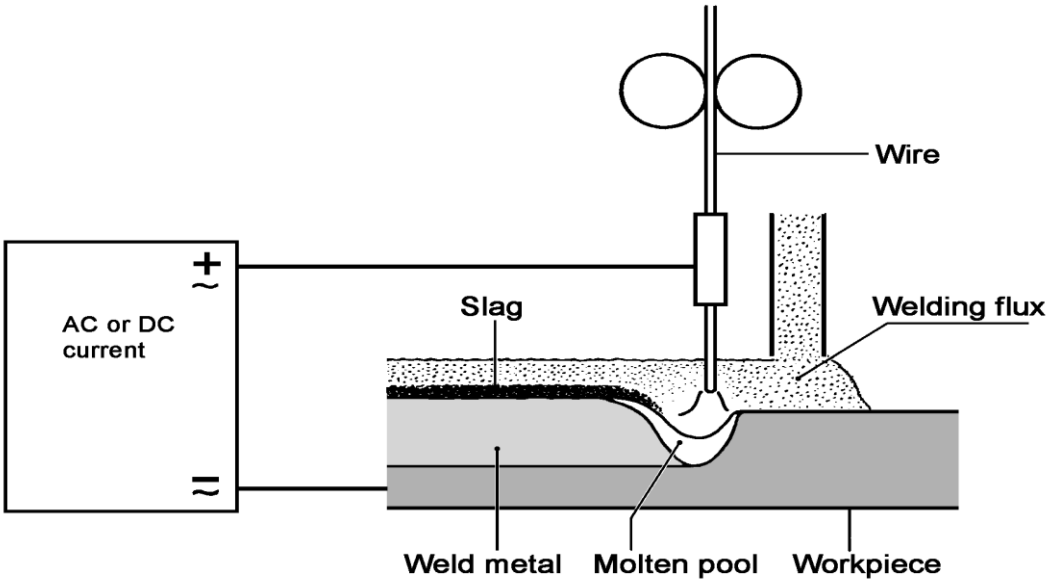

Figure 1.3 Principle of submerged arc welding [10]

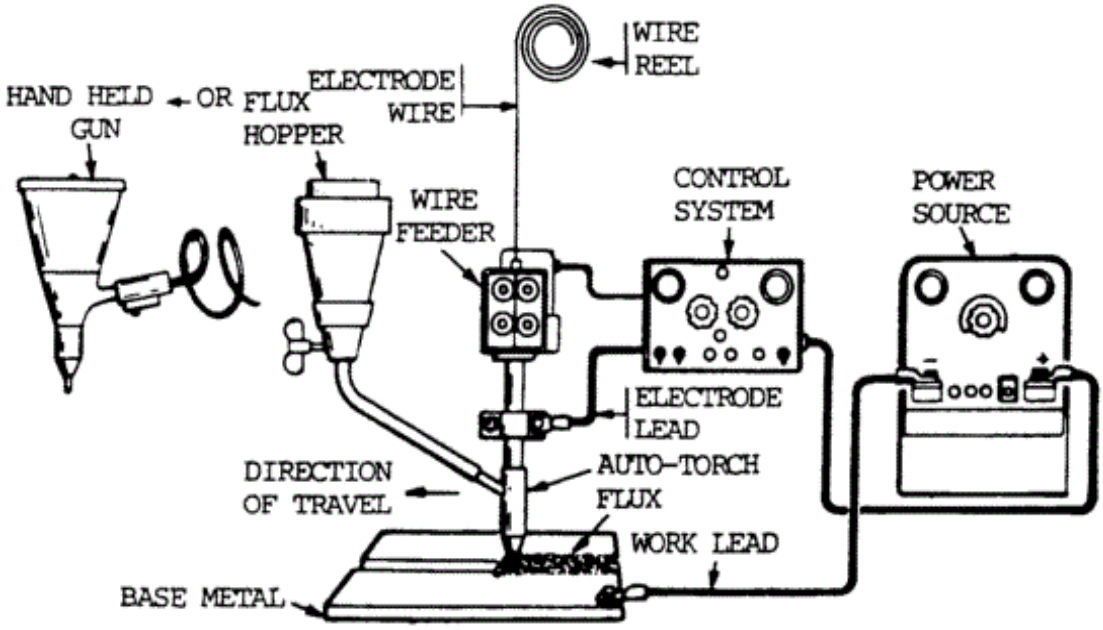

Figure 1.4 Block diagram of a SAW machine [10]

1.2.2 CONTROLING OF ELECTRODE FEED WIRE

Welding current is the main source upon which rate of melting or deposition rate of electrode depends. The wire electrodes are used, to be fed at a controlled rate to maintain constant arc length and rate of melt-off. Figure 1.5 shows the mechanism of feeding the wire in SAW. Melt-off rate or deposition rate is expressed in kg/hour.

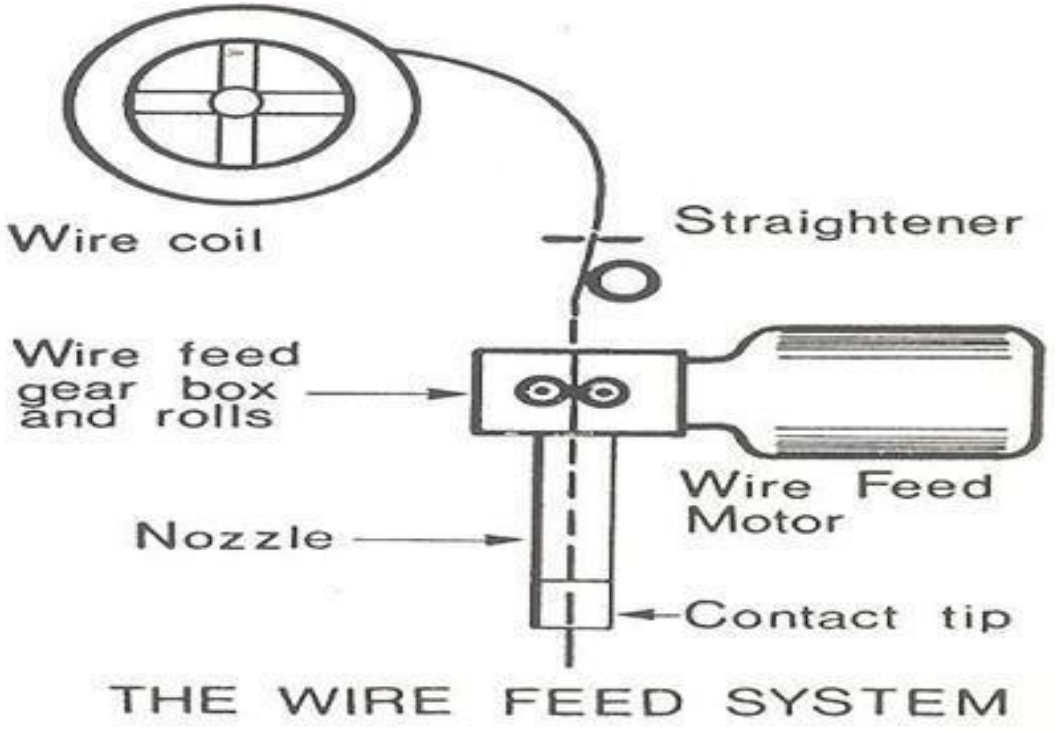

Figure 1.5 The wire feeding system [10]

1.2.3 CONSUMABLE MATERIALS

Two main items which are generally used as consumable materials for submerged arc welding; these are electrodes (filler wire) and flux. Recently, a third component has become commonly used is iron powder.

Filler wire/Electrode

The filler wires are generally copper plated in order to ensure good current transfer to it from the contact jaws, and to reduce wear of the jaws. The copper, in other words, is not intended for corrosion protection in the usual meaning, and the coils of filler wires must be protected against moisture in the same way as must other filler materials. Figure 1.6 illustrates the various types of electrode or filler wire.

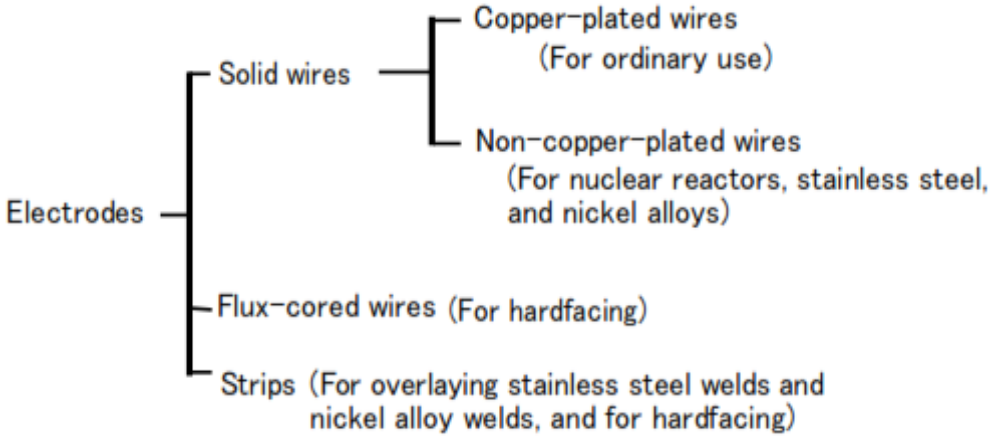

Figure 1.6 Types of electrode [11]

The wires may be of various types such as solid or tubular and, in the case of solid wire, be round or rectangular in cross-section. Solid filler wires of round section are used for fabrication welding and cladding, while rectangular section wires are known as strip electrodes which are generally used only for cladding. Tubular wire electrodes are also very suitable for cladding, as the alloying elements necessary can be contained in the hollow centre of the wire. Both strip electrodes and tubular wire electrodes are important parts of the field of welding technology devoted to cladding.

Flux

The granulated flux which is granulated to a definite size shields the weld zone and thus protects molten weld from atmospheric contamination. They clean weld metal and can modify its chemical composition and mechanical properties as well. Most metals in their molten states are oxidized by the atmospheric oxygen. To prevent this oxidation and other unwanted chemical reactions flux is used. It is used to help the welding process easier and ensures a sound weld. As yet, there is no universal flux suitable for all purposes. The flux may consist of fluorides of calcium (CaF_2) and oxides of calcium (CaO), magnesium (MgO), silicon, aluminum and manganese. Alloying elements may be added as per requirements. Flux composition optimises for the use in combination with filler wires of varying metallurgical characteristics. These combinations can be provided in three ways which are: with all the necessary alloying elements i) in the filler wire, ii) in the flux or in the filler wire and iii) flux and filler wire together.

Flux can be classified as a fused, sintered or agglomerating type.

- Fused flux:- A fused flux is a homogeneous flux having size 0.2 to 1.6 mm thickness/average dia, i.e. the substances in the flux have been melted together to form

a glass like substance, which is then crushed and ground before finally being classified to a suitable grain size. The main components of fused flux are quartz, limestone and manganese dioxide (MnO_2) with small quantities of fluorspar and aluminium oxide (Al_2O_3) which are melted in an electric arc furnace where the manganese dioxide (MnO_2) is reduced to MnO.

- Agglomerated flux:- The particles in an agglomerated flux have been formed by 'rolling' of the various constituents on a rotating dish, drum or cone, with waterglass as an additive. The resulting product has then been dried in a rotary kiln at a temperature of 800–900°C. After drying, the flux is classified to give approximately the same grain size (0.2 to 1.6 mm thickness) as that of a fused flux. The manufacturing of this flux is easier then fused flux.
- Sintered flux:- These type of fluxes are produced by sintering the various components to produce blocks, which are then crushed and classified.

Fused fluxes are non-hygroscopic therefore particularly suitable for outdoor welding and in high-humidity environments. Agglomerated fluxes may be hygroscopic and should be handled with the same care as recommended for electrodes for manual welding. Benefits and drawbacks of different fluxes are listed in Table 1.4.

Table 1.4 Advantages and disadvantages of fluxes

Type of flux	Benefits	Drawbacks
Fused	Non-hygroscopic High grain strength	Alloying elements such as Cr and Ni cannot be incorporated in the flux High specific density (approx. 1.6 kg/l)
Agglomerated	Alloying elements such as Cr and Ni can be included in the flux Low specific density (approx. 0.8 kg/l)	Hygroscopic Relatively low grain strength
Sintered	Relatively low hygroscopicity Relatively low density (approx. 1.3 kg/l)	Alloying elements cannot usually be included in the flux Relatively low grain strength

Basicity index of SAW fluxes

Basicity index of a welding flux shows the metallurgical behaviour of the flux. It is the ratio between basic and acid compounds (oxides and fluorides) of which the flux is composed of. Welding fluxes can be divided into three groups; which is given in Table 1.5.

In the present work ESAB OK Flux 10.71 L has been used which is an agglomerated basic flux, having basicity index 1.4. It has very high current capacity on both A.C. and D.C. and very good operability characteristics both in single and multi-wire system.

Table 1.5 Classification of welding fluxes

Type of welding flux	Basicity index
Acid fluxes	<0.9
Neutral fluxes	0.9 - 1.2
Basic fluxes	>1.2

Table 1.6 describes the classification and requirements for submerged arc welding wire and fluxes.

Table 1.6 Classification and requirements for submerged arc welding wires and fluxes

Classification (1)		Chemical composition of wire (%)						
		C	Mn	Si	S	P	Cu	Others
Wires	EL8	0.10 max.	0.25-0.60	0.07 max.	0.030 max.	0.030 max.	0.35 max.	0.50 max.
	EL12	0.04-0.14	0.25-0.60	0.10 max.				
	EM12K	0.05-0.15	0.80-1.25	0.10-0.35				
	EH14	0.10-0.20	1.70-2.20	0.10 max.				

Iron Powder

In order to increase the productivity in welding materials over 20 mm thick, additives in the form of cold materials such as iron powder or cold wire can be used in filling passes. For the same energy input per unit length of weld, the addition of iron powder results in a smaller heat affected zone than does conventional submerged arc welding, which is beneficial in respect of the quality (strength) of the weld. The energy input per unit length of weld reduces in proportion to the increasing amount of iron powder.

Iron powder is usually alloyed with manganese (about 1.8%), although nickel-alloyed powder is also available [12].

1.2.4 SELECTION OF WELDING PARAMETERS IN SAW

Selection of welding parameters of SAW depend upon the shape and size of the work-piece, and must be selected to ensure satisfactory penetration and correct shape of the weld.

Starting from this basic requirement, one selects the appropriate values of filler wire size, arc voltage, welding current, electrode stick-out and welding speed. Selection of process parameters has great influence on the quality of a welded connection. Research in this respect is still being continued to identify the optimal parametric condition/combination. More emphasis is being given and is needed, particularly with reference to dissimilar welding.

Arc voltage:- The arc voltage determines the shape and width of the arc and also it influences penetration. In welding very high arc voltage produces a wider weld and on the other hand, very low arc voltage results in a high, round weld. Arc voltage is directly proportional to the arc length. Thus by increasing the arc length the arc voltage increases so that more heat is available for melting of the base metal and the flux. But increased arc length leads to spread of the arc column which increases the weld width and decrease in depth of penetration. Figure 1.7 shows the effect of arc voltage on bead shape when current is constant.

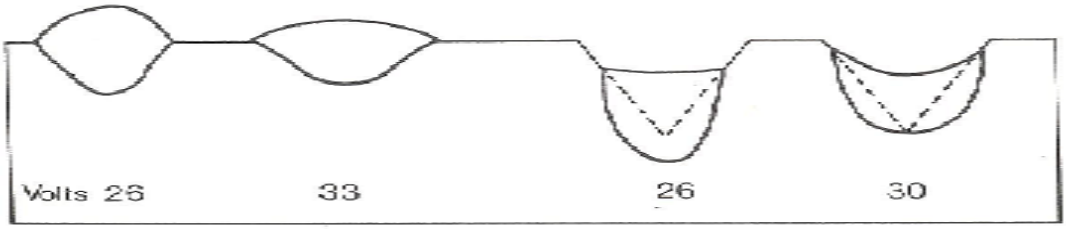

Figure 1.7 Effect of arc voltage on bead shape [12]

Figure 1.8 represents the effect of welding arc voltage and arc length on bead shape.

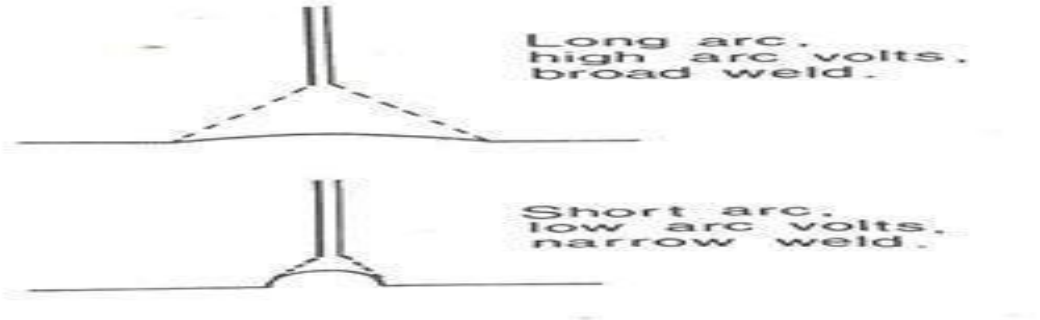

Figure 1.8 Effect of welding arc voltage and arc length on bead shape [12]

Welding current:- Welding current is the most important parameter for penetration. The welding current depends on the thickness of the metal and the type of joint. The current has no great effect on the width of the weld bead. A very high current can burn through, while very low current can penetrate insufficiently.

Welding current is proportional to the wire feed speed which affects the deposition rate. If the welding current increases the rate of melting of the filler wire also increases. For a

given welding current, the deposition rate will be higher if the filler wire is negative with respect to the workpiece than if the wire is positive, but the penetration will be reduced. Figure 1.9 shows the effect of welding current on weld bead shape.

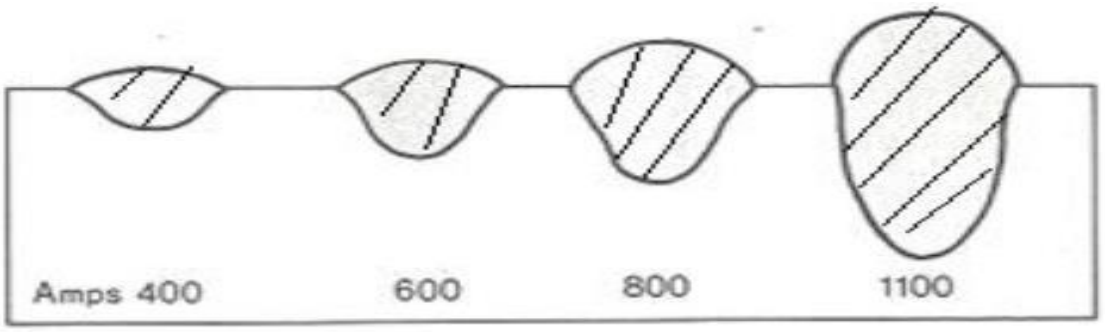

Figure 1.9 Effect of welding current on bead shape [12]

Welding speed:- The welding speed also affects the penetration. For a given welding current and arc voltage if the speed increases penetration will decrease and the weld will be narrower while reducing the speed increases penetration and results in a wider weld. At high travel speed transformation of thermal energy between the weld deposit and the parent metal decreases due to which increases the tendencies for undercut, arc blow, porosity and irregular bead shape. As the welding speed decreases, penetration and reinforcement increase but too slow a speed results in poor penetration. If the welding speed is to be changed while penetration is kept constant, it is necessary to compensate by adjustment of the welding current (increase or decrease). The effect of travel speed on bead shape is shown in Figure 1.10.

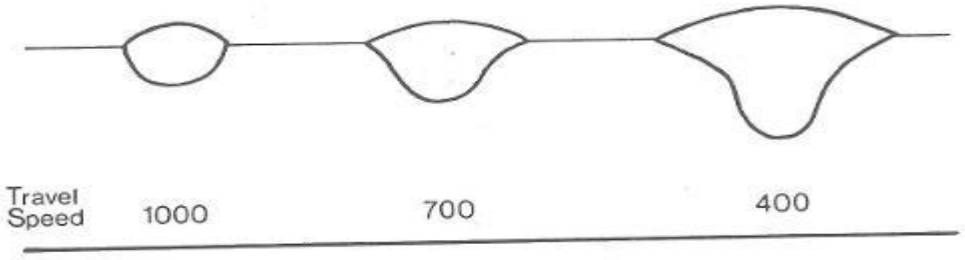

Figure 1.10 Effect of travel speed on bead shape [12]

Stick-out length:- The stick-out of the wire is the distance from the contact tip to the surface of the workpiece. In the present study it is taken as the electrode extension from the tip of nozzle. Figure 1.11 shows the distance of stick-out length- S.

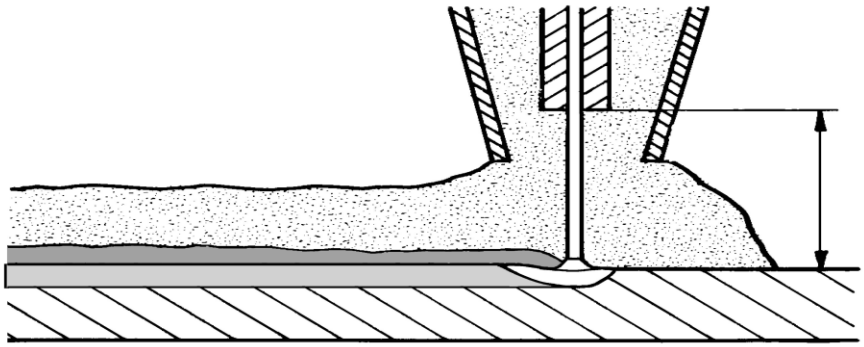

Figure 1.11 Stick-out distance [12]

It is the important parameter which affects the resistive heating of the tip of the wire electrode. If the stick-out is short, little heat will be developed in the wire and penetration will be greater. As the stick-out length is increased, so the temperature of the wire increases and penetration is reduced, while the rate of deposition is increased. It is desirable to be able to adjust the flux depth, depending on the amount of molten metal in the bead.

Wire angle:- The angle between the filler wire and the workpiece determines the position of the weld, its appearance and its penetration. There are three types of wire angle: backhand, vertical and forehand. Table 1.7 depicts the effect of wire angle on weld penetration and width.

Table 1.7 Effect of wire angle on weld penetration and width

Electrode angle	Backhand	Vertical	Forehand
Penetration	High	Normal	Low
Weld convexity	Narrow (high)	Normal	Wide (low)
Tendency to undercutting	High	Normal	Slight

In the present work vertical wire angle of electrode is taken. Vertical filler wire angle is most commonly used, but when tandem and multi-wire systems are used both forehand and backhand wire angles are used in order to achieve the required welding performance.

1.3 CARBON STEEL

Carbon steel also called plain carbon steel is the metal alloy which is made up of the mainly two components iron and carbon. In the carbon steel carbon is the main interstitial alloying constituent which varies in the range of 0.12 to 2.0%. Steel (sometimes C is less than 0.12%) is considered to be carbon steel when no minimum content is specified or required for chromium, cobalt, molybdenum, nickel, niobium, titanium, tungsten, vanadium or zirconium,

or any other element to be added to obtain a desired alloying effect when the specified minimum for copper does not exceed 0.40%; or when the maximum content specified for any of the following elements does not exceed the percentages noted: manganese 1.65, silicon 0.60, copper 0.60. When the carbon percentage increases then steel becomes harder and stronger after heat treating. Mild steel is also a type of carbon steel.

1.3.1 CLASSIFICATION OF CARBON STEEL

There are four types of carbon steel based on the amount of carbon percentage in the alloy: low carbon steel, medium carbon steel, high carbon steel and very high carbon steel. Lower carbon steels are softer and more easily formed, and steels with higher carbon content are harder and stronger, but less ductile, and they become more difficult to machine and weld. Below are the properties of the grades of carbon steel:

a) Low carbon steel (Mild steel):- It contains 0.05%-0.25% carbon and up to 0.4% manganese. It is also known as mild steel; it is a low-cost material that is easy to shape. While not as hard as higher-carbon steels, carburizing can increase its surface hardness.

b) Medium carbon steel:- It has 0.29%-0.54% carbon, with 0.60%-1.65% manganese. Medium carbon steel is ductile and strong, with long wearing properties.

c) High carbon steel:- High carbon steel, having 0.55%-0.95% carbon, with 0.30%-0.90% manganese, is very strong and holds shape well, making it ideal for springs and wire.

d) Very high carbon steel:- This type of carbon steel has 0.96%-2.1% carbon. Its high carbon content makes it an extremely strong material. Due to its brittleness, this grade requires special handling.

However, in the literature, carbon steels are not always classified exactly in the same manner as mentioned here.

1.3.2 MILD STEEL

Mild steel is an iron alloy that contains less than 0.25% carbon. The term mild steel is sometimes referred to mean almost the same variety as low carbon steel. A little bit of variation in specifying or defining mild steel can be found in text books and literature. Mild steel is very reactive and will readily revert back to iron oxide (rust) in the presence of water, oxygen and ions. The readiness of steel to oxidize on exterior exposure means that it must be adequately protected from the elements in order to meet and exceed its design life. Mild steel is the most common form of steel as its price is relatively low while it provides material properties that are acceptable for many applications.

1.4 STAINLESS STEEL

Stainless steel is an alloy of iron with a minimum of 10.5% chromium and a small amount of carbon, plus some other elements in certain grades. Chromium produces a thin layer of oxide on the surface of the steel known as the 'passive layer'. This prevents any further corrosion of the surface. Increasing the amount of chromium gives an increased resistance to corrosion.

Stainless steel also contains varying amounts of carbon, silicon and manganese. Other elements such as nickel and molybdenum may be added to impart other useful properties such as enhanced formability, strength and increased corrosion resistance. Stainless steel does not readily corrode, rust or stain with water as ordinary steel does. However, it is not fully stain-proof in low-oxygen, high-salinity, or poor air-circulation environments. For greater hardness and strength, more carbon is added. With proper heat treatment, these steels are used for such products as razor blades, cutlery and tools and as many other household and engineering components. Welding of stainless steel to mild steel is the area of work in the present investigation.

1.4.1 CLASSIFICATION OF STAINLESS STEELS

There are many number of different systems currently used to designate stainless steel. Most commonly, the AISI system, used in USA is adopted. In the AISI system, austenitic grades are in the 200 and 300 series, martensitic and ferritic are in the 400 series. Figure 1.12 illustrates the families of stainless steels.

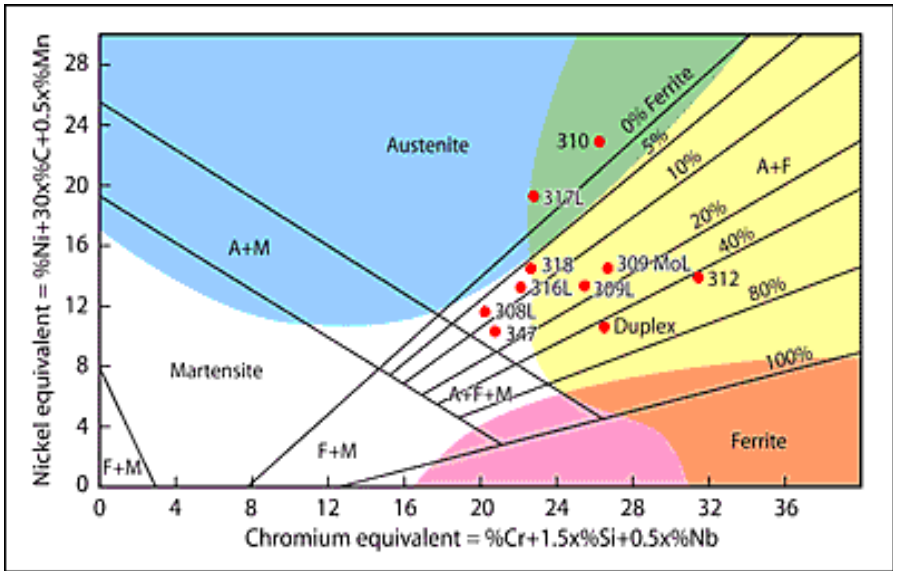

Figure 1.12 Families of stainless steel [13]

a) Austenitic stainless steels:- It is very common and most widely used type of stainless steels having carbon percentage upto 0.15%. It has FCC crystal structure and called γ-iron. They have an austenitic crystalline structure and contain a maximum of 0.15% carbon, a minimum of 16%-26% chromium and sufficient nickel (10-20%) and/or manganese to retain an austenitic structure at all temperatures from the cryogenic region to the melting point of the alloy. Austenite steels make up over 70% of total stainless steel production.

They have two series AISI 300-series and AISI 200-series. AISI 300-series include 301, 302, 303 Se, 304, 304 L, 304 LN, 308, 309, 310, 316, 316 L, 316 LN, 321, 330, 347 etc, and contain chromium (16-26%) and nickel (10-22%). AISI 304 austenitic stainless steel is most widely used and also known as 18/8 for its composition of 18% chromium and 8% nickel. The second most common austenite steel is 316 grade which is also called marine grade stainless steel.

AISI 200-series include 202, 201, 205 etc and they contain chromium, nickel and manganese (5-18%). Decreasing nickel content and increasing manganese results in weak corrosion resistance. Austenitic steel AISI 201 grade is hardenable through cold working. AISI 202 type steel is a general purpose stainless steel.

b) Ferritic stainless steels:- These steels are nonhardenable iron-chromium alloys having BCC crystal structure. Ferritic stainless steels have better engineering properties and usually less expensive than austenitic grades, but have reduced corrosion resistance, because of the lower chromium and nickel content. They are available in AISI 400-series which include 405, 409, 430, 439, 442, 446 etc types. AISI 409 is the most commonly used ferritic stainless steel. They contain upto 0.20% carbon and 11-18% Cr and small amount of ferritic stabilizers, such as aluminium, niobium and titanium. These stabilizers are ferritic at all temperatures, do not transform to austenite and therefore, are not hardenable by heat treatment. Ferritic stainless steel contains 10.5%-27% chromium and very little nickel, if any, but some types can contain lead. Most compositions include molybdenum; some, aluminium or titanium. Common ferritic grades include 18Cr-2Mo, 26Cr-1Mo, 29Cr-4Mo, and 29Cr-4Mo-2Ni.

c) Martensitic stainless steel:- These types of steels have similar in composition to the ferritic steel group but contain higher carbon and lower chromium to permit hardening by heat treatment. They have not as corrosion resistant as the other two classes but are extremely strong and tough and can be hardened by heat treatment. Martensitic stainless steel contains chromium (12–14%), molybdenum (0.2–1%), nickel (less than 2%), and carbon (about 0.1–1%) (giving it more hardness but making the material a bit more brittle). It is quenched and

magnetic. This group includes types AISI 403, 410, 414, 416, 420, 422, 431 and 440. They transform to austenite phase on heating and, therefore, can be hardened by formation of martensite on rapid quenching.

d) Duplex stainless steels:- These steels contain the mixed microstructure of austenite and ferrite. Duplex stainless steel is used to produce in equal proportion of austenite and ferrite, although in commercial alloys the ratio may be 40/60. They solidify as 100% ferrite, but about half of the ferrite transforms to austenite during cooling through temperatures above approx. 1900°F (1040°C). Duplex stainless steels have roughly twice the strength compared to austenitic stainless steels and also improved resistance to localized corrosion, particularly pitting, crevice corrosion and stress corrosion cracking. They are characterized by high chromium (19–32%) and molybdenum (up to 5%) and lower nickel contents than austenitic stainless steels. Duplex grades are characterized into groups based on their alloy content and corrosion resistance. Lean duplex refers to grades such as UNS S32101, S32304 etc. Standard duplex is 22% chromium with UNS S31803/S32205 known as 2205; it is the most widely used variety. Super duplex grades have 25% chromium or more and some common examples are S32760, S32750 and S32550 (Ferralium). Hyper duplex refers to duplex grades with a pitting resistance equivalent (PRE) > 48 and at the moment only UNS S32707 and S33207 are available [14].

1.4.2 WELDING OF FERRITIC STAINLESS STEEL

Most of the stainless steels are considered to be of good weldability and may be welded by several welding processes including the arc welding processes, resistance welding, electron and laser beam welding, friction welding and brazing. For any of these processes, joint surfaces and any filler metal must be clean.

The ferritic stainless steels contain 10.5 to 30% Cr, up to 0.20% C and sometimes ferrite promoters Al, Nb (Cb), Ti and Mo. They are ferritic at all temperatures, do not transform to austenite and therefore, are not hardenable by heat treatment. This group includes the more common types AISI 405, 409, 430, 442 and 446. To weld ferritic stainless steel is possible, although they are less fool proof than the austenites. The lack of Ni increases the risk of grain growth and the formation of unwanted phases as a result of the heating. Such effects may cause brittleness and reduced corrosion resistance, and therefore, one has to be more careful when welding the ferrites as compared with the austenites, in particular with regard to the heat input. The thicker the steel, the more important it is to keep the heat input

low in order to avoid unwanted side effects.

Now a days ferritic steels are much easier to weld due to the fact that the higher alloyed ferrites are "stabilized" by adding titanium (Ti) and/or niobium (Nb), both of which stabilize against grain growth during welding. It is essential to employ stabilizers in sufficient quantities, e.g. Ti and/or Nb, both strong carbide formers and blocking grain growth. To weld the ferritic stainless steels, filler metals should be used which match or exceed the Cr level of the base alloy. Austenitic types AISI 309 and 312 may be used for dissimilar joints. To minimize grain growth, weld heat input should be minimized, preheat should be limited to 300-450°F and used only for the higher carbon ferritic stainless steels (e.g., AISI 430, 434, 442 and 446). Many of the highly alloyed ferritic stainless steels are only available in sheet and tube forms and are usually welded by GTA without filler metal.

In the present work one of the base materials used for dissimilar welding is ferritic stainless steel AISI 409.

1.5 TESTING AND INSPECTION OF WELD

Quality control is used throughout the welding industry to monitor the quality of the items produced. Inspection of the weld is the throughout observation of the products to ensure the desired qualities. Testing on the other hand is the physical performance of operations to determine quantitative measurement of mechanical or other properties. Inspections are carried out in three stages i.e. before welding, during welding and after the welding is over. Before welding, proper specifications of base metals, electrodes, filler materials, shielding gases etc. should be ensured. During welding proper cleaning and clamping of base metals etc. are necessary. After welding, various destructive and nondestructive tests are carried out. For detail analysis, microstructural study of welded joint is required. In the present study, some nondestructive tests, destructive tests and microstructural study have been done. Tests must be made to qualify the processes and the operators. Thus, testing and inspection determine whether or not the quality standards of materials and workmanship are being met. Welds are often tested for soundness, strength and toughness by mechanical tests.

Testing and inspection of welds can be grouped into two basic categories, namely;

- Non-destructive testing
- Destructive testing

1.5.1 NON-DESTRUCTIVE TESTING

Inspections and tests of a weld that do not destroy any portion of the completed weld are called non-destructive testing (NDT). Five basic methods are commonly used to examine finished welds: visual, liquid penetrant, magnetic particle, ultrasonic and radiographic (X-ray). All the non-destructive tests have good potential to check the flaw in weldment. In the present work visual inspection test has been conducted.

Visual inspection:- A visual inspection (VT) is one of the most important methods of inspection and is widely used for acceptance of welds. VT is also used to identify bad welds before other more expensive or time consuming forms of inspection are performed. Visual inspection is easy to apply, quick, and relatively inexpensive. Visual testing equipment includes rulers, fillet weld gauges, squares, magnifying glasses, and reference weld samples. It is an effective quality control method that will ensure procedure conformity and will catch errors at early stages. Visual inspection is the best buy in NDE, but it must take place prior to, during and after welding.

1.5.2 DESTRUCTIVE TESTING

Inspections and tests that destroy the completed weld, or samples of the completed weld, are called destructive tests. Destructive tests are used for welder qualification and certification, as well as welding procedure qualifications. In large production runs, destructive tests are often made by pulling apart sample units. It is often less expensive to scrap a part to make a destructive quality test than to test the parts using more expensive non-destructive tests. Destructive tests as applied to welds are: tensile test, bend test, impact test, hardness test, nick-break test, etch test, fatigue test etc.

In the present work tensile test, hardness test and microstructure studies of the weld specimens have been carried out.

Tensile test:- Tensile tests are used to compare the weldment to the base metal mechanical properties like ultimate tensile strength, yield strength etc and specification requirements. The weldment is sliced into coupons, and then each end of the coupon is pulled in opposite directions until the coupon fails (breaks). Tensile test gives an indication about the tensile strength and ductility of a weld.

Tensile properties of the weld joints namely yield and ultimate strength and ductility (%age elongation, %age reduction in area) can be obtained either in ambient condition or in special environment (low temperature, high temperature, corrosion etc.) depending upon the

requirement of the application using tensile test which is usually conducted at constant strain rate (i.e. 0.001 mm/s). Tensile properties of the weld joint are obtained in two ways: a) taking specimen from transverse direction of weld joint consisting base metal HAZ-weld metal-HAZ-base metal and b) all weld metal specimen. Tensile test results must be supported by respective engineering stress and strain diagram indicating modulus of elasticity, elongation at fracture, yield and ultimate strength.

1.6 OPTIMIZATION AND PREDICTION

Making use of prediction is a crucial, but under-explored area in respect of dissimilar welding of submerged arc welding. Process optimization is also relevant: however a suitable design of experiments is to be made first. There are many numbers of techniques of design of experiments available for use such as Taguchi's orthogonal array, response surface design, full factorial design etc. Response surface analysis of the output parameters is carried out for response prediction. There are several single and multivariable optimization techniques available for use such as principle component analysis, genetic algorithm, Grey-Taguchi analysis, simulated annealing, teaching-learning based optimization etc. Details of the optimization techniques including design of experiments are discussed in chapter 2.

1.7 DISSIMILAR WELDING

Joining dissimilar materials is often more difficult than joining the same materials or alloys with minor differences in composition; however, many dissimilar materials can be joined successfully with the appropriate joining process and specialized procedures. A number of factors must be taken into consideration when designing a dissimilar material joint, including: joint design and material thicknesses, differences in melting temperature, thermal expansion-contraction mismatch during joining and in service, formation of brittle intermetallic compounds during joining which may lead to brittle joints, heating and cooling rate effects on the microstructure of the joint (which may affect the strength), precision control of heat input and needs for special filler materials during joining. Successful dissimilar metal joints are often vital for the technical performance and commercial success of a design, frequently requiring proprietary development work etc.

The most common and important example of dissimilar metal joining is that of welding stainless steel to carbon manganese steel or to low alloy steel. The most common application is attachments or transitions. The problem of making welds between dissimilar metals relates to the transition zone between the metals and the intermetallic compounds formed in this

transition zone. Welding of dissimilar metals involves different types of metals, with distinct chemical and microstructural composition. The two dissimilar metals involved in welding process have different mechanical properties and microstructures which in turn may affect selection of welding parameters like weld current, hold time, weld force etc. The difference in chemical composition of metals may also be due to several factors such as age hardening, oxidation etc. The study of mechanical properties is important because welded structure may be installed at highly sensitive and risky place. Problem of formation of inter-metallic compound may arise which affect the weld quality. For the fusion welding processes it is necessary to investigate the phase diagram of the two metals involved. If there is mutual solubility of the two metals, the dissimilar joints can be made more successfully though not easily. If there is little or no solubility between the two metals to be joined the weld joint will not be successful and the intermetallic compounds that are formed, between the dissimilar metals, must be investigated to determine their crack sensitivity, ductility, susceptibility to corrosion etc. The microstructure of this intermetallic compound is important [15].

1.8 LITERATURE REVIEW

In the context of the present work, a literature survey is made. This survey covers submerged arc welding, welding of stainless steels, performance testing of welds, process optimization, mathematical modeling, statistical analysis of experimental data, welding of dissimilar metals, microstructures in dissimilar welding and relevant aspects. In the process of writing the earlier sections, some references [1-15] have already been cited. Though the present work is concerned with welding of ferritic stainless steel to mild steel by submerged arc welding, literature survey also includes welding of ferritic stainless steel to ferritic stainless steel, weld microstructure in such welding, joining of various combinations of materials, process optimization methods and techniques applied to both similar and dissimilar welding not only by submerged arc welding only but also by other welding processes. Microstructural aspects, parametric studies, mathematical models in respect of both similar and dissimilar welding of several combinations have also been addressed in this literature survey.

Lakshminarayanan[16] investigated the effect of autogenous arc welding processes on tensile and impact properties of ferritic stainless steel conformed to AISI 409M grade. Tensile and impact properties, microhardness, microstructure, and fracture surface morphology of continuous current gas tungsten arc welding (CCGTAW), pulsed current gas tungsten arc

welding (PCGTAW), and plasma arc welding (PAW) joints were evaluated and the results were compared.

Hong et al.[17] investigated the characterization of corrosion resistance in a ferritic stainless steel stabilized with Ti addition. The author mentioned that ferrite stainless steel, with cheap prices and low thermal expansion coefficients due to no addition of nickel, was excellent in corrosion properties and high temperature corrosion resistance compared with cheap prices, widely used in automobile industry. 3 kinds of welding wire, where adjusted Ti contents of a stabilizing element were added to AISI 436 stainless steel, to perform FCAW (Flux Cored Arc Welding) and thus to evaluate microstructures and corrosive properties. The specimen having no Ti additive was transformed into ferrite + martensite structure, while the specimen having Ti additives into fully ferrite structure.

Reddy et al.[18] attempted to weld ferritic stainless steel by electron beam welding(EBW). Single-pass autogeneous welds, free of volumetric defects, were produced at a welding speed of 1000 mm/min. They concluded that the coarse ferritic grains in the base metal were changed into equi-axed axial grains and columnar grains as a result of characteristic rapid solidification of electron beam welds. Tensile testing indicated overmatching of the weld metal relative to the base metal. The joints exhibited acceptable impact toughness and bend strength properties.

Mohandas et al.[19] made a comparative evaluation of gas tungsten and shielded metal arc welds of AISI 430 ferritic stainless steel. In the square butt joint titanium was added as a powder obtained from crushed titanium sponge for grain refining, also copper was added as a foil for austenite stabilizer. A mixture of 2% O_2 and 98% argon was used. From the investigation it was concluded that gas tungsten arc welds exhibiting equi-axed grain morphology had greater tensile and yield strength, compared to shielded metal arc welds.

Shahid et al.[20] carried out mechanical and microstructural analyses of dissimilar metal welds of stainless steel to mild steel by autogenous processes.

Mishra et al.[21] studied dissimilar joints of mild steel and stainless steel by TIG welding and MIG welding. The percentage dilutions of joints were calculated and tensile strength of dissimilar metal joints were investigated. The results were compared for different joints made by TIG and MIG welding processes and it was observed that TIG welded dissimilar metal joints had better physical properties than MIG welded joints. It might be because of less porosity in dissimilar metal welds during TIG welding and carbon precipitation which came out due to welding being also less. The low percentage of free

carbon allowed the product (welded stainless steel with mild steel) better corrosion resistivity, ductility and strength.

Taban et al.[22] investigated the characteristics of dissimilar welds between ferritic stainless steel modified 12% Cr and carbon steel S355. In this research, 20-mm thick, modified X_2CrNi_{12} ferritic stainless steel conforming in composition to Grades UNS S41003 in ASTM A240 and 1.4003 in EN 10088-2 and EN 10028-7 with a carbon content below 0.015% was welded to non-alloy S355 steel by means of shielded metal arc (SMA) and submerged arc (SA) welding processes using AISI 309 type of filler metal. Microstructural examinations were carried out including macro and micrographs, hardness and ferrite content measurements, and grain size analysis.

Rossini et al.[23] carried out investigation on dissimilar laser welding of advanced high strength steel sheets for the automotive industry. To support the use of advanced high strength steels in car body design and fabrication, an investigation was carried out on dissimilar butt laser welding between Twinning Induced Plasticity (TWIP) steels, Dual Phase (DP) steels, hot stamping boron (22MnB5) steel and Transformation Induced Plasticity (TRIP) steels. The base materials and the weldments were fully characterized by means of metallography, microhardness, and tensile tests. The dissimilar joints between the DP, 22MnB5 and TRIP steels exhibit good resistance properties.

Akella et al.[24] made a welding simulation of dissimilar materials SS304 and copper. In this work a finite element model for dissimilar welding of 304 steel & copper is done. A simple 3D sequential thermal followed by structural analysis is done using ANSYS software. Temperature dependent thermal and structural properties were used. This study will provide an insight to the designer for obtaining feasibility of providing such a weld and for further fatigue life studies.

Behm et al.[25] studied on laser beam welding of dissimilar material combinations of austenitic high manganese (FeMn) and ferrite steels. Particularly dissimilar material combination of FeMn and ferrite steel are in the centre of interest for industrial applications. This study revealed that metallurgical properties of dissimilar welding seams could be influenced considerably by laser beam welding, resulting in a change of the mechanical properties of the seam which was practicable without using filler material.

Kumar[26] through their research paper, presented friction stir welding of dissimilar materials with completely different base metals. Weld imperfection such as intermetallic compounds and cracking, which were not likely to occur during welding of dissimilar alloys with similar chemical composition, were frequently observed in welding of dissimilar

materials such as Al to Mg, Al to steel. Sound welds between dissimilar materials could be achieved with proper process design. In this work, influences of welding conditions, such as welding parameters, placement of work-piece, placement of welding tool with respect to the interface of work-pieces, on weld integrity, microstructure, and mechanical properties of dissimilar welds had been explored.

Chen et al.[27] made dissimilar joining of Ti_3Al-based alloy to Ni-based super alloy by arc welding technology using gradient filler alloys. In this study, Ti–Al–Nb, Ti–Ni–Nb and Ni–Cr–Nb system alloys were designed and incorporated in order to construct a gradient structure at the surface of the joined Ti_3Al base material. And the Ti_3Al based alloy and Ni based super alloy were successfully joined together using gas tungsten arc (GTA) welding technology. The microstructure evolution, mechanical properties and fractured behaviours of the joints were investigated.

Sun et al.[28] investigated on laser welding of butt joints of Al/steel dissimilar materials. Dissimilar metals of AA6013 aluminum alloy and Q235 low carbon steel of 2.5 mm thickness were butt joined using a 10 kW fiber laser welding system with ER4043 filler metal. The study indicated that it was feasible to join aluminum alloy to steel by butt joints when zinc layer was hot-dip galvanized at the steel's groove face in advance, and better weld appearance could be obtained at appropriate welding parameters. The joints had dual characteristics of a welding joint on the aluminum side and a brazing joint on the steel side.

Some other researchers also highlighted useful aspects of dissimilar welding [29-38].

McPherson et al.[39] performed submerged arc welding of ferritic stainless steel and duplex stainless steel. A number of welds were produced using a Y preparation and a V preparation with one pass from each side and using a square edge preparation with one pass only. The basicity index of the flux used in all the cases was 2.3. The use of the higher alloyed 317L consumable counteracted the dilution effects from the parent plates and as a result, acceptable strength level had been maintained.

Patel and Gohil[40] presented the comprehensive research review on effect of welding parameters on quality of welds. Best quality and cost effective welds could be achieved by proper understanding the weld metal properties and the influence of welding parameters. The joint quality could be assessed in terms of properties such as weld-bead geometry, mechanical properties and distortion.

Moshi et al.[41] made a review paper on factors influencing submerged arc welding on stainless steel. In this paper, submerged arc welding process and the effect of process parameters on quality of welding had been reviewed from various researches and the authors

also discussed in detail about submerged arc welding and its inherent benefits such as higher metal deposition rate, good strength of the joint and good surface appearance. The authors mentioned that this welding process was often preferred because it offered high production rate, high melting efficiency and ease of automation. The review is concerned with factors influencing the quality of weld in stainless steel by submerged arc welding; the review may be very helpful for predicting the best welding conditions for stainless steel.

Chandel et al.[42] through their research paper, presented theoretical predictions of the effect of current, electrode polarity, electrode diameter and electrode extension on the melting rate, bead height, bead width and weld penetration, in submerged arc welding.

Pandey et al.[43] showed in their work that welding current and voltage had appreciable influence on element transfer, as well as on weld composition. Weldment properties such as strength, toughness and solidification cracking behaviour were affected by chemical composition of the weld. They investigated the influence of submerged arc welding (SAW) parameters and flux basicity index on the weld chemistry and transfer of elements like manganese, silicon, carbon and sulphur.

Ghosh et al.[44] used graphical technique to predict submerged arc welding yield parameters and studied the effect of main factors, viz. current, wire feed rate, travel speed and stick-out and the interactions among the main factors on the welding bead parameters. The interactions depicted the level of confounded character of the main factors with respect to the significant yield parameters of the process.

Bang et al.[45] investigated the effects of flux composition on the chemical composition, tensile strength, and impact toughness of weld metal in submerged arc welding. Depending on the wire/flux combination, different chemical compositions of weld metals were obtained. The Pcm index calculated from the chemical composition of weld metals, accordingly, varied from 0.153 to 0.196 depending on the combination. The tensile strength of weld metal increased almost linearly with an increase in the Pcm index.

Nathan et al.[46] studied the effect of welding processes on mechanical and microstructural characteristics of high strength low alloy naval grade steel joints. Naval grade high strength low alloy (HSLA) steels can be easily welded by all types of fusion welding processes. However, fusion welding of these steels leads to the problems such as cold cracking, residual stress, distortion and fatigue damage. These problems can be eliminated by solid state welding process such as friction stir welding (FSW). In this investigation, a comparative evaluation of mechanical (tensile, impact, hardness) properties and microstructural features of shielded metal arc(SMA), gas metal arc(GMA) and friction stir

welded (FSW) naval grade HSLA steel joints was carried out. It was found that the use of FSW process eliminated the problems related to fusion welding processes and also resulted in the superior mechanical properties compared to GMA and SMA welded joints.

Kanjilal et al.[47] developed a prediction model for submerged arc weld metal chemical composition in terms of flux ingredients with the help of statistical experiments for mixture. Experiments were performed to obtain bead-on-plate weld deposits at some specific process parameters (current, voltage, speed, electrode extension) using CaO_2-MgOCaF_2-Al_2O_3 flux system. While studying the combined effect of flux and welding parameters on chemical composition and mechanical properties of submerged arc weld metal, the authors concluded that individual flux ingredients and welding parameters had individual as well as interaction effects on responses.

Chattopadhyaya et al.[48] addressed the issue associated with the uncertainties involved with the heat affected zone (HAZ) in and around the weldment produced by SAW process. They assessed the heat affected zone of submerged arc welding of structural steel plates through the analysis of the grain structure by means of digital image processing techniques. It was concluded that the grains were predominantly of smaller variety and the counts for larger grain were almost negligible.

Shukla and Pandey[49] studied the influence of the process parameters on the weld deposit area and microstructure using bead on plate submerged arc welding process. It was found that the weld deposit area was affected by weld parameters like welding wire feed rate, welding speed, open circuit voltage, and contact-tube to-work distance. The effect of welding current on weld deposit area had been studied independently by making a separate model for welding current. This was due to the fact that it was not possible to control the current in welding in semi-automatic processes unless it was a constant current welding process. Since the open circuit voltage was also one of the parameters, therefore, controlled variation of both the parameters was not possible. The adequacy of the model was tested by analysis of variance technique and the significance of the coefficient was tested by student's 't' test.

Chandel and Malik[50] studied the effect of welding parameters on the wire feed speed (W.F.S.) for the submerged arc welding process. The results had shown that the welding current, electrode polarity, electrode wire diameter and electrode stick-out influenced the wire feed speed. The arc voltage had not any influence on the W.F.S.

Pandey et al.[51] investigated the influence of submerged arc welding (SAW) parameters and flux basicity index on the weld chemistry and transfer of elements manganese, silicon, carbon and sulphur. Five fluxes and different values of the welding parameters were

used for study. The welds were produced as a bead on a mild steel plate. The weld-metal composition showed, in general, gains of silicon and loss of carbon, manganese and sulphur elements. The results had shown that welding current and voltage had an appreciable influence on element transfer, as well as on weld composition. Weldment's properties such as strength, toughness and solidification cracking behaviour were affected by chemical composition.

Lakshminarayanan et al.[52] studied the evaluation of microstructure and mechanical properties of laser beam welded AISI 409 grade ferritic stainless steel. The joints were subjected to optical microscope, scanning electron fractograph, microhardness, traverse and longitudinal tensile bead and charpy impact toughness testing. The coarse ferrite grains in the base metal were changed into dendritic grains as a result of rapid solidification of laser beam welds. It was also reported that the joint exhibited acceptable impact toughness and bend strength properties.

Kacar and Baylan[53] investigated the microstructure and property relationships in dissimilar welds between martensitic and austenitic stainless steels. Both austenitic and duplex stainless steel electrodes were used to join this combination. Defect free welds were made with each welding consumable. It was found that the tensile strength of weldment, which was produced by duplex electrode (E2209-17), was slightly lower than that of austenitic electrode (E308L-16). This investigation had shown that both filler metals could be used to join austenitic stainless steel to the martensitic stainless steel.

Belyakov et al.[54] carried out microstructure evolution in ferritic stainless steels during large strain deformation. Deformation microstructures were studied in ferritic stainless steels during cold bar rolling and swaging to total true strains about 7. Two steels, i.e, Fe-22Cr-3Ni and Fe-18Cr-7Ni with coarse-grained ferritic and fine-grained martensitic initial microstructures, respectively, were selected as starting materials. Microstructure evolution in the both steels was characterized by the development of highly elongated (sub) grains aligned along the rolling/swaging axis. The hardness of the Fe-22Cr-3Ni steel increased with cold working within the studied strain range, while that of the Fe-18Cr-7Ni approached a saturation after fast work hardening at strains below 3, leading to an apparent steady-state behaviour.

Yajiang Li et al.[55] studied microstructure and fracture morphology in the welding zone of Cr18Mo2 ferritic stainless steel. Microstructure, precipitates and fracture morphology in the weld metal and the heat affected zone (HAZ) of Cr18Mo2 ferritic stainless steel had been studied by means of metalloscope, SEM, TEM and X-ray diffractometer. Experimental

results indicated that crystalline grain coarsening in HAZ was one of the reasons resulting in the embrittlement fracture in the welding zone of the ferritic stainless steel. Some precipitates (TiC, TiN and Cr2N) in the steel promoted production and development of the brittle cracks. In practical applications, the welding heat input should be as small as possible to prevent embrittlement caused by HAZ grain coarsening.

Gharibshahiyan et al.[56] described the effect of microstructure on hardness and toughness of low carbon welded steel using inert gas welding. The heat affected zone (HAZ), had a great influence on the properties of welded joints since it could alter the microstructure and residual stresses. In this work, the effect of welding parameters and heat input on the HAZ and grain growth had been investigated. The role of grain size on hardness and toughness of low carbon steel had also been studied. It was observed that, at high heat input, coarse grains appeared in the HAZ which resulted in lower hardness values in this zone.

Boumerzoug et al.[57] did the investigation on the effect of welding on microstructure and mechanical properties of an industrial low carbon steel. In this work, the effect of arc welding on microstructures and mechanical properties of industrial low carbon steel (0.19 wt. % C) was studied. This steel is used for making gas storage cylinders. In order to realize the objective, optical microscopy, EBSD, X-ray diffraction, and hardness tests were used. Different zones and some phases were identified. New microstructural phenomena were observed by using EBSD technique.

Kotus et al.[58] investigated the influence of welding method on microstructural creation of welded joints. This paper is focused on the analysis of the influence of welding technology on the microstructure production and quality of the welded joint. Steel of class STN 41 1375 was selected for the experiment, the samples were welded by arc welding including two methods: a manual one by coated electrode and gas metal arc welding method. Macro and microstructural analyses of the experimental welded joints confirmed that the welding parameters affected the welded joint structure in terms of the grain size and character of the structural phase.

Joarder et al.[59] made an extensive study on the microstructure of weld metal and heat affected zone of plain carbon steel plate in SAW. They noticed that depending on the number, size and distribution of inclusions, the weld metal microstructure varied. They also noted that a limited number of large inclusions helped in the formation of acicular ferrite, whereas a large number of smaller inclusions favoured grain boundary ferrite formation.

Rudrapati et al.[60] conducted experiment as per L9 orthogonal array of Taguchi method. Grey based Taguchi method had been used to optimize the grinding parameters to

minimize surface roughness parameters Ra and Rq simultaneously. The analysis of signal to noise ratio had been applied to investigate the effects of grinding parameters and optimize them.

Ene and Scutelnicu[61] had carried out experiments for optimizing the process in order to get the best quality and productivity results. They carried out experiments by using the hybrid method, which combined the Taguchi approach with the Grey Relational Analysis. They were able to provide answers to multi criteria optimization of an industrial process. The aim of the investigation was to identify the optimal process control parameters, able to produce the desired and predefined characteristics of the submerged arc weld bead geometry.

Chandel and Seow[62] presented the mathematical prediction of the effect of current, polarity used, electrode diameter and its extension on the melting rate, bead height, bead width and weld penetration in SAW. They concluded that for a given current (heat input) the melting rate could be increased by using electrode negative polarity, longer electrode extension, and smaller diameter electrodes. There were two other ways to increase the deposition rate without increasing the heat input; these were: (i) using a twin-arc mode and (ii) adding metal powders, as per their findings.

Tarng et al.[63] used Fuzzy Logic in the Taguchi method to optimize the submerged arc welding process parameter with multiple performance characteristics. An orthogonal array, signal to noise ratio, multi response performance index and analysis of variance had been employed. The process parameters namely arc current, arc voltage, welding speed, electrode extrusion and pre-heat temperature had been optimized with the deposition rate and the dilution.

Reddy et al.[64] carried out the application of factorial design approach for optimizing four submerged arc welding parameters viz. arc voltage, welding speed and nozzle to plate distance. Governing mathematical models were developed for the submerged arc welding of 6mm-thick MS plates using 3.15-mm diameter MS electrodes. The main and interaction effects of the process control variables on important bead geometry parameters were determined quantitatively and their influence was presented. Design Expert 8 software had been used to develop a set of solutions with their desirability values, these solutions were used to get the optimized results.

Bamankar and Sawant[65] carried out research on controlling metal transfer modes in SAW process. Mode of metal transfer may influence quality of weld. Quality has now become an important issue in today's manufacturing world. Experiments were conducted using submerged arc process parameters viz. welding current, arc voltage and welding speed

(Trolley speed) on mild steel of 12 mm thickness, to study the effect of these parameters on penetration depth. The experiments were designed using Taguchi method (with Taguchi L9 orthogonal array) considering three factors and three levels.

Mallaiah et al.[66] examined the influence of grain refining elements on mechanical properties of AISI 430 ferritic stainless steel weldments by Taguchi approach. Based on Taguchi orthogonal array with regression equations, the authors developed an equation for predicting the mechanical properties of ferritic stainless steel welds within range of grain refining elements. The authors also correlated the mechanical properties of AISI 430 ferritic stainless steel and austenite content with microstructure and fracture feature.

Kumanan et al.[67] used Taguchi technique and regression analysis to determine the optimal process parameters for submerged arc welding (SAW). The planned experiments were conducted in the semi-automatic submerged arc welding machine and the signal-to-noise ratios were computed to determine the optimum parameters. The percentage contribution of each factor was validated by analysis of variance (ANOVA) technique. Multiple regression analysis (MRA) was conducted using statistical package for social science (SPSS) software and the mathematical model was built to predict the bead geometry for any given welding conditions.

Karaoglu et al.[68] derived a mathematical model while carrying out sensitivity analysis of parameters and fine tuning requirements of the weld bead geometry. Changeable process parameters such as welding current, welding voltage and welding speed were used as design variables. The objective function was formed using width, height and penetration of the weld bead. Experimental part of the study was based on three level factorial designs of three process parameters. Effects of all three design parameters on the bead width and bead height showed that even small changes in these parameters played an important role in the quality of weld geometry. The results also revealed that the penetration was almost non-sensitive to the variations in voltage and speed.

Dhas et al.[69] optimized the parameters of submerged arc weld using non-conventional techniques. Data were collected as per Taguchi's design of experiments and regression analysis was carried out to establish input–output relationship of the process. By this relationship, an attempt was made to minimize weld bead width, a good indicator of bead geometry, using optimization procedures based on the genetic algorithm (GA) and particle swarm optimization (PSO) algorithm to determine optimal weld parameters. The optimized values obtained from these techniques were compared with experimental results. PSO model

gave better results than GA model. Also PSO converged to the global optimum solution at the faster rate.

Tarng et al.[70] used grey-based Taguchi method for optimization of the submerged arc welding (SAW) process parameters in hard-facing with considerations of multiple weld qualities. The grey relational analysis was adopted to solve the SAW process with multiple weld qualities. A grey relational grade obtained from the grey relational analysis was used as the performance characteristic in the Taguchi method. Then, optimal process parameters were determined by using the parameter design proposed by the Taguchi method. Experimental results had shown that optimal SAW process parameters in hard facing could be determined effectively so as to improve multiple weld qualities through this new approach.

Sallehuddin et al[71] used grey relational analysis (GRA) to determine the most influential factors that affected the grain crop yield in China from 1990 to 2002. GRA was employed to search for grey relational grade (GRG), which was used to describe the relationships among the factors and to determine the important factors that significantly influenced some defined objectives.

Ghosh et al.[72] attempted to uncover an important area of quality engineering applied to a critical manufacturing process through design of experiments for optimization of submerged arc welding process. The submerged arc welding process was selected because of the complex set of variables involved in the process as well as its significant applications in the manufacturing of critical equipment. The main objectives of the study was the identification of main factors, viz. current, wire feed rate, travel speed and stick out, there way of affecting the welding bead parameters, influence of the interactions among the main factors and finally to determine the optimum settings of the main factors.

Some other resources [73-80] have also helped by providing useful information during the present study; some of these are mentioned in subsequent chapters.

1.9 SCOPE AND OBJECTIVE OF THE PRESENT WORK

The literature survey reveals that welding of dissimilar materials is a challenging area of research, important as well. More investigations are needed covering various aspects relevant to dissimilar welding.

Submerged arc welding (SAW) has become a very important welding process because of its ability to deposit large amounts of metal with high penetration. In recent years different new welding processes have come into use but still SAW is extensively used in industrial applications. Submerged arc welding is among the most widely used techniques in industrial

applications such as ship building, pressure vessels, nuclear power plants, windmill construction, container fabrications etc. It is quite prominent because of its inherent advantages of deep penetration, smooth bead and superior quality. It has been used for welding thicker materials but by controlling the input parameters it can be used for welding of thinner plates of thickness 5-8 mm as well. There are many numbers of publications available about the wide area of welding. But there remains the need of extensive research in various aspects including techniques, process control, process analysis, quality evaluation, process optimization etc., particularly in respect of dissimilar welding. Dissimilar welding is a challenging area of research and is now more and more in demand. There is thus the need of extensive research not only in the context of dissimilar welding which is already in demand, but also in the context of various combinations of the materials, which may or may not be in demand at present, but because of development of research in the field, will be very promising in the days to come. In this context, among various aspects of interest, some important ones are: selection of suitable technique of welding, selection of desirable or required combination of the dissimilar materials, determination of suitable levels of input parameters, process optimization and microstructural studies. Literature survey, indeed, indicates that investigations have been carried out on various aspects of submerged arc welding, many of which are in the context of welding of mild steel and stainless steel. One can also find from the literature survey that some work has indeed been done in the area of dissimilar welding but it is not enough. There are several aspects: one is the combination of the materials which has to be welded and the other aspect is the method of welding applied. Evaluation of the quality of the weld in terms of ultimate joint strength, microstructural characteristic, percentage elongation, hardness, HAZ width etc. is very much important and all of these aspects need to be investigated extensively. It is expected that only through extensive research, knowledge-base can be developed. So far as dissimilar welding of stainless steel to mild steel is concerned, publications are very few, particularly in respect of the technique: submerged arc welding. It may also be noted that use of mild steel electrode/filler wire in joining stainless steel to mild steel has been rarely found in the literature. In some specific areas of joining and repairing, stainless steel may be joined to mild steel by mild steel filler material.

Keeping in consideration of the above, the present work has been planned to investigate some aspects of dissimilar welding of ferritic stainless steel AISI 409 to mild steel by submerged arc welding. Ferritic stainless steel is used in many applications such as automatic exhaust and fuel lines, architectural trim, cooking utensils, bank vaults etc. Though

publications are rare in so far as joining of ferritic stainless steel to mild steel, industry people very often come across to the need of joining this stainless steel to plain carbon steel particularly in exhaust lines and equipment. Research in this respect seems to be useful for precise/control and better results of such type of dissimilar welding. This will also provide scope of utilizing welding of ferritic stainless steel to mild steel in many more possible applications. Welding has been done of butt joint at varied input parameters. These input parameters are: current, traverse speed and stick-out, they have been varied in several levels. Taguchi's L9 orthogonal array of design of experiments has been adopted. The influence of the levels of the parameters on quality of the weld has been studied and analysed. Nine samples have been prepared by welding of 8 mm thick both mild steel and ferritic stainless steel plates. After welding, quality of the weld has been judged through visual inspection, micro-hardness test, scanning electron microscopy, microstructural study and tensile testing of all the nine samples produced by welding. Results of all these tests and observations have been analyzed. In the present work, process optimization has been done and ANOVA (analysis of variation) has been carried out. The objective is also to develop mathematical models to relate the responses (ultimate tensile strength, percentage elongation, hardness and HAZ width) with the input parameters. Response surface/contour plots have been generated as well-based on the mathematical models developed. Significance of the input parameters on the performance (individual and overall responses) of the welded joint has been tested by ANOVA.

Both single-objective optimization and multi-objective optimization have been kept under the purview of the objective of the present work. In the plan and objective of the present work, emphasis has also been given to microstructural study. Microstructures developed in the weld, HAZ adjacent to mild steel and HAZ adjacent to ferritic stainless steel have been examined under metallurgical microscope and discussed. Scanning electron microscopy has also been aimed at, to a limited extent.

Finally, based on all the observations, test results and analyses some useful conclusions are made. And this is the end–objective of the present work i.e. arriving at some conclusive points with regard to dissimilar welding of ferritic stainless steel to mild steel by submerged arc welding.

CHAPTER 2

2. FUNDAMENTALS OF DESIGN OF EXPERIMENTS AND OPTIMIZATION METHODOLOGIES

In the present study, Taguchi's orthogonal array has been used for design of experiments. Also process optimization has been carried out. Multi objective optimization has been the target. In this chapter, some fundamentals of Taguchi's orthogonal array, some other methods of design of experiments, Grey-Taguchi analysis, response surface methodology (RSM), genetic algorithm, simulated annealing, ANOVA and teaching-learning based optimization (TLBO) etc. are discussed.

Every experimenter has to plan and conduct experiments to obtain enough and relevant data so that he can infer the science behind the observed phenomenon. It can do so by,

Trial-and-error approach:

This refers to performing a series of experiments each of which gives some understanding. This requires making measurements after every experiment so that analysis of observed data will allow him to decide what to do next- "which parameters should be varied and by how much". Many a times such series does not progress much as negative results may discourage or will not allow a selection of parameters which ought to be changed in the next experiment. Therefore, such experimentation usually ends well before the numbers of experiments reach a double digit. The data is insufficient to draw any significant conclusions and the main problem (of understanding the science) still remains unsolved.

Design of experiments (conventional):

A well planned set of experiments, in which all parameters of interest are varied over a specified range, is a much better approach to obtain systematic data. Mathematically speaking, such a complete set of experiments ought to give desired results. Usually the number of experiments and resources (materials and time) required are prohibitively large. Often the experimenter decides to perform a subset of the complete set of experiments to save on time and money! However, it does not easily lend itself to understanding of science behind the phenomenon. The analysis is not very easy (though it may be easy for the mathematician/statistician) and thus effects of various parameters on the observed data are not readily apparent. In many cases, particularly those in which some optimization is required, the

method does not point to the BEST settings of parameters. A classic example illustrating the drawback of design of experiments is found in the planning of a world cup event, say football. While all matches are well arranged with respect to the different teams and different venues on different dates and yet the planning does not care about the result of any match (win or lose)! Obviously, such a strategy is not desirable for conducting scientific experiments (except for co-ordinating various institutions, committees, people, equipment, materials etc.).

Taguchi method:

Dr. Taguchi of Nippon Telephones and Telegraph Company, Japan has developed a method based on "ORTHOGONAL ARRAY" experiments, which gives much reduced "variance" for the experiment with "optimum settings" of control parameters. Thus the marriage of design of experiments with optimization of control parameters to obtain best results is achieved in the Taguchi method. "Orthogonal arrays" (OA) provide a set of well balanced (minimum) experiments and Dr. Taguchi's signal-to-noise ratios (S/N), which are log functions of desired output, serve as objective functions for optimization, help in data analysis and prediction of optimum results.

2.1 TAGUCHI DESIGN METHOD

When Japan began its reconstruction efforts after World War II, it faced acute shortage of good quality raw material, high quality manufacturing equipment and skilled engineers. The challenge was to produce high quality products and continue to improve the quality under those circumstances. The task of developing a methodology to meet the challenge was assigned to Dr. Genichi Taguchi. Through his research in the 1950s and early 1960s, Dr. Taguchi developed the foundation of robust design and validated its basic philosophies by applying them in the development of many products.

2.1.1 TAGUCHI METHODOLOGY

The Taguchi method involves reducing the variation in a process through robust design of experiments. The overall objective of the method is to produce high quality product at low cost to the manufacturer. Taguchi’s philosophy is an efficient tool for the design of high quality manufacturing system. Taguchi developed a method for designing experiments to investigate how different parameters affect the mean and variance of a process performance characteristic that defines how well the process is functioning. Dr. Genichi Taguchi, a Japanese quality management consultant, has developed a method based on orthogonal array

experiments, which provides much reduced variance for the experiment with optimum setting of process control parameters. Thus the marriage of design of experiments (DOE) with parametric optimization of process to obtain desired results is achieved in the Taguchi method. The experimental design proposed by Taguchi involves using orthogonal arrays to organize the parameters affecting the process and the levels at which they should be varied. Instead of having to test all possible combinations like the factorial design, the Taguchi method tests pairs of combinations. This allows for the collection of the necessary data to determine which factors affect product quality most significantly with a minimum amount of experimentation, thus saving time and resources. The Taguchi method is best used when there are an intermediate number of variables (3 to 50), few interactions between variables, and when only a few variables contribute significantly. Orthogonal array (OA) provides a set of well balanced (minimum experimental runs) experiments and Taguchi's signal-to-noise ratio (S/N), which is logarithmic functions of desired output; serve as objective functions for optimization. This technique helps in data analysis and prediction of optimum results. In order to evaluate optimal parameter settings, Taguchi method uses a statistical measure of performance called signal-to-noise ratio. The S/N ratio takes both the mean and the variability into account. The S/N ratio is the ratio of the mean (signal) to the standard deviation (noise). The standard S/N ratios generally used are as follows: Nominal is the best (NB), lower the better (LB) and higher the better (HB). The optimal setting is the parameter combination, which has the highest S/N ratio. Among the available methods, Taguchi design is one of the most powerful DOE methods for analyzing of experiments. It is widely recognized in many fields particularly in the development of new products and processes in quality control. The salient features of the method are as follows:

a). It is a simple, efficient and systematic method to optimize product/process to improve the performance or reduce the cost.

b). It helps arrive at the best parameters for the optimal conditions with the least number of analytical investigations.

c). It is a scientifically disciplined mechanism for evaluating and implementing improvements in products, processes, materials, equipment and facilities.

d). Therefore, the Taguchi method has great potential in the area of low cost experimentation. Thus it becomes an attractive and widely accepted tool to engineers and scientists.

2.1.2 TAGUCHI METHOD OF DESIGN OF EXPERIMENTS

Design of experiments (DOE) is an important aspect of Taguchi method. It is applicable

both to numerical experiment and for the model fitting of physical experiments as well. The objective of DOE is the selection of the points where the response should be evaluated. Most of the criteria for optimal design of experiments are associated with the mathematical model of the process. Generally, these mathematical models are polynomials with an unknown structure, so the corresponding experiments are designed only for every particular problem. The choice of the design of experiments can have a large influence on the accuracy of the approximation and the cost of constructing the response surface.

The general steps involved in the Taguchi method are as follows:

1). Defining the process objective, or more specifically, a target value for a performance measure of the process. The target of a process may also be a minimum or maximum. The deviation in the performance characteristic from the target value is used to define the loss function for the process.

2). Determining the design parameters affecting the process. Parameters are variables within the process that affect the performance measure such as temperatures, pressures, etc. that can be easily controlled.

3). Creating orthogonal arrays for the parameter design indicating the number of and conditions for each experiment. The selection of orthogonal arrays is based on the number of parameters and the levels of variation for each parameter, and will be expounded below.

4). Conducting the experiments indicated in the completed array to collect data on the effect on the performance measure.

5). Completing data analysis to determine the effect of the different parameters on the performance measure.

Knowing the number of parameters and the number of levels, the proper orthogonal array can be selected. Using the array selector Table 2.1 shown below, the name of the appropriate array can be found by looking at the column and row corresponding to the number of parameters and number of levels. Once the name has been determined (the subscript represents the number of experiments that must be completed), the predefined array can be looked up.

Table 2.1 Array selector [73]

Number of Levels	Number of Parameters (P)																														
	2	3	4	5	6	7	8	9	10	11	12	13	14	15	16	17	18	19	20	21	22	23	24	25	26	27	28	29	30	31
2	L4	L4	L8	L8	L8	L8	L12	L12	L12	L12	L16	L16	L16	L16	L32	L32	L32	L32	L32	L32	L32	L32	L32	L32	L32	L32	L32	L32	L32	L32
3	L9	L9	L9	L18	L18	L18	L18	L27	L27	L27	L27	L27	L36	L36	L36	L36	L36	L36	L36	L36	L36	L36								
4	L'16	L'16	L'16	L'16	L'32	L'32	L'32	L'32	L'32																					
5	L25	L25	L25	L25	L25	L50	L50	L50	L50	L50	L50																			

Taguchi method has been successfully applied in manufacturing field for nearly three decades to robustly design products or processes having a single quality parameter. Some researchers have used Taguchi's orthogonal array (OA) experiment for selection of optimum levels of process parameter setting in welding.

OTHER TYPES OF DESIGN OF EXPERIMENTS

- **Full factorials design:-** As their name implies, full factorial experiments look completely at all factors included in the experimentation. In full factorials, one studies all of the possible treatment combinations that are associated with the factors and their levels. They look at the effects that the main factors and all the interactions between factors have on the measured responses. If one uses more than two levels for each factor, he can also study whether the effect on the response is linear or if there is curvature in the experimental region for each factor and for the interactions. Full factorial experiments can require many experimental runs if many factors at many levels are investigated.
- **Fractional factorials:-** Fractional factorials look at more factors with fewer runs. Using a fractional factorial involves making a major assumption- that higher order interactions (those between three or more factors) are not significant. Fractional factorial designs are derived from full factorial matrices by substituting higher order interactions with new factors. To increase the efficiency of experimentation, fractional factorials give up some power in analysing the effects on the response. Fractional factorials will still look at the main factor effects, but they lead to compromises when looking into interaction effects.
- **Screening experiments:-** Screening experiments are the ultimate fractional factorial experiments. These experiments assume that all interactions, even two-way interactions, are not significant. They literally screen the factors, or variables, in the process and determine which the critical variables are that affect the process output(s).

  There are two major families of screening experiments:

  - Drs. Plackett and Burman developed the original family of screening experiment matrices in the 1940s.
  - Dr. Taguchi adapted the Plackett–Burman screening designs. He modified the Plackett–Burman design approach so that the experimenter could assume that interactions were not significant, yet could test for some two-way interactions at the same time.

- **Response surface analysis:-** Response surface analysis is an off-line optimization technique. Usually, 2 factors are studied; but 3 or more can also be studied. With response surface analysis, one runs a series of full factorial experiments and map the response to generate mathematical equations that describe how factors affect the response.
- **EVOP:-** EVOP (evolutionary operations) is an online optimization technique. Usually, two factors are studied using small, step changes in factor levels to incrementally explore the operating bounds of the process.
- **Mixture experiments:-** The designs looked at so far work fine for variables like temperature, pressure, or time and even for material substitutions. But they will not work in situations where one needs to study how changes in the formulation affect the final properties of a material. When dealing with formulations, there are added constraints on the experimenter. When dealing with composition, the sum of all of the weight fractions of all the components must add up to 1.0 and each of the individual components must have a weight fraction between 0 and 1.0. Mixture experiments provide techniques to operate within these constraints.
- **Experimental strategy:-** When setting up an experimental strategy, it is usually best to start with screening experiments to separate out the important (significant) factors from the many factors in a process. From there one can experiment further on the significant factors and study their interactions with fractional factorial or full factorial experiments. In some cases, once the power factors are identified, one may want to optimize the response using the power factors in one of the two major DOE techniques for optimizing processes, response surface analysis (RSM) or EVOP [73].

2.1.3 TAGUCHI DESIGN FOR OPTIMIZATION OF SINGLE PERFORMANCE CHARACTERISTIC:

Robust design method

Robust design method, also called the Taguchi method, pioneered by Dr. Genichi Taguchi, greatly improves engineering productivity. By consciously considering the noise factors (environmental variation during the product's usage, manufacturing variation, and component deterioration) and the cost of failure in the field, the robust design method helps ensure customer satisfaction. Robust design focuses on improving the fundamental function of the product or process, thus facilitating flexible designs and concurrent engineering.

Indeed, it is the most powerful method available to reduce product cost, improve quality, and simultaneously reduce development interval. The robustness strategy uses five primary tools:

1). P-diagram is used to classify the variables associated with the product into noise, control, Signal (input) and response (output) factors.

2). Ideal function is used to mathematically specify the ideal form of the signal-response relationship as embodied by the design concept for making the higher-level system work perfectly.

3). Quadratic loss function (also known as quality loss function) is used to quantify the loss incurred by the user due to deviation from target performance.

4). Signal-to-Noise ratio is used for predicting the field quality through laboratory experiments.

5). Orthogonal arrays are used for gathering dependable information about control factors (design parameters) with a small number of experiments.

Robust design is an engineering methodology for obtaining product and process conditions, which possess minimum sensitivity to the various causes of variation to produce high quality products with low development and manufacturing cost. Taguchi's parameter design is an important tool for robust design. Taguchi design provides a powerful and efficient method for designing products that operate consistently and optimally over a variety of conditions. The Taguchi design, also known as an orthogonal array, is a method of designing experiments that usually requires only a fraction of the full factorial combinations. In this design the array is orthogonal which ensures the design is balanced so that factor levels are weighted equally. Because of this, an orthogonal array is one in which each factor can be evaluated independently of all the other factors.

Quality measurement

To measure quality, Taguchi defines a quality loss function. The quality loss function (Figure 2.1) is a continuous function that is defined in terms of the deviation of a design parameter from an ideal or target value. Loss includes costs to operate, failure to function, maintenance and repair costs, customer dissatisfaction, injuries caused by poor design and similar costs. Defective products that are detected, repaired, reworked or scrapped before shipment are not considered part of this loss. Taguchi's view on the nature of the quality loss function represents a fundamental paradigm shift (particularly in the U.S.) in the way in which manufacturers consider whether or not a product is good. Products that meet tolerances also inflict quality loss.

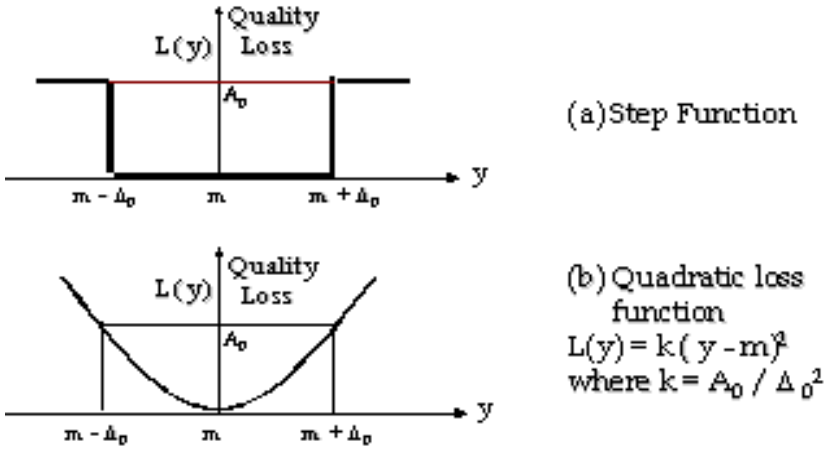

Figure 2.1 Quality loss function [74]

m: target value for a critical product characteristic

+/- Δ_0: allowed deviation from the target

A_0: loss due to a defective product

Then the quality loss, 'L', suffered by an average customer due to a product with 'y' as value of the characteristic is given by the equation 2.1:

$$\mathbf{L = k*(y - m)^2} \qquad (2.1)$$

Where $k = (A_0/\Delta_0^2)$

Taguchi design

Taguchi method treats optimization problems in two categories,

a) Static problems (batch process optimization):- Generally, a process to be optimized has several control factors which directly decide the target or desired value of the output. The optimization then involves determining the best control factor levels so that the output is at the target value. Such a problem is called as a "static problem". This is best explained using a P-diagram which is shown in Figure 2.2 ('P' stands for process or product). Noise is shown to be present in the process but should have no effect on the output. This is the primary aim of the Taguchi experiments- to minimize variations in output even though noise is present in the process. The process is then said to have become robust.

Taguchi calls the variations as noise factor. A noise factor is a source of variation that is impossible or difficult to control and that affects the functional characteristics of the product.

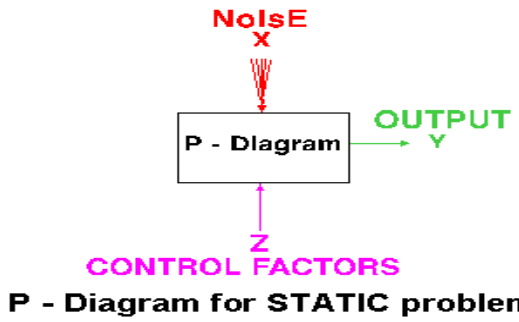

Figure 2.2 P-diagram for static problem [73]

Signal to Noise(S/N) Ratio

There are three forms of signal to noise (S/N) ratio that are of common interest for optimization of static problems, as per Taguchi's approach; The S/N ratio is denoted by "n" in the following equations.

i) Smaller-the-better:

$$\mathbf{n = -10\ Log_{10}[mean\ of\ square\ of\ measured\ data]} \quad (2.2)$$

This is usually the chosen S/N ratio for all undesirable characteristics like 'defects' etc. for which the ideal value is zero. Also, when an ideal value is finite and its maximum or minimum value is defined (like maximum purity is 100% or maximum Tc is 92K or minimum time for making a telephone connection is 1 sec) then the difference between measured data and ideal value is expected to be as small as possible. The generic form of S/N ratio then becomes,

$$\mathbf{n = -10\ Log_{10}[mean\ of\ sum\ of\ squares\ of\ \{measured - ideal\}]} \quad (2.3)$$

ii) Larger-the-better:

$$\mathbf{n = -10\ Log_{10}[mean\ of\ sum\ squares\ of\ reciprocal\ of\ measured\ data]} \quad (2.4)$$

This is often converted to smaller-the-better by taking the reciprocal of the measured data and next, taking the S/N ratio as in the smaller-the-better case.

(iii) Nominal-the-best:

$$\mathbf{n= -10\ Log_{10}(Square\ of\ means/variance)} \quad (2.5)$$

This case arises when a specified value is the most desired, meaning that neither a smaller nor a larger value is desired.

b) Dynamic problems (technology development):- If the product to be optimized has a signal input that directly decides the output, the optimization involves determining the best control factor levels so that the 'input signal/output' ratio is closest to the desired relationship. Such a problem is called as a "DYNAMIC PROBLEM". This is best explained by a P-

diagram which is shown in Figure 2.3. Again, the primary aim of the Taguchi experiments- to minimize variations in output even though noise is present in the process- is achieved by getting improved linearity in the input/output relationship.

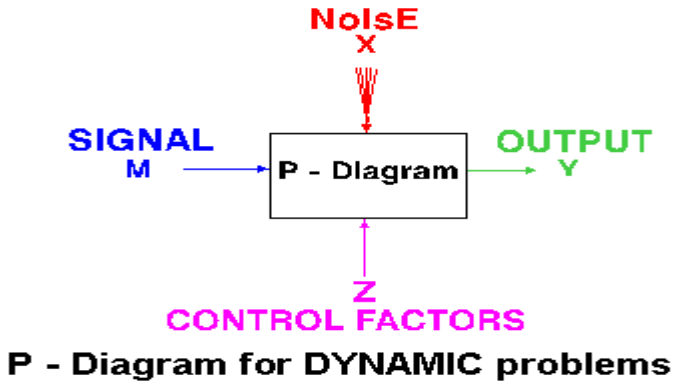

Figure 2.3 P- diagram for dynamic problem [73]

In dynamic problem, many applications are found where the output is supposed to follow input signal in a predetermined manner. Generally, a linear relationship between 'input' and 'output' is desirable. Taguchi method is a scientifically disciplined mechanism for evaluating and implementing improvements in products, processes, materials, equipment and facilities. These improvements are aimed for improving the desired characteristics; reducing the number of defects by studying the key variables controlling the process and optimizing the procedures or design to yield the best results simultaneously. The method is applicable over a wide range of engineering fields like manufacturing raw materials, sub systems, products for professional and consumer markets. In fact, the method can be applied to any engineering fabrication, computer aided-design, banking and service sectors etc.

2.2 GREY TAGUCHI ANALYSIS

Grey Taguchi method is the combination of orthogonal array (OA) design of experiments (DOE) with grey relational analysis (GRA) which enables the determination of the optimal combination of submerged arc welding parameters as example for multiple process response. Taguchi method associated with Grey relational analysis represents new approach towards optimization of any kind of process operation. GRA is employed to search for grey relational grade (GRG), which can be used to describe the relationships among the factors and to determine the important factors that significantly influence some defined objectives. In a complex and multivariate time series system, many factors simultaneously influence the system to determine the state of development of the system. GRA analysis is already proved to be simple and accurate method for selecting factors especially for those

problems with unique characteristic. In Grey relational analysis, when the range of sequence is large or the standard value is enormous, the function of factors is neglected. Therefore, one has to pre-process the data which are related to a group of sequences ranging from zero to one, which is called "grey relational generation". It is a process of transferring the original sequence to a comparable sequence which can be done in three different approaches.

The first approach is data pre-processing. Data pre-processing is usually required when the range or unit in one data sequence is different from others or the sequence scatter range is too large. Therefore, data must be normalized, scaled and polarized first into a comparable sequence before proceeding to other steps. The processing is called generation of grey relation or standard processing.

If the expectancy is the larger-the-better, then it can be expressed by

$$x^*(k) = \frac{x_i^o(k) - \min x_i^o(k)}{\max x_i^o(k) - \min x_i^o(k)} \tag{2.6}$$

If the expectancy is the smaller-the-better, then it can be expressed by

$$x^*(k) = \frac{\max x_i^o(k) - x_i^o(k)}{\max x_i^o(k) - \min x_i^o(k)} \tag{2.7}$$

Where $x_i^0(k)$ is the original sequence, $x_i^*(k)$ the sequence after data processing, max $x_i^0(k)$ and min $x_i^0(k)$ are the largest and smallest value of $x_i^0(k)$, respectively.

The second step is to locate the grey relational coefficient by using following equation

$$\xi_i(k) = \frac{\Delta \min + \zeta \Delta \max}{\Delta_{0,i}(k) + \zeta \Delta \max} \tag{2.8}$$

Where $\Delta o, i(k)$ is the deviation sequence of the reference sequence (x_0) and the comparability sequence (x_i), i.e. $|x_0(k) - x_i(k)|$, where $x_0(k)$ is the ideal result (=1) and ξ is the distinguishing coefficient set between zero and unity; in the present study, $\xi = 0.5$ is used because it offers moderate distinguishing effect and stability.

After the grey relational coefficient is derived, grey relational grade (GRG) is calculated by averaging the value of grey relational coefficients (GRC). GRG is defined as the numerical measure of the relevancy between two systems or two sequences such as the reference sequence and the comparability sequence.

$$\gamma_i = \frac{1}{n} \sum_{k=1}^{n} \xi_i(k) \tag{2.9}$$

Where 'γ_i' represents GRG; the level of correlation between the reference sequence and the comparability sequence. The evaluated GRG fluctuates from 0 to 1 and equals 1 if these two sequences are identically coincidental. The overall performance characteristic of the multiple response process depends on the calculated Grey relational grade. This approach converts a multiple response process optimization problem into a single response optimization situation with the objective function related to overall Grey relational grade. The optimal parametric combination is then evaluated which would result highest Grey relational grade. The optimal factor setting for maximizing overall Grey relational grade can be performed by Taguchi method.

In the context of the present work, ultimate tensile strength, percentage elongation and hardness at weld should follow larger-the-better criterion and for HAZ width at mild steel and ferritic stainless steel should follow smaller-the-better criterion. Normalized values for these responses are calculated by using eqs. (2.6) and (2.7) respectively. Then the GRC value is calculated by equation (2.8). Now the average of all GRC values is calculated by eq. (2.9) to get the value of GRG. Now based on the GRG values, Taguchi multi objective optimization method has been applied, based on S/N ratio concept [75].

2.3 RESPONSE SURFACE METHODOLOGY (RSM)

Response surface methodology (RSM) is a collection of mathematical and statistical techniques, generally used for empirical model building and analysing a problem. Response surface methodology is a very useful and modern technique for the prediction and optimization of welding characteristics and many other cases. The objective of RSM is to optimize a response (output variable) which is influenced by several independent input variables. To determine the optimum operating conditions of a system or to determine a region of the factor space in which operating requirements are satisfied, a design of experiments is employed. In the present study, ultimate tensile strength, percentage elongation and hardness at weld in submerged arc welding has been predicted and some other as well by RSM. In this section, overview of RSM has been given briefly. RSM can also be used for process optimization.

The most extensive applications of RSM are in the particular situations where several input variables potentially influence some quality characteristics (responses) of the process. The field of RSM consists of the experimental strategy for exploring the space of the independent process variables, empirical statistical modelling to develop a relationship

between the yield and process variables and optimizing the process variables that produce desirable values of the response. If process yield y is a function of two variables x_1 and x_2, then it can be written as

$$\mathbf{y = f\,(x_1, x_2) + \varepsilon} \qquad (2.10)$$

The variables x_1 and x_2 are independent variables where the response y depends on them. The dependent variable y is a function of x_1, x_2, and the experimental error term, denoted as ε. The error term ε represents any measurement error on the response, as well as other type of variations not counted in 'f'. It is a statistical error that is assumed to distribute normally with zero mean and variance 's^2'. In most RSM problems, the true response function 'f' is unknown. In order to develop a proper approximation for 'f', the experimenter usually starts with a low-order polynomial in some small region. If the response can be defined by a linear function of independent variables, then the approximating function is a first-order model. A first-order model with 2 independent variables can be expressed as

$$\mathbf{y = \beta_0 + \beta_1 x_1 + \beta_2 x_2 + \varepsilon} \qquad (2.11)$$

If there is a curvature in the response surface, then a higher degree polynomial should be used. The approximating function with 2 variables is called a second-order model:

$$\mathbf{y = \beta_0 + \beta_1 x_1 + \beta_2 x_2 + \beta_{11} x_{11}^2 + \beta_{22} x_{22}^2 + \beta_{12} x_1 x_2 + \varepsilon} \qquad (2.12)$$

Some other forms are also utilized like:

$$\mathbf{y = \beta_0 + \beta_1 x_1 + \beta_2 x_2 + \beta_{12} x_1 x_2 + \varepsilon} \qquad (2.13)$$

In general all RSM problems use either one or the mixture of the both of these models. In each model, the levels of each factor are independent of the levels of other factors. In order to get the most efficient result in the approximation of polynomials the proper experimental design must be used to collect data. Once the data are collected, the method of least square is used to estimate the parameters in the polynomials. The response surface analysis is performed by using the fitted surface. The response surface designs are types of designs for fitting response surface. Therefore, the objective of studying RSM can be accomplish by

- understanding the topography of the response surface (local maximum, local minimum, ridge lines), and
- finding the region where the optimal response occurs. The goal is to move rapidly and efficiently along a path to get to a maximum or a minimum response so that the response is optimized [76].

2.4 GENETIC ALGORITHM

Genetic Algorithm (GA) is a nondeterministic stochastic optimization process based on the theories of evolution and natural selection to solve a complex problem within a solution space. It is an efficient method for nonlinear global optimization problems. The advantage of GA is that objective function does not need to be differentiable. This makes this algorithm suitable for solving some complex problems which are multimodal, discontinuous or noisy in nature. Even, it is beneficial to use GA for solving inverse problems.

GA uses a binary coding system; variables are first coded in some string structures. Specific lengths of strings are used, composed of 0 and 1 instead of encoded input variables. The accuracy of the solution depends on the string length. As string length increases, accuracy increases. GA searches a set of possible solutions. Therefore, it is effective in finding a global optimal point by preventing it from converging to a local optimal point. The transition rule used in the genetic algorithm is probabilistic rather than deterministic. GA is naturally suited for maximization problems. Minimization problems are usually transformed into maximization problem by using a fitness function (Fi). The fitness function does not have to be either continuous or differentiable. In general, a fitness function is first derived from the objective function and used in successive genetic operations. In GA, fitness is used to allocate reproductive traits to the individuals in the population and thus act as some measure of goodness to be maximized. This means that individuals with higher fitness value will have higher probability of being selected as candidates for further examination. Certain genetic operators require that the fitness function be non-negative, although certain operators need not have this requirement. For maximization problems, the fitness function can be considered to be the same as the objective function. For minimization problems, to generate non-negative values in all the cases and to reflect the relative fitness of individual string, it is necessary to map the underlying natural objective function to fitness function form. A number of such transformations are possible. A commonly adopted fitness mappings is like this:

$$\mathbf{F(x) = 1/(1+f(x))} \tag{2.14}$$

Genetic algorithm uses three genetic operators- reproduction, crossover and mutation- to produce systematically the next generation population from a given generation. The new population is further evaluated to find the fitness values and tested for the convergence of the process. One cycle of reproduction, crossover, mutation and the evaluation of the fitness values is known as a generation in GA. If the convergence criterion is not satisfied, the population is iteratively operated by the three operators and the resulting new population is

evaluated for the fitness values. The procedure is continued through several generations until the convergence criterion is satisfied and the process is terminated [77].

2.5 ANALYSIS OF VARIANCE (ANOVA)

Analysis of variance (ANOVA) is a collection of statistical models used to analyse the differences among group means and their associated procedures (such as 'variation' among and between groups), developed by statistician and evolutionary biologist Ronald Fisher. In the ANOVA setting, the observed variance in a particular variable is partitioned into components attributable to different sources of variation. In its simplest form, ANOVA provides a statistical test of whether or not the means of several groups are equal, and therefore generalizes the t-test to more than two groups. As doing multiple two-sample t-tests would result in an increased chance of committing a statistical type I error, ANOVA's are useful in comparing (testing) three or more means (groups or variables) for statistical significance.

2.5.1 ASSUMPTIONS OF ANOVA

The analysis of variance has been studied from several approaches, the most common of which uses a linear model that relates the response to the treatments and blocks. Even when the statistical model is nonlinear, it can be approximated by a linear model for which an analysis of variance may be appropriate.

2.5.2 CHARACTERISTICS OF ANOVA

ANOVA is used in the analysis of comparative experiments, those in which only the difference in outcomes is of interest. The statistical significance of the experiment is determined by a ratio of two variances. This ratio is independent of several possible alterations to the experimental observations. Adding a constant to all observations does not alter significance. Multiplying all observations by a constant does not alter significance. So ANOVA statistical significance results are independent of constant bias and scaling errors as well as the units used in expressing the observations. In the era of mechanical calculation it was common to subtract a constant from all observations (when equivalent to dropping leading digits) to simplify data entry. This is an example of data coding.

Taguchi replaces the full factorial experiments with lean, less expensive, faster, partial factorial experiments. Taguchi's design for the partial factorial is based on specially developed orthogonal arrays as mentioned earlier. Since the partial experiment is only a

sample of the full experiment, the analysis of the partial experiment must include an analysis of the confidence that can be placed in the results. Fortunately, there is a standard statistical technique called analysis of variance (ANOVA) which is routinely used to provide a measure of confidence. The technique does not directly analyse the data, but rather determines the variability (variance) of the data. Confidence is measured from the variance. Analysis provides the variance of controllable and noise factors. By understanding the source and magnitude of variance, robust operating conditions can be predicted. This is a second benefit of the methodology.

The purpose of the analysis of variance (ANOVA) is to investigate which design parameters significantly affect the quality characteristic. This is accomplished by separating the total variability of the S/N ratio, which is measured by the sum of the squared deviations from the total mean S/N ratio from each of the design parameters and the error. The total sum of squared deviations SST from the mean ratio '$\mathbf{n'_m}$ can be calculated as:

$$\mathbf{SS_T = \sum_i^k (n_i - n_m)^2} \tag{2.15}$$

where 'k' is the number of experiments in the orthogonal array and '$\mathbf{n_m}$' is the mean S/N ratio for the 'ith' experiment.

In ANOVA table mean square deviation is defined as:

$$MS = \frac{SS(sum\ of\ squared\ deviation)}{DF(degree\ of\ freedom)} \tag{2.16}$$

F-value of Fisher's F ratio (Variance ratio) is defined as:

$$F = \frac{MS\ for\ a\ term}{MS\ for\ the\ error\ term} \tag{2.17}$$

Depending on F-value, P-value (probability of significance) is then calculated. If the P-value for a term appears less than 0.05 (95% confidence level) then it can be concluded that, the effect of the factor(s)/interaction of factors is significant on the selected response [78].

2.6 SIMULATED ANNEALING (SA)

Simulated annealing (SA) is a probabilistic technique for approximating the global optimum of a given function. Specifically, it is a metaheuristic to approximate global optimization in a large search space. The name of this algorithm comes from the analogous process of a liquid freezing and crystallizing or a metal cooling and annealing. At high temperatures, a liquid consists of randomly dispersed molecules resulting in a high energy state. When carefully decreasing the temperature from this point, the particles slowly arrange

themselves into a highly structured lattice (solid phase). It is crucial throughout this process that the system reaches a steady state before the temperature decreases to the next level. When the temperature is sufficiently low enough, the system reaches its ground state or the point at which the energy of the solid is minimized. If cooling is not performed slowly enough, the system is no longer at its minimal energy state, analogous to the process of quenching. The key idea behind simulated annealing is to minimize the cost function using an appropriate annealing schedule that cools the system slow enough to find the optimal solution.

Simulated annealing acts similarly to local optimization in that it always accepts changes which reduce the cost. Where it improves local optimization, it accepts increased cost function changes with a certain probability described by a Boltzmann distribution. That is, a system changes its configuration from E_1 to E_2 with probability p defined by: $p = e^{(dE/T)}$. This acceptance rule is also known as the Metropolis criterion. The formula can be verified because when $E_2<E_1$, the value of p is greater than 1 and changes are always accepted. If $E_2>E_1$, a randomly generated number between 0 and 1 is compared to p. If the random number is less than or equal to p, the change is accepted even though the cost function has increased. One last thing to note about this distribution is its dependence on the temperature T. Because the temperature is decremented as the algorithm progresses, the likelihood of accepting an uphill change also decreases [79].

2.7 TEACHING-LEARNING BASED OPTIMIZATION (TLBO)

Teaching-Learning based Optimization (TLBO) algorithm is a global optimization method originally developed by Rao. It is a population- based iterative learning algorithm that exhibits some common characteristics with other evolutionary computation (EC) algorithms. However, TLBO searches for an optimum through each learner trying to achieve the experience of the teacher, which is treated as the most learned person in the society, thereby obtaining the optimum results, rather than through learners undergoing genetic operations like selection, crossover, and mutation. Due to its simple concept and high efficiency, TLBO has become a very attractive optimization technique and has been successfully applied to many real world problems.

In any evolutionary algorithms the convergence rate is given prime importance for solving an optimization problem over quality of solutions. TLBO in general produces improved results in compared to other EC techniques like Genetic Algorithm (GA), Particle Swarm Optimization (PSO), Differential Evolution (DE), and Artificial Bee Colony (ABC). However, in real- world real time applications, the major thrust is always on convergence

time. To make TLBO suitable for such applications, one focuses on improving the convergence time while without compromising the quality of results [80].

This optimization method is based on the effect of the influence of a teacher on the output of learners in a class. It is a population based method and like other population based methods it uses a population of solutions to proceed to the global solution. A group of learners constitute the population in TLBO. In any optimization algorithms there are numbers of different design variables. The different design variables in TLBO are analogous to different subjects offered to learners and the learners' result is analogous to the 'fitness', as in other population-based optimization techniques. As the teacher is considered the most learned person in the society, the best solution so far is analogous to Teacher in TLBO. The process of TLBO is divided into two parts. The first part consists of the "Teacher phase" and the second part consists of the "Learner phase". The "Teacher phase" means learning from the teacher and the "Learner phase" means learning through the interaction between learners. In the sub-sections the procedure of implementation of TLBO is discussed.

Initialization

Followings are the notations used for describing the TLBO

N : number of learners in class i.e. "class size"

D : number of courses offered to the learners

MAXIT: maximum number of allowable iterations

The population 'X' is randomly initialized by a search space bounded by matrix of 'N' rows and 'D' columns. The 'jth' parameter of the 'ith' learner is assigned values randomly using the equation

$$x^{0}_{(i,j)} = x_j^{min} + rand \times \left(x_j^{max} - x_j^{min} \right) \tag{2.18}$$

where 'rand' represents a uniformly distributed random variable within the range (0, 1), x_j^{min} and x_j^{max} represent the minimum and maximum value for 'j^{th}' parameter. The parameters of 'i^{th}' learner for the generation g are given by

$$X^{g}_{(i)} = \left[x^{g}_{(i,1)}, x^{g}_{(i,2)}, x^{g}_{(i,3)}, \ldots\ldots, x^{g}_{(i,j)}, \ldots\ldots, x^{g}_{(i,D)} \right] \tag{2.19}$$

(i) Teacher phase

The mean parameter Mg of each subject of the learners in the class at generation g is given as

$$M^g = \left[m_1^g, m_2^g, ..., m_j^g, ..., m_D^g\right] \tag{2.20}$$

The learner with the minimum objective function value is considered as the teacher for respective iteration. The Teacher phase makes the algorithm proceed by shifting the mean of the learners towards its teacher. To obtain a new set of improved learners a random weighted differential vector is formed from the current mean and the desired mean parameters and added to the existing population of learners.

$$Xnew_{(i)}^g = X_{(i)}^g + rand \times \left(X_{Teacher}^g - T_F M^g\right) \tag{2.21}$$

'T_F' is the teaching factor which decides the value of mean to be changed. Value of 'T_F' can be either 1 or 2. The value of 'T_F' is decided randomly with equal probability as,

$$T_F = round\,[1 + rand(0,1)\{2-1\}] \tag{2.22}$$

Where 'T_F' is not a parameter of the TLBO algorithm. The value of 'T_F' is not given as an input to the algorithm and its value is randomly decided by the algorithm using eq. (2.22). After conducting a number of experiments on many benchmark functions it is concluded that the algorithm performs better if the value of 'T_F' is between 1 and 2. However, the algorithm is found to perform much better if the value of 'T_F' is either 1 or 2 and hence to simplify the algorithm, the teaching factor is suggested to be taking either 1 or 2 depending on the rounding up criteria given by Eq. (5).

If '$Xnew_{(i)}^g$' is found to be a superior learner than '$X_{(i)}^g$' in generation 'g', than it replaces inferior learner in the matrix.

(ii) Learner phase

In this phase the interaction of learners with one another takes place. The process of mutual interaction tends to increase the knowledge of the learner. The random interaction among learners improves his or her knowledge. For a given learner $X_{(i)}^g$, another learner $X_{(r)}^g$ is randomly selected ($i \neq r$). The 'i^{th}' parameter of the matrix 'Xnew' in the learner phase is given as

$$Xnew_{(i)}^{g} = \begin{cases} X_{(i)}^{g} + rand \times \left(X_{(i)}^{g} - X_{(r)}^{g}\right) & if\ f\left(X_{(i)}^{g}\right) < f\left(X_{(r)}^{g}\right) \\ X_{(i)}^{g} + rand \times \left(X_{(r)}^{g} - X_{(i)}^{g}\right) & otherwise \end{cases} \tag{2.23}$$

2.7.1 TLBO ALGORITHM

The TLBO algorithm may briefly be described with the following steps:

Step-1: A random population is generated according to the number of students in the class and number of subjects offered. It may mathematically be expressed as

$$P = \begin{bmatrix} x_{1,1} & \cdot & x_{1,j} & \cdot & x_{1,d} \\ \cdot & \cdot & \cdot & \cdot & \cdot \\ x_{i,1} & \cdot & x_{i,j} & \cdot & x_{i,d} \\ \cdot & \cdot & \cdot & \cdot & \cdot \\ x_{n,1} & \cdot & x_{n,j} & \cdot & x_{n,d} \end{bmatrix} \tag{2.24}$$

where '$x_{i,}j$' is the initial grade of the 'j^{th}' subject of the 'i^{th}' student.

Step 2: The average grade of each subject offered in the class. The mean grade of the 'j^{th}' subject is given by

$$\mu_j = mean\left(x_{1,j},\ x_{2,j},\ .,\ .,\ x_{i,j},\ .,\ .,\ x_{n,j}\right) \tag{2.25}$$

Step 3: Based on the overall grade point (objective value) the students (population) are sorted from best to worst.

Step 4: The grade point of each subject (control variables) of each of the individual student is improved. Improvement of grade points may be depicted as follows:

For i = 1: NP

For j = 1: ND

$$x_{i,j}^{t+1} = x_{i,j}^{t} + rand \times \left[x_{teacher_j} - round(1 + r_1) \times \mu_j\right]$$

End

Step 5: Every student improves grade point of each subject through the mutual interaction with the other students. The modification of the grade points using the concept of learning phase may be illustrated as follows:

For I = 1:N_P

a = randperm (N_P);

l = a(1);

Xi = x(i,:); X_l = x(l,:);

if f(Xi) < f(X_l)

for j = 1: N_D

$$x_{i,j}^{t+1} = x_{i,j}^{t} + rand \times \left(x_{i,j}^{t} - x_{l,j}^{t}\right)$$

end

else if f(Xi) > f(X_l)

for j = 1:N_D

$$x_{i,j}^{t+1} = x_{i,j}^{t} + rand \times \left(x_{l,j}^{t} - x_{i,j}^{t}\right)$$

End

Figure 2.4 Flow chart of learning phase

In the present work Taguchi's S/N ratio concept has been used for single objective optimization. For multi-objective optimization Taguchi-based grey relation analysis has been employed. As an extension of the present work, the comparative usefulness of other techniques, specially the TLBO and GA will be studied in future.

CHAPTER 3

3. EXPERIMENTAL PLAN, SET UP AND PROCEDURE

An experiment is characterized by the treatments and experimental units to be used, the way treatments are assigned to units, and the responses that are measured. Some mechanical and metallurgical properties of submerged arc welded butt joints between ferritic stainless steel (AISI 409) and mild steel (AISI 1018) have been studied in the present work. 8 mm thickness has been used for both of these two materials, for dissimilar butt welding. Continuous electrode wire of low carbon steel ESAB SA1 (E8) is used. The effects of input parameters: welding current (C), stickout length (S) and travel speed (T) on the ultimate tensile strength (UTS), percentage elongation, hardness and HAZ width of the welded samples have been experimented and analyzed. 3 levels of each factor; current, stick-out and travel speed have been employed for a set of planned experiments. Process optimization and microstructural study have also been carried out. Experimental plan, set up and procedure have been discussed in this chapter.

3.1 EXPERIMENTAL PLAN

In the present work, experiments are done in a planned experimental order, named design of experiments. Taguchi's orthogonal array is the main source of planning of the experiments of the present work. Some fundamentals of design of experiments are described in Chapter 2. Taguchi's L9 orthogonal array has been selected, considering three factors, and three levels of each factor. The input parameters are current, traverse speed and stick-out length.

Table 3.1 Process parameters and their levels

Process parameters	Unit	Symbols	Values	Level 1	Level 2	Level 3
Current	A	C	Numerical	250	300	350
			Coded	1	2	3
Traverse speed	mm/s	T	Numerical	37.5	50.0	62.5
			Coded	1	2	3
Stickout length	mm	S	Numerical	15	20	25
			Coded	1	2	3

Thus nine butt welded samples have been prepared using different levels of current, traverse speed and stick-out length. The output responses measured are ultimate tensile strength, percentage elongation, hardness and HAZ width. Based on the trial runs and

literature survey, the levels of the factors are selected. Table 3.1 shows the factors and their levels used in the experiments.

Experimental runs corresponding to the factors and levels shown in Table 3.1, are listed in Table 3.2.

Table 3.2 Experimental design matrix as per L9 orthogonal array

Sample No./Experiment No.	Current		Traverse speed		Stickout length	
	Level	Value (A)	Level	Value (mm/s)	Level	Value (mm)
1.	1	250	1	37.5	1	15
2.	1	250	2	50.0	2	20
3.	1	250	3	62.5	3	25
4.	2	300	1	37.5	2	20
5.	2	300	2	50.0	3	25
6.	2	300	3	62.5	1	15
7.	3	350	1	37.5	3	25
8.	3	350	2	50.0	1	15
9.	3	350	3	62.5	2	20

Butt joints of dissimilar materials – ferritic stainless steel (AISI 409) to mild steel (AISI 1018) are made using different parametric conditions as listed in Table 3.2

3.2 EXPERIMENTAL SETUP

The experimental set up used to carry out welding, is mainly the submerged arc welding machine with its accessories. After welding, other equipment and instruments have been used as well.

3.2.1 EQUIPMENT AND INSTRUMENTS USED

The main set-up of the experiments includes the SAW welding machine.

Welding machine

Welding has been done on a single wire submerged arc welding machine. Important specifications are given here under. The photographic view of the set-up of the SAW machine is given in Figure 3.1.

Figure 3.1 Photographic view of the submerged arc welding machine

SAW welding machine:

Major specifications of the SAW welding machine used in the study are:-

a) Make : INDARC AUTOWELD MAJOR (Maker: IOL Ltd.India).
Type : CPRA 800(S) with AWM (LW) tractor for single wire

b) POWER SUPPLY UNIT:

Mains supply, Ph x V, Hz	: 3 x 415, 50
Fuse rating at 415V, A (M	: 60
Input power kVA (Max)	: 47
Open circuit voltage, V DC	: 22-55
Welding current range	: 300 A /32 V -1000 A/44 V
Welding current at 100% Duty cycle, A	: 800
Insulation class	: F
Type of cooling	: Forced Air
Dimensions, l x w x h, mm	: 830 x 670 x 1400
Weight, Kg	: 440

c) WELDING HEAD:

Wire (single) diameter range, mm	: 2.4 – 5.0 (Standard), 6.3 (Optional)
Wire feed speed, cm/min	: 50 – 450
Welding current, A	: 1200 max (800A continuous)
Vertical adjustment, mm	: 140
Horizontal adjustment, m	: 140
Swivel arrangement, De	: 360^0
Torch tilt, Deg ±	: 450
Speed range of tractor, cm/min	: 0 – 150
Hopper capacity, Kg	: 5
Wheel center of tractor, cm	: 350
Dimension, l x w x h, mm	: 1368 x 410 x 114

Instron universal testing machine:

Tensile tests have been done on Instron universal testing machine at Fatigue fracture damage analysis (FFDA) laboratory, Mechanical Engineering Department, Jadavpur University. The specimens are clamped by using hydraulic chuck, as shown in the Figure 3.2. A photographic view of the machine is also shown (Figure 3.2).

Figure 3.2 Photographic view of Instron universal testing machine

Major Specification of Instron universal testing machine are:-

Model number	: 5589
Serial number	: 95/1058
Maximum capacity	: 600 kN
Maximum Temperature	: 1000^0 C

Metallurgical microscope:

Leica metallurgical microscope is used for study of microstructures and measurement of HAZ width of the welded samples in the present work. The photographic view of the microscope is given in Figure 3.3. Major specifications are also shown.

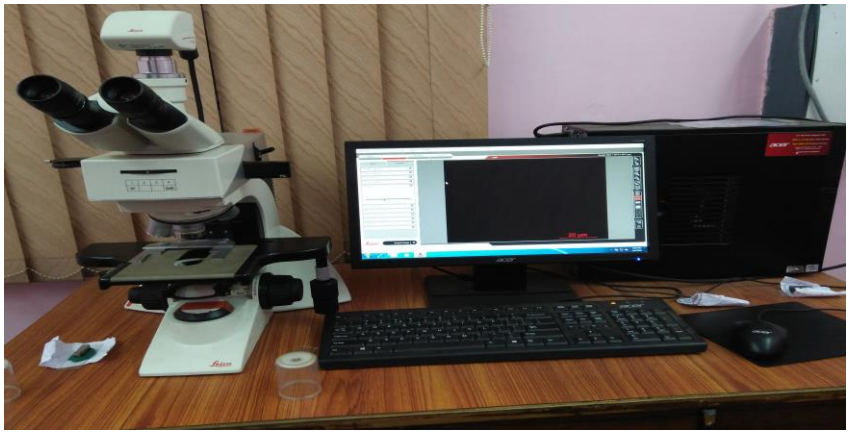

Figure 3.3 Photographic view of the microscope

Major specifications of the metallurgical microscope are:-

Model code : Leica L2
Model number : DMLM/118886055
Focusing : 2 gear focusing/ 3 gear focusing
Incident light : Sturdy incident light axis with 4x and 5x reflector turrets
Power supply : 90-250 for 12 V 100 W, frequency 50-60 Hz

Micro-hardness tester:

This instrument has been used to measure hardness at different regions of the weldment. There are several methods used for the measurement of hardness and each method is based on a defined principle. In the present study, hardness of all the samples has been measured by a Leco LM 248AT micro-hardness tester (Figure 3.4). Some important specifications are also mentioned. It is a Vickers hardness tester which is used to determine the micro-hardness of welded samples. Vickers indenter made of diamond in the form of square based pyramid is used for indenting purpose. Hardness values are in Vickers scale i.e., HV.

Figure 3.4 Photographic view of the Leco LM248AT micro-hardness tester

Specifications of micro-hardness tester:-

Model number : LM 248AT
Software : Amh 43
Zoom : 10x – 50x
Indentation load : 10 gf – 1 kgf

SEM Equipment

This instrument has been used to visualize the weld beads at varied magnifications. Study under scanning electron microscope has revealed crack, discontinuities and some other

features in the weld beads. The photographic view of the SEM is given in Figure 3.5. Some relevant information of this instrument includes:

Figure 3.5 Photographic view of the set-up of scanning electron microscope

Specifications of SEM Equipment:-

Make : Jeol
Model : JSM 6300
Electron resolution : 1.0 nm (at 15 kV)
Electron optics : electron gun

Besides the equipment and instruments mentioned above, power hack saw and shaping machine have also been required for preparing the specimens for hardness testing, microstructural studies, tensile testing etc.

3.2.2 BASE MATERIALS, FLUX AND ELECTRODE WIRE

In the present study, each of the nine samples, ferritic stainless steel sheet and mild steel sheet both having dimensions of 50 mm x 50 mm x 8 mm are welded by submerged arc welding. V edge preparation with 55^{o} included angle has been done. Low carbon steel electrode: ESAB SA1 (E8) of 2.5 mm diameter has been used. Granular flux of basicity index of 1.4 (OK flux 10.71L) is used in this study. Mild steel AISI 1018 (0.10% Carbon with other usual elements) is used in the present work. Chemical composition of AISI 409 ferritic stainless steel, AISI 1018 mild steel and electrode wire are given in the Table 3.3, Table 3.4 and Table 3.5 respectively.

Table 3.3 Chemical composition of AISI 409 stainless steel

Composition	C	Cr	Ni	Mn	Ti	Si	P	S
Wt %	Max 0.08	10.05 – 11.75	0.50	Max 1.00	6xC – 0.75	Max 1.00	Max 0.045	Max 0.02/0.03

Table 3.4 Chemical composition of AISI 1018 mild steel

Composition	C	Fe	Mn	P	S
Wt %	0.14 - 0.20	98.81 - 99.26	0.60 – 0.90	Max 0.04	Max 0.05

Table 3.5 Chemical composition of filler wire ESAB SA1 (E8)

Composition	C	Mn	Si	S	P	Cu
Wt %	0.08	1.45	0.15	0.02	0.02	0.2

3.3 EXPERIMENTAL PROCEDURE

In the present investigation, dissimilar welding between ferritic stainless steel and mild steel has been done. Nine butt joints are made. Thickness of each sample is 8 mm; dimensions of both the materials are: 50 mm x 50 mm x 8 mm. V– edge preparation has been made on both the materials such that 55^0 included angle is formed (Figure 3.6). Ferritic stainless steel AISI 409 and mild steel AISI 1018 have been joined together by submerged arc welding as mentioned earlier. Welding set-up has been prepared, tested and made ready for doing welding. Butt joints are made by welding two pieces; one of AISI 409 ferritic stainless steel and another of AISI 1018 mild steel. Nine welded samples are made, by carrying out welding at different levels of current, traverse speed and stick-out length, as per Taguchi's orthogonal array design of experiments, given in Table 3.2. Photographic view of the welding set-up and some sample specimens are shown in Figure 3.7 and Figure 3.8 respectively.

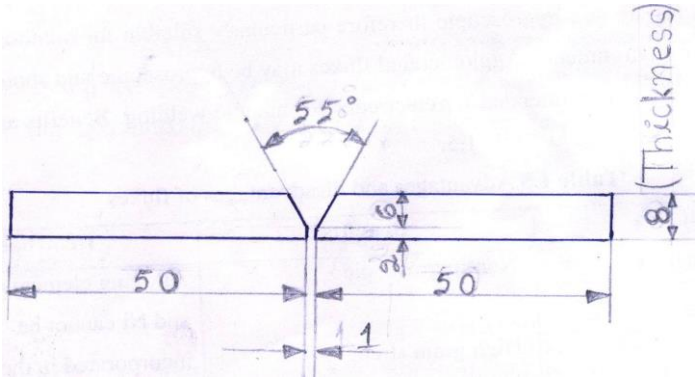

Figure 3.6 Dimensions of the specimen prepared for SAW

Figure 3.7 Welding set up

Figure 3.8 photographic views of some samples after welding

The width of each butt joint is made wide (50 mm) because from each sample joint,

several specimens are prepared for different tests/studies. These specimens are i) tensile test specimen (without notch), ii) notched tensile test specimen, iii) specimen for hardness test, iv) SEM test specimen and v) specimen for microstructural study. Specimens for microstructural study and hardness test are made shorter in size. For study under microscope, the specimens were ground, polished suitably and finally etched with a suitable etchant made up of ethylene glycol, nitric acid and ethanol.

The tensile test specimens (un–notched and notched) are obtained by machining to the derived shape and dimensions as given in Figure 3.9 (a-b).

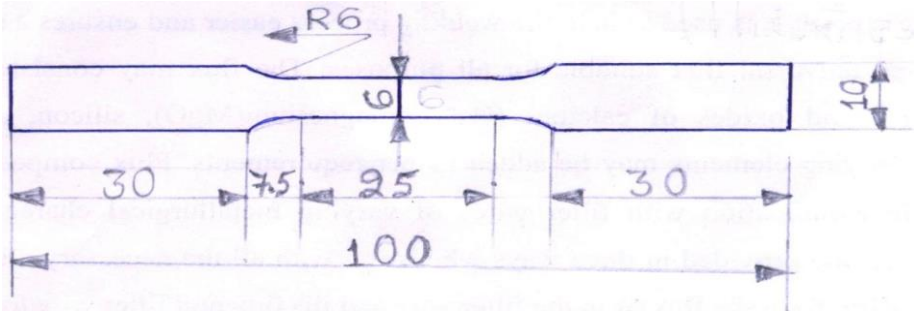

Figure 3.9(a) Dimensions of the un-notched specimen prepared for tensile test

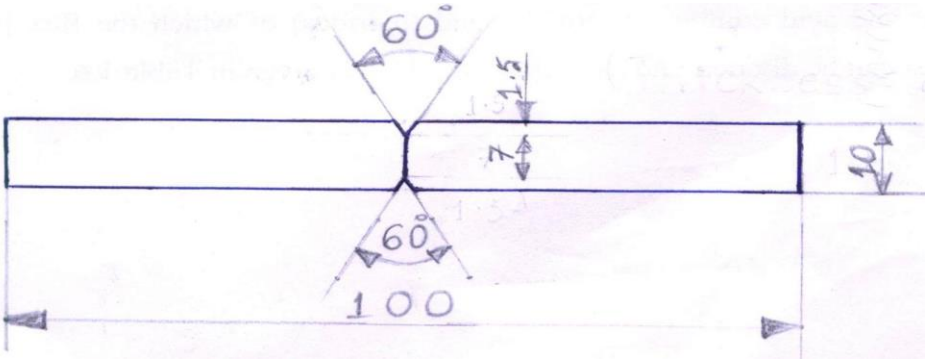

Figure 3.9(b) Dimensions of the notched specimen prepared for tensile test

Figure 3.10(a) and Figure 3.10(b) show the photographic view of tensile test specimens of un–notched and notched sample respectively.

Figure 3.10(a) Photographic view of tensile test specimen of un–notched sample

Figure 3.10(b) Photographic view of tensile test of notched specimen

Now tensile test specimens are made by machining the welded samples. Photographic view of a tensile test specimen is shown in Figure 3.10 (a-b). The dimensions of each of the tensile test specimens are given in Figure 3.9 (a-b). Tensile test specimens are tested on Instron universal testing machine, housed at fatigue fracture damage analysis (FFDA) Laboratory, Mechanical Engineering Department, Jadavpur University and relevant observations are made. A hydraulic jaw is used during testing for gripping the samples. During preparation of the tensile test specimen small portion is cut out from the samples for microstructural study. Again from each of these cut-out pieces, the middle portion has been taken out and finally prepared for microstructural study. Along with microstructural study, HAZ width has also been measured for all the nine samples. And in each case HAZ width at mild steel side and also at ferritic stainless steel side has been measured. Widths at several regions within HAZ have been measured and then averaged.

Visual Inspection of the nine samples has been performed after welding. From the welded samples, a small section has been cut out from the middle portion and finally prepared for the scanning electron microscopy, hardness test and subsequently for microstructural studies(as mentioned earlier).

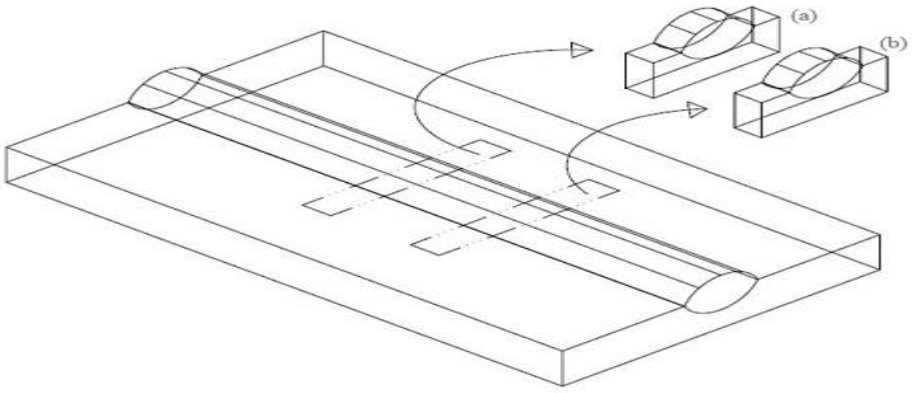

Figure 3.11 Sample preparations for (a) micro-hardness test (b) optical microscopy (under SEM & metallurgical microscope)

The cut out pieces (Figure 3.11) have been ground, polished and finally etched to obtain samples for microstructural studies. All the polished specimens are etched with the etchant

made up of 20 ml ethylene glycol, 20 ml HNO_3, and 100 ml ethanol. The microstructures of the weldments are studied using Leica Microscope. Jeol SEM machine having modal no. JSM 6300 is used for the study of scanning electron microscopy. Micro-hardness test has also been performed for each of the samples. While doing this, hardness value has been measured at several points in different zones: weld metal, HAZ, and base metal. Leica micro-hardness tester has been used for this purpose.

The results of all the above mentioned experiments, tests and studies are given and discussed in the next chapter. Process optimization, data analyses and mathematical modelling have also been done, based on the observed results. This is included in chapter 5.

CHAPTER 4

4. RESULTS AND DISCUSSION

The details of experimental plan, procedure and set up have been discussed in Chapter 3. In this chapter the experimental results are presented and discussed, which include discussion on microstructural study as well.

4.1 VISUAL INSPECTION: RESULTS AND DISCUSSION

After welding, visual inspection of the welded samples has been carried out and the observed results are summarized in Table 4.1. Results of visual inspection indicate that defects like lack of penetration, undercut, incomplete fusion, non-uniform reinforcement etc. have occurred in some of the samples. And under certain parametric conditions no defects are found in a few samples by visual inspection like sample nos. 1, 6 and 9. These defects found in several samples may be due to fluctuation of voltage, incorrect parameter setting, lack of environment suitability and also may due to semi-automatic machine set up etc. These defects may come from any irregularities in the base metal and filler wire as well. [Current is denoted by (C), speed is denoted by (T) and stick-out length is denoted by (S)].

Table 4.1 Results of visual inspection

Sample No.	Sample Code	Defects
1.	C-1/T-1/S-1	No defect
2.	C-1/T-2/S-2	Non uniform bead width
3.	C-1/T-3/S-3	Non uniform width
4.	C-2/T-1/S-2	Non uniform reinforcement
5.	C-2/T-2/S-3	Lack of penetration
6.	C-2/T-3/S-1	No defect
7.	C-3/T-1/S-3	Incomplete penetration
8.	C-3/T-2/S-1	Undercut at one end
9.	C-3/T-3/S-2	No defect

For undercut there are several reasons like excessive voltage, too large melt area of the

base metal, high travel speed, low heat input etc. The major defect is lack of penetration and it occurs due to faster speed, improper selection of welding parameter, improper washing and cleaning, presence of impurities, oxides and scales etc.

4.2 RESULTS OF TENSILE TEST AND DISCUSSION

Tensile test has been performed on Instron machine, to examine the regions from where failure/fracture has occurred and to find important mechanical properties of the welded samples. The results of tensile tests are given in Table 4.2 and 4.3.

4.2.1 RESULTS OF TENSILE TEST OF UN-NOTCHED SPECIMENS AND DISCUSSION

The results include yield strength (MPa), ultimate tensile strength (MPa), breaking strength (MPa), percentage elongation (%) and elongation at break (mm) of the welded samples. The tensile test results indicate that for most of the samples, tensile strength is satisfactory. During tensile testing it is noted that, excepting one sample (sample no. 4), failure has occurred within the base material or through the adjacent HAZ region at mild steel side. It is generally desired that failure does not occur within the weld region.

Table 4.2 Tensile test result of welded specimens without notch

Sample No.	Sample Identity	Ultimate tensile strength (MPa)	Percentage elongation (PE)	Yield strength (MPa)	Breaking strength (MPa)	Elongation at break (mm)
1	C-1/T-1/S-1	455	14.0	198	93	3.6
2	C-1/T-2/S-2	447	10.6	299	91	2.6
3	C-1/T-3/S-3	494	17.8	185	152	4.7
4	C-2/T-1/S-2	423	12.9	176	85	3.3
5	C-2/T-2/S-3	551	14.0	182	113	3.5
6	C-2/T-3/S-1	606	17.6	188	122	4.4
7	C-3/T-1/S-3	501	11.7	196	101	3.2
8	C-3/T-2/S-1	442	18.8	204	89	4.8
9	C-3/T-3/S-2	545	18.9	198	111	4.7

From Table 4.2 it is found that under some parametric conditions of current, traverse speed and stick-out length, ultimate tensile strength values are remarkably good. For the sample no. 6, ultimate tensile strength is maximum and for the sample no. 4, ultimate tensile strength is minimum. The maximum (sample no. 6) and minimum (sample no. 4) values of UTS are 606 MPa and 423 MPa respectively.

UTS for all samples lies between 440 MPa – 551 MPa except for sample no. 4 and sample no. 6 in which it is found to be 423 MPa and 606 MPa respectively. Only for a few samples UTS is found to be a little bit low but not significantly low (sample nos. 2, 4 and 8). The UTS value of sample no. 6 is more i.e., 606 MPa this may be because of formation of intermetallic components or complex combination of different base materials and filler rod and the resulting behavior during melting and subsequent cooling under particular parametric conditions. The values of percentage elongation are quite satisfactory ranging from 12.9 % - 18.9 % for all the samples except sample nos. 2 & 7 where these values are 10.6 % and 11.7 % respectively. This may be linked with the defects found in the welded specimens in visual inspection. The highest value of percentage elongation is observed to be 18.9 % (for sample no. 9). For many other samples also (like sample nos. 3, 6, 8 and 9) sufficiently high values of percentage elongation are found. The lowest value of percentage elongation is exhibited in the sample no. 2 (10.6 %). In so far as yield strength is concerned, the results given in Table 4.2 are found to be satisfactory. Maximum yield strength (299 MPa) is observed for sample no. 2 and minimum yield strength (176 MPa) is found for sample no. 4. The breaking strength is found in the range from 91 MPa to 152 MPa for all samples except sample nos. 4 and 8, for which the values are 85 MPa and 89 MPa respectively. The highest value of breaking strength is observed in sample no. 3 and lowest value is found in sample no. 4. Elongation at the break is satisfactorily good, it is within the range of 2.6 mm to 4.8 mm. The highest value of elongation at the break is found in sample no. 8 and the lowest value of elongation at the break is found in sample no. 2.

The above results point to the fact that dissimilar welding between ferritic stainless steel and mild steel, done by submerged arc welding using mild steel filler wire, has produced satisfactory joint (because excepting sample no. 4, no one has failed within the weld region and because UTS and PE values for most of the samples are fair). Stress-Strain curves, corresponding to tensile test results of all the samples are shown in Figures 4.1 (a) – 4.1(i). Typical ductile behavior is observed in almost all the stress – strain curves.

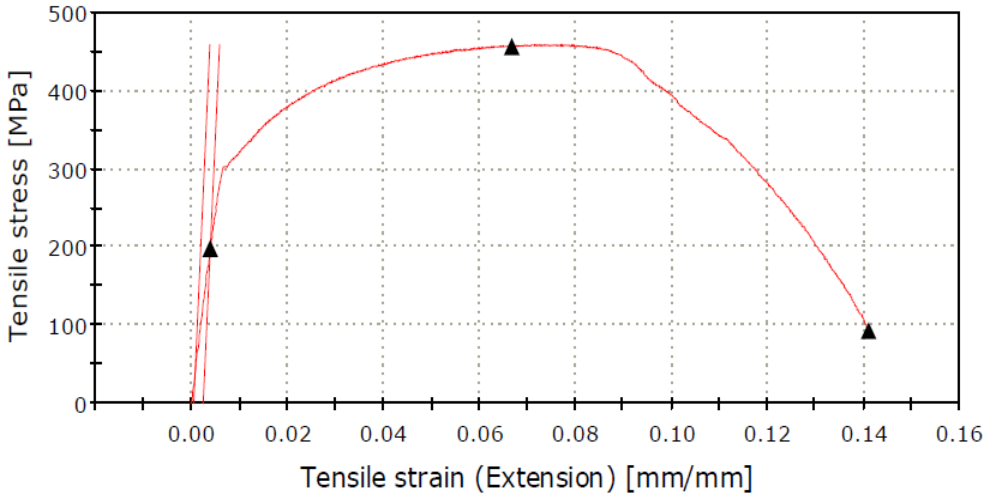

Figure 4.1(a) Stress-strain curve of sample no. 1

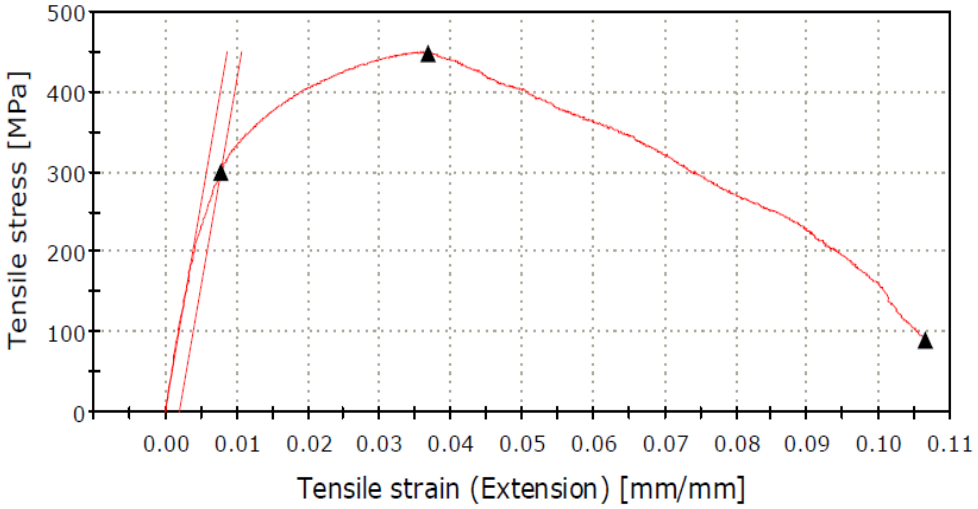

Figure 4.1(b) Stress-strain curve of sample no. 2

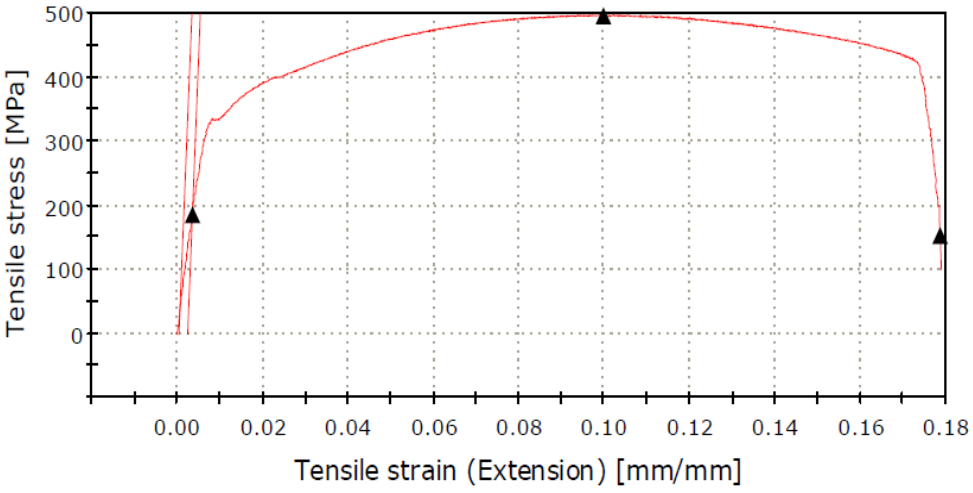

Figure 4.1(c) Stress-strain curve of sample no. 3

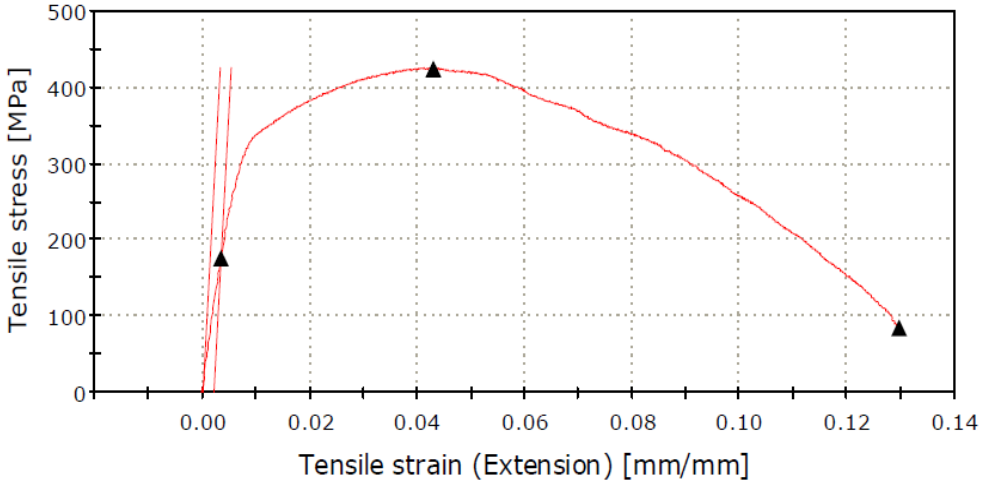

Figure 4.1(d) Stress-strain curve of sample no. 4

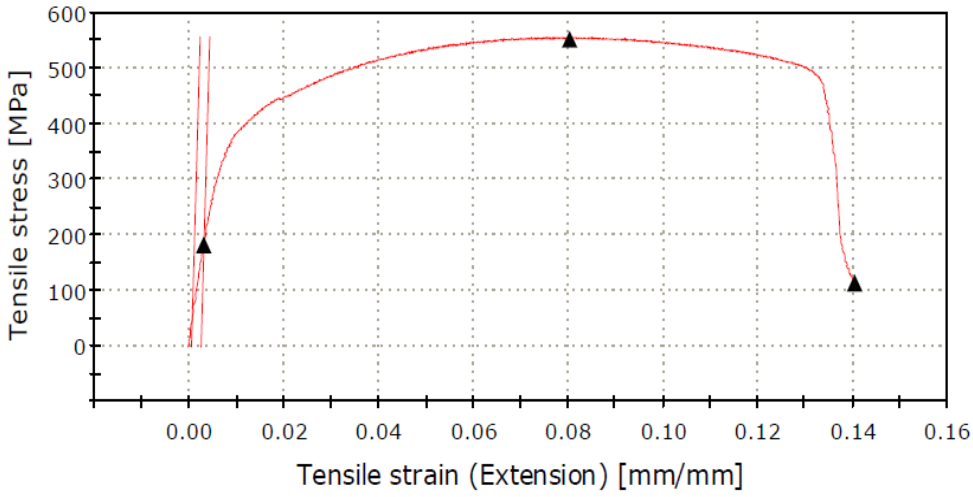

Figure 4.1(e) Stress-strain curve of sample no. 5

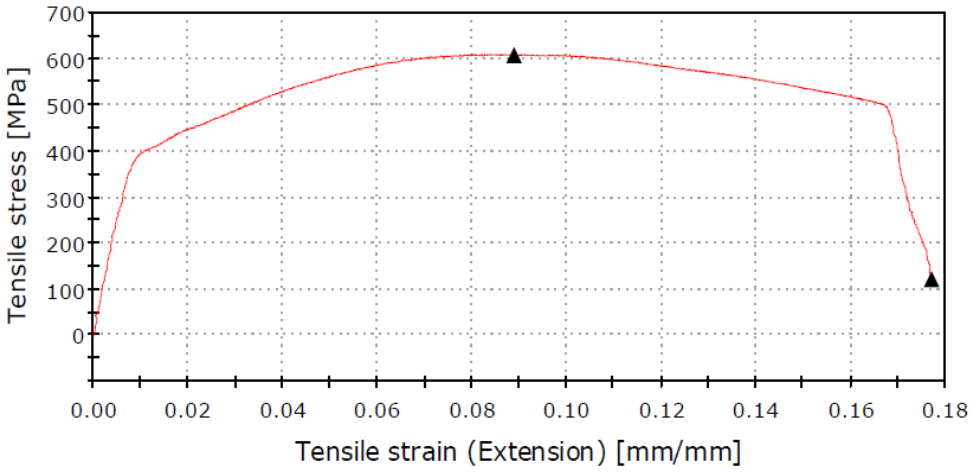

Figure 4.1(f) Stress-strain curve of sample no. 6

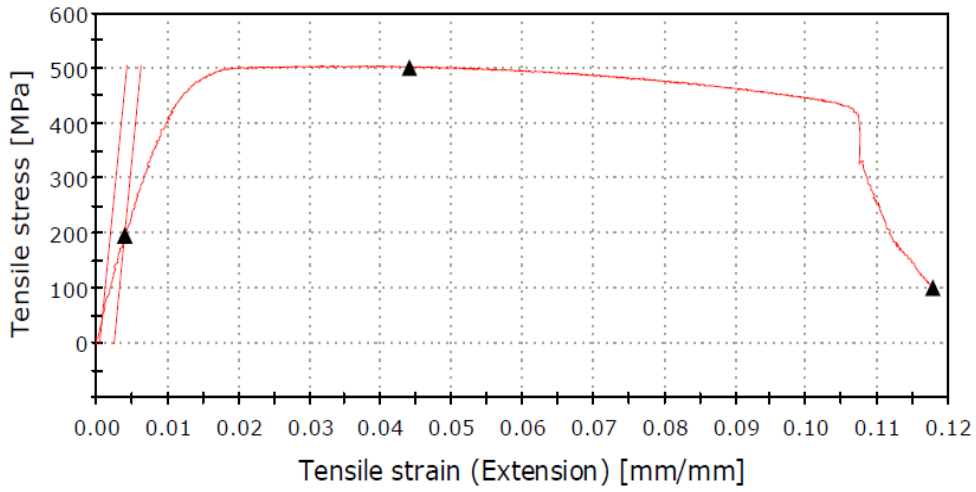

Figure 4.1(g) Stress-strain curve of sample no. 7

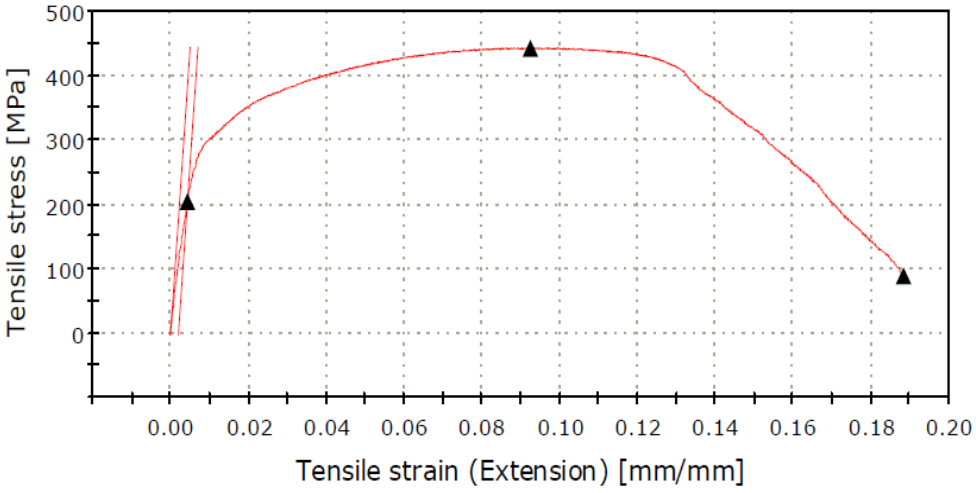

Figure 4.1(h) Stress-strain curve of sample no. 8

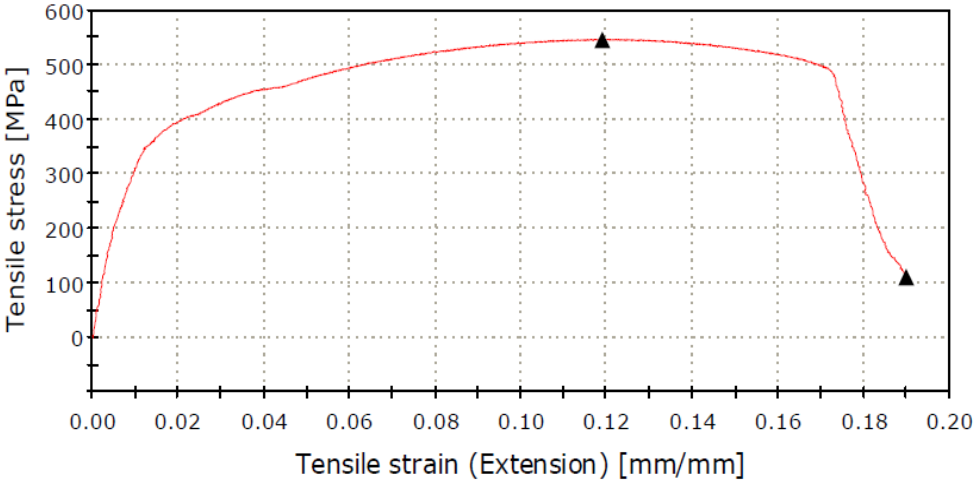

Figure 4.1(i) Stress-strain curve of sample no. 9

Further it may be mentioned that the weld zone in the joint, is the result of i) ferritic stainless steel base material, ii) mild steel base material and iii) mild steel electrode (filler wire). The levels of the input parameters, heat input, and cooling rate influence the microstructures developed during heating and subsequent cooling, apart from the fact that compositions of dissimilar materials and dilution have direct effect on the metallurgy and mechanical properties of the joint. These can be discussed again while discussing about study of microstructures. However, in so far as the strength of the joint is concerned, the results of the study reveal that under suitable combination of input parameters, sound joint is obtained. UTS is found to be in between the UTS values of AISI 409 (ferritic stainless steel) and AISI 1018 (mild steel). In certain cases UTS of the joint is very near to UTS of AISI 409, or more. The UTS of mild steel AISI 1018 and ferritic stainless steel AISI 409 is 440 MPa and 560 MPa respectively.

4.2.2 TENSILE TEST RESULTS OF NOTCHED SPECIMENS

The results include ultimate tensile strength (MPa), percentage elongation (%), yield strength (MPa), breaking strength (MPa), and elongation at break (mm) of the welded samples. The tensile test results indicate that for most of the samples, tensile strength is satisfactory. The purpose of this set of experiments is to identify whether the variation of the input parameters has resulted in change in the mechanical properties, specifically in the weld region. Intentionally, therefore, the centre portion of the weld is notched, so that the joint fails at the notch i.e. within weld as cross section is made smaller at that region. Ultimate strength is found to be good enough in almost each of the samples. At all combination of parameters joint strength is sufficiently good with the exception for sample no. 2. Thus, it appears that for C (250 A) i.e. current at level 1, traverse speed T (50.0 mm/s) at level 2 and stick–out length S (20 mm) at level 1, is not good for making a strong joint. It may be noted that for few samples ultimate strength and percentage elongation are observed to be very high. This needs further investigation from material science and metallurgical points of view. Some discussion in this respect can be made while discussing on hardness results and microstructural study. However, in the future plan of work, more detailed study in this respect is expected to be carried out.

From Table 4.3 it is found that under some parametric conditions of current, traverse speed and stick-out length, ultimate tensile strength values are remarkably good. For the sample no. 5, ultimate tensile strength is maximum and for the sample no. 2, ultimate tensile strength is minimum. The maximum (sample no. 5) and minimum (sample no. 2) value of UTS are 657 MPa and 447 MPa respectively.

Table 4.3 Tensile test result of welded specimens with notch

Sample No	Sample Identity	Ultimate tensile strength (MPa)	Percentage elongation (PE)	Yield strength (MPa)	Breaking strength (MPa)	Elongation at break (mm)
1	C-1/T-1/S-1	539	4.2	182	538	1.06
2	C-1/T-2/S-2	447	10.6	280	160	10.6
3	C-1/T-3/S-3	632	49.4	459	146	12.3
4	C-2/T-1/S-2	526	5.7	166	467	1.4
5	C-2/T-2/S-3	657	49.6	224	139	12.4
6	C-2/T-3/S-1	592	47.4	357	119	11.8
7	C-3/T-1/S-3	599	45.5	152	137	11.3
8	C-3/T-2/S-1	507	7.3	242	503	1.82
9	C-3/T-3/S-2	615	48.5	352	191	12.1

The above results point to the fact that dissimilar welding between ferritic stainless steel and mild steel, done by submerged arc welding- using mild steel filler wire, has produced satisfactory joint. Stress-strain curves, corresponding to tensile test results of all the notched samples are shown in Figures 4.2(a) - 4.2(i). Typical ductile behaviour is observed in almost all the stress – strain curves.

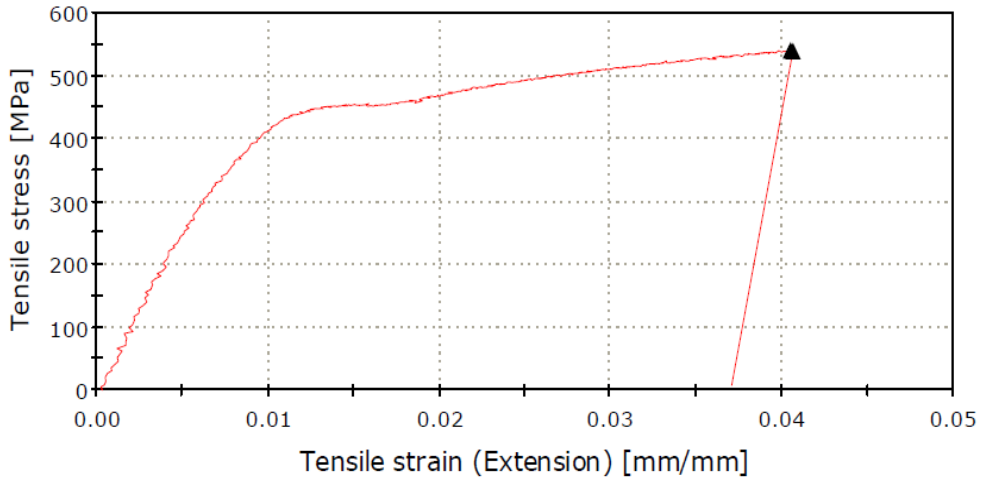

Figure 4.2(a) Stress-strain curve of sample no. 1

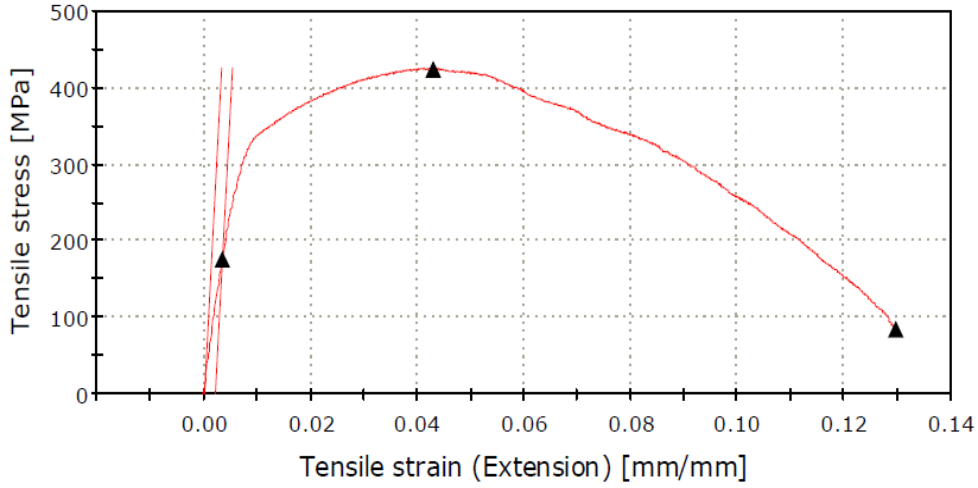

Figure 4.2(b) Stress-strain curve of sample no. 2

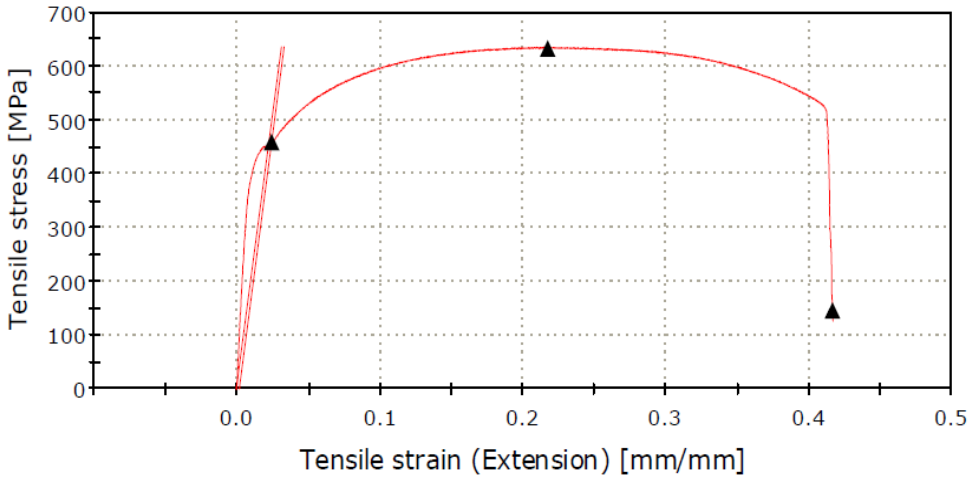

Figure 4.2(c) Stress-strain curve of sample no. 3

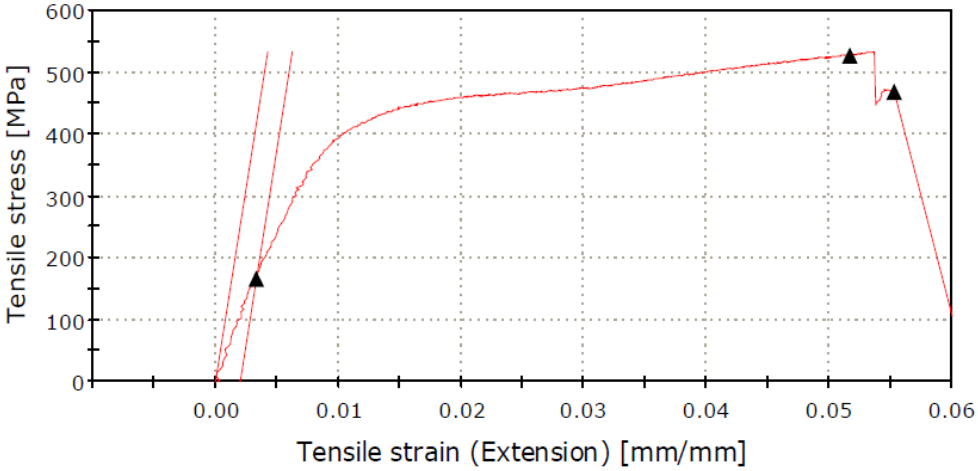

Figure 4.2(d) Stress-strain curve of sample no. 4

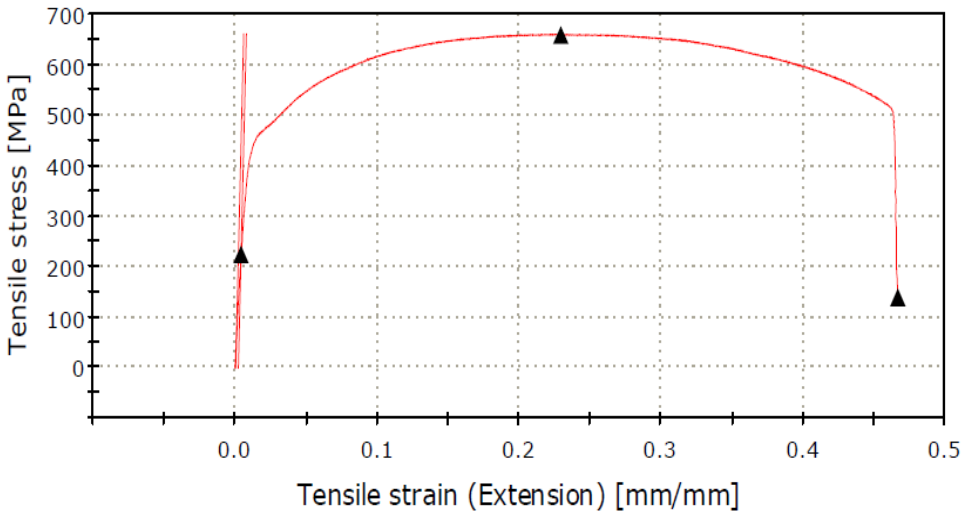

Figure 4.2(e) Stress-strain curve of sample no. 5

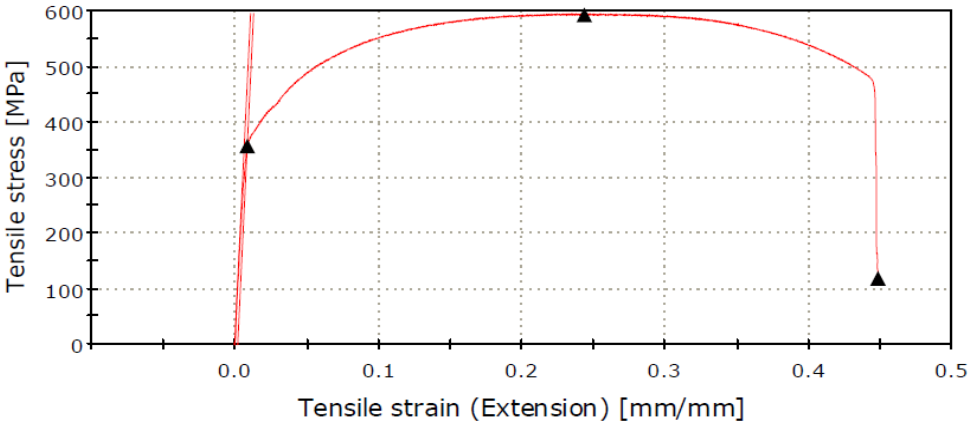

Figure 4.2(f) Stress-strain curve of sample no. 6

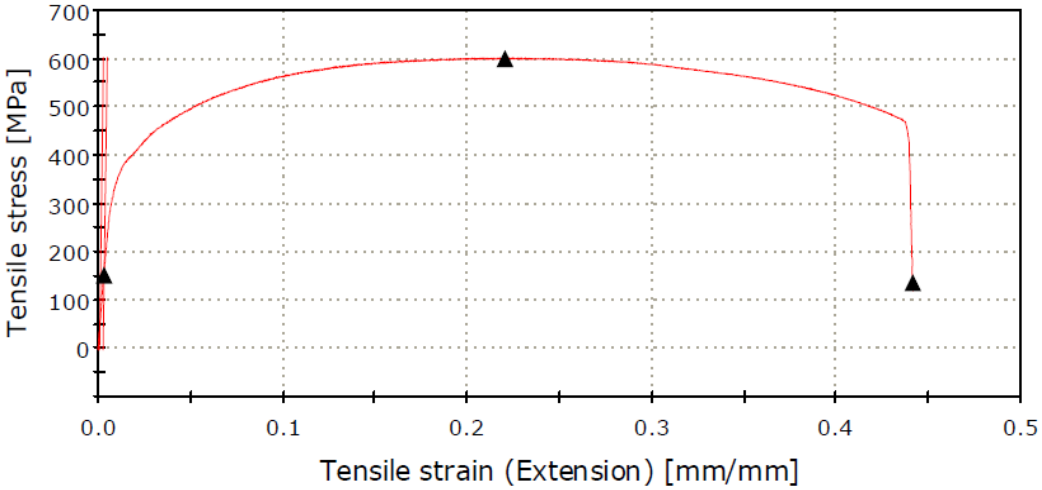

Figure 4.2(g) Stress-strain curve of sample no. 7

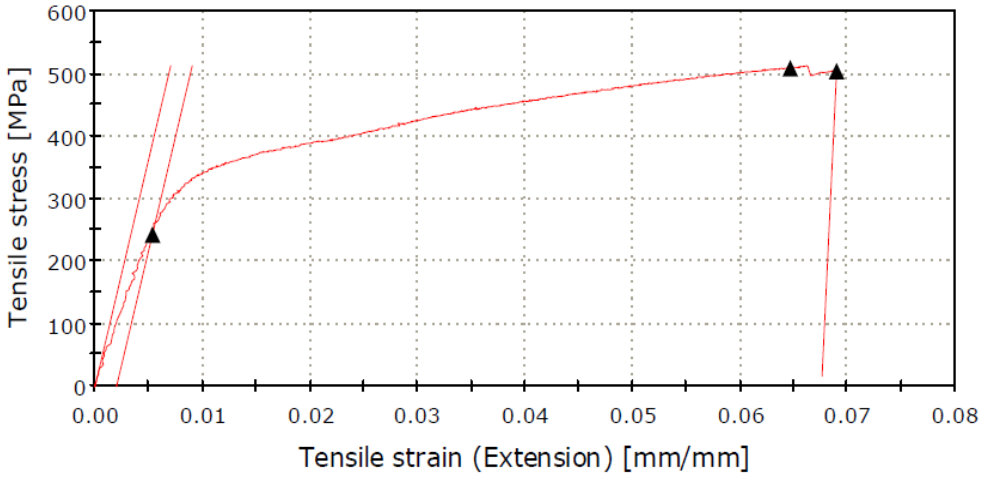

Figure 4.2(h) Stress-strain curve of sample no. 8

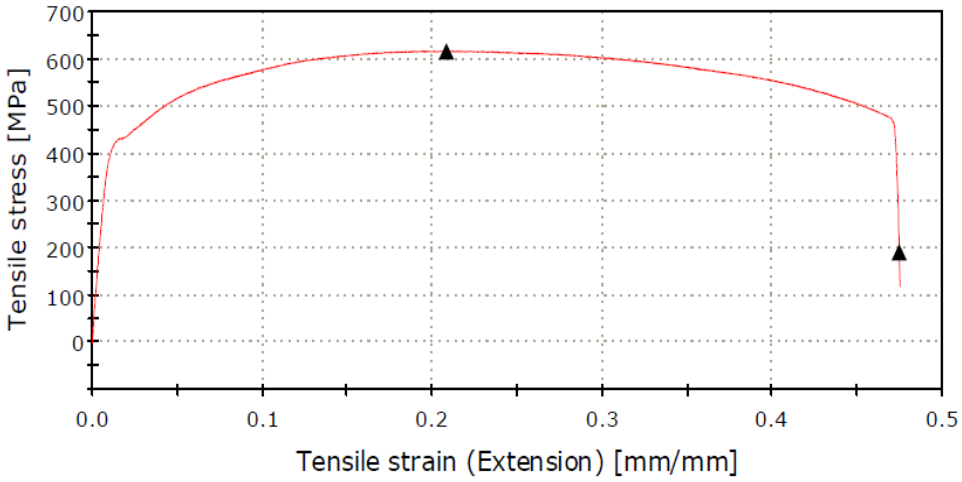

Figure 4.2(i) Stress-strain curve of sample no. 9

The results of tensile tests of both with and without notch welded samples are used further for ANOVA, mathematical modelling and process optimization. These are included in chapter 5.

4.3 RESULTS OF MICRO-HARDNESS TEST AND DISCUSSION

Hardness measures the resistance of a material to indentation. It is a very important property related to welded joint because different types of microstructures are observed in different zones: base metal, HAZ and weld zone of the weld sample. Different zones usually exhibit different hardness characteristics. Generally hardness indicates resistance to abrasion, scratching, shaping etc. With increase in hardness, resistance to wear increases, but increase in hardness also increases brittleness of a material.

Hardness test has been carried out at different zones of all the nine samples in Vicker's scale (i.e. in HV). For each sample, hardness has been measured at 5 different positions around 1, 2, 3, 4 and 5 as shown in Figure 4.3. At each position hardness has been measured thrice near about that location and average value is determined. The average hardness values at five locations are listed in Table 4.4. Changes in the hardness value corresponding to the change in locations of the welded samples are shown by using graphs in Figures 4.4(a) - 4.4(i). From these figures it is found that for most of the samples, the nature of variation in hardness values along the position 1 - 2 – 3 – 4 - 5 is almost similar.

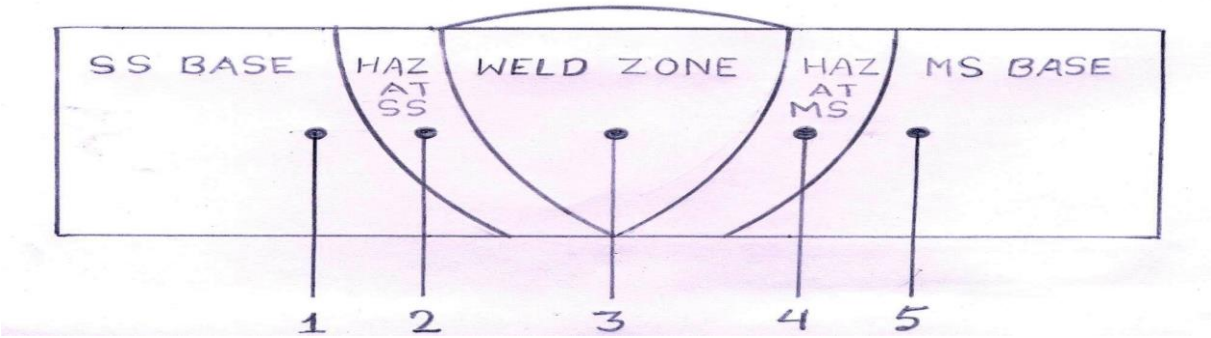

Figure 4.3 Schematic diagram showing positions of hardness measure

Table 4.4 Micro-hardness in HV values of welded samples

Sample no.	Ferritic stainless steel base zone (1)	HAZ zone near ferritic stainless steel (2)	Weld zone (3)	HAZ zone near mild steel (4)	Mild steel base zone (5)
1	386.2	327.76	339.2	292.4	168.2
2	388.8	322.46	328.76	326.8	170.36
3	386.16	333.03	348.5	287.9	172.26
4	385.1	309.96	334.43	337.1	167.16
5	387.25	321.1	342.3	312.4	171.8
6	389.46	376.23	325.3	302.9	169.86
7	386.7	319.0	336.73	347.8	170.6
8	388.6	312.83	337.43	279.9	171.0
9	384.86	320.53	338.16	367.8	169.8

Corresponding hardness vs. position graphs are drawn for all the samples and are shown in the Figure 4.4(a) - Figure 4.4(i).

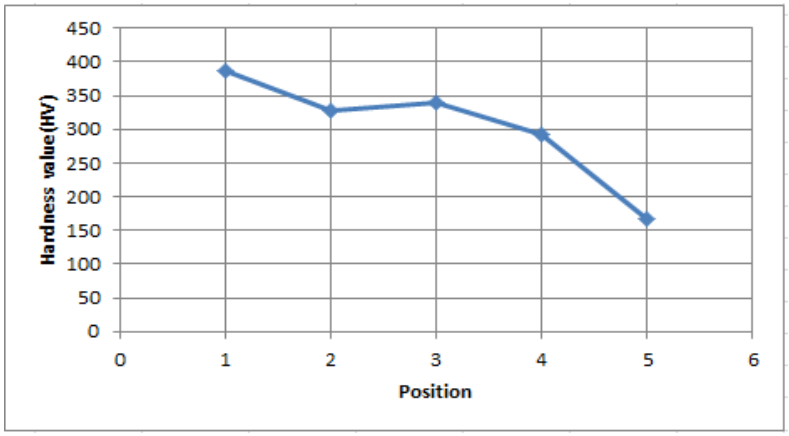

Figure 4.4(a) Hardness graph for sample no. 1

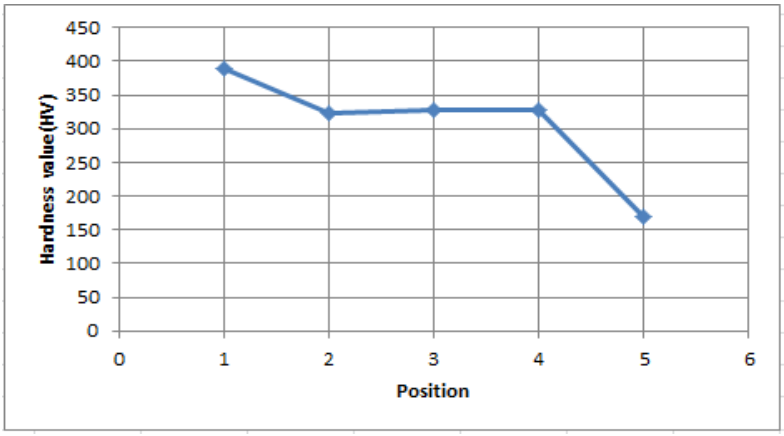

Figure 4.4(b) Hardness graph for sample no. 2

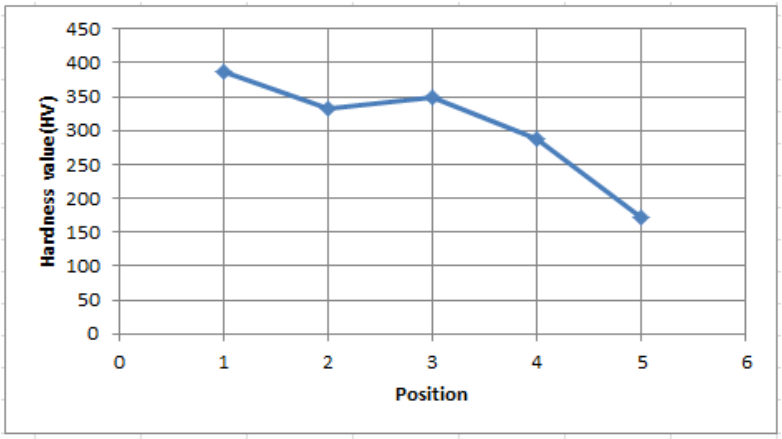

Figure 4.4(c) Hardness graph for sample no. 3

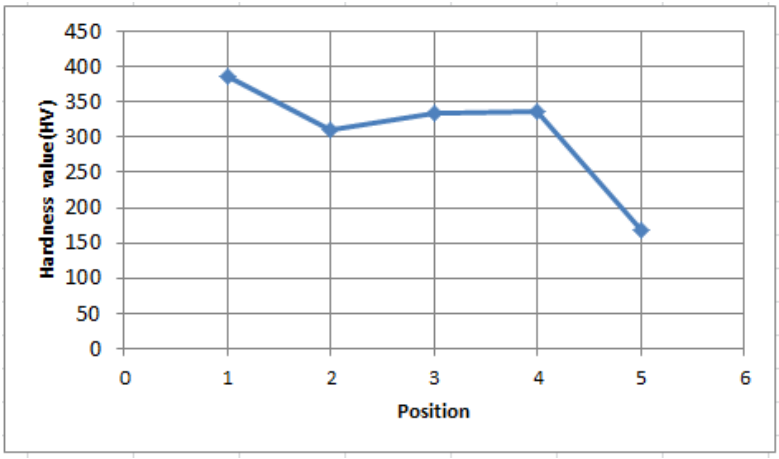

Figure 4.4(d) Hardness graph for sample no. 4

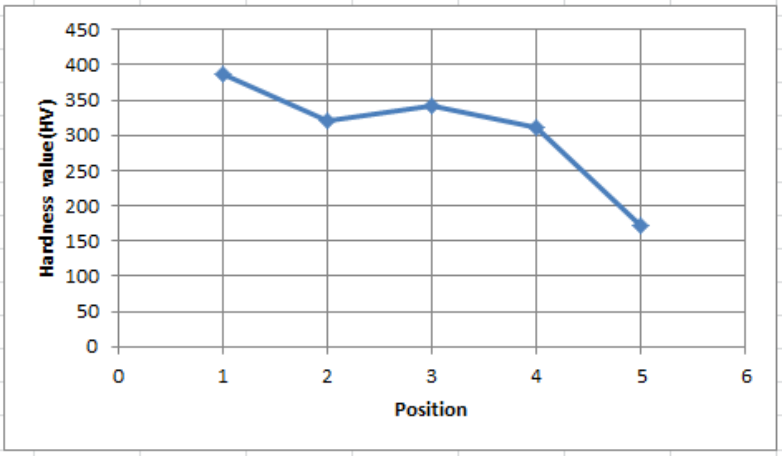

Figure 4.4(e) Hardness graph for sample no. 5

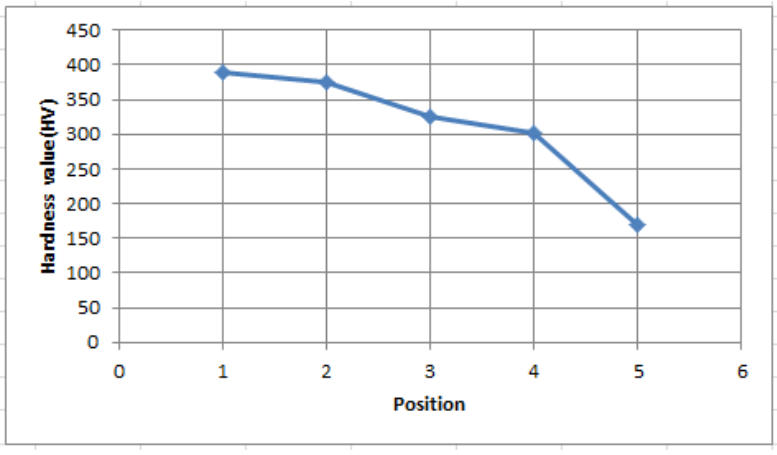

Figure 4.4(f) Hardness graph for sample no. 6

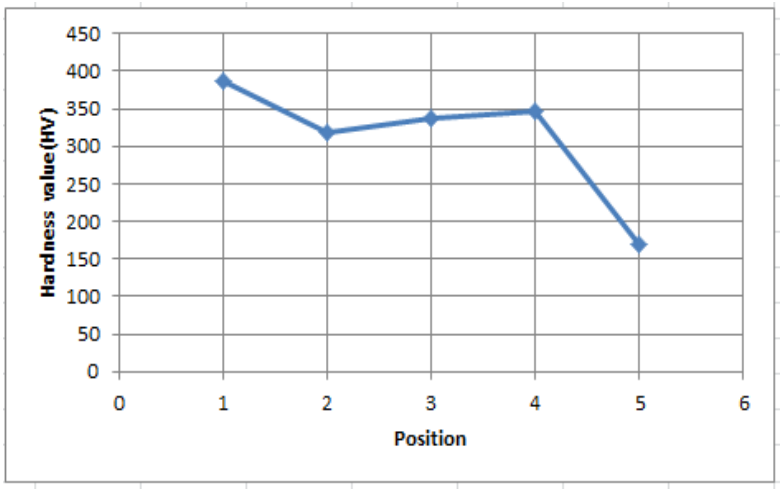

Figure 4.4(g) Hardness graph for sample no. 7

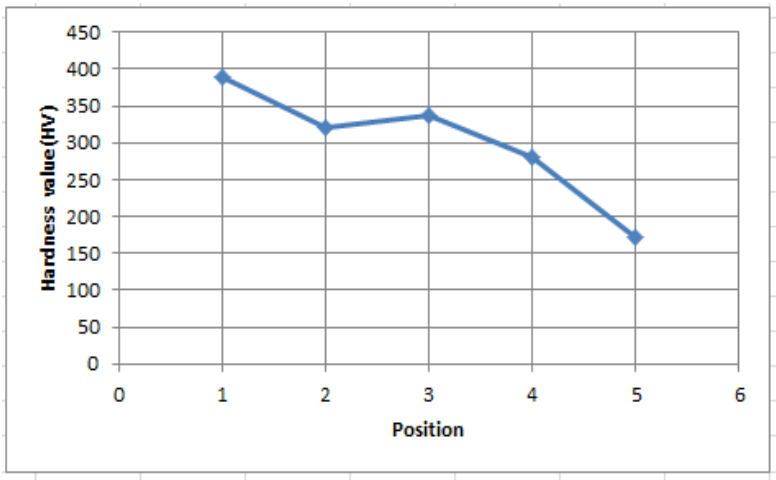

Figure 4.4(h) Hardness graph for sample no. 8

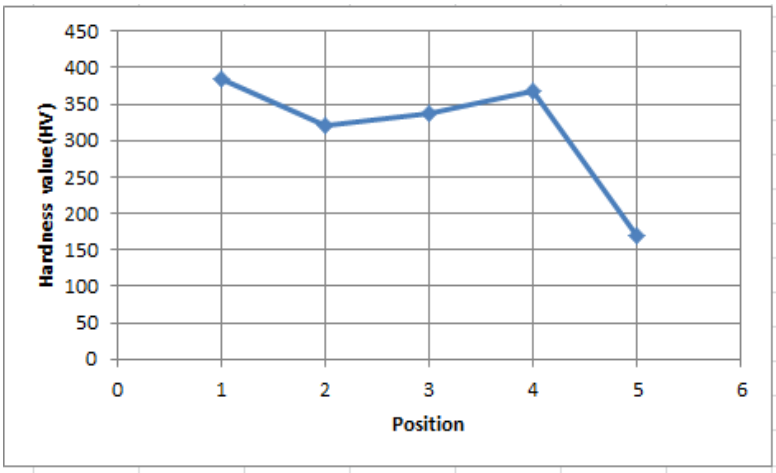

Figure 4.4(i) Hardness graph for sample no. 9

Within the weld, excepting for sample no. 6, hardness is generally found to be slightly more than hardness of HAZ at both sides. As obvious, hardness at stainless steel base material is highest among the hardness at different zones. However, there is slight increase in hardness value within the region mild steel base to HAZ and slight decrease in hardness value within the region ferritic stainless steel base to HAZ in sample numbers 1, 2, 3, 4, 5 and 8. And also for these samples hardness value increases from HAZ region to weld region from the both sides of the base materials. For the sample no. 6 hardness value continuously decreases from ferritic steel base to mild steel base. In the sample nos. 7 and 9, the value of hardness inreases in the HAZ region of mild steel. Still, hardness values in both HAZ and weld metal are found to be higher than mild steel base metal hardness, in all the samples but it is lesser than ferritic stainless steel base metal hardness. It is found that hardness ranges from 384.86 – 389.46 HV at ferritic stainless steel base metal, 309.96 – 376.23 HV at HAZ region near ferritic stainless steel, 325.3 – 348.5 HV at weld, 267.7 – 367.8 HV at HAZ region near mild steel and 167.16 – 172.26 HV at mild steel region.

In welding, uniform mechanical properties and microstructures throughout the different regions (weld metal, HAZ and base metal) are desired, though very difficult to achieve. Hardness is one of the several characteristics, which represent quality or mechanical property of the weldment. The data in Table 4.4 suggest that, variation in the levels of the input parameters has influenced hardness of the welded samples at its different zones, though the trend of this variation is not same for all the samples. Hardness values in different regions of the welded samples also indicate the effect of heating and cooling cycle of the nine samples, made under varied conditions of welding. Now, weld consists of both parent material and electrode material. Compositions of these two materials are not exactly same, and in dissimilar welding there are three different materials. Further, heat input rate, cooling rate and many other factors influence the final microstructure of the weld metal. Hardness of weld metal is thus dependent on the development of the type of microstructure developed in the weld region. Variation of weld-metal hardness with respect to base metal, as found from the graphs and data can be attributed to the phenomena described above. Mechanical properties of weld are influenced by the properties of the base material, the levels of the input parameters, and many more factors. As mentioned earlier, it is desirable (though difficult) to achieve uniform properties of weld, HAZ and base material. Hardness values of base material of the different samples reveal the mechanical characteristics of the base/parent material. Hardness value of base material is measured adjacent to HAZ. Variation in base metal hardness may be due to some non-uniform characteristics of base metal arising out of a little amount of

variation in microstructure/composition of the parent material in nine samples, though all the pieces have been obtained from the same stock.

4.4 RESULTS OF HAZ WIDTH AND MICROSTRUCTURAL STUDY AND DISCUSSION

4.4.1 RESULTS OF HAZ WIDTH AND DISCUSSION

In case of single pass weld, the weld zone is generally divided into two main regions: the fusion zone, or weld metal, and the heat-affected zone (HAZ). Within the fusion zone, the peak temperature exceeds the melting point of the base metal, and the chemical composition of the weld metal will depend on the choice of welding consumables and the operating conditions. HAZ zone is the subsequent zone of fusion zone in which HAZ width of a C-Mn steel is the region heated from lower critical temperature (i.e., 723℃) to the temperature just below the melting point temperature of welded materials (i.e. 1464℃). HAZ width is a function of the process parameters of SAW process and these, in turns, depend on the heat input as heat input is the function of voltage, travel speed, wire feed rate, stick out etc. Table 4.5 shows the values of HAZ width variation of ferritic stainless steel side and mild steel side.

Table 4.5 HAZ width values of welded samples

Sample no.	HAZ width at FSS side in (microns)	HAZ width at MS side in (microns)
1	762.412	742.643
2	678.801	730.830
3	744.487	624.468
4	713.571	728.193
5	742.675	760.001
6	679.660	718.393
7	567.245	712.875
8	714.306	617.841
9	526.562	613.594

The value of HAZ width at ferritic stainless steel side lies between 678.801 µm to 762.412 µm. For the sample no. 7 and 9 the value of ferritic stainless steel HAZ width is low and these are 567.245 µm and 526.562 µm respectively. The range of HAZ width at mild steel

side is 613.594 µm–760.001 µm. For most of the samples, the HAZ width value of mild steel is more than that of ferritic stainless steel except for the sample nos. 1, 3 and 8. This may occur due to variation in heat input and input parameters.

The optimum setting of input variables has been found in order to minimize the HAZ width, which has been reported in the next chapter.

4.4.2 RESULTS OF MICROSTRUCTURAL STUDY AND DISCUSSION

Study of microstructures has been made for all the welded samples and the photographs are taken of base metal, HAZ and weld region by the Leica DM LM metallurgical microscope for each of the samples. Some typical microstructural views of several samples are shown in Figures 4.5-4.14. The microstructures reveal some variations. The reasons of these variations may be many, like varied parametric combinations, non-uniform manual mode of welding, joint and environmental conditions etc.

The microstructures of base materials: mild steel and ferritic stainless steel have been shown in Figure 4.5 (a) and Figure 4.5 (b) respectively. In the microstructure of mild steel ferrite is present at the grain boundaries of austenite which has later transformed to the pearlitic. For ferritic stainless steel the microstructure is the mixture of ferrite and chromium carbides ($Cr_{23}C_6$).

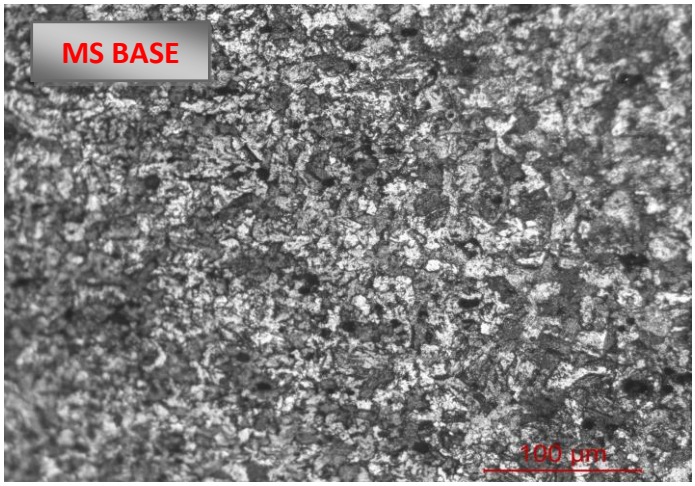

Figure 4.5(a) Mild steel base

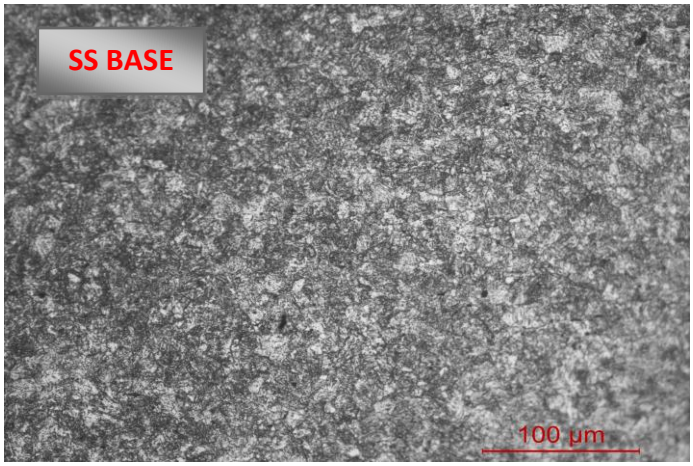

Figure 4.5(b) Stainless steel base

In the present work dissimilar welding of ferritic stainless steel to mild steel has been carried out by submerged arc welding with mild steel filler wire. So there are three types of material, mild steel base, mild steel wire and ferritic stainless steel base. So a complex type of weld microstructure is expected. Analysis is very critical. But still it can be observed that evidences of both mild steel and stainless steel are there in weld metal microstructure (Figure 4.6 (c)). Since the welding of the nine samples has been done at different conditions of input parameters, grain size and distribution of different phases are found to be a little bit varied among them. Microstructure also depends upon the characteristics of the base materials as well as filler material, particularly in dissimilar welding. It is a challenging work to study the microstructure in dissimilar welding where both the base materials are different and filler material is expected to play its role as well. Both the mechanical properties and thermal properties of materials are different. Microstructure also depends on welding conditions.

Microstructure also depends upon the heating cycle and cooling cycle. The temperature of welding has a considerable effect on microstructure. If large heat is applied then the flowability of material increases and it affects the HAZ. If low heat is available then different type of HAZ is found. If the cooling rate is high finer grains are produced but when cooling rate is low then coarse grain structure is produced.

Therefore, there are some variations in the microstructures of the welded regions. For example, in Figure 4.6 (c), in the weld region dominant phase is more or less equi-axed ferrite in which precipitation of minor amount of scattered titanium nitride or carbide is found. The grains are finer and uniformly distributed. In Figure 4.7 (c), it is observed that weld region consists relatively homogeneous ferrite grains in which accicular ferrite structure is formed within the grains. Figure 4.8 (c) indicates that welded region contains fully ferrite and precipitation of scattered carbides as well. In Figure 4.9 (c) the weld metal composition gives

the evidence of both ferrite and carbide regions with primary ferrite solidification. The grains are finer and uniformly distributed. In Figure 4.11 (c) carbon migration has been observed from carbon steel base metals across the fusion boundary in to the transition region. This migration can result in local microstructural changes in both the HAZ and transition region.

In general weld microstructure is found to contain fine grains with much less variation with change in input parameters. Hardness in weld zone as discussed earlier is found to be more or less consistent with the observations in microstructures.

The photo micrograph shown in Figure 4.6 (a) shows the fusion boundary region. It also reveals dramatic change in microstructure across the fusion boundary. Here weld metal and HAZ are mainly ferritic allowing ferritic grain growth across the fusion boundary. These boundaries may be sites for carbide precipitation, particularly if significant carbon migration from the base metal has occurred. It consists of pearlite with mixture of ferrite. In the mild steel side grains become finer and HAZ side it is mixture of ferrite and pearlite. Figure 4.8(a) shows the mixture of ferrite and precipitation of carbide in lesser amount. In this microstructure ferrite grains become finer. For the other microstructures there is no appreciable change has been occurred due to change of input parameters.

Ferritic phase is predominant in the HAZ region adjacent to stainless steel as shown in Figure 4.6(b). Figure shows that ferrite grains are quite large and grain boundaries have a continuous layer of martensite. The ‘peppery’ structure at the grain interiors represents carbides or nitrides. In Figure 4.9(b) also the same feature is observed. In addition, in the context of Figure 4.9(b), it may be mentioned that microstructure evolution along the fusion boundary in dissimilar welds made with stainless steel to other can be quite complex. In this situation, where the base is ferritic at temperature; near the melting point and the weld metal is ferrite, normal epitaxial growth may be suppressed. In this case ferrite weld metal solidifies in contact with ferrite base metal. The microstructure shown in Figure 4.6(b) has some precipitates of carbides and nitrides. In Figure 4.8(b) precipitation of carbides and nitrides are shown, as well as grains are also elongated along the direction of cooling. For the other microstructures no appreciable change has been noticed due to change of weld parameters.

In the same manner HAZ near mild steel side and HAZ near ferritic stainless steel side may be interpreted from all the relevant microstructures (Figures 4.6-4.14).

The above findings from microstructural study cannot be directly compared with published result. Because, though there are some publications relating to ferritic stainless steel to mild steel welding, no such publications show the use of mild steel as filler wire and

publications are very few in number. However, microstructures observed here are not far different from those observed by Lakshminarayanan et al.[52] and Andrey Belyakov et al. [54].

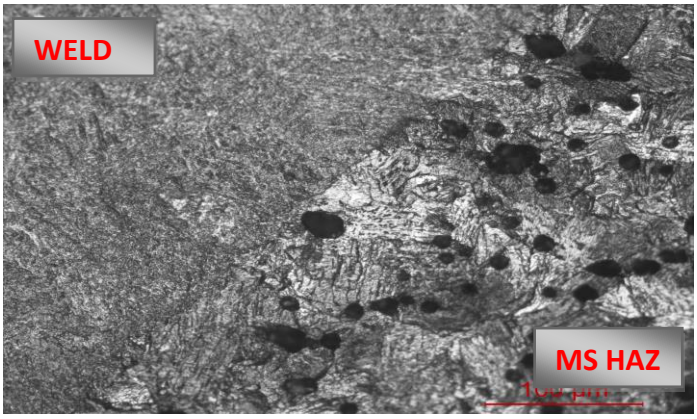

a) MS HAZ + WELD

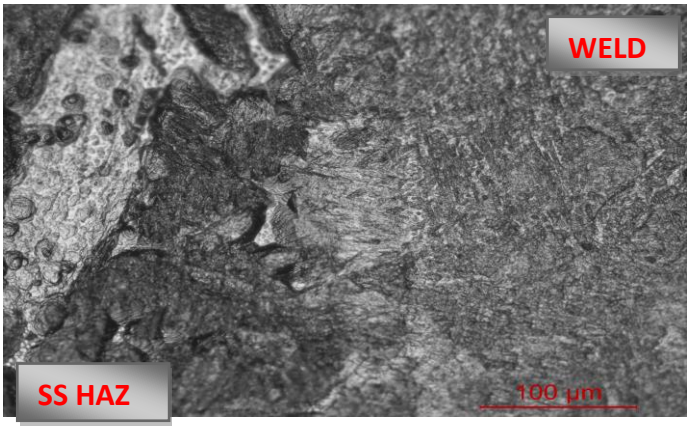

b) SS HAZ + WELD

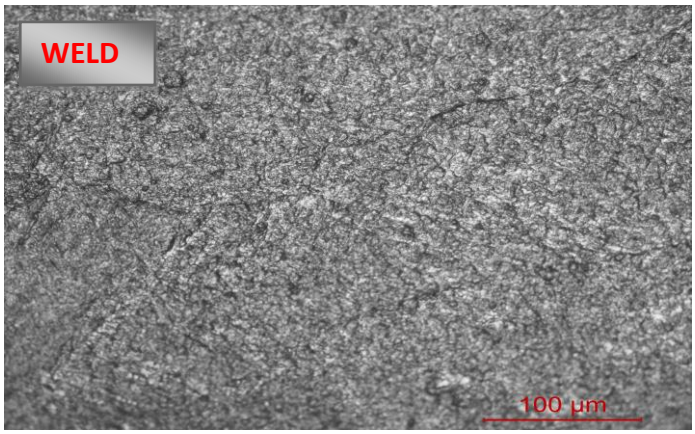

c) WELD REGION

Figure 4.6 Microstructures of sample no. 1

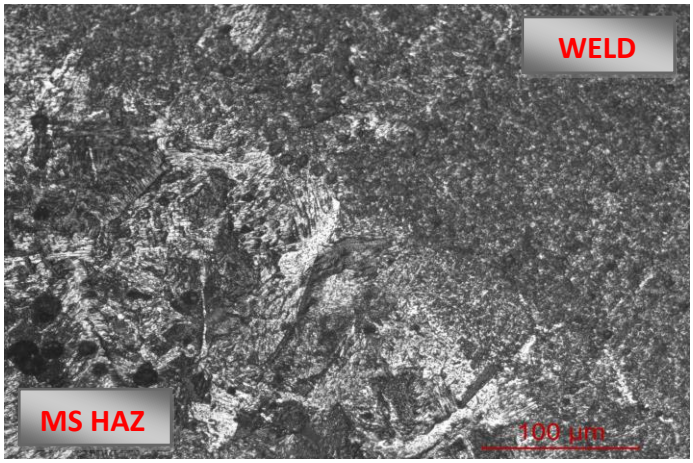

a) MS HAZ + WELD

b) SS HAZ + WELD

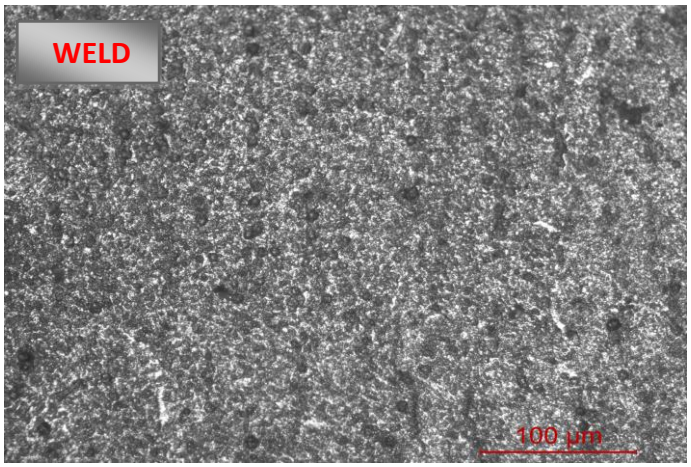

c) WELD REGION

Figure 4.7 Microstructures of sample no. 2

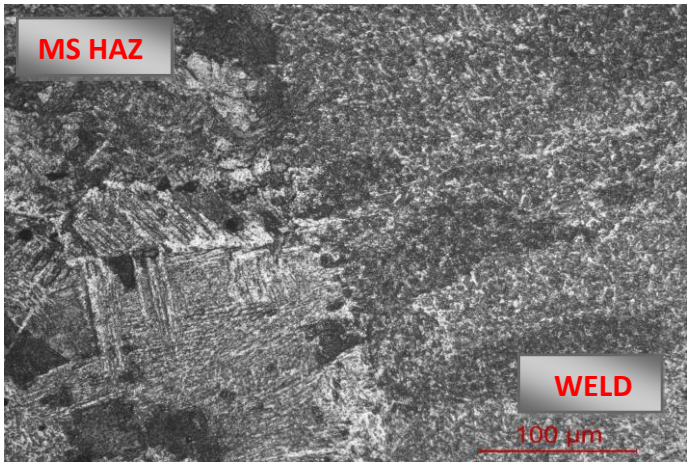

a) MS HAZ + WELD

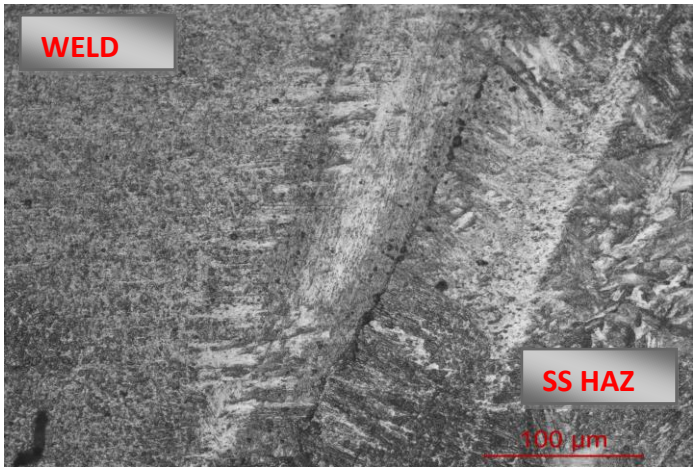

b) SS HAZ + WELD

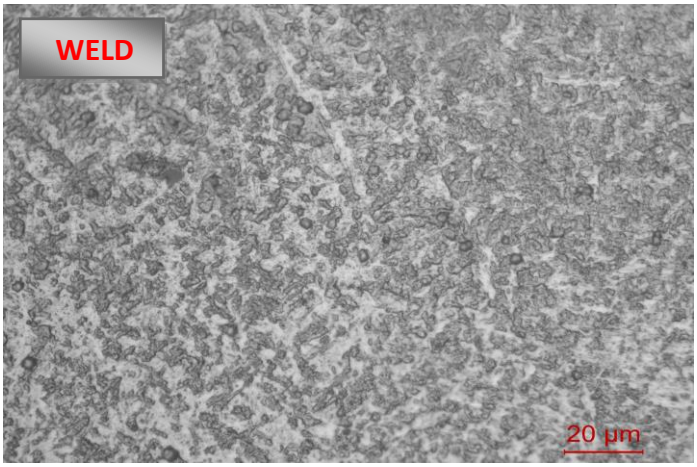

c) WELD REGION

Figure 4.8 Microstructures of sample no. 3

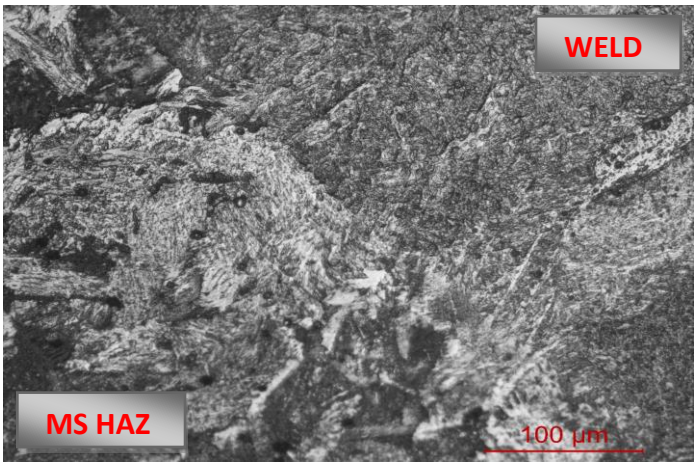

a) MS HAZ + WELD

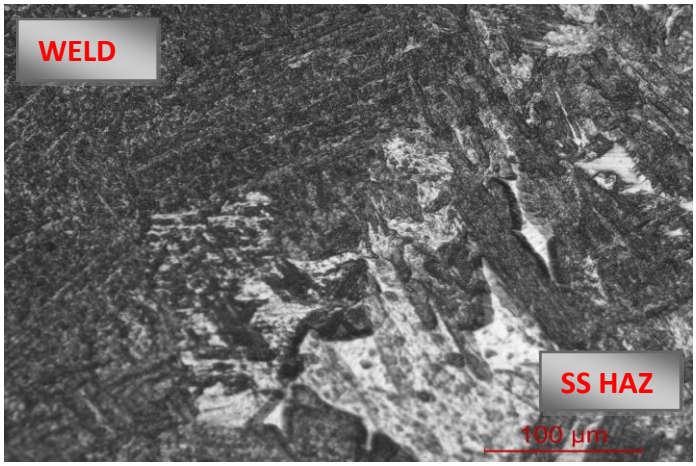

b) SS HAZ + WELD

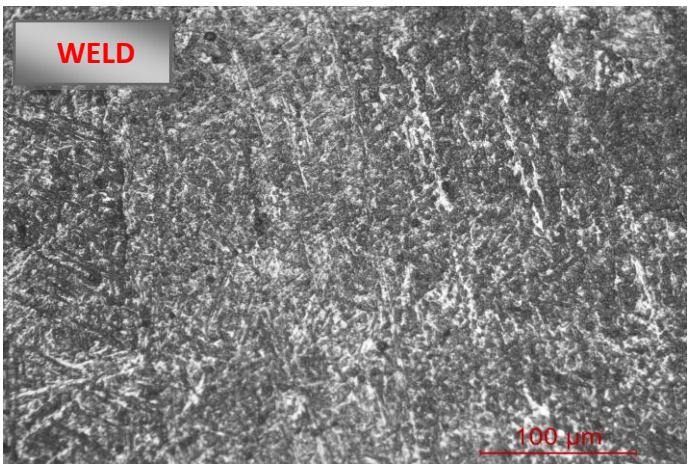

c) WELD REGION

Figure 4.9 Microstructures of sample no. 4

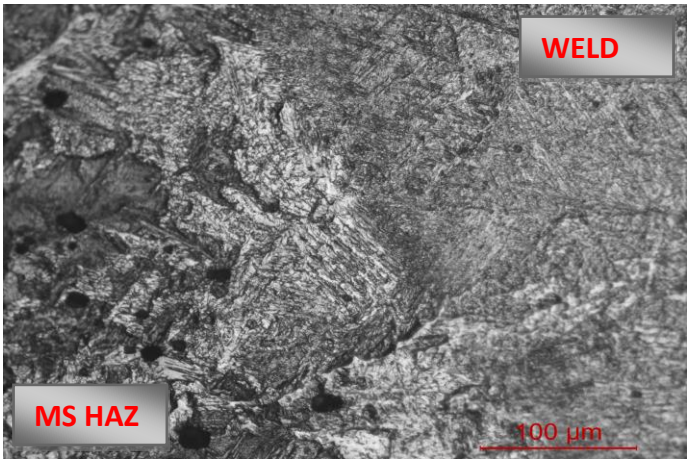

a) MS HAZ + WELD

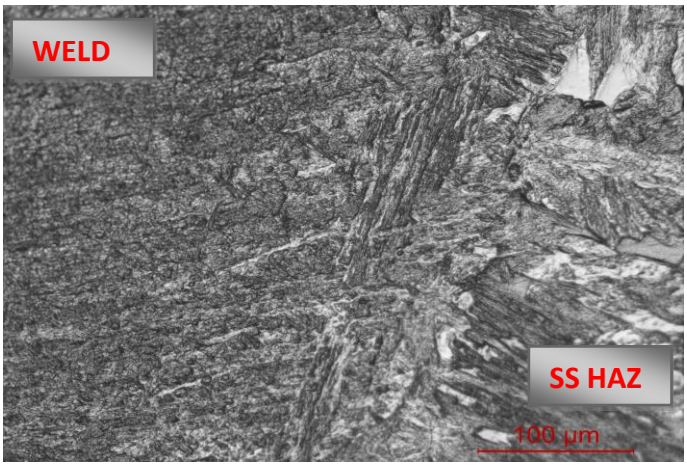

b) SS HAZ + WELD

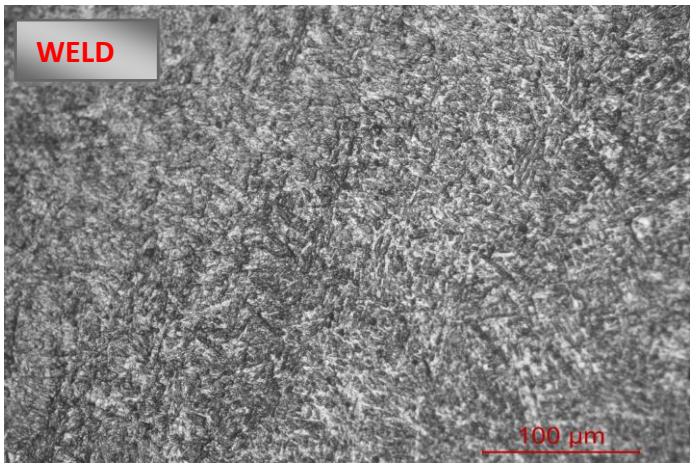

c) WELD REGION

Figure 4.10 Microstructures of sample no. 5

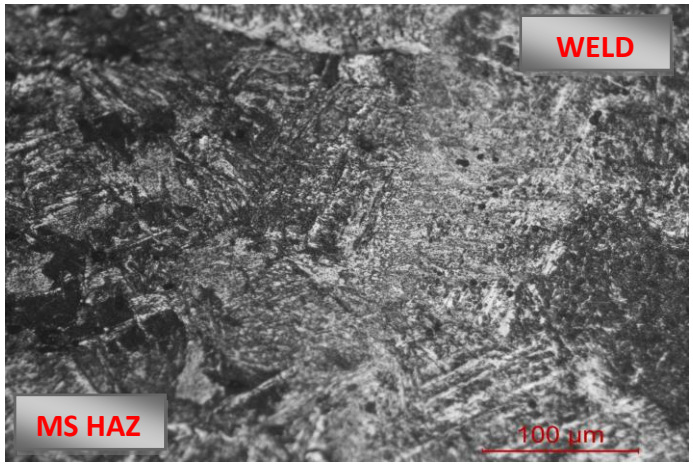

a) MS HAZ + WELD

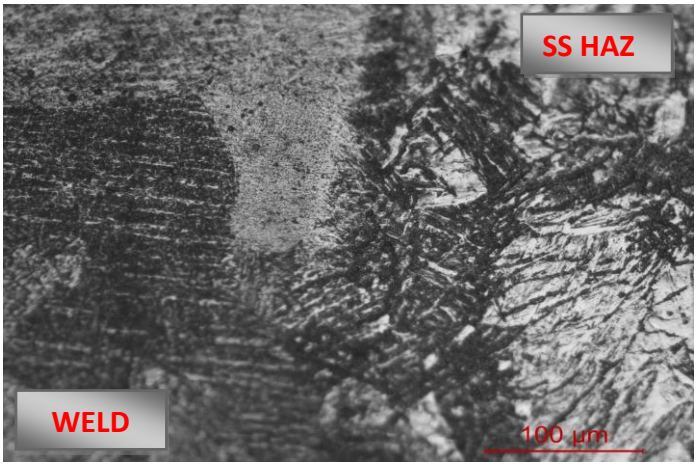

b) SS HAZ + WELD

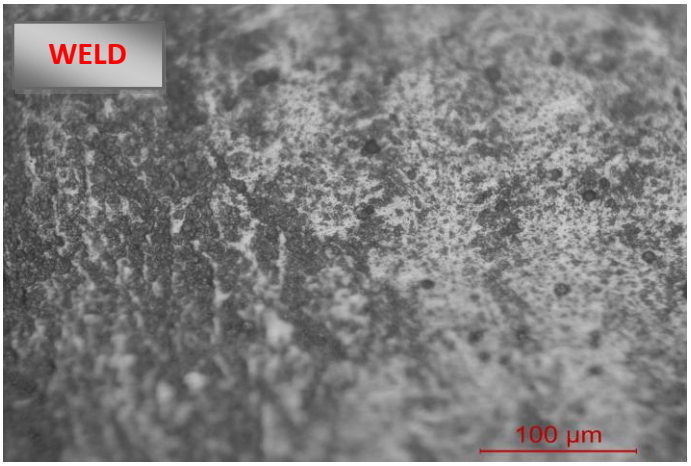

c) WELD REGION

Figure 4.11 Microstructures of sample no. 6

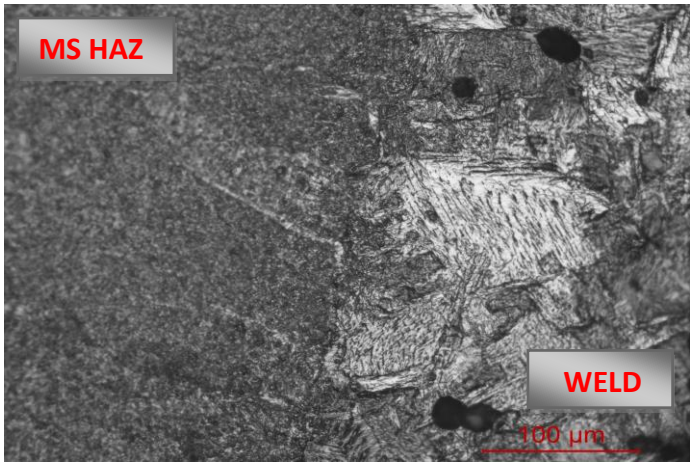

a) MS HAZ + WELD

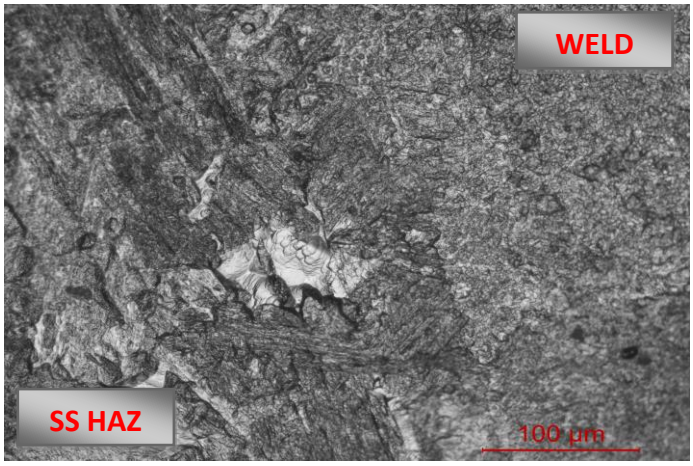

b) SS HAZ + WELD

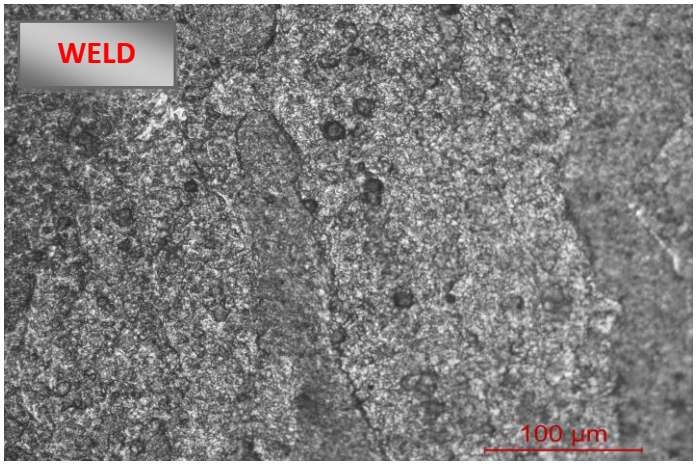

c) WELD REGION

Figure 4.12 Microstructures of sample no. 7

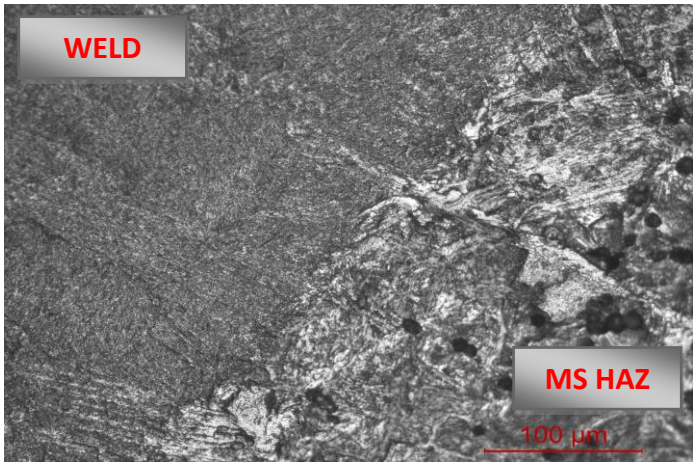

a) MS HAZ + WELD

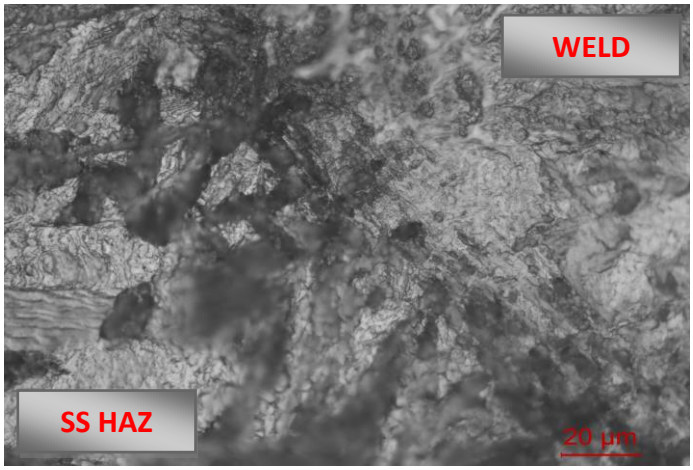

b) SS HAZ + WELD

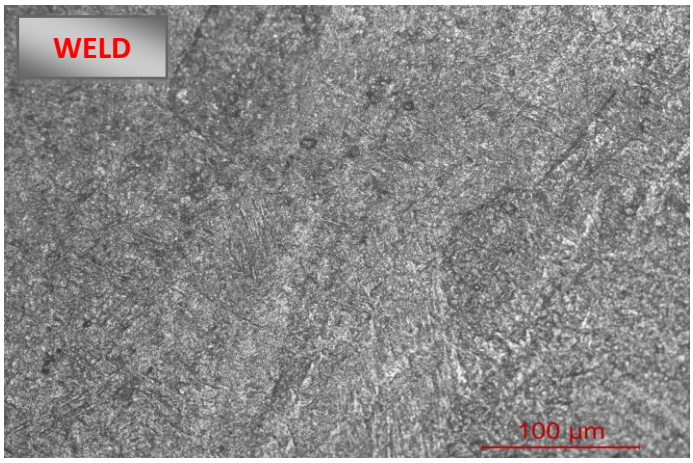

c) WELD REGION

Figure 4.13 Microstructures of sample no. 8

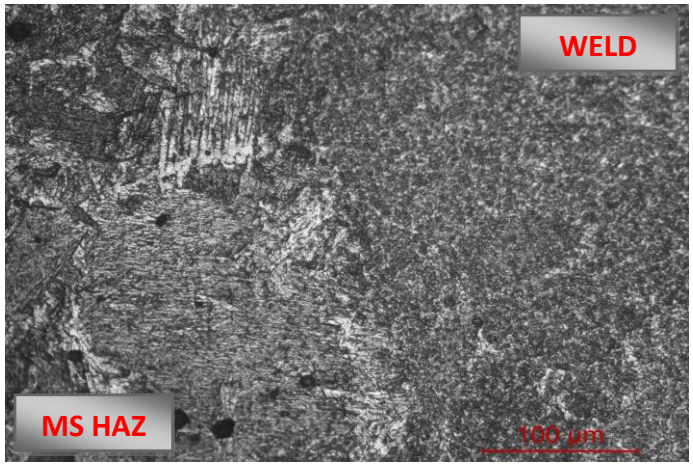

a) MS HAZ + WELD

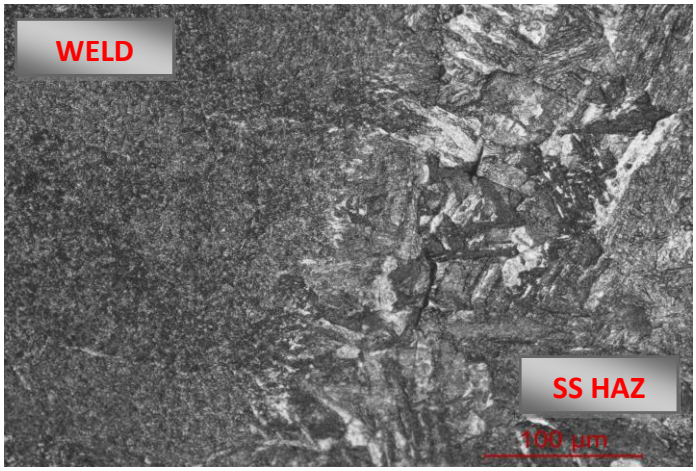

b) SS HAZ + WELD

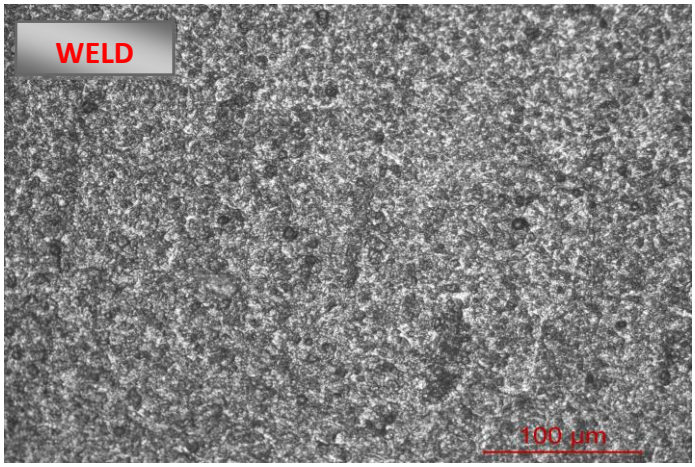

c) WELD REGION

Figure 4.14 Microstructures of sample no. 9

4.5 RESULTS OF SCANNING ELECTRON MICROSCOPY (SEM) AND DISCUSSION

A scanning electron microscop (SEM) is a type of electron microscope that produces images of a sample by scanning it with a focused beam of electrons. The electrons interact with atoms in the sample, producing various signals that contain information about the sample's surface topography. The electron beam is generally scanned in a raster scan pattern, and the beam's position is combined with the detected signal to produce an image. SEM can achieve resolution better than 1 nanometre. Specimens can be observed in high vacuum, in low vacuum, in wet conditions (in environmental SEM), and at a wide range of cryogenic or elevated temperatures.

In the present work SEM is performed on model JSM 6300 Jeol scanning machine. Figures 4.15-4.16 represent the SEM images of two welded samples, 1 and 5, with some defects in few cases. Figure 4.15(a)–4.15(c) show the SEM image of sample no. 1 and remaining figures, Figure 4.16(a)–4.5(e) show the sample no. 5.

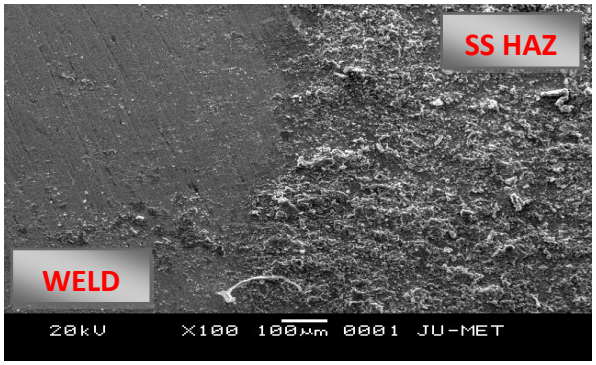

a) SS HAZ + WELD

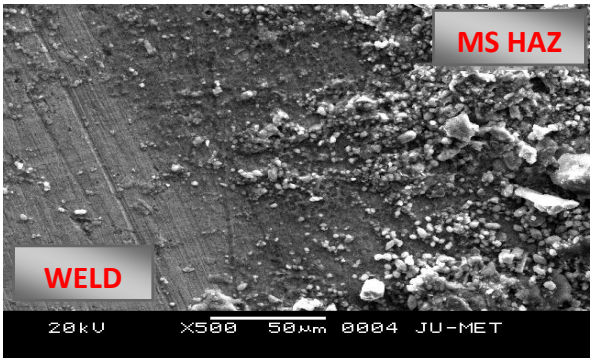

b) MS HAZ + WELD

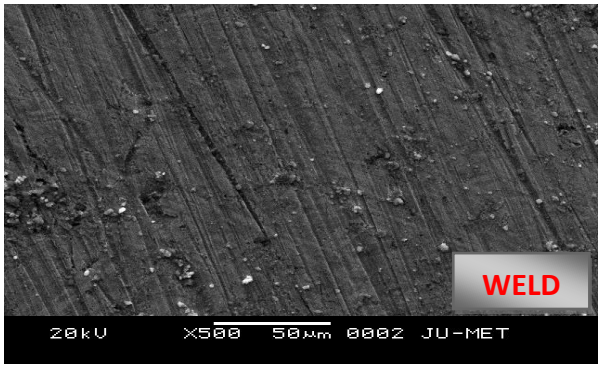

c) WELD REGION

Figure 4.15 SEM images of sample no. 1

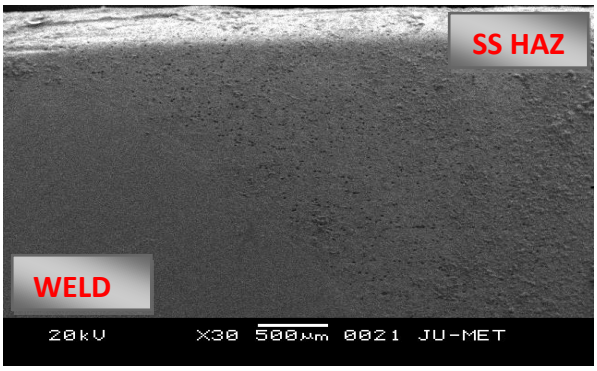

a) SS HAZ + WELD

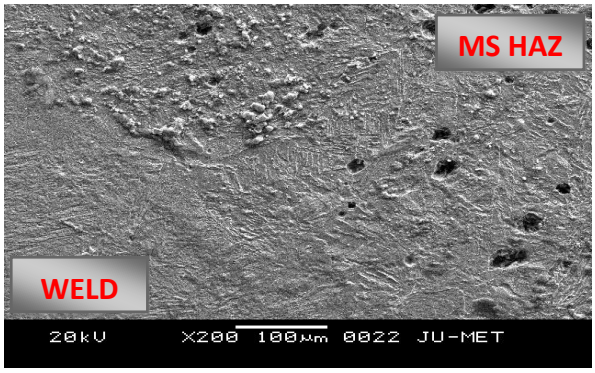

b) MS HAZ + WELD

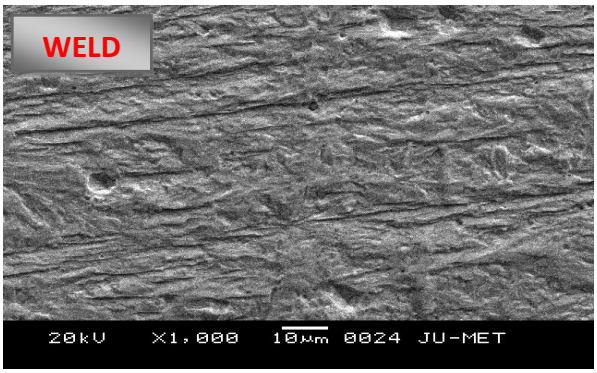

c) WELD REGION

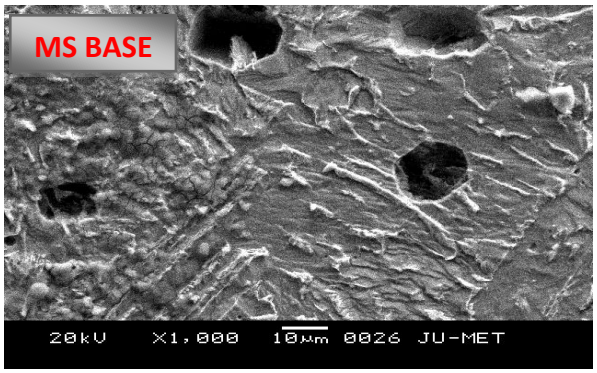

d) MS BASE

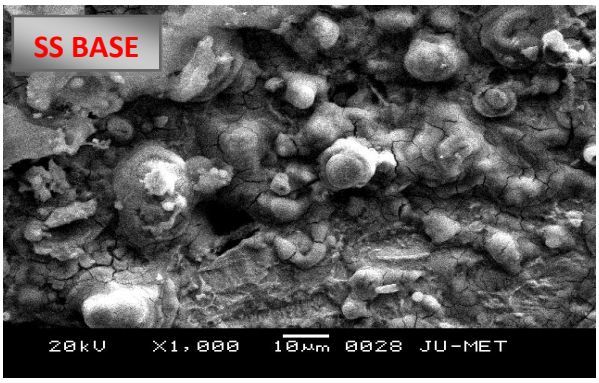

(e) SS BASE

Figure 4.16 SEM images of sample no. 5

Only two samples have been considered for SEM images (sample nos. 1 and 5). In these figures, in most of the samples three different regions are clearly identified-weld, HAZ and base. From the SEM photographic view, sample no. 1 is found to be almost defect free, due to favourable parametric combination of input parameters. In some figures, magnified SEM images reveal some defects like hot cracks (Figures 4.15 (c)), corrosion defects (Figure

4.16 (e)) and slag inclusions/impurities (Figures 4.15 (c)). Representative weld region and HAZ region are shown at higher magnification in Figures 4.15 (c), and 4.16 (c).

More extensive study by scanning electron microscopy is kept under consideration for future study, as an extension of the present work.

CHAPTER 5

5. DATA ANALYSIS AND PROCESS OPTIMIZATION

In the present study response surface methodology (RSM) is used for developing mathematical model and response prediction. Ultimate tensile strength (UTS), percentage elongation (PE), hardness at weld, HAZ width at mild steel plate and HAZ width at ferritic stainless steel plate are the response parameters whereas; current, traverse speed and stick-out length are the input parameters. Analysis of variance (ANOVA) has been applied to check adequacy of the model. Taguchi's S/N ratio concept has been used for single objective optimization for which the optimum parametric condition is identified for maximization of UTS, PE and hardness at weld, and minimization of HAZ widths at mild steel plate and ferritic stainless steel plate separately-individually. Grey-based Taguchi method has been used for multi-objective optimization. It is used to determine the optimum parametric condition for maximization of UTS, PE and hardness at weld as well as minimization of HAZ widths at MS plate and FSS plate simultaneously. Response surface plots and contour plots have also been made for each of the responses. Confirmatory tests have been conducted and validated with optimized parametric settings, proposed by, Taguchi (for single optimization) and Grey-Taguchi analysis (for multi-response optimization).

5.1 DATA ANALYSIS FOR ULTIMATE TENSILE STRENGTH (UTS)

In this section, response surface analyses of ultimate tensile strength (UTS) have been done using MINITAB 17 software. At first a mathematical model is developed. Response surface plots and contour plots are then generated.

5.1.1 MAIN EFFECTS PLOT FOR UTS

Main effects plot for UTS has been obtained by considering data in Table 3.2. This plot shows the nature of the relationship between UTS and input parameters. Figure 5.1 shows that with increase in current UTS increases up to the maximum limit, then decreases. However, UTS value increases with increase in the value of traverse speed. UTS first decreases and then increases with increase in stick-out. This figure indicates that change in input parameters, influence the UTS, but not in a consistent manner. By examining Table 5.1 it appears that the parameter "speed" influences UTS most strongly, because for speed the rank is found to be 1.

Table 5.1 Mean response table for ultimate tensile strength (UTS)

Level 1	Current (C)	Speed (T)	Stick-out length (S)
1	465.3	459.7	501.0
2	526.7	480.0	471.7
3	496.0	548.3	515.3
Delta	61.3	88.7	43.7
Rank	2	1	3

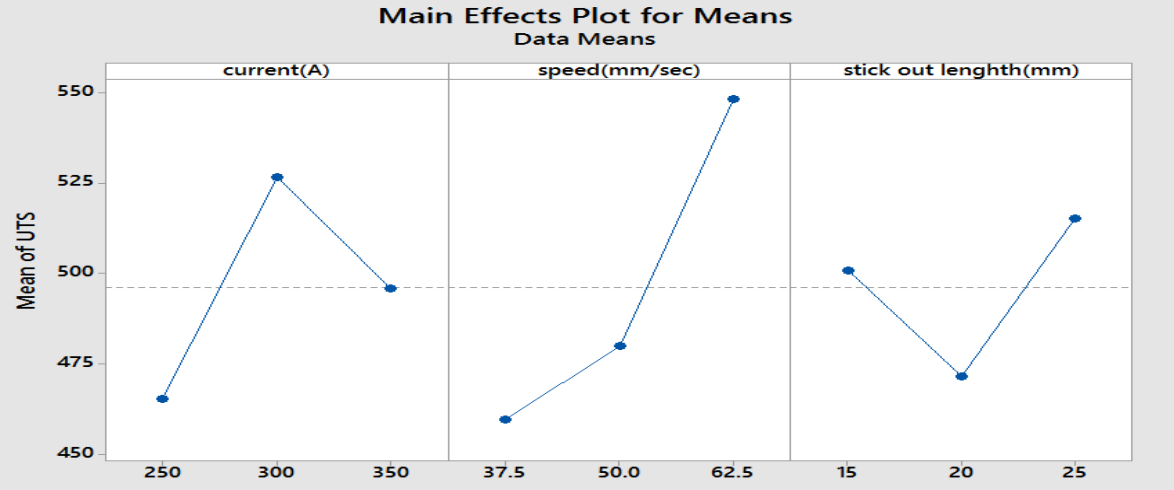

Figure 5.1 Main effects plot for means of UTS

5.1.2 MATHEMATICAL MODELING FOR UTS

Mathematical modeling has been done by RSM of the type given by eq. (2.12), discussed in chapter 2. The inner interaction terms and squared terms are neglected and cross interaction terms are used. This is equivalent to the type of eq. (2.13).

UTS has been expressed in terms of the process variables welding current (C), traverse speed (T) and stick-out length (S) in the form:

$$\mathbf{UTS = \beta_0 + \beta_1(C) + \beta_2(T) + \beta_3(S) + \beta_{12}(CT) + \beta_{13}(CS) + \beta_{23}(TS)} \quad (5.1)$$

Where β_0 is the constant coefficient,

β_1, β_2 and β_3 are the coefficients of current, traverse speed and stick-out respectively.

β_{12}, β_{13} and β_{23} are the coefficients of CT, CS and TS respectively.

The final mathematical model to estimate UTS in terms of uncoded values is given as

$$\mathbf{Y_{UTS} = 969.302 - 2.34857(C) + 15.9048(T) - 68.9048(S) - 0.0361143(CT) + 0.209714(CS) + 0.096(TS)} \quad (5.2)$$

Where Y_{UTS} is in MPa, C is in A, T is in mm/sec and S is in mm.

5.1.3 RESPONSE SURFACE PLOTS AND CONTOUR PLOTS FOR UTS

Surface and contour plots for all the responses are generated for all possible conditions. But the plots generated at middle value of the third parameter (while combined effect of other two factors on the response is being considered) are presented here. This is followed here for surface and contour plots of all the responses, including UTS.

Surface plots are used to predict the response value (i.e. UTS) at some given combination of any two parameters, while the third parameter is held at some fixed level. For this purpose, necessary program is made and run for developing the response surface plots. These are made on the basis of eq. (5.2) developed above. MINITAB 17 software is used for the purpose. The response surface plots for ultimate tensile strength (UTS) are shown in Figures 5.2–5.4. These plots indicate interaction effects on the response variables. If the surface plots reveal much curvature or bend then interaction effect is more. If the response surface does not show much curvature, bend or twist interaction effect is less. All most all the response surface plots (Figures 5.2–5.4) reveal interaction effects. For example, in Figure 5.3 twist in the response is very distinct, identifying that the interaction effect of current (C) and stick-out length (S) on UTS is significant. In Figure 5.4 the surface plot shows that interaction between current (C) and speed (T) has strong effect on the response UTS.

The contour plots are two dimensional plots which are helpful in the prediction of the response under some given combination of any two parameters while the third parameter is held at some constant level. Each line or contour in the contour plots represents constant response line. The plots are particularly necessary when the stationary point is a saddle point or is remote from the design region. Contour plots for UTS are shown in Figures 5.5-5.7. These plots indicate interaction effect on the response variables. If the contour plots reveal much curvature or bend then interaction effect is more. If the lines are straighter, then the interaction effect is less. For example, in Figure 5.5 lines are curved, it means that there is interaction effect between stick-out length (S) and speed (T) at middle value of current. In Figure 5.6 the lines are more curved. It shows that there is more interaction effect between stick-out length (S) and current (C).

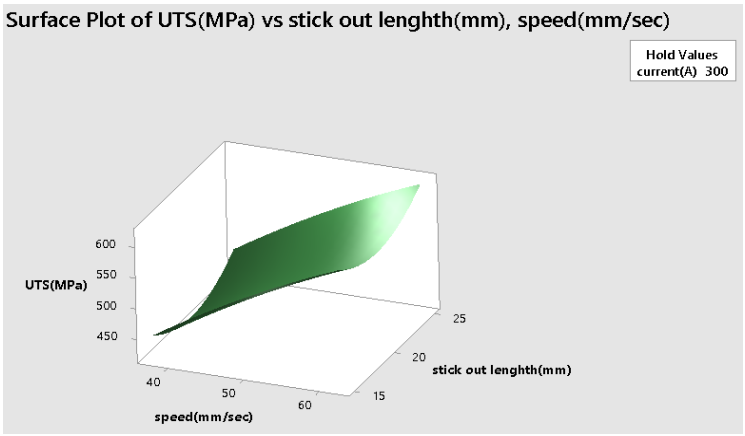

Figure 5.2 Response surface plot showing combined effects of S and T on UTS when C is kept constant (C_{mid} = 300 A)

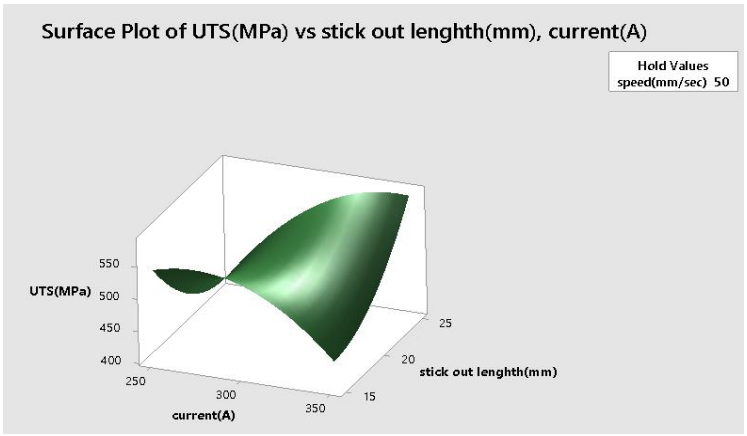

Figure 5.3 Response surface plot showing combined effects of C and S on UTS when T is kept constant (T_{mid} = 50 mm/sec)

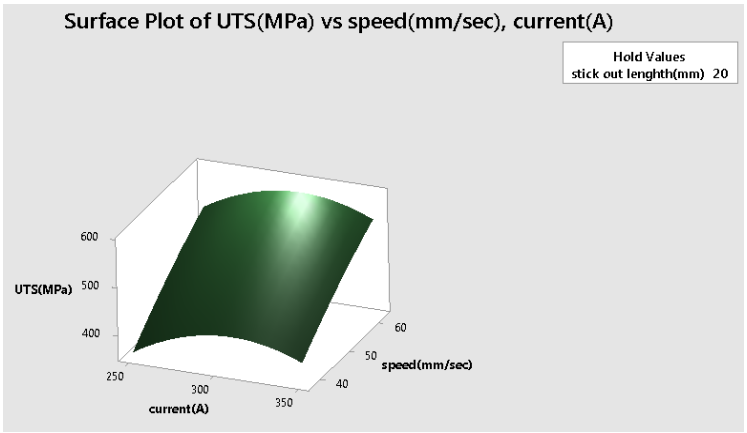

Figure 5.4 Response surface plot showing combined effects of C and T on UTS when S is kept constant (S_{mid} = 20 mm)

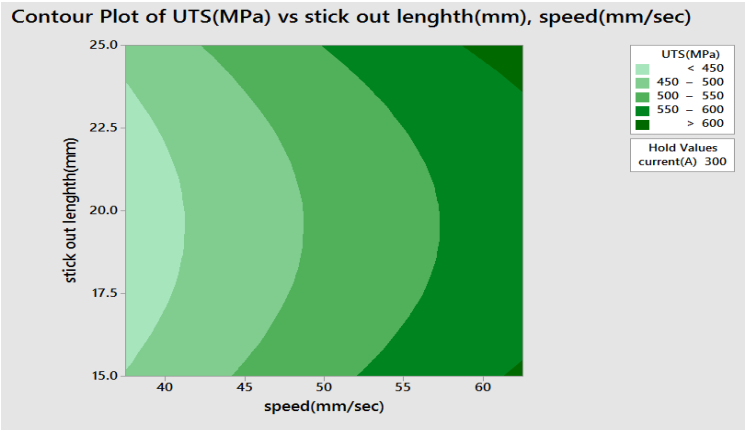

Figure 5.5 Contour plot showing combined effects of S and T on UTS when C is kept constant (C_{mid} = 300 A)

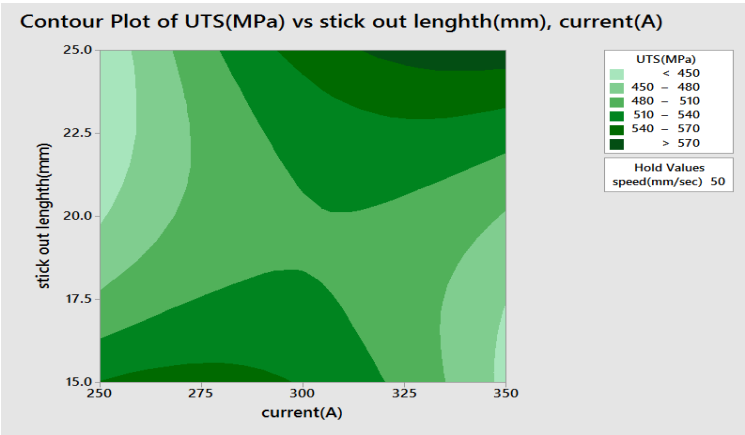

Figure 5.6 Contour plot showing combined effects of S and C on UTS when T is constant (T_{mid} = 50 mm/sec)

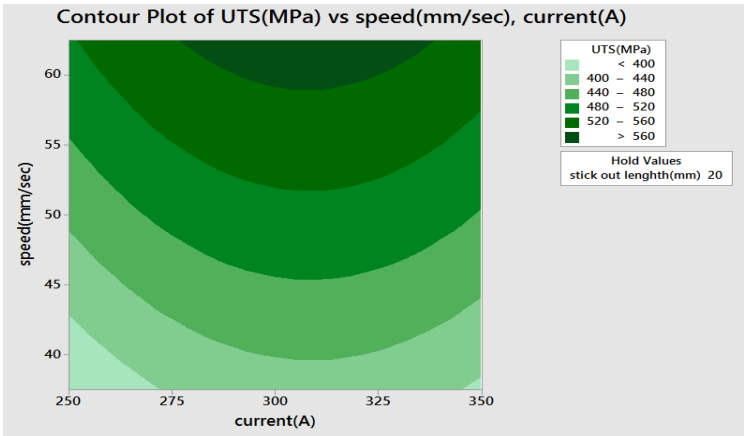

Figure 5.7 Contour plot showing combined effects of C and T on UTS when S is kept constant (S_{mid} = 20 mm)

5.2 DATA ANALYSIS FOR PERCENTAGE ELONGATION (PE)

Statistical analysis of observed data of percentage elongation is done and discussed here.

5.2.1 MAIN EFFECTS PLOT FOR PERCENTAGE ELONGATION (PE)

Data in Table 3.2 have been converted to mean responses for percentage elongation and these are listed in Table 5.2. Table 5.2 indicates that speed (T) is the factor which influences PE the most, as Rank is 1 for speed. Next main effects plot for means is drawn, which is shown in Figure 5.8. From Figure 5.8 the trend is found to be inconsistent with stick-out length; in this case PE value decreases first and then increases. The value of PE is increasing with increase in current and speed. Thus trend between PE and current, between PE and speed are more or less consistent.

Table 5.2 Mean response table for percentage elongation

Level 1	Current(C)	Speed(T)	Stick-out length(S)
1	14.13	12.87	16.80
2	14.83	14.47	14.13
3	16.47	18.10	14.50
Delta	2.33	523	2.67
Rank	3	1	2

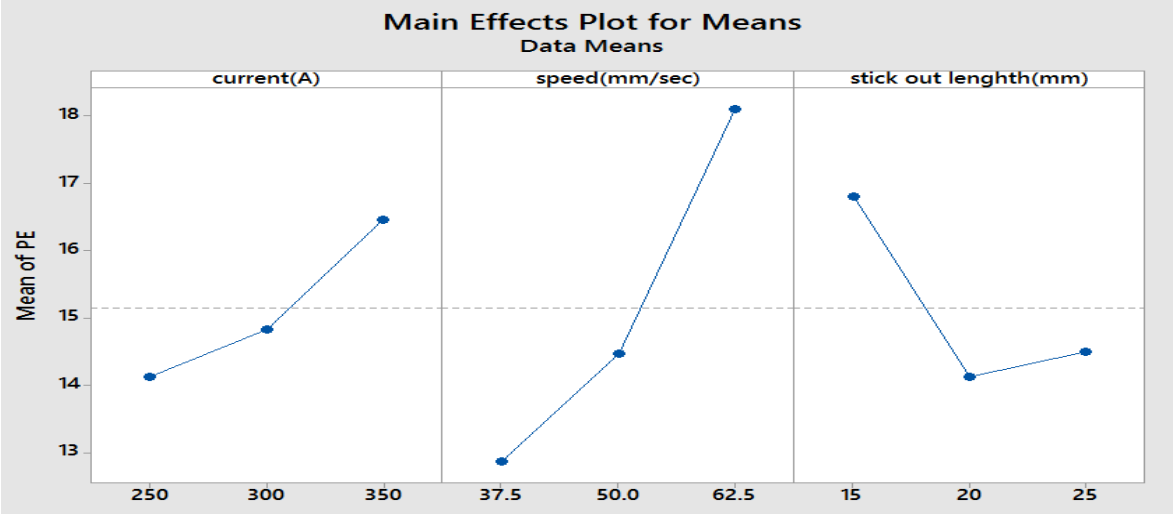

Figure 5.8 Main effects plot for means of percentage elongation

5.2.2 MATHEMATICAL MODELING FOR PE

As mentioned earlier, relationship has been modeled by response surface methodology,

utilizing the observed data in Table 3.2. The inner interaction terms and squared terms are neglected and two-factor interaction terms are used from the eq. (2.12). Percentage elongation (PE) has been expressed in terms of the process variables welding current (C), traverse speed (T) and stick-out length (S). The form of equation is already mentioned in eq. (2.13), chapter 2.

$$\mathbf{PE = \beta_0 + \beta_1(C) + \beta_2(T) + \beta_3(S) + \beta_{12}(CT) + \beta_{13}(CS) + \beta_{23}(TS)} \quad (5.3)$$

The final mathematical model to estimate percentage elongation in terms of uncoded values is given as

$$\mathbf{Y_{PE} = -2.14444 + 0.0846667(C) + 0.276571(T) - 0.566667(S) - 9.37143E - 04(CT) - 0.0012(CS) + 0.0114286(TS)} \quad (5.4)$$

Where Y_{PE} is in percentage, C is in A, T is in mm/sec and S is in mm.

5.2.3 RESPONSE SURFACE PLOTS AND CONTOUR PLOTS FOR PERCENTAGE ELONGATION (PE)

Response surface plots for percentage elongation (PE) have been shown in Figures 5.9-5.11. Figure 5.9 reveals that interaction effect of S – T on PE is pronounced. The same idea is conveyed by the contour plot 5.12. Other surface and contour plots can also be utilized to predict interaction effects and also to select suitable combination of any two parameters (while third parameter is held at some constant level), for achieving the desired PE. Contour plots for percentage elongation (PE) have been shown in Figures 5.12-5.14.

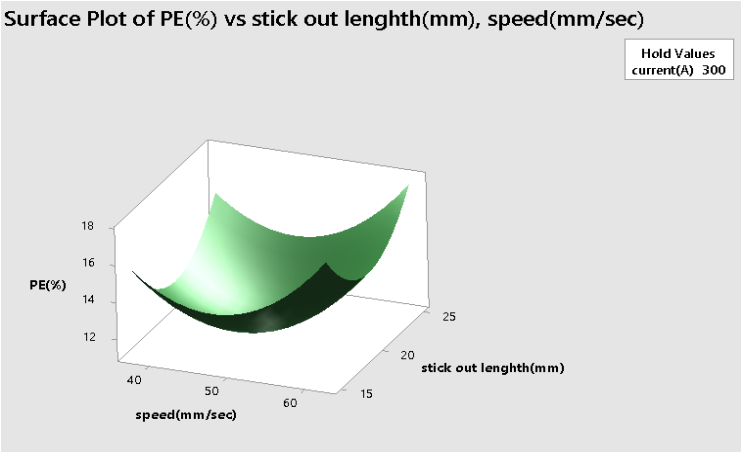

Figure 5.9 Response surface plot showing combined effects of S and T on PE when C is kept constant (C_{mid} = 300 A)

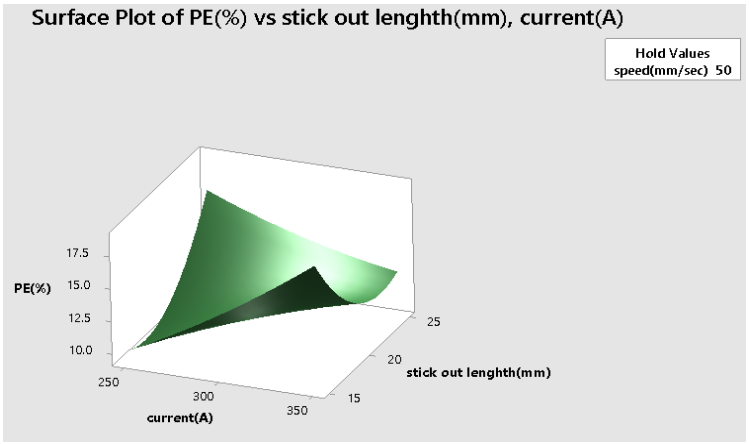

Figure 5.10 Response surface plot showing combined effects of S and C on PE when T is kept constant (T_{mid} =50 mm/sec)

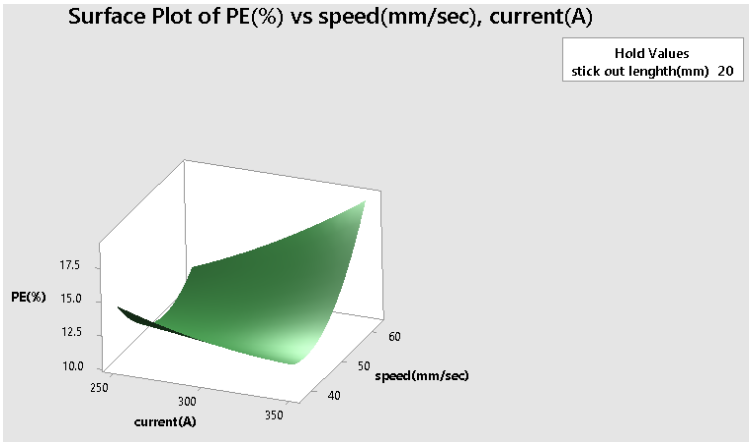

Figure 5.11 Response surface plot showing combined effects of C and T on PE when S is kept constant (S_{mid} 20 mm)

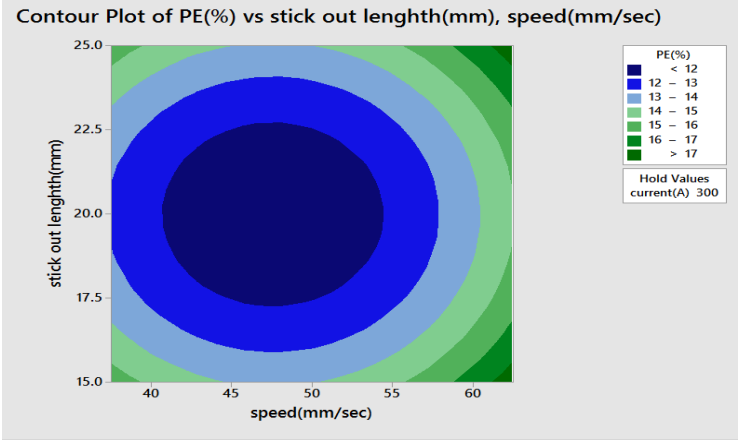

Figure 5.12 Contour plot showing combined effects of S and T on UTS when C is constant (C_{mid} = 300 A)

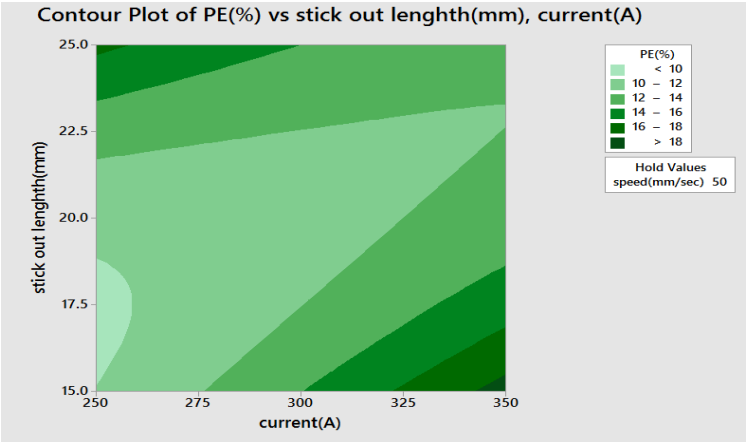

Figure 5.13 Contour plot showing combined effects of S and C on PE when T is kept constant (T_{mid} = 50)

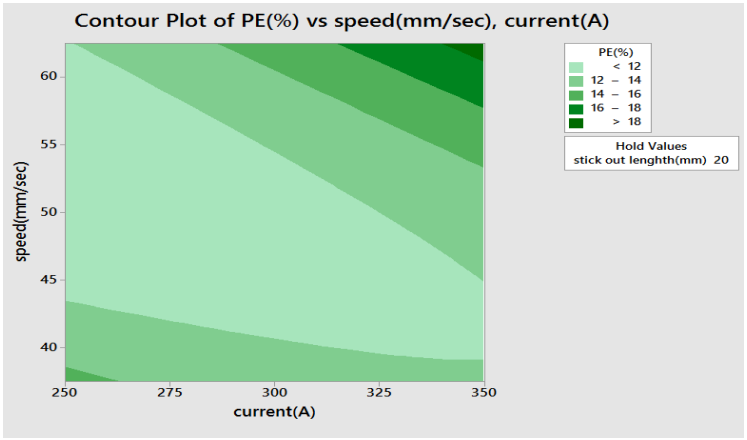

Figure 5.14 Contour plot showing combined effects of C and T on PE when S is kept constant (S_{mid} = 20)

5.3 DATA ANALYSIS FOR HARDNESS AT WELD (HAW)

Analysis of observed data of hardness at weld is made through main effects plot, mathematical modelling, surface plots and contour plots.

5.3.1 MAIN EFFECTS PLOT FOR HARDNESS AT WELD (HAW)

Main effects plot for hardness at weld has been obtained by considering data in the Table 3.2. This plot shows the nature of the relationship between hardness at weld and input parameters. Figure 5.15 shows that hardness at weld decreases first and then increases in the next level for all the input parameters. There is thus consistent trend between weld hardness and input parameters. Mean response table for hardness at weld is given in Table 5.3. Further stick-out length (S) is found to be the most influential factor for HAW, because its Rank is 1.

Table 5.3 Mean response table for hardness at weld

Level 1	Current(C)	Speed(T)	Stick-out length(S)
1	338.8	336.8	334.0
2	334.0	336.2	333.8
3	337.4	337.3	342.5
Delta	48	1.2	8.7
Rank	2	3	1

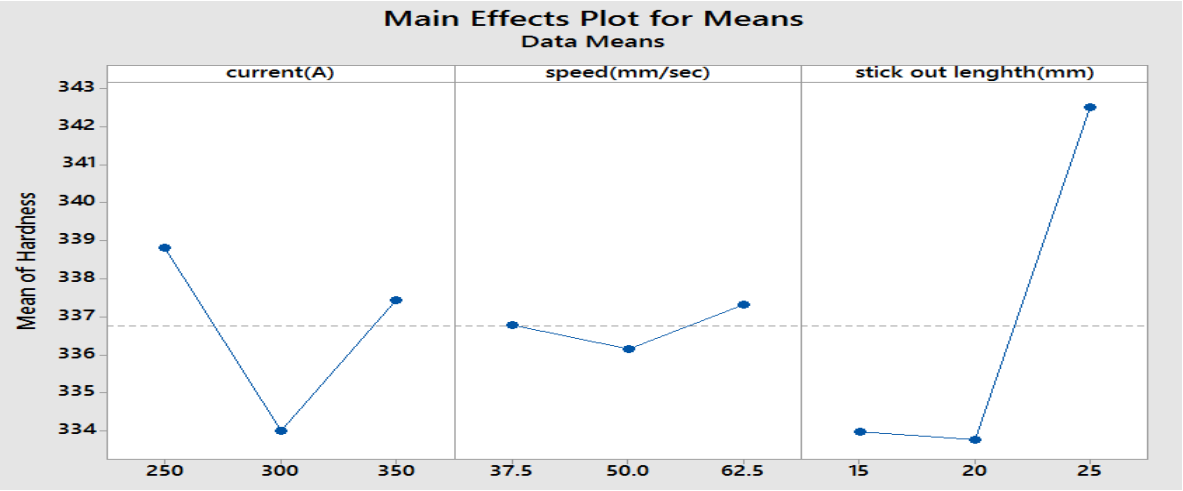

Figure 5.15 Main effects plot for means of hardness at weld

5.3.2 MATHEMATICAL MODELING FOR HARDNESS AT WELD

Considering the form of relationship in a manner same as discussed in earlier sections, the mathematical model developed for hardness at weld ($\mathbf{Y_{HAW}}$) is given by

$$\mathbf{Y_{HAW} = 356.571 - 0.0263810(C) - 5.84305(T) + 14.3057(S) + 0.0154971(CT) - 0.0436571(CS) + 0.0256(TS)} \quad (5.5)$$

Where Y_{HAW} is in HV, C is in A, T is in mm/sec and S is in mm.

5.3.3 RESPONSE SURFACE PLOTS AND CONTOUR PLOTS FOR HARDNESS AT WELD (HAW)

Response surface plots and contour plots for hardness at weld are shown in Figures 5.16 - 5.21. Combined effects of any two parameters on hardness at weld are illustrated through these plots, while the third parameter in each case, have been kept constant at middle value. Figures 5.16 - 5.18 indicate two factor interaction effects of S – T, S – C and C – T on weld hardness. However, interaction effect C – T is found to be somewhat more stronger than S – T

and S – C, on hardness at weld. The contour plots (Figures 5.19 – 5.20) also lead to the same conclusion as bend in the contour lines in Figure 5.21 is more.

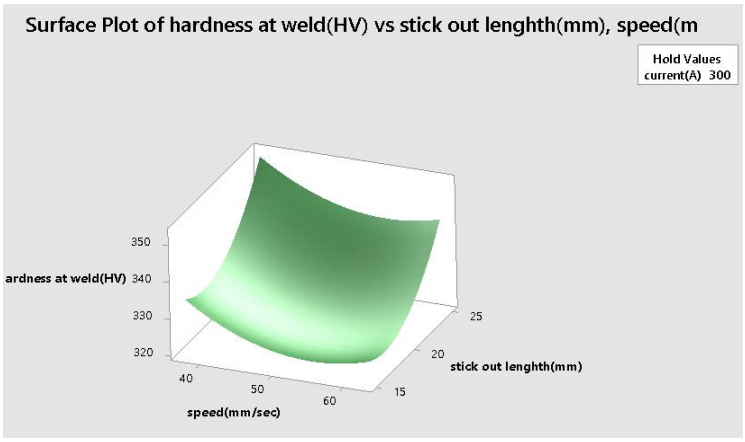

Figure 5.16 Response surface plot showing combined effects of S and T on hardness at weld when C is kept constant (C_{mid} = 300A)

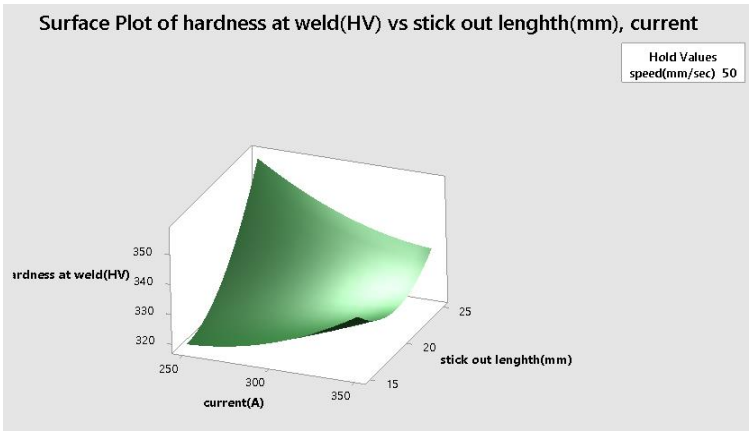

Figure 5.17 Response surface plot showing combined effects of S and C on hardness at weld when T is kept constant (T_{mid} = 50 mm/sec)

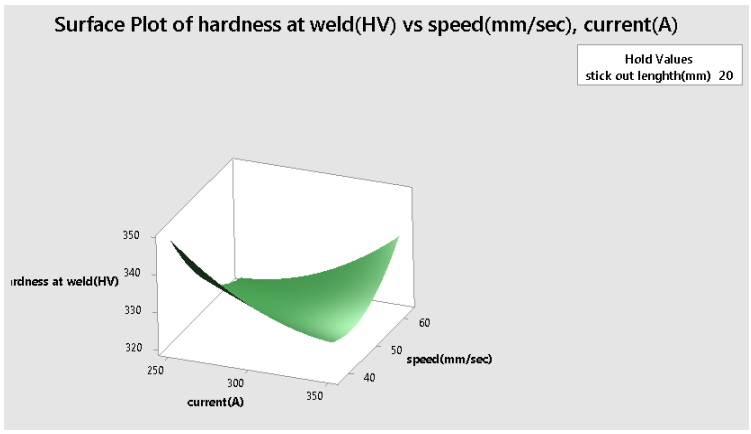

Figure 5.18 Response surface plot showing combined effects of C and T on hardness at weld when S is kept constant (S_{mid} = 20 mm)

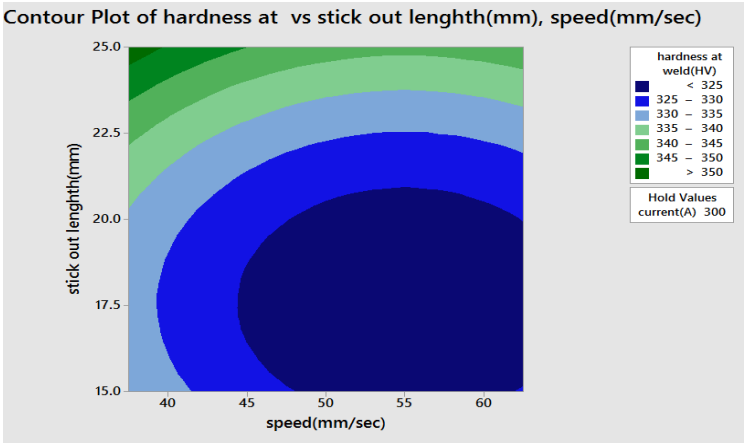

Figure 5.19 Contour plot showing combined effects of S and T on hardness at weld when C is constant (C_{mid} = 300 A)

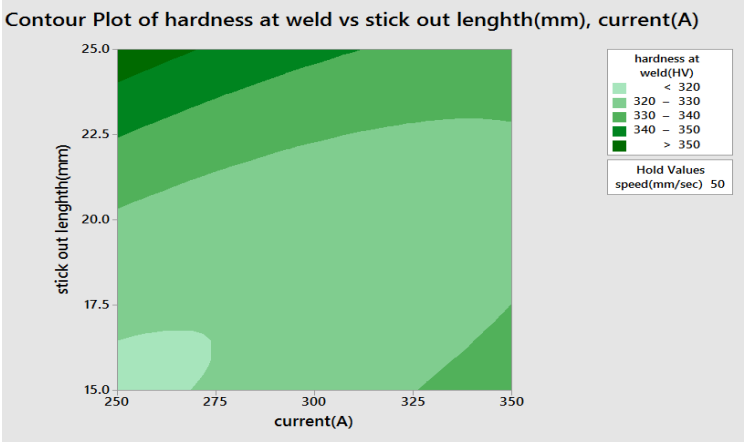

Figure 5.20 Contour plot showing combined effects of C and S on hardness at weld when T is kept constant (T_{mid} = 50 mm/sec)

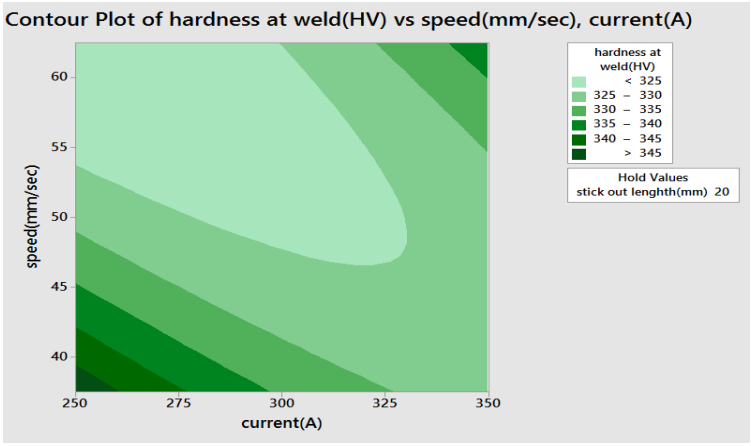

Figure 5.21 Contour plot showing combined effects of C and T on hardness at weld when S is kept constant (S_{mid} = 20 mm)

5.4 DATA ANALYSIS FOR HAZ WIDTH AT MILD STEEL PLATE

In this section, response surface analyses of HAZ width at mild steel have been done using MINITAB 17 software. Mathematical models are developed first. Response surface plots and contour plots are then generated.

5.4.1 MAIN EFFECTS PLOT FOR HAZ WIDTH AT MILD STEEL PLATE

Mean responses table for HAZ at mild steel is prepared and shown in Table 5.4. Current "C" (Rank 1) is found to be the most important factor which influences HAZ width at mild steel.

Main effects plot for HAZ width at MS has been generated by considering data in the Table 3.2. This plot shows the nature of the relationship between HAZ at MS and input parameters. Figure 5.22 shows that with increase in current, HAZ at MS increases up to the maximum limit and then decreases. But by increasing the stick-out, HAZ at MS first decreases a little bit and then increases beyond the second level. HAZ width at MS is in consistent trend with speed; it decreases with increase in speed.

Table 5.4 Mean response table for HAZ width at mild steel

Level 1	Current(C)	Speed(T)	Stick-out length(S)
1	699.3	727.9	693.0
2	735.5	702.9	690.9
3	648.1	652.2	699.1
Delta	874	75.8	8.2
Rank	1	2	3

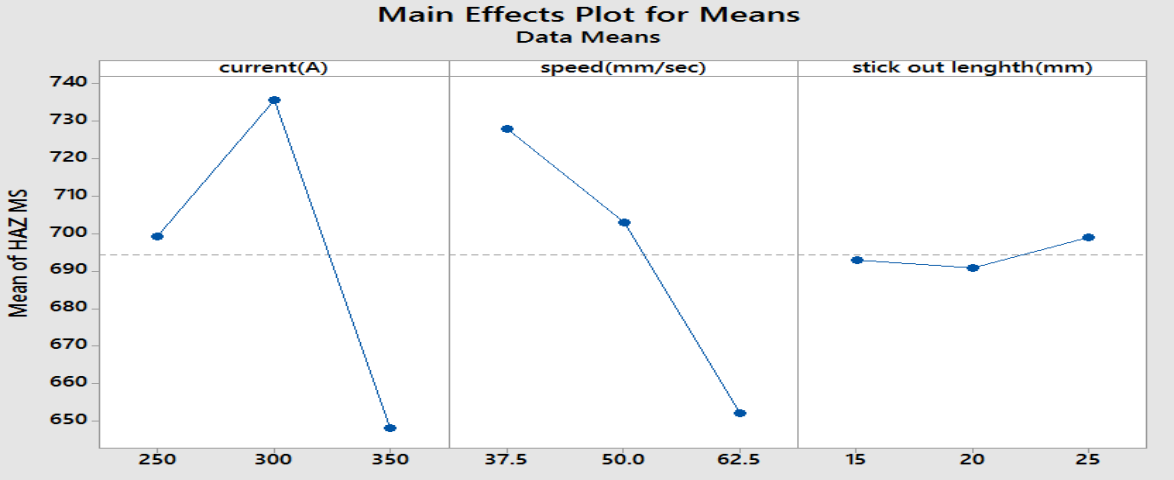

Figure 5.22 Main effects plot for means of HAZ width at MS

5.4.2 MATHEMATICAL MODELING FOR HAZ WIDTH AT MS

Using RSM and utilizing software MINITAB 17, the mathematical model for HAZ width at mild steel is found to be:

$$\mathbf{Y_{HAZ\ at\ MS} = 698.052 - 4.13602(C) - 12.1589(T) + 120.835(S) + 0.117568(CT) - 0.170823(CS) - 1.32583(TS)} \quad (5.6)$$

Where $Y_{HAZ\ at\ MS}$ is in microns, C is in A, T is in mm/sec and S is in mm

5.4.3 RESPONSE SURFACE PLOTS AND CONTOUR PLOTS FOR HAZ WIDTH AT MS

Figures 5.23 – 5.28 represent surface plots and contour plots for the response: HAZ width at MS. The constant parameter, in each case has been kept at its middle value (i.e. at second level). These plots indicate that all the two factor interaction effects do exit. Figure 5.25 suggests that the interaction effect of C – T on HAZ width at MS is much stranger than in other cases.

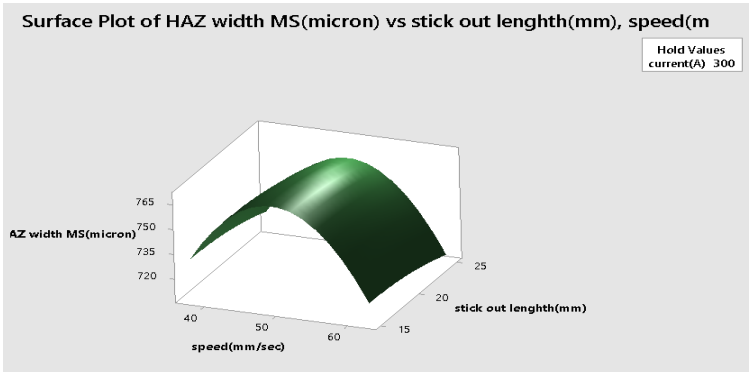

Figure 5.23 Response surface plot showing combined effects of S and T on HAZ at MS when C is kept constant (C_{mid} = 300A)

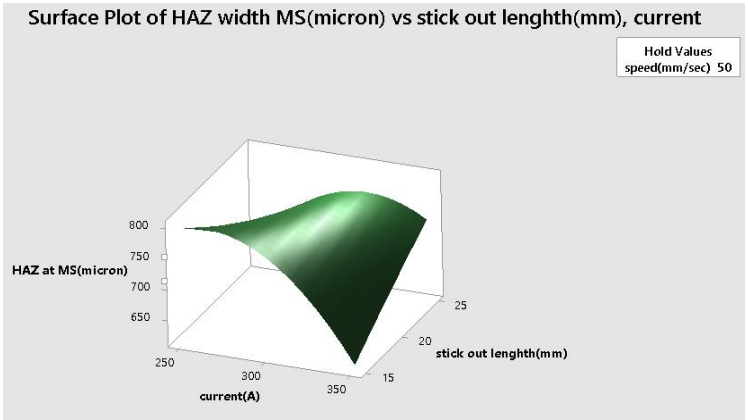

Figure 5.24 Response surface plot showing combined effects of S and C on HAZ at MS when T is kept constant (T_{mid} = 50mm/sec)

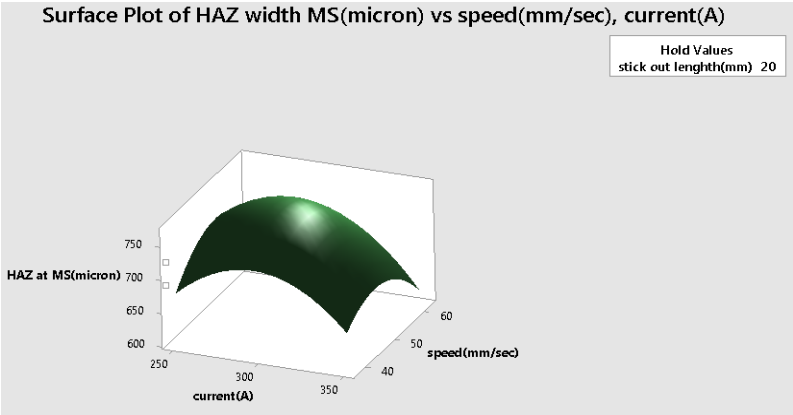

Figure 5.25 Response surface plot showing combined effects of C and T on HAZ at MS when S is kept constant (S_{mid} = 20 mm)

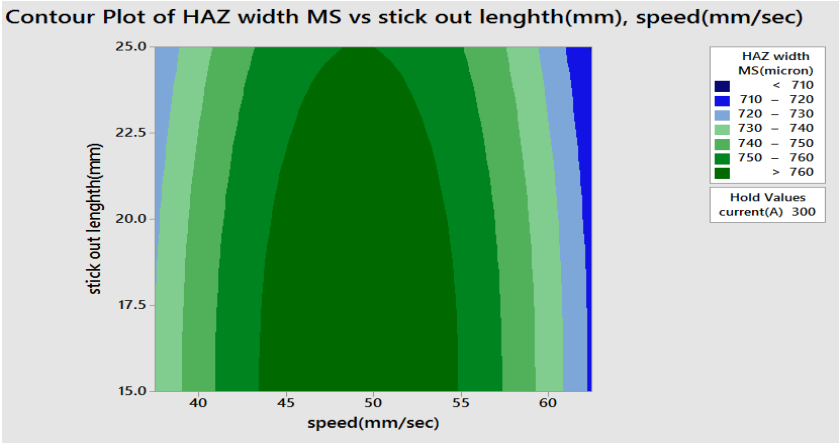

Figure 5.26 Contour plot showing combined effects of S and T on HAZ at MS when C is constant (C_{mid} = 300 A)

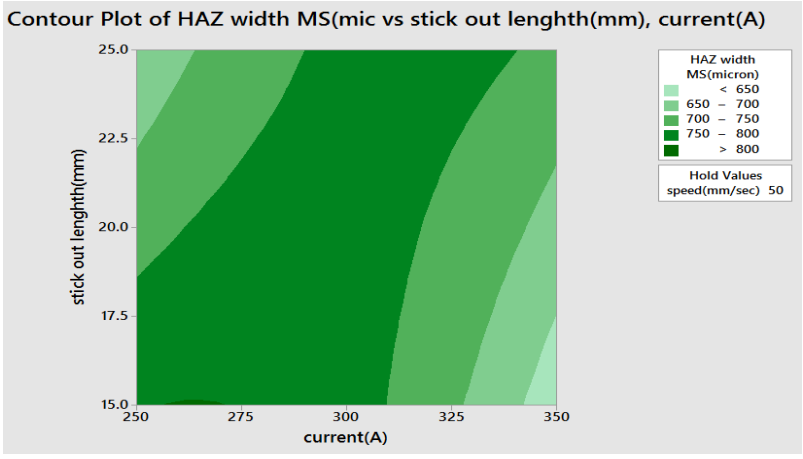

Figure 5.27 Contour plot showing combined effects of C and S on HAZ at MS when T is kept constant (T_{mid} = 50 mm/sec)

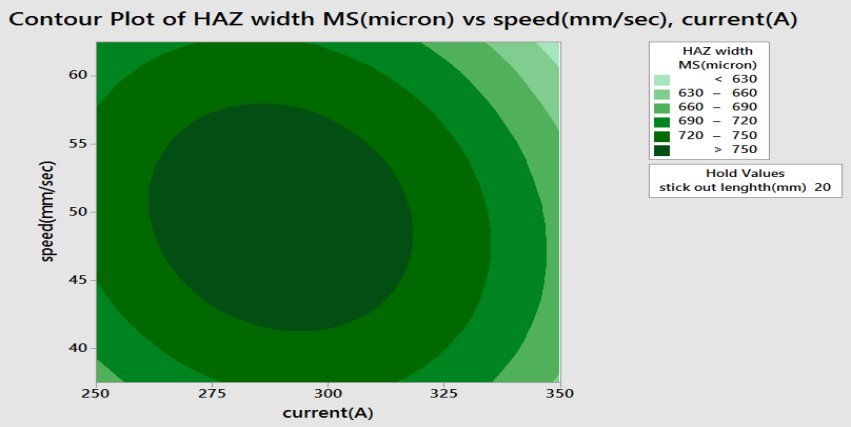

Figure 5.28 Contour plot showing combined effects of C and T on HAZ at MS when S is kept constant (S_{mid} = 20 mm)

5.5 DATA ANALYSIS FOR HAZ WIDTH AT FERRITIC STAINLESS STEEL (FSS) PLATE

The same procedure, as in previous section, is followed.

5.5.1 MAIN EFFECTS PLOT FOR HAZ WIDTH AT FERRITIC STAINLESS STEEL

Mean response table shown in Table 5.5 reveals that current (C) is the most important factor which contributes to HAZ width at FSS. Its Rank is 1 in Table 5.5. Next main effects plot for means of HAZ width at ferritic stainless steel side is made (Figure 5.29). From Table 5.5, it is observed that current is the most dominating factor in so far as HAZ width at FSS is concerned, as the corresponding Rank is 1. From Figure 5.29, no consistent trend is found between i) HAZ at FSS and traverse speed and ii) HAZ at FSS and stick-out length. However, with increase in current HAZ width is found to decrease, though not purely linearly

Table 5.5 Mean response table for HAZ width at FSS

Level 1	Current(C)	Speed(T)	Stick-out length(S)
1	728.6	681.1	718.8
2	712.0	711.9	639.6
3	602.7	650.2	684.8
Delta	125.9	61.7	79.1
Rank	1	3	2

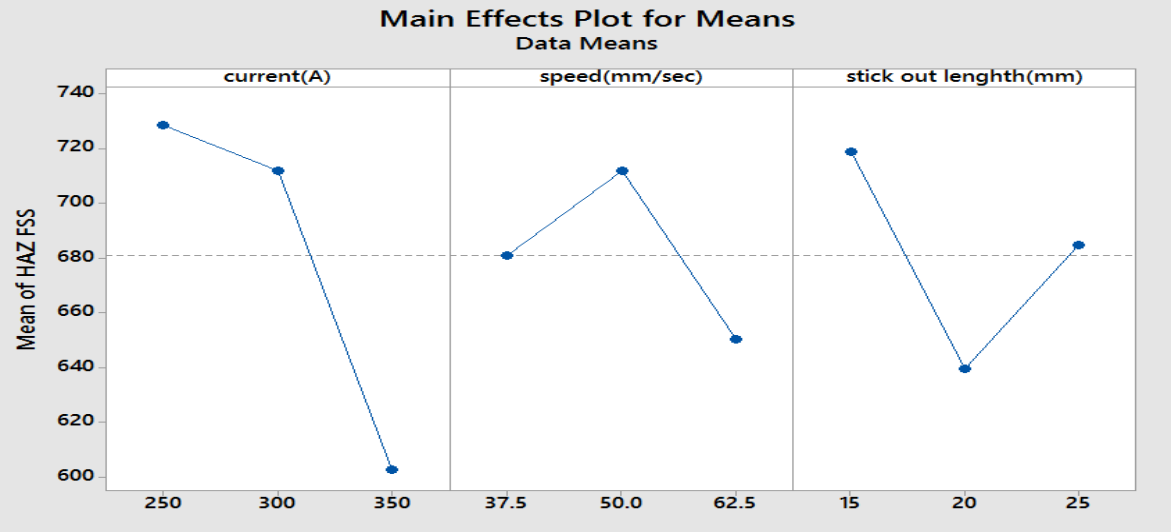

Figure 5.29 Main effects plot for means of HAZ at FSS

5.5.2 MATHEMATICAL MODELING FOR HAZ WIDTH AT FSS

As mentioned earlier, relationship has been modeled by response surface methodology by utilizing the observed data in Table 3.2. The inner interaction terms and squared terms are neglected and cross interaction terms are used from the eq. (2.12). The final mathematical model to estimate HAZ at FSS in terms of uncoded values is given as

$$\mathbf{Y_{HAZ\ at\ FSS} = 860.797 - 1.54818(C) - 4.87497(T) + 47.0337(S) + 0.0293349(CT) - 0.0940571(CS) - 0.304983(TS)} \quad (5.7)$$

Where $Y_{HAZ\ at\ FSS}$ is in microns, C is in A, T is in mm/sec and S is in mm

5.5.3 RESPONSE SURFACE PLOTS AND CONTOUR PLOTS FOR HAZ WIDTH AT FSS PLATE

From surface and contour plots shown in Figures 5.30 – 5.35 it appears that all the two factor interaction effects are important in respect of HAZ width at FSS. However, it seems that interaction effect of S – T, on HAZ at FSS, is the strongest one as the corresponding surface plot (Figure 5.30) shows much twist and contour plot as well, (Figure 5.33) reveals significant bending in the contour lines. All the response surface plots and contour plots can be utilized for selecting the combination of any two parameters to achieve the desired response, while the third parameter is kept constant at one of its level.

Surface plots and contour plots for other combinations are also possible, as mentioned earlier (the third parameter being set at other two levels as well). Some of these are included in the Appendix.

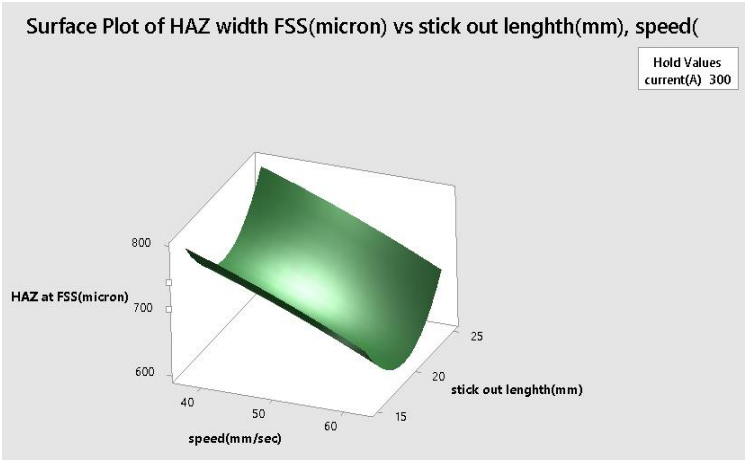

Figure 5.30 Response surface plot showing combined effects of S and T on HAZ at FSS when C is kept constant (C_{mid} = 300 A)

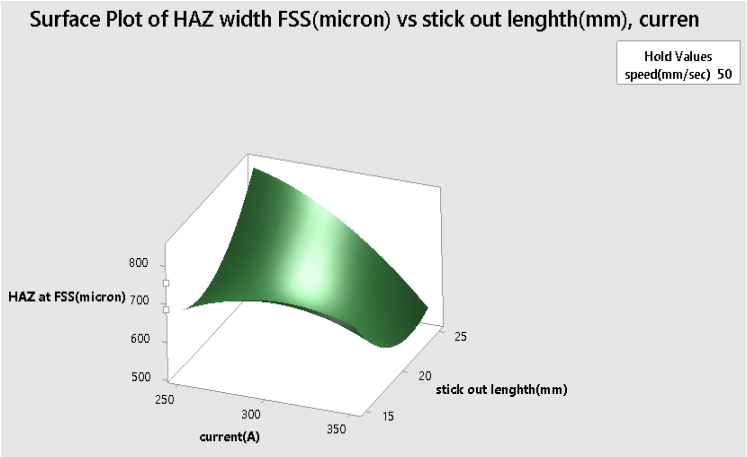

Figure 5.31 Response surface plot showing combined effects of S and C on HAZ at SS when T is kept constant (T_{mid} = 50 mm/sec)

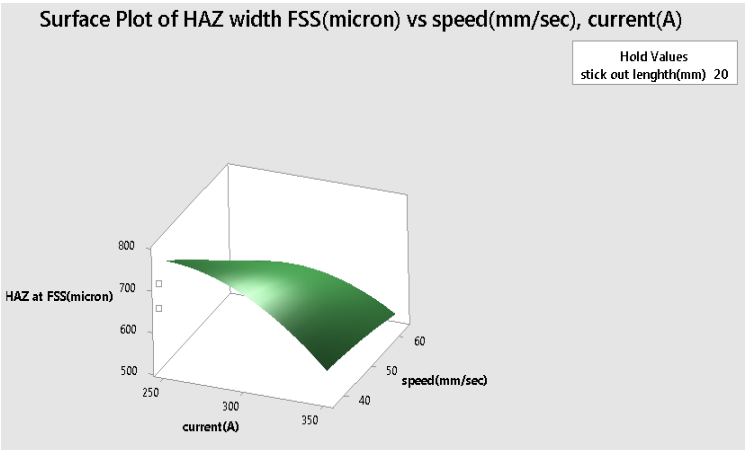

Figure 5.32 Response surface plot showing combined effects of C and T on HAZ at FSS when S is kept constant (S_{mid} = 20 mm)

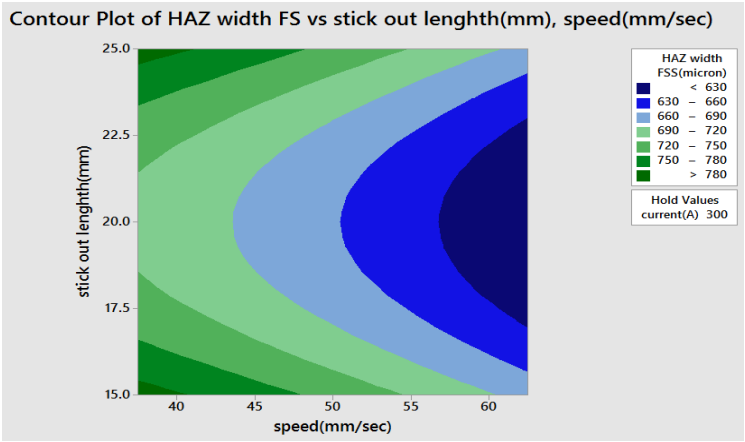

Figure 5.33 Contour plot showing combined effects of S and T on HAZ at FSS when C is constant (C_{mid} = 300 A)

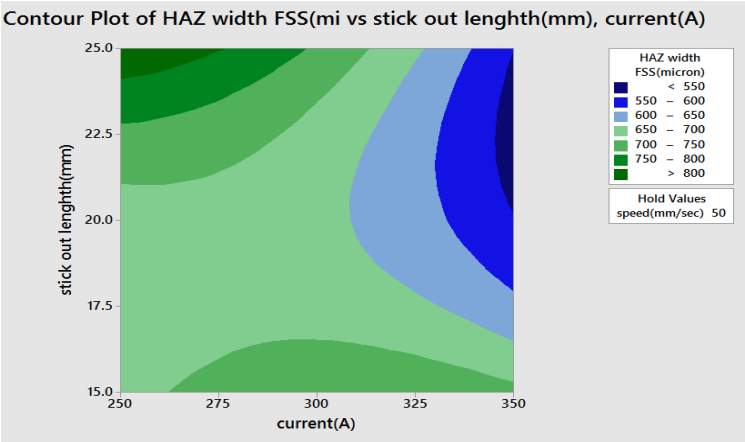

Figure 5.34 Contour plot showing combined effects of C and S on HAZ at FSS when T is kept constant (T_{mid} = 50 mm/sec)

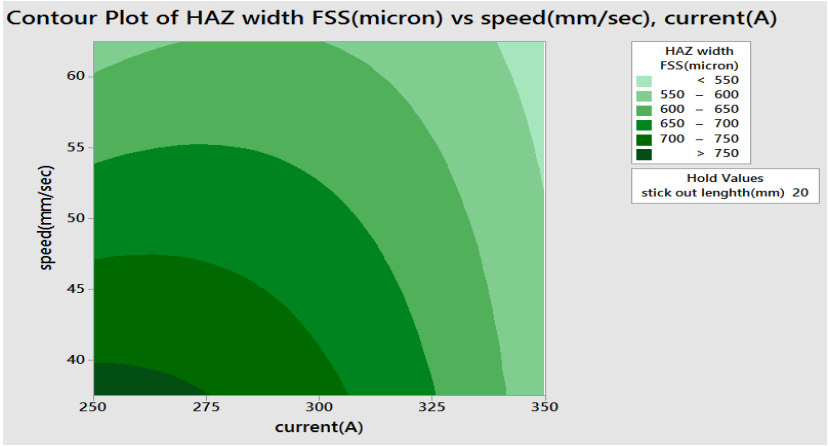

Figure 5.35 Contour plot showing combined effects of C and T on HAZ at FSS when S is kept constant (S_{mid} = 20 mm)

5.6 PROCESS OPTIMIZATION

Optimization techniques are applied on the observed data corresponding to Taguchi's L9 orthogonal array experiments. First, optimization has been carried out separately for maximization of i) ultimate tensile strength (UTS), ii) percentage elongation (PE), iii) hardness at weld, and minimization of iv) HAZ at mild steel side and v) HAZ at ferritic stainless steel side by Taguchi's method. Next, multi-objective optimization has been done, in which simultaneous maximization of ultimate tensile strength, percentage elongation, hardness at weld and minimization of HAZ width at mild steel side and HAZ width at ferritic stainless steel side have been performed. Grey-based Taguchi method has been used for this purpose.

5.6.1 SINGLE OBJECTIVE OPTIMIZATION FOR ULTIMATE TENSILE STRENGTH (UTS) BY TAGUCHI METHOD

Taguchi method uses a statistical measure of performance called signal to noise (S/N) ratio. The S/N ratio is the ratio of the mean (signal) to the standard deviation (noise). It depends on the quality of the product or process. The standard S/N ratio used is as follows: nominal is the better, larger is the better and lower is the better. For maximization of the responses larger is the better has been used and for the minimization of the responses smaller is better has been used in the present work.

Mean S/N ratio table is given in Table 5.6. Main effects plot for S/N ratios is shown in Figure 5.36, obtained by using MINITAB 17 software.

Table 5.6 Mean S/N ratio table for UTS

Level 1	**Current(C)**	**Speed(T)**	**Stick-out length(S)**
1	53.66	52.98	53.91
2	54.17	53.40	53.40
3	53.63	55.08	54.15
Delta	0.54	2.10	0.75
Rank	3	1	2

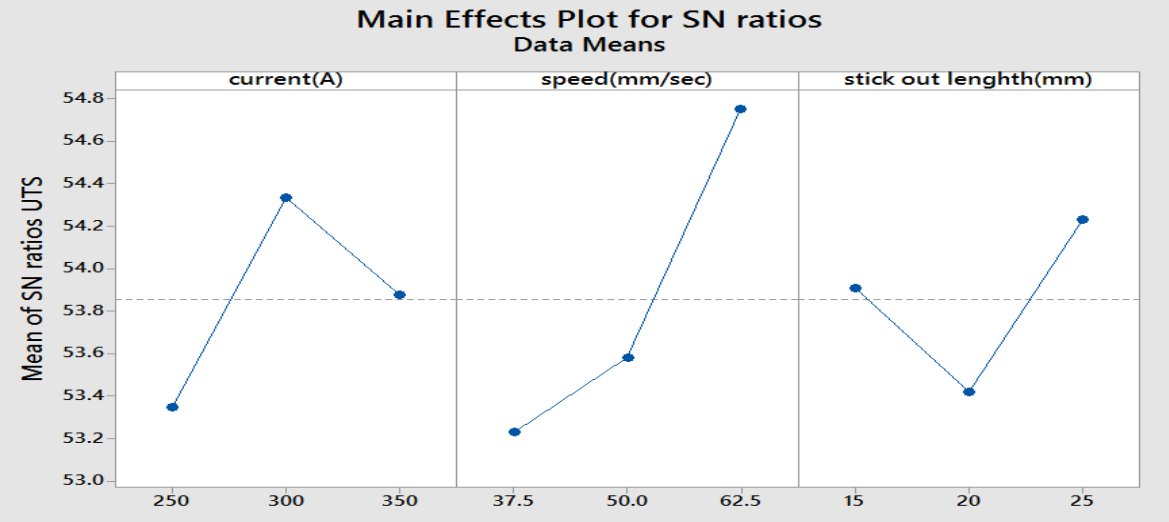

Figure 5.36 Main effects plot for S/N ratios of ultimate tensile strength

From Figure 5.36, it is found that current at level 2, speed at level 3 and stick-out length at level 3 [**C2 T3 S3**] (i.e. current = 300 A, speed = 62.5 mm/sec and stick-out = 25 mm.) is the parametric condition which will give maximum value of ultimate tensile strength (UTS), within the range which has been used in the experiments. This parametric combination is based on the level of the each factor at which S/N ratio value is maximum.

ANOVA for UTS

Analysis of variance (ANOVA) using MINITAB 17 software has been performed to determine the contribution of process parameters on ultimate tensile strength. Table 5.7 shows the results of analysis of variance for ultimate tensile strength. If P-value is less than 0.05, the corresponding factor is said to have significant influence on the response, at 95% level of confidence. So Table 5.7 gives the idea that none of the individual or interaction terms influences UTS significantly at 95 % confidence level. However, on examining the P-values it is found that among the individual terms/parameters, influence of speed on UTS is the highest (P=0.085) and that of the current is the lowest (P=0.555). The determination factor (R-sq) indicates the goodness of fit of the model. The value of R-sq of this model is 92.8% which is greater than 80%. This implies that at least 92.8% of the variability in data for the response is explained by the model. This indicates that the proposed mathematical model for UTS is adequate.

Table 5.7 ANOVA table for means of UTS

Source	DF	Seq SS	Adj SS	Adj MS	F	P
Current(C)	2	0.5547	0.5547	0.2774	0.80	0.555
Speed(T)	2	7.4302	7.4302	3.7151	10.76	0.085
Stick-out length(S)	2	0.8841	0.8841	0.4421	1.28	0.439
Residual Error	2	0.6907	0.6907	0.3453		
Total	8	9.5598		R-sq =92.8%	R-sq(adj) =71.1%	

Where DF = Degree of freedom, SS = Sum of squared deviation, MS = Mean squared deviation F = Fisher's ratio, P = Probability of significance.

5.6.2 SINGLE OBJECTIVE OPTIMIZATION FOR PERCENTAGE ELONGATION (PE) BY TAGUCHI METHOD

Same procedure as discussed above is followed for optimization of percentage elongation (PE). The corresponding mean S/N ratio values are calculated and shown in Table 5.8. As larger is the better criterion is required, eq. 2.4 as discussed in chapter 2 is used for calculation of S/N ratios. Main effects plot for S/N ratios is shown in Figure 5.37, using MINITAB 17 software.

Table 5.8 Mean S/N ratio table for PE

Level	Current(C)	Speed(T)	Stick-out length(S)
1	23.93	22.17	24.75
2	23.66	24.09	23.87
3	24.13	25.46	23.10
Delta	0.47	3.29	1.65
Rank	3	1	2

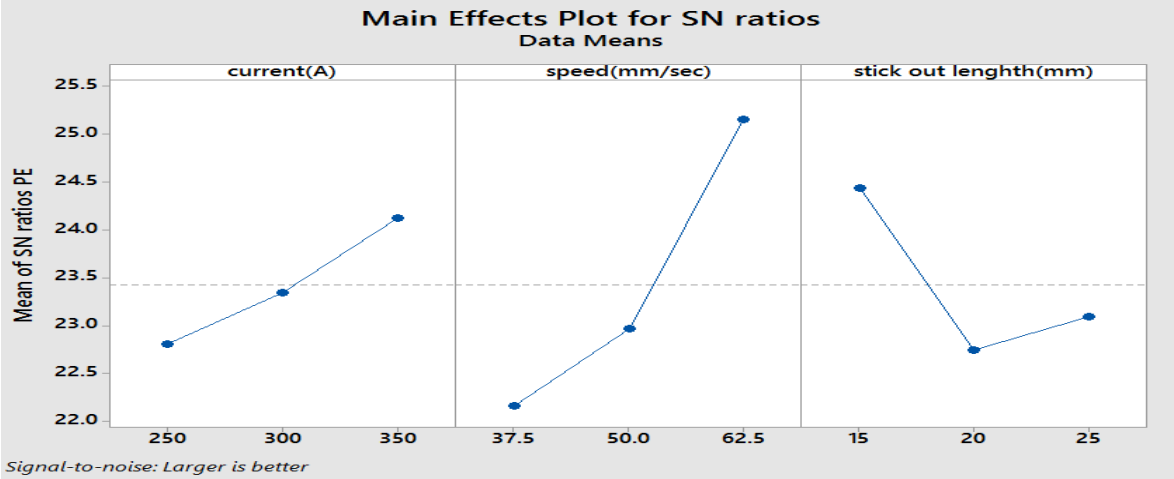

Figure 5.37 Main effects plot for S/N ratios of percentage elongation

From the plots shown in Figure 5.37, the optimized condition for maximum percentage elongation is current at level 3, speed at level 3 and stick-out length at level 1 [C3 T3 S1] (i.e. current = 350 A, speed = 62.5 mm/sec and stick-out length = 15 mm.), corresponding to the highest value of S/N ratio relating to these parameters.

ANOVA for PE

The table 5.9 shows the results of analysis of variance for percentage elongation has been obtained by using MINITAB 17 software.

Table 5.9 Analysis of variance for PE

Source	DF	Seq SS	Adj SS	Adj MS	F	P
Current(C)	2	0.3281	0.3281	0.089678	0.65	0.605
Speed(T)	2	16.4368	16.4368	0.015511	32.72	0.030
Stick-out length(S)	2	4.1003	4.1003	0.003344	8.16	0.109
Residual Error	2	0.5024	0.5024	0.009478		
Total	8	21.3675		R-sq =97.6%	R-sq(adj) =90.6%	

Where DF = Degree of freedom, SS = Sum of squared deviation, MS = Mean squared deviation F = Fisher's ratio, P = Probability of significance.

On examining the P-values from Table 5.9, it is observed that speed is the most significant factor because corresponding P value is the lowest and it is 0.030. The P-values of stick-out length and current are 0.109 and 0.605 respectively, which do not influence the

response significantly. Thus as P-value corresponding to speed is less than 0.05, this parameter can be considered significant at 95% confidence level. (R-sq) is the determination factor which indicates the goodness of fit of the model. The value of R-sq of the model is 97.6% which is greater than 80%. This shows that at least 97.6% of the variability in data for the response is explained by the model.

5.6.3 SINGLE OBJECTIVE OPTIMIZATION FOR HARDNESS AT WELD BY TAGUCHI METHOD

The procedure as discussed earlier is followed for optimization of hardness at weld. Larger S/N ratio indicates that better signal is obtained and lesser noise is occurred. The effect of process parameters on the performance is indicated by S/N ratio. As larger is the better criterion is required, eq. 2.4 as discussed in chapter 2 is used for calculation of S/N ratios. Mean S/N ratio table is given in Table 5.10. Main effects plot for S/N ratio is shown in Figure 5.38, using MINITAB 17 software.

Table 5.10 Mean S/N ratio table for hardness at weld

Level	Current(C)	Speed(T)	Stick-out length(S)
1	50.91	50.55	50.29
2	50.29	50.85	50.78
3	50.56	50.37	50.69
Delta	0.62	0.47	0.50
Rank	1	3	2

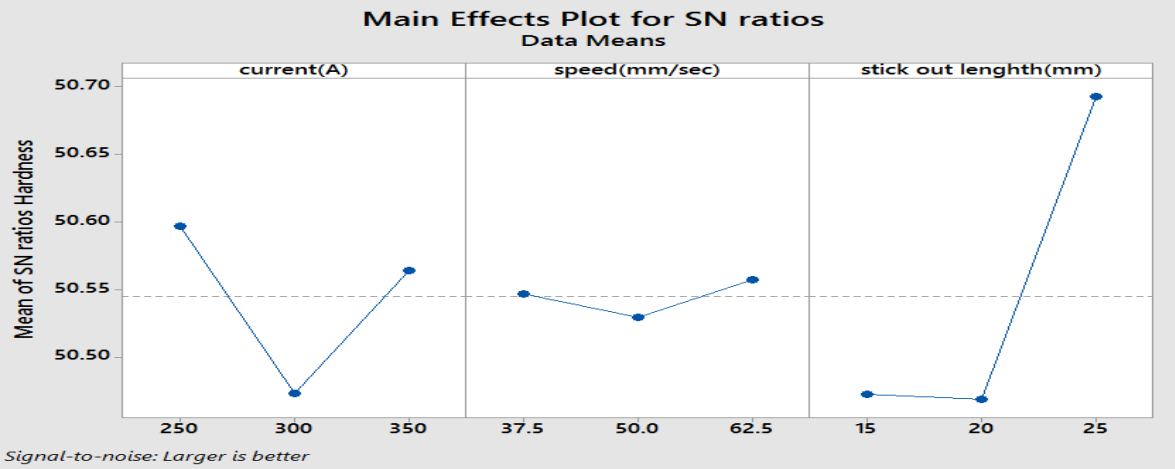

Figure 5.38 Main effects plot for S/N ratios of hardness at weld

The main effects plot of S/N ratios in Figure 5.38 demonstrates that the optimum condition for hardness at weld is current at level 1, speed at level 3 and stick-out length at level 3 [C1 T3 S3] (i.e. current = 250 A, speed = 62.5 mm/sec and stick-out length = 25 mm.).

This is finalised corresponding to the levels of the factors at which S/N ratio values are maximum.

ANOVA for hardness at weld

The analysis of variance for hardness at weld is shown in Table 5.11. After the examination of P-values it is observed that current is the most significant factor because corresponding P-value (P = 0.047) is the lowest and it is below 0.05. The P-values of stick-out length (P = 0.065) and traverse speed (P = 0.077) are greater than 0.05, so they are considered to be not so significant factors which influence hardness at weld (at 95% confidence level). However, the corresponding P-values are not far beyond 0.05. R-sq value indicates the goodness of fit of the model. The value of R-sq of the model is 97.9% which is greater than 80%. This implies that at least 97.9% of the variability in data for the response is explained by the model. This indicates that the proposed model is adequate.

Table 5.11 Analysis of variance for means of hardness at weld

Source	DF	Seq SS	Adj SS	Adj MS	F	P
Current(C)	2	0.58662	0.58662	0.29331	20.39	0.047
Speed(T)	2	0.34295	0.34295	0.17148	11.92	0.077
Stick-out length(S)	2	0.41656	0.41656	0.20828	14.48	0.065
Residual Error	2	0.02877	0.02877	0.01438		
Total	8	1.37491		R-sq =97.9%	R-sq(adj) =91.6%	

Where DF = Degree of freedom, SS = Sum of squared deviation, MS = Mean squared deviation F = Fisher's ratio, P = Probability of significance.

5.6.4 SINGLE OBJECTIVE OPTIMIZATION FOR HAZ WIDTH AT MS PLATE BY TAGUCHI METHOD

The mean S/N ratio table for HAZ width at MS plate is shown in Table 5.12. As smaller is the better criterion is required, eq. 2.2 as discussed in chapter 2 is used for calculation of S/N ratios. Main effects plot for S/N ratio is shown in Figure 5.39, using MINITAB 17 software.

Table 5.12 Mean S/N ratio table for HAZ width at mild steel side

Level	**Current(C)**	**Speed(T)**	**Stick-out length(S)**
1	-56.87	-56.80	-56.79
2	-57.17	-56.75	-56.76
3	-55.77	-56.26	-56.27
Delta	1.40	0.54	0.52
Rank	1	2	3

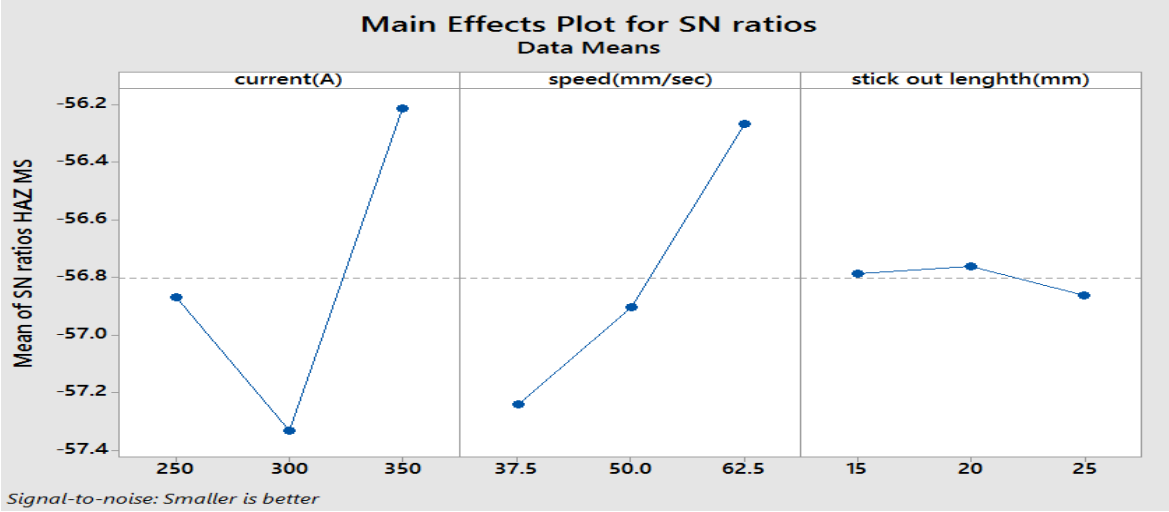

Figure 5.39 Main effects plot for S/N ratios of HAZ at MS

From the plots shown in Figure 5.39, the optimized condition for minimum HAZ width at MS side is current at level 3, speed at level 3 and stick-out length at level 2 [C3 T3 S2] (i.e. current = 350 A, speed = 62.5 mm/sec and stick-out length = 20 mm.), corresponding to the lowest value of S/N ratio relating to these parameters.

ANOVA for HAZ width at MS plate

Analysis of variance (ANOVA) using MINITAB 17 software has been carried out to determine the contribution of process parameters on HAZ width at MS side. The table 5.13 shows the results of analysis of variance for HAZ width at MS side. Table 5.13 indicates that no parameter has significant role in influencing HAZ width at MS side at 95% confidence level. All P-values are greater than 0.05. However, it is found that among the individual terms/parameters, influence of current on HAZ at MS is the highest (P = 0.100) and that of the stick-out is lowest (P = 0.413). The R-sq value listed in Table 5.13 suggests that the analysis is adequately valid because R-sq (= 92.3%) value is greater than 80%.

Table 5.13 Analysis of variance for means for HAZ width at mild steel side

Source	DF	Seq SS	Adj SS	Adj MS	F	P
Current(C)	2	3.2450	3.2450	1.6225	9.04	0.100
Speed(T)	2	0.5244	0.5244	0.2622	1.46	0.406
Stick-out length(S)	2	0.5114	0.5114	0.2557	1.42	0.413
Residual Error	2	0.3591	0.3591	0.1796		
Total	8	4.6399		R-sq = 92.3%	R-sq(adj) = 69.0%	

Where DF = Degree of freedom, SS = Sum of squared deviation, MS = Mean squared deviation F = Fisher's ratio, P = Probability of significance.

5.6.5 SINGLE OBJECTIVE OPTIMIZATION FOR HAZ WIDTH AT FSS PLATE BY TAGUCHI METHOD

As discussed earlier, same procedure is followed for optimization of HAZ width at FSS plate. The corresponding mean S/N ratio values are calculated and shown in Table 5.14. As smaller is the better criterion is required, eq. 2.2 as discussed in chapter 2 is used for calculation of S/N ratios where ideal value is taken to be zero. By using MINITAB 17 software, the main effects plot for S/N ratio, in respect of HAZ width at ferritic stainless steel side is found and it is shown in Figure 5.40.

Table 5.14 Mean S/N ratio table for HAZ width at ferritic stainless steel (FSS) side

Level	Current(C)	Speed(T)	Stick-out length(S)
1	-57.24	-56.60	-56.42
2	-57.04	-56.34	-56.04
3	-54.82	-56.17	-56.64
Delta	2.41	0.43	0.60
Rank	1	3	2

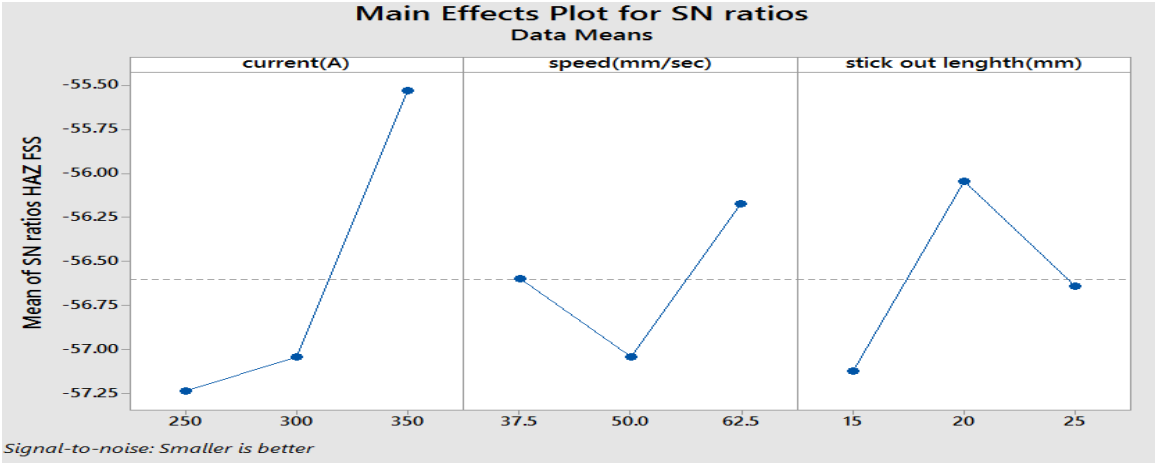

Figure 5.40 Main effects plot for S/N ratios of HAZ width at FSS

It is observed from this plot shown in Figure 5.40, the parametric condition for minimum HAZ width at FSS side is: current at level 3, speed at level 3 and stick-out length at level 2 [C3 T3 S2] (i.e. current = 350 A, speed = 62.5 mm/sec and stick-out length = 20 mm.). This is based on the level of each factor at which S/N ratio value is minimum.

ANOVA for HAZ width at FSS plate

The table 5.15 is the ANOVA table for HAZ width at ferritic stainless steel side. If P-value in the table is less than 0.05 then the corresponding variable is considered as statistically significant at 95% confidence level. On examining the P-values from the Table 5.15, it is observed that current (P = 0.025) is the most significant factor because corresponding P-value is the lowest and it is below 0.05. The P-values of speed and stick-out are greater than 0.05, so they are not considered to be so significant parameters. The determination factor R-sq value is 97.6% which is greater than 80%. This means that at least 97.6% of the variability in data for the response is explained by the model and the model is adequate.

Table 5.15 Analysis of variation for means for HAZ width at ferritic steel side

Source	DF	Seq SS	Adj SS	Adj MS	F	P
Current(C)	2	10.7921	10.7921	5.3961	38.34	0.025
Speed(T)	2	0.2752	0.2752	0.1376	0.98	0.506
Stick-out length(S)	2	0.5490	0.5490	0.2745	1.95	0.339
Residual Error	2	0.2815	0.2815	0.1407		
Total	8	11.8977		R-sq = 97.6%	R-sq(adj) = 69.0%	

Where DF = Degree of freedom, SS = Sum of squared deviation, MS = Mean squared deviation F = Fisher‟s ratio, P = Probability of significance.

Confirmatory test:

Confirmatory tests for all the responses individually, have not been fully carried out yet. However, the confirmatory test to validate the predicted optimal condition for multi objective optimization is carried out and discussed in section 5.7.4. For validating the five individual optimum parametric settings, predicted by single objective optimization methodology (for UTS, PE, weld hardness, HAZ width at MS side and HAZ width at FSS side separately), confirmatory tests have been planned and are in process. (Few of these are completed and the results indicate acceptability of the predicted optimal conditions)

One such validity test in respect of single objective optimization of hardness at weld is given below; however the optimum parametric setting in the case is same as sample no. 3.

Hardness at weld at optimal condition = 348.5 HV

Hardness at weld at random condition = 310.8 HV

In confirmatory tests, two samples have been welded, one as per the optimized combination of parameters obtained from optimization technique while other with a random combination (current 240 A, traverse speed 60 mm/sec and stick-out length 28 mm) of the parameters.

5.7 MULTI-OBJECTIVE OPTIMIZATION BY GREY-BASED TAGUCHI METHOD

In order to solve multi-objective problem of minimization of HAZ width at mild steel side, HAZ width at ferritic stainless steel side and maximization of ultimate tensile strength, percentage elongation and hardness at weld - all taken together, grey relational analysis along with Taguchi method has been applied in the present study. The Grey-Taguchi method is an effective optimization tool to optimize two or more responses simultaneously. This procedure includes the following steps.

I. The experiments are carried out as per Taguchi’s orthogonal array design matrix.
II. All the response values are normalized.
III. Grey relational coefficients are obtained.
IV. Grey relational grades are calculated by taking the average of the grey relational coefficients.

V. Taguchi method is used on grey relational analysis using the concept of S/N ratio.

VI. The optimal levels of the parameters are selected.

VII. ANOVA has been done to identify the significance of the each parameter on the selected response.

5.7.1 GREY RELATIONAL ANALYSIS

In the grey relational analysis, the responses tabulated in Table 3.2, in chapter 3 are normalized initially. In this step, a linear normalization of the experimental results for the responses such as ultimate tensile strength, percentage elongation, hardness at weld, HAZ width at mild steel side and HAZ width at ferritic stainless steel side are performed in the range of 0 to 1. This process is called grey relational generation. For larger-the-better characteristics, the normalized values are calculated by using eq. (2.6) in chapter 2. For smaller-the-better quality characteristics (HAZ width at both MS and FSS side), normalized values are calculated by using eq. (2.7), which is already discussed in chapter 2.

The results achieved through eq. (2.6) and eq. (2.7) (from chapter 2) are depicted in the Table 5.16

Table 5.16 Normalized values of the responses

Experiment No	UTS	PE	Hardness at weld	HAZ width at MS	HAZ width at FSS
1	0.174863388	0.409638554	0.599137931	0.118559905	0
2	0.131147541	0	0.149137931	0.199245938	0.354509222
3	0.387978142	0.86746988	1	0.925727595	0.076001696
4	0	0.277108434	0.393534483	0.217257372	0.207085012
5	0.699453552	0.409638554	0.732758621	0	0.083684545
6	1	0.843373494	0	0.28415991	0.350867077
7	0.426229508	0.13253012	0.492672414	0.321883516	0.82750477
8	0.103825137	0.987951807	0.522844828	0.970991824	0.203968624
9	0.666666667	1	0.554310345	1	1

5.7.2 CALCULATION OF GREY RELATIONAL COEFFICIENTS

Grey relational coefficients are obtained in order to relate the ideal and actual

experimental results. Table 5.17 demonstrates the grey relational coefficients for each experiment of the L9 orthogonal array of Taguchi design matrix. After normalization, grey relational co-efficient (GRC) is calculated by eq. 2.8 as mentioned in chapter 2.

Table 5.17 Values of grey relational coefficients corresponding to 9 experiments

Experiment No	UTS	PE	Hardness at weld	HAZ width at MS	HAZ width at FSS
1	0.195095949	0.25304878	0.332855093	0.184938584	0.166666667
2	0.187116564	0.166666667	0.190319934	0.199849301	0.236549002
3	0.246298789	0.601449275	1	0.72920205	0.177936212
4	0.166666667	0.216710183	0.247995724	0.203512084	0.201427113
5	0.399563319	0.25304878	0.42804428	0.166666667	0.179160827
6	1	0.560810811	0.166666667	0.218378735	0.235534384
7	0.258474576	0.187358916	0.282754418	0.227760216	0.536919627
8	0.182452642	0.943181818	0.295353278	0.873331265	0.200796887
9	0.375	1	0.309746328	1	1

5.7.3 CALCULATION OF GREY RELATIONAL GRADES

Now a weighing method is used to integrate the grey relational coefficient of each experiment into the grey relational grade. The overall assessment of the multiply quality characteristics is based on the grey relational grade which is given by eq. (2.9) from chapter 2. In calculating the grey relational grade, the weighting ratio for all the responses is set as 1:1, i.e each characteristics has equal importance or relative weighting. The evaluated values of grey relational grades are depicted in the Table 5.18. The higher the value of grey relational grade, better is the desired response.

S/N ratios of grey relational grade have been calculated by "Minitab 17" software and demonstrated in Table 5.19, where the value of delta is higher in case of speed. Therefore speed has the more impact on the overall grey relational grade. Large value of grey relational grade is the objective, always.

Table 5.18 Calculated values of grey relational grade

Experiment No.	Grey Relational Grade
1	0.045304203
2	0.039220059
3	0.110195453
4	0.041452471
5	0.057059355
6	0.087255624
7	0.05973071
8	0.099804636
9	0.147389853

Table 5.19 Response table for S/N ratio of grey relational grade

Level	Current (A)	Speed (mm/sec)	Stick-out (mm)
1	-24.72	-26.33	-22.69
2	-24.57	-24.34	-24.14
3	-20.37	-18.99	-22.84
Delta	4.35	7.34	1.44
Rank	2	1	3

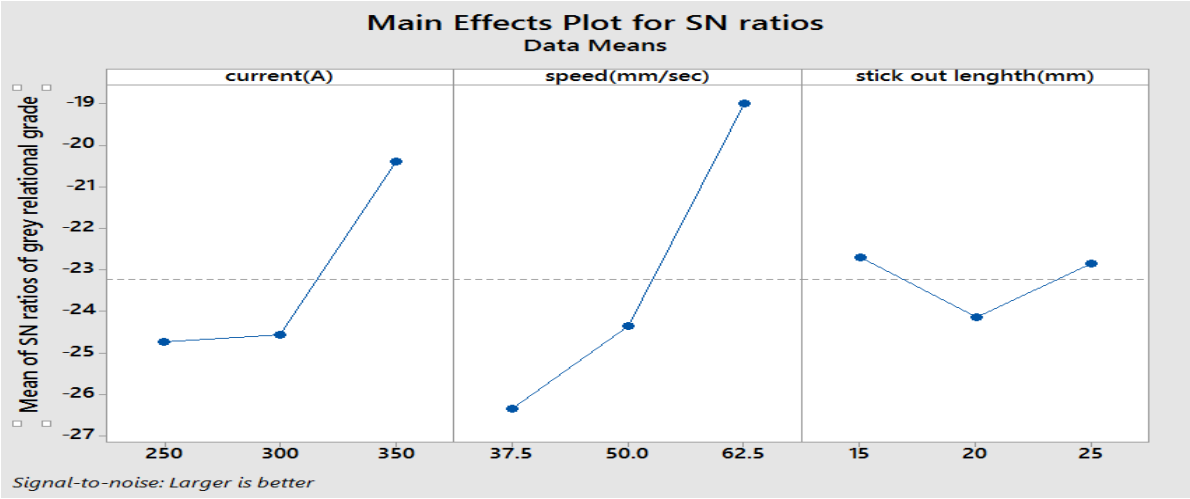

Figure 5.41 Main effects plot for S/N ratios for grey relational grade

Main effects plot for S/N ratios for grey relational grade is shown in Figure 5.41. It is examined that for multi-response optimization, the optimum parametric configuration is current at level 3, speed at level 3 and stick-out length at level 1 [C3 T3 S1] (i.e. current = 350 A, speed = 62.5 mm/sec and stick-out length = 15 mm.) corresponding to the levels of the highest S/N ratio values of grey relational grades of these parameters.

ANOVA for multiple-response characteristic

Table 5.20 shows analysis of variance for grey relational grade. Analysis of variance (ANOVA) is done to identify the impact of the input parameters on the overall multi-objective output response. ANOVA is carried out by comparing the P-values of the parameter. If P-values in the table are less than 0.05 than the corresponding variables are considered statistically significant, at 95% confidence level.

In Table 5.20, the P-value for current is 0.401, P-value for traverse speed is 0.538 and for stick-out length it is 0.557. Thus, it is observed that contribution of current is the highest on the overall objective, though none of the factors is found to be significant at 95% confidence level, as P value in no case is less than 0.05. While preparing ANOVA here, interaction terms are not considered.

Table 5.20 Analysis of variance for grey relational grade

Source	DF	Seq SS	Adj SS	Adj MS	F	P
Current(C)	2	0.003273	0.003273	0.001636	1.50	0.401
Speed(T)	2	0.001877	0.001877	0.000939	0.86	0.538
Stick-out length(S)	2	0.001739	0.001739	0.000870	0.79	0.557
Residual Error	2	0.002188	0.002188	0.001094		
Total	8	0.009078				

5.7.4 CONFIRMATORY TEST

Confirmatory tests have been performed to validate the above optimized condition. In confirmatory tests, two samples have been welded, one as per the optimized condition of parameters found from optimization technique while other with a random combination (current = 330 A, traverse speed = 58 mm/sec and stick-out = 12mm) of the parameters. The results obtained are:

UTS at optimized condition = 595 MPa

UTS at random condition = 539 MPa

Percentage elongation (PE) at optimized condition = 18.6 %

Percentage elongation (PE) at random condition = 16.2 %

Hardness at weld at optimal condition = 360.7 HV

Hardness at weld at random condition = 330.8 HV

HAZ width at MS side at optimal condition = 606.594 microns

HAZ width at MS side at random condition = 632.826 microns

HAZ width at FSS side at optimal condition = 516.561 microns

HAZ width at FSS side at random condition = 540.254 microns

The results are found to be satisfactory. The results indicate the validity of the optimization technique adopted in the study. Also, it is found that the UTS, PE, hardness at weld, HAZ width at both MS and FSS values are better than those observed in the experimental runs.

CHAPTER 6

6. CONCLUSIONS AND FUTURE SCOPE OF WORK

6.1 CONCLUSIONS

In the present work dissimilar welding of ferritic stainless steel AISI 409 to mild steel AISI 1018 has been done by submerged arc welding (SAW) using mild steel as filler wire, at various levels of current (C), traverse speed (T) and stick-out length (S). Plate thickness = 8 mm. Based on the results of the experiments, microstructural studies and analysis of the data, following conclusions are made.

- The results of present study indicate that welding between ferritic stainless steel AISI 409 and mild steel AISI 1018 by submerged arc welding, using mild steel filler wire, can produce satisfactory butt joint under suitable parametric combination.

- Visual inspection shows some defects like undercut, incomplete penetration, non-uniform reinforcement and lack of fusion in some samples. However, under certain combinations of current, traverse speed and stick-out length, some welded samples are found to be defect free.

- Observed data in tensile test indicate that ultimate tensile strength is satisfactory for many of the joints made at different levels of current, traverse speed and stick-out length. However, some parametric conditions have been identified which have produced joints of excellent tensile strength. The conditions leading to poor tensile strength are also indicated for few samples. Percentage elongation values obtained in tensile testing are also found to be good for most of the samples, with exception in few cases.

- In tensile test, except for one sample, none of the sample has failed in the weld region, failure has occurred within the base material or through the adjacent HAZ region at mild steel side. It indicates that the quality of the welded joint is good.

- From the micro-hardness tests it is observed that the hardness value increases from base region to HAZ and HAZ to weld region for some of the samples. However,

consistency in this trend is not observed for all the samples.

- SEM results show some defects in a sample in the form of slag inclusions, crack propagation etc. Few samples are found almost defect free as well. SEM pictures also reveal, HAZ width of both sides (FSS and MS) etc., clearly.

- The microstructure of mild steel contains the mixture of ferrite and pearlite in which ferrite is present at the grain boundaries of austenite which has later transformed to pearlite. For ferritic stainless steel the microstructure has ferrite and precipitation of chromium carbide. In the weld region the microstructure is fully ferritic and contains scattered titanium nitride or carbide precipitation. The grains are finer and uniformly distributed throughout the weld. In some samples weld region contains relatively homogeneous ferrite grains in which accicular ferrite structure is formed within the grains. Ferritic phase is predominant in the HAZ region adjacent to stainless steel.

- Mathematical models have been developed to correlate input parameters with ultimate tensile strength (UTS), percentage elongation (PE), hardness at weld, HAZ width at MS side and HAZ width at FSS side. Response surface plots and contour plots are generated by using mathematical models developed for UTS, PE, hardness at weld, HAZ at MS and HAZ at FSS. These plots are useful for prediction of the response(s) at some given combination of any two parameters while the third parameter is held constant at one of its levels. Significance of the various interactions like current - speed, stickout length - speed, stickout length - current, on the responses: UTS, PE, hardness at weld, HAZ at MS and HAZ at FSS can also be interpreted from these plots.

- In single objective optimization, Taguchi's S/N ratio concept is utilized and it is found that the optimum condition for maximum i) UTS is [C2 T3 S3] (i.e. current = 300 A, speed = 62.5 mm/sec, stick-out = 25 mm), ii) PE is [C3 T3 S1] (i.e. current = 350 A, speed = 62.5 mm/sec and stick-out length = 15 mm) and iii) hardness at weld is [C1 T3 S3] (i.e. current = 250 A, speed = 62.5 mm/sec and stick-out length = 25 mm.), and the optimum condition for minimum iv) HAZ width at MS is [C3 T3 S2] (i.e. current = 350 A, speed = 62.5 mm/sec and stick-out length = 20 mm) and v) HAZ width at FSS is [C3 T3 S2] (i.e. current = 350A, speed = 62.5 mm/sec and stick-out length = 20 mm).

- Multi-objective optimization carried out by Grey-Taguchi method, showed that the optimum parametric setting is: current = 350 A, traverse speed = 62.5 mm/sec and stick-out length = 15 mm [C3 T3 S1], for simultaneous maximization of UTS, PE, hardness at weld and minimization of HAZ width at MS and FSS.

- The optimum condition determined by multi-objective optimization technique (Taguchi and Grey-Taguchi method) has been validated by confirmatory tests

6.2 FUTURE SCOPE OF WORK

- In the present study, dissimilar welding of AISI 409 stainless steel to mild steel AISI 1018 has been carried out by submerged arc welding (SAW) using mild steel filler wire. In future, experiments and analyses may be carried out for joining other varieties of stainless steel to mild steel.

- The parameters like electrode stick out, electrode wire diameter, composition of filler wire and voltage may also be included as variable input parameters in future study.

- Different combinations of filler wire and flux can be studied in future.

- Effects of different types of edge preparation for joint strength can also be studied.

- More elaborate study of microstructure characteristics, scanning electron microscopy and hardness test at different regions also provide scope of future work.

- Few of the other optimization techniques like simulated annealing, RSM, principle component analysis, genetic algorithm, ETLBO may be used in future work and suitability of them may be examined.

REFERENCES

[1] R.S. Parmar, "Welding processes and technology, 2nd edition", Khanna Publications, New Delhi-1997.

[2] O.P. Khanna, "Welding Technology", Dhanpat Rai & Sons, 1986.

[3] https://www.weldinginfocenter.com/history

[4] www.weldguru.com/welding-history

[5] The ABC's of Arc Welding and Inspection, Published by KOBE STEEL, LTD.

[6] A. Ghosh & A.K., Mallik, "Manufacturing Science", East-West Press Private Limited, New Delhi-2008.

[7] http://nhml.com/weld-discrepancies

[8] www.slideshare.net/welding-inspection

[9] www.slideshare.net/surface-preparation

[10] http://www.weldguru.com

[11] http://www.hobartbrothers.com/downloads/subarcbrochure_web.pdf.

[12] www.esab.com/submerged-arc welding and http://shodhganga.inflibnet.ac.in:8080/jspui/bitstream/10603/13984/7/07chapter%202.pdf

[13] www.nhml.com

[14] www.asminternational.org/content/ASM/.../06940G_Chapter_1.pdf, dated 11/08/2012

[15] Gas Tungsten Arc Welding Handbook/inspection and testing of weld joint & http://www.totalmateria.com

[16] A K Lakshminarayanan, K Shanmugam, V Balasubramanian, "*Effect of Autogenous Arc Welding Processes on Tensile and Impact Properties of Ferritic Stainless Steel Joints*", journal of iron and steel research, international. 2009, 16(1): 62-68, 16

[17] Ja young Hong, Yong taek Shin, Hae Woo Lee, "*Characterization of Corrosion Resistance in a Ferritic Stainless Steel Stabilized with Ti Addition*", Int. J. Electrochem. Sci.,

9 (2014) 7325 – 7334

[18] T. Mohandas, G. Reddy Madhusudan, N. Mohammad, "*A comparative evaluation of gas tungsten and shielded metal arc welds of a "ferritic" stainless steel*", Journal of Materials Processing Technology, 94 (1999), pp, 133-140.

[19] T. Mohandas, V.V. Satyanarayana, G. Madhusudhan Reddy, "*Dissimar matal friction welding of austenitic - ferritic stainless steel*", Journal of Materials Processing Technology, Volume 160, Issue 2, 20 March 2005, pp. 128-137.

[20] Farhan Shahid, R.K Rajkumar, Fatin Hamimi, "*Investigating the dissimilar weld joints of aisi 302 austenitic stainless steel and low carbon steel*", International Journal of Scientific and Research Publications, 2, Issue 11, (November 2012), pp. 1-5.

[21] Radha Raman Mishra, Visnu Kumar Tiwari, Rajesha S, "*A study of tensile strength of MIG and TIG welded dissimilar joints of mild steel and stainless steel*", International Journal of Advances in Materials Science and Engineering, 3, April 2014, pp. 23-32.

[22] E. Taban, E. Deleu, A. Dhooge, and E. Kaluc. "*Evaluation of Dissimilar Welds between Ferritic Stainless Steel Modified 12% Cr and Carbon Steel S355*", supplement to the welding journal, december 2008.

[23] M. Rossini, P. Russo Spena, L. Cortese, P. Matteis, D. Firrao, "*Investigation on dissimilar laser welding of advanced high strength steel sheets for the automotive industry*", Materials Science and Engineering: A, Volume 628, 25 March 2015, Pages 288-296

[24] Mr. Suresh Akella, Mr. Vemanaboina Harinadh, Mr. Yaggadi Krishna, Mr. Ramesh Kumar Buddu, "*A Welding Simulation of Dissimilar Materials SS304 and Copper* ", Procedia Materials Science, Volume 5, 2014, Pages 2440-2449.

[25] Velten Behm, Matthias Höfemann, Ansgar Hatscher, André Springer, Stefan Kaierle, David Hein, Manuel Otto, Ludger Overmeyer, "*Investigations on Laser Beam Welding Dissimilar Material Combinations of Austenitic High Manganese (FeMn) and Ferrite Steels*", Physics Procedia, Volume 56, 2014, Pages 610-619.

[26] Nilesh Kumar, Wei Yuan, Rajiv S. Mishra, *"Chapter 5 - Friction Stir Welding of Dissimilar Materials, Friction Stir Welding of Dissimilar Alloys and Materials",* 2015, Pages 71-114

[27] Bing-Qing Chen, Hua-Ping Xiong, Bing-Bing Sun, Bo-Rui Du, Zhen-Wei Wei, Bo Chen, *"Dissimilar joining of Ti3Al-based alloy to Ni-based superalloy by arc welding technology using gradient filler alloys",* Materials & Design, Volume 87, 15 December 2015, Pages 732-741.

[28] Junhao Sun, Qi Yan, Wei Gao, Jian Huang, *"Investigation of laser welding on butt joints of Al/steel dissimilar materials",* Materials & Design, Volume 83, 15 October 2015, Pages 120-128.

[29] P. Čičo, D. Kalincová, M. Kotus, *"Influence of welding method on microstructural creation of welded joints"*, Vol. 57, 2011 (Special Issue): S50–S56.

[30] International Stainless Steel Forum Rue Colonel Bourg 120 B-1140 Brussels Belgium.

[31] V.I. Isaev, A.N. Cherepanov, V.P. Shapeev, "*Numerical study of Heat Modes of laser welding of dissimilar metals with an intermediate insert",* Heat and Mass Transfer, 99, (2016), pages 711-720.

[32] Z. Shen, Y. Chen, M. Haghshenas, A.P. Gerlich, *"Role of welding parameters on interfacial bonding in dissimilar steel/aluminum friction stir welds",* Engineering Science and Technology 18, (20150, pages 270-277.

[33] Xiao-yong WANG, Da-qian SUN, Shi-qiang YIN, Dong-yang LIU, *"Microstructures and mechanical properties of metal inert-gas arc welded Mg–steel dissimilar joints",* Transactions of Nonferrous Metals Society of China, Volume 25, (2015), Pages 2533-2542.

[34] K. Devendranath Ramkumar, Anshuman Singh, Shubham Raghuvanshi, Ankur Bajpai, Tathagat Solanki, M. Arivarasu, N. Arivazhagan, S. Narayanan, "*Metallurgical and mechanical characterization of dissimilar welds of austenitic stainless steel and super-duplex stainless steel – A comparative study",* Manufacturing Processes, 19, (2015), Pages 212-232.

[35] Aboulfazl Moteshakker, Iman Danaee, *"Microstructure and Corrosion Resistance of Dissimilar Weld-Joints between Duplex Stainless Steel 2205 and Austenitic Stainless Steel 316L",* Materials Science & Technology, 32, (2016), Pages 282-290.

[36] V.K. Patel, D.L. Chen, S.D. Bhole, *"Dissimilar ultrasonic spot welding of Mg-Al and Mg-high strength low alloy steel",* heoretical and Applied Mechanics, 4, (2014).

[37] Rakesh Chaudhari, Asha Ingle, Kanak Kalita, *"Stress Analysis of Dissimilar Metal Weld*

between Carbon Steel and Stainless Steel formed by Transition Grading Technique", Materials Today: 2, (2015), pages 1657-1664.

[38] H. Naffakh, M. Shamanian, F. Ashrafizadeh, *"Dissimilar welding of AISI 310 austenitic stainless steel to nickel-based alloy Inconel 657",* Materials Processing Technology, 209, (2009), pages 3628-3639.

[39] N.A. McPherson, K. Chi, T.N. Baker, *"Submerged arc welding of stainless steel and the challenge from the laser welding process",* Journal of materials processing technology,134, (2003), pp. 174-179.

[40] Patel, A.M., and Gohil, A.V., (2013), *"Effect of arc welding parameters controlling submerged arc welding (SAW) process",* International journal of pure and applied research in engineering and technology, ISSN: 2319-507X, Volume 1(6), pp.37-51.

[41] A. Arul Marcel Moshi, S. R. Sundara Bharathi, R. Rajeshkumar and R. Kumar*, "factors influencing submerged arc welding on stainless steel - a review",* ARPN Journal of Engineering and Applied Sciences Vol. 11, no. 2, January 2016.

[42]. Chandel, R.S., Seow, H.P. and Cheong, F.L. (1997) *"Effect of increasing deposition rate on the bead geometry of submerged arc welds",* Journal of Materials Processing Technology.72, pp.124 – 128.

[43]. Pandey, N.D., Bharti, A. and Gupta, S.R., (1994*), "Effect of submerged arc welding parameters and fluxes on element transfer behaviour and weld-metal chemistry"* Journal of Materials Processing Technology, 40: pp.195-211.

[44]. Ghosh, P.K. and Ahmed, M. (1999), *"Characterization of mechanical properties of multipass submerged arc weld by model analysis of its microstructure facilitated by aid of computer"* Indian Welding Journal, 32,4, pp.32-42.

[45] Kook-soo Bang, Chan Park, Hong-chul Jung, Jong-bong Lee, *"Effects of flux composition on the element transfer and mechanical properties of weld metal in submerged arc welding",* Met. Mater. Int., 15, (2009), pp. 471-477.

[46] S. Ragu Nathan, V. Balasubramanian, S. Malarvizhi, A.G. Rao, *"Effect of welding processes on mechanical and microstructural characteristics of high strength low alloy naval grade steel joints",* Defence Technology 11 (2015) 308-317.

[47] J. Kanjilal, N.D. Pandey, A. Bharti, S.R. Gupta, *"Effect of submerged arc welding parameters and fluxes on element transfer behaviour and weld-metal chemistry",* journal of Materials Processing Technology, Volume 40, Issues 1–2, January 1994, Pages 195-211.

[48] S. Chattopdhyaya , A.Ghosh,*"Assessment of heat affected zone of submerged arc welding process through digital image processing",* Procedia Engineering, 10, (2011), pp. 2782-2785.

[49] Shukla and Pandey, *"Influence of the process parameters on the weld deposit area and microstructure and bead on plate submerged arc welding process",* journal on Materials of Processing Technology, 95, 1-3, 1999, pp. 246-261.

[50] R.S. Chandel, L. Malik, "*Relationship between wire feed speed and submerged arcwelding parameters",* Proceedings of the International Conference on Welding for Challenging Environments", 15–17 October 1985, pp. 245-251.

[51] N.D. Pandey, A. Bharti, S.R. Gupta, *"Effect of submerged arc welding parameters and fluxes on element transfer behaviour and weld-metal chemistry",* Journal of Materials Processing Technology,40, Issues 1–2, January 1994, pp.195–211.

[52] A K Lakshminarayanan, V Balasubramanian, *"Evaluation of microstructure and mechanical properties of laser beam welded AISI 409m grade ferritic stainless steel",* Journal of iron and steel research, international. 2012, 19(1): 72-78.

[53] Ramazan Kacar and Orhan Baylan, *"An investigation of microstructure/property relationships in dissimilar welds between martensitic and austenitic stainless steels",* Materials and Design, 25, (2004), pp. 317–329.

[54] Andrey Belyakov, Yuuji Kimura, Yoshitaka Adachi and Kaneaki Tsuzaki, *"Microstructure evolution in ferritic stainless steels during large strain deformation",* Materials Transactions, Vol. 45, No. 9 (2004) pp. 2812 to 2821.

[55] Yajiang Li, Zengda ZOU and M. Thompson, *"Microstructure and fracture morphology in the welding zone of $Cr_{18}Mo_2$ ferritic stainless steel",* J. Mater. Sci. Technol., Vol. 12, 1996.

[56] Ehsan Gharibshahiyan, Abbas Honarbakhsh Raouf, Nader Parvin, Mehdi Rahimian, *"The effect of microstructure on hardness and toughness of low carbon welded steel using inert gas welding",* Materials and Design 32 (2011) 2042–2048.

[57] Zakaria Boumerzoug, Chemseddine Derfouf, Thierry Baudin, *"effect of welding on microstructure and mechanical properties of an industrial low carbon steel",* Engineering, 2010, 2, 502-506.

[58] Bulent Kurt Kotus, Adnan Çalik, *"Interface structure of diffusion bonded duplex stainless steel and medium carbon steel couple",* Materials Characterization, Volume 60, Issue 9, September 2009, Pages 1035-1040.

[59]. Joarder, A., Saha, S.C. and Ghose, A.K., (1991), *"Study of submerged arc weld metal and heat-affected zone microstructures of plain carbon steel",* Weld. J. Suppl. Res, 70, 6, pp. 141–146.

[60]. Rudrapati, R., Bandyopadhyay, A, A., Pal, P.K., (2013), *"Multi-objective optimization in traverse cut cylindrical grinding",* Advanced Materials Manufacturing & Characterization Volume 3 Issue 1, pp.335-339.

[61]. Ene, N., Scutelnicu, E., (2013), *"Application of the taguchi method combined with grey relational analysis for the optimization of the submerged arc welding process",* Annals of the University Dunarea de Jos of Galati: Fascicle XII,; Vol. 24, p.23.

[62]. Chandel, R.S., Seow, H.P. and Cheong, F.L. (1997*) "Effect of increasing deposition rate on the bead geometry of submerged arc welds",* Journal of Materials Processing Technology.72, pp.124 – 128.

[63]. Tarng, Y.S., Yang, W.H. and Juang, S.C., (2000), *"The use of fuzzy logic in the taguchi method for the optimization of the submerged arc welding process",* International Journal of Advanced Manufacturing Technology, 16, pp.688–694.

[64] G. M. Reddy, P. K. Ghosh, A. Khanna*,"The influence of electrode polarity and welding current on mechanical properties of submerged arc weld",* Indian Welding Journal, 23, Issue 3, (1991), pp.145-150.

[65] P.B.Bamankar, S.M.Sawant, *"Study of the effect of process parameters on depth of penetration and bead width in SAW (submerged arc welding) process",* International Journal of Advanced Engineering Research and Studies, E-ISSN2249–8974, 2, Issue 3, (2013).

[66] G. Mallaiah, A. Kumar, P. Ravinder Reddy, G. Madhusudhan, *"Influence of grain refining elements on mechanical properties of AISI 430 ferritic steel weldments - Taguchi*

approach", Materials and Design 36, (2012), pp. 443-450.

[67] S Kumanan, J Edwin Raja Dhas,, K Gowthaman, *"Determination of submerged arc welding process parameters using Taguchi method and regression analysis",* Indian Journal of Engineering & Materials Sciences, 14, (2007), pp. 177-183.

[68] Serdar Karaoglu, Abdullah Secgin, *"Sensitivity analysis of submerged arc welding process parameters",* Journal of materials processing technology, 202, (2008), pp. 500–507.

[69] J. Edwin Raja Dhas, S. Kumanan, *"Optimization of parameters of submerged arc weld using non conventional techniques",* Applied Soft Computing, 11, (2011), pp. 5198–5204.

[70] Y.S. Tarng, S.C. Juang, C.H. Chang, *"The use of grey-based Taguchi methods to determine submerged arc welding process parameters in hardfacing",* Journal of Materials Processing Technology, 128, (2002), pp. 1–6.

[71] Roselina Sallehuddin, Siti Mariyam Hj. Shamsuddin, Siti Zaiton Mohd Hashim, *"Grey Relational Analysis And Its Application On Multivariate Time Series".* (http://comp.utm.my/pars/files/2013/04/Grey-Relational-Analysis-And-Its-Application-On-Multivariate-Time-Series.pdf)

[72] Aniruddha Ghosh, Somnath Chattopadhyaya, P.K.Sarkar, *"Critical analysis of confounded parameters of SAW process",* Procedia Engineering, 10, (2011), pp. 2786–2790.

[73] S. M., Phadke, "*Quality Engineering Using Robust Design*", Prentice Hall, Englewood Cliffs, N.J., 1989.

[74]. Kanjilal, P., Pal, T.K. and Majumdar, S.K., (2006), *"Combined effect of flux and welding parameters on chemical composition and mechanical properties of submerged arc weld meta l"* Journal of Materials Processing Technology, 171,pp.223-231.

[75] NPTEL LECTURES, Module 5, Design for Reliability and Quality.

[76] D.C. Montgomery, "*Design and analysis of experiments*", 7th Edition, Wiley-India.

[77] K. Deb, *"Optimization for engineering design: Algorithms and Examples",* Prentice Hall, (1998), India.

[78] www.ee.iitb.ac.in

[79] A. Ghosh: Master dgree thesis entitled *"Gas metal arc welding of austenitic stainless steel – experiments, modeling and analysis"*, submitted at Jadavpur University, Kolkata, 2013.

[80] Rao, R.V. & Savsani, V.J. & Vakharia, D.P. (2011). *Teaching-learning-based optimization: A novel method for constrained mechanical design optimization problems*. Computer-Aided Design, 43 (3), 303-315.

APPENDIX

A. Some more photographic views of microstructures

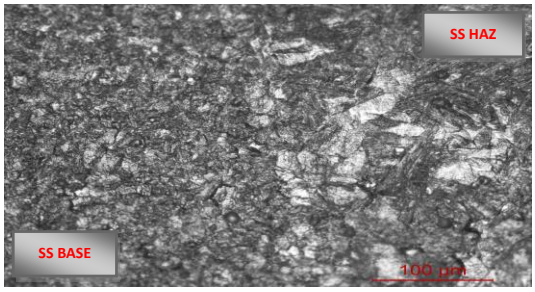

a) Ferritic base + HAZ

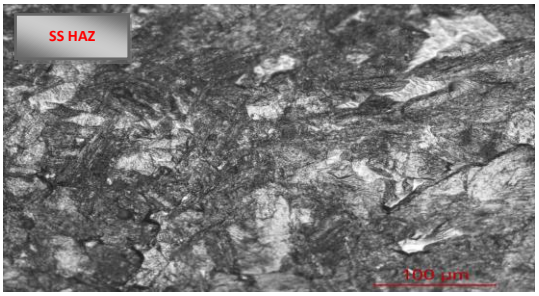

b) Ferritic HAZ

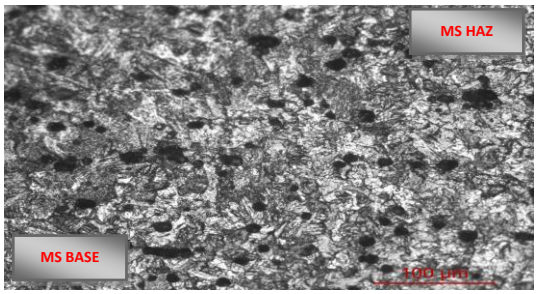

c) MS base + HAZ

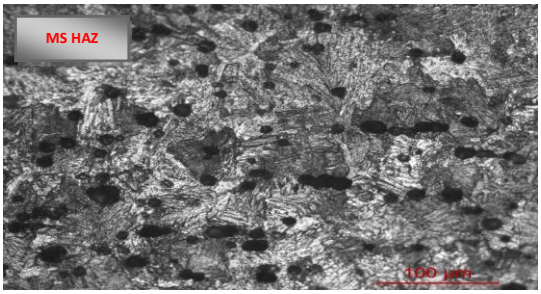

d) MS HAZ

Figure A.1 Microstructure of sample no. 1 (x 200)

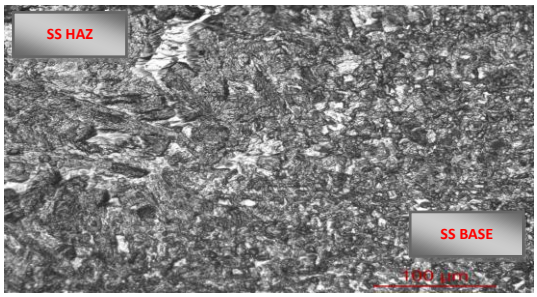

a) Ferritic base + HAZ

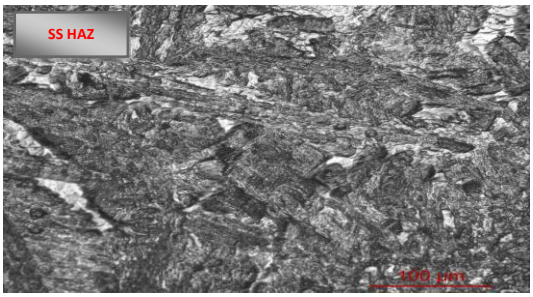

b) Ferritic HAZ

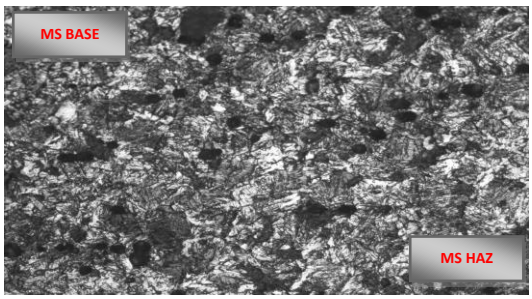

c) MS base + HAZ

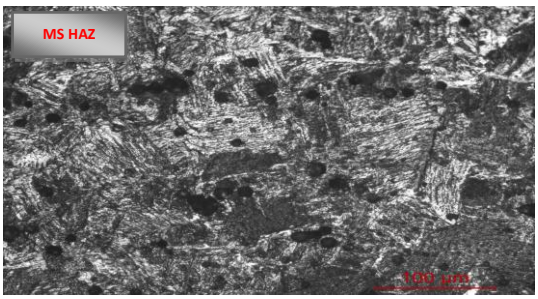

d) MS HAZ

Figure A.2 Microstructure of sample no. 2 (x 200)

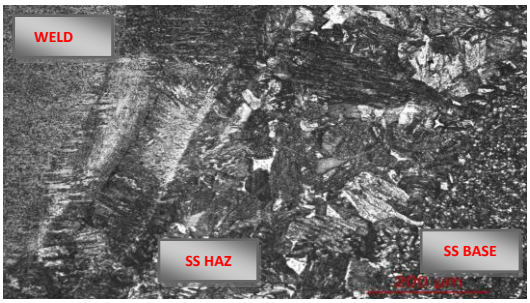

a) Ferritic base + HAZ + weld

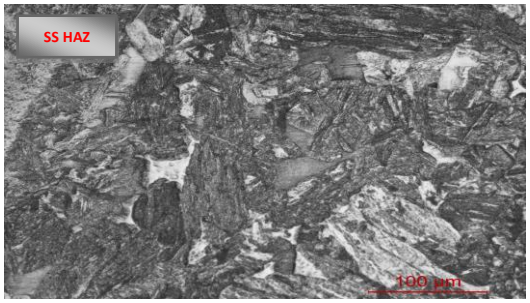

b) Ferritic HAZ

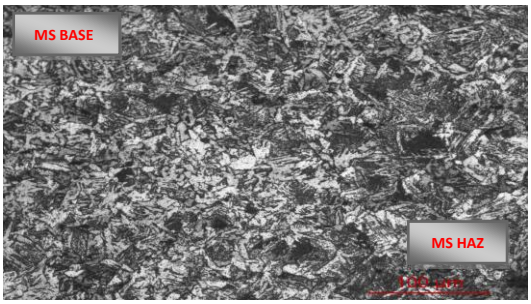

c) MS base + HAZ

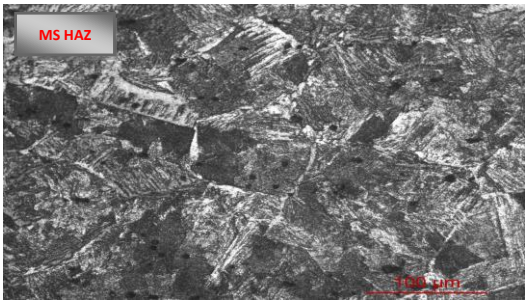

d) MS HAZ

Figure A.3 Microstructure of sample no. 3 (x 200)

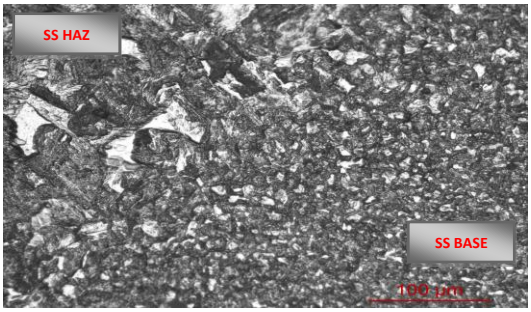

a) Ferritic base + HAZ

b) Ferritic HAZ

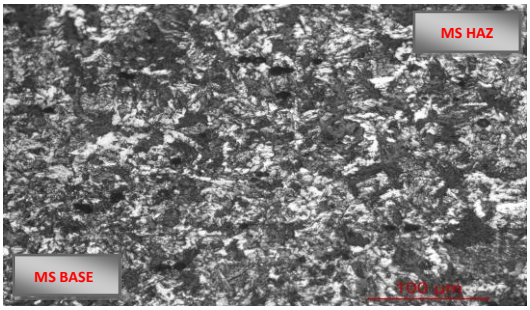

c) MS base + HAZ

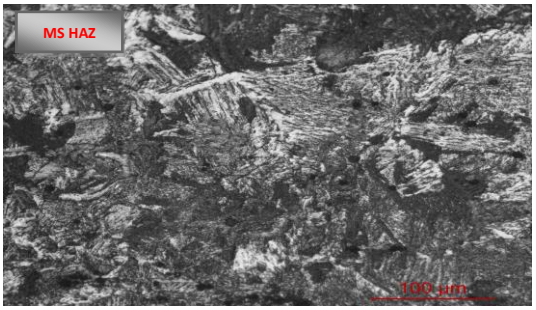

d) MS HAZ

Figure A.4 Microstructure of sample no. 4 (x 200)

B. Response surface plots and Contour plots

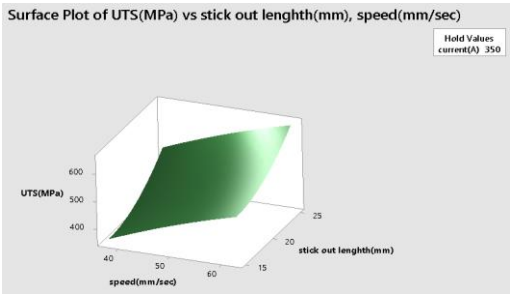

a) At highest value of current (350 A)

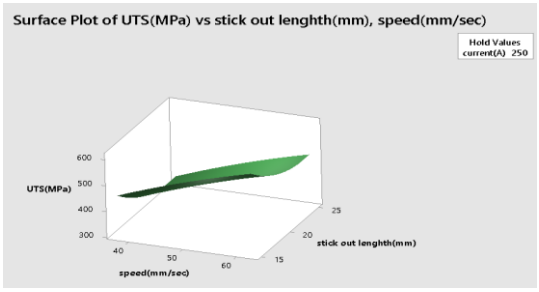

b) At lowest value of current (250 A)

Figure B.1 Response surface plots showing combined effects of S and T on UTS when C is kept constant

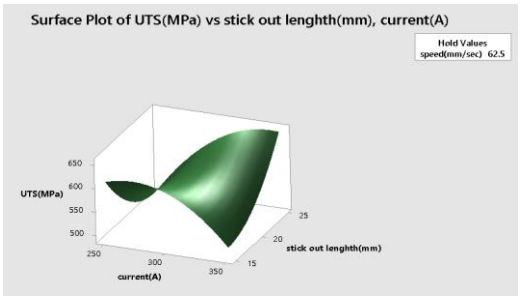

a) At highest value of speed (62.5 mm/sec.)

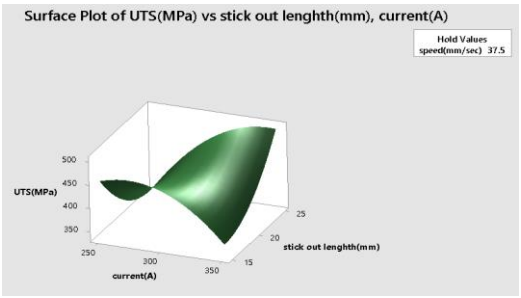

b) At lowest value of speed (37.5 mm/sec.)

Figure B.2 Response surface plots showing combined effects of C and S on UTS when T is kept constant

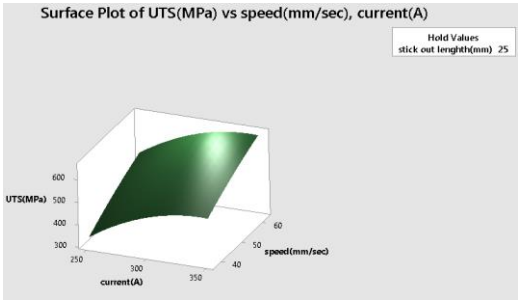

a) At highest value of stick-out length (25 mm)

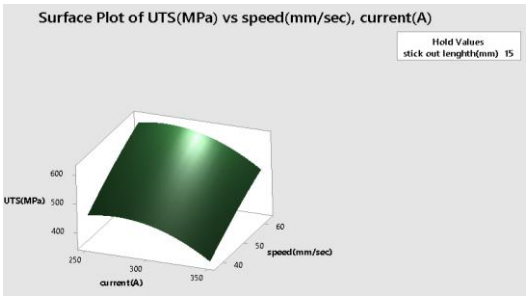

b) At lowest value of Stick-out length (15 mm)

Figure B.3 Response surface plots showing combined effects of C and T on UTS when S is kept constant

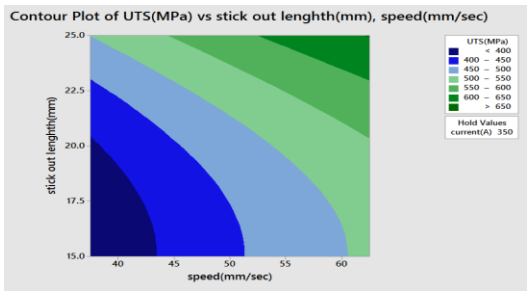

a) At highest value of current (350 A)

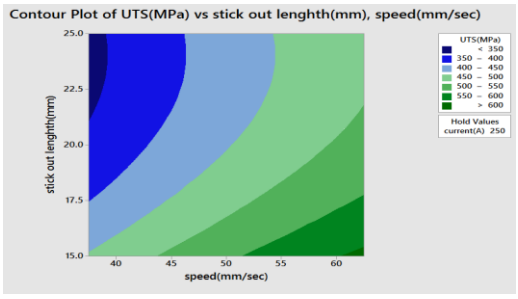

b) At lowest value of current (250 A)

Figure B.4 Contour plots showing combined effects of S and T on UTS when C is constant

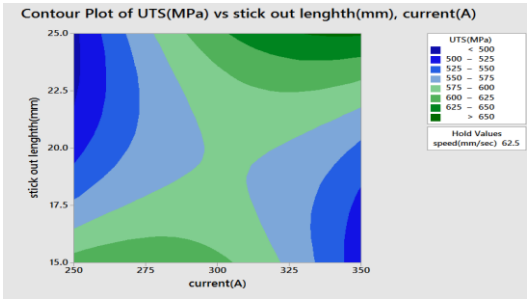

a) At highest value of speed (62.5 mm/sec.)

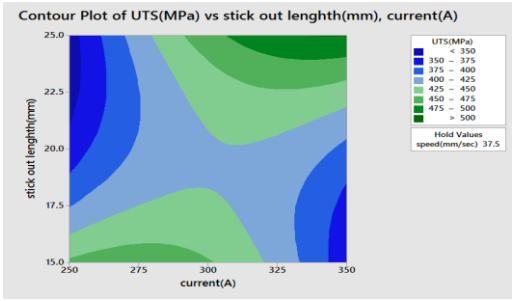

b) At lowest value of speed (37.5 mm/sec.)

Figure B.5 Contour plots showing combined effects of S and C on UTS when T is constant

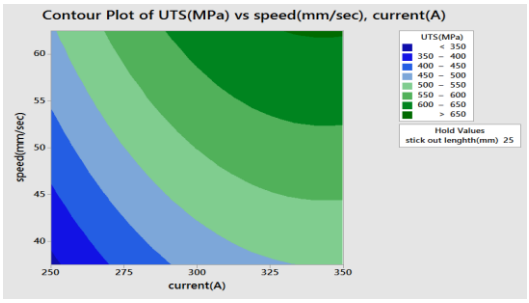

a) At highest value of stick-out length (25 mm)

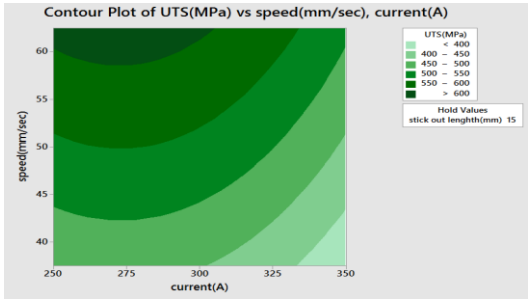

b) At lowest value of stick-out length (15 mm)

Figure B.6 Contour plots showing combined effects of C and T on UTS when S is constant

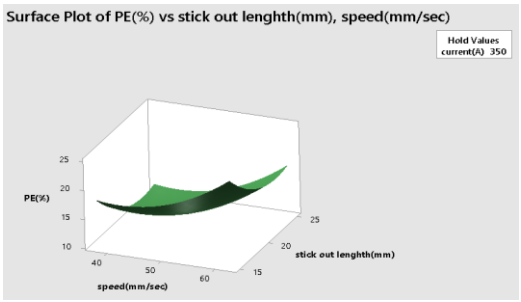

a) At highest value of current (350 A)

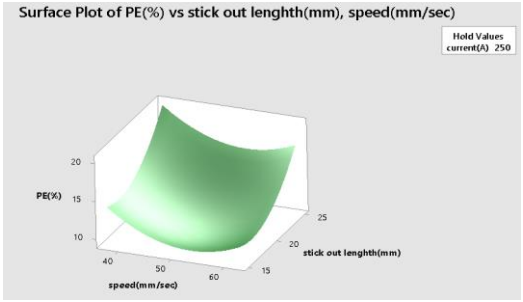

b) At lowest value of current (250 A)

Figure B.7 Response surface plots showing combined effects of S and T on PE when C is kept constant

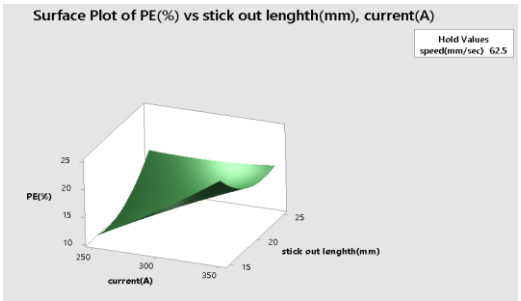

a) At highest value of speed (62.5 mm/sec.)

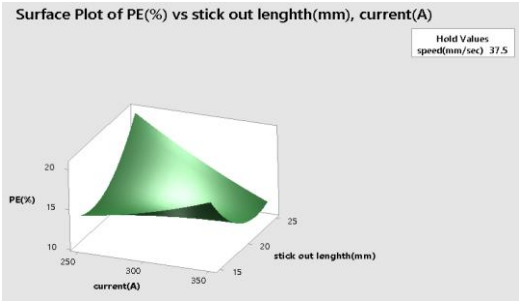

b) At lowest value of speed (37.5 mm/sec.)

Figure B.8 Response surface plots showing combined effects of S and C on PE when T is kept constant

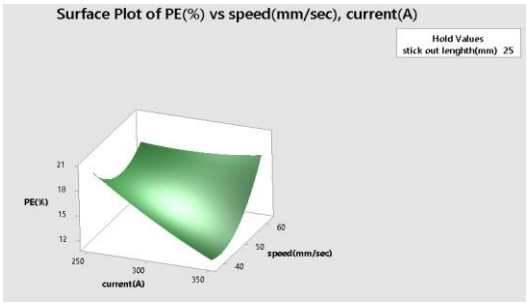

a) At highest value of stick-out length (25 mm)

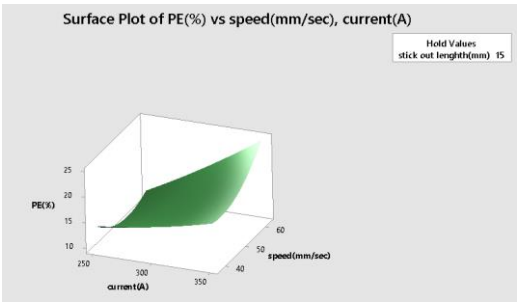

b) At lowest value of stick-out length (15 mm)

Figure B.9 Response surface plots showing combined effects of C and T on PE when S is kept constant

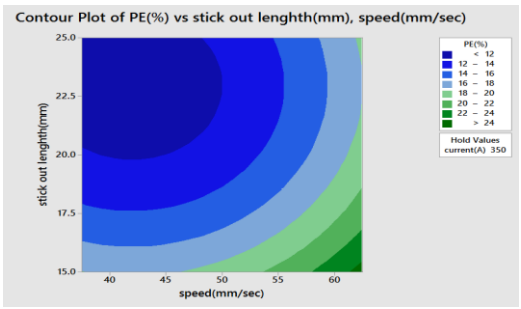

a) At highest value of current (350 A)

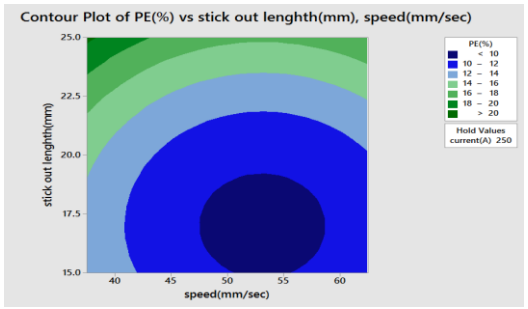

b) At lowest value of current (250 A)

Figure B.10 Contour plots showing combined effects of S and T on UTS when C is constant

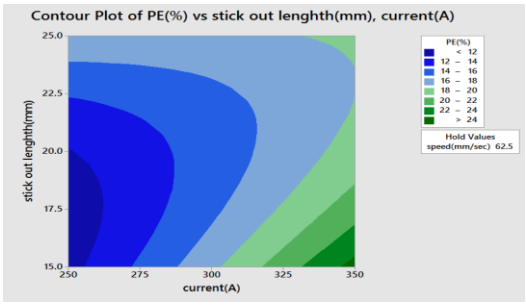

a) At highest value of speed (62.5 mm/sec.)

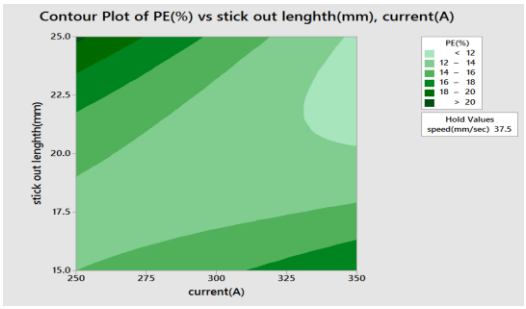

b) At lowest value of speed (37.5 mm/sec.)

Figure B.11 Contour plots showing combined effects of S and C on PE when T is constant

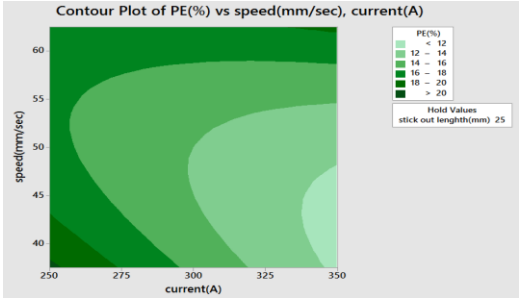

a) At highest value of stick-out length (25 mm)

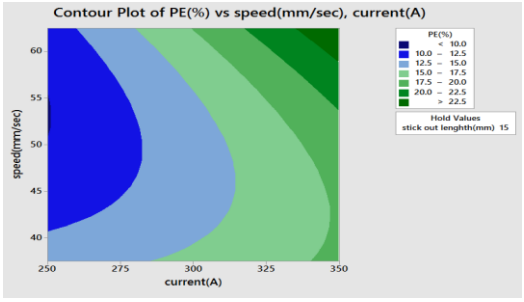

b) At lowest value of stick-out length (15 mm)

Figure B.12 Contour plots showing combined effects of C and T on PE when S is Constant

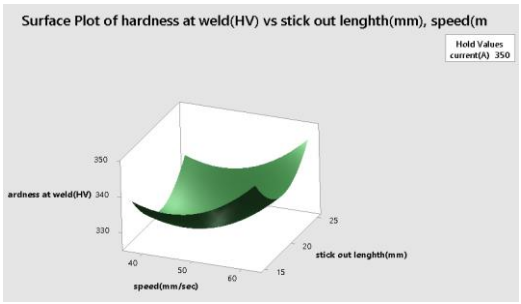

a) At highest value of current (350 A)

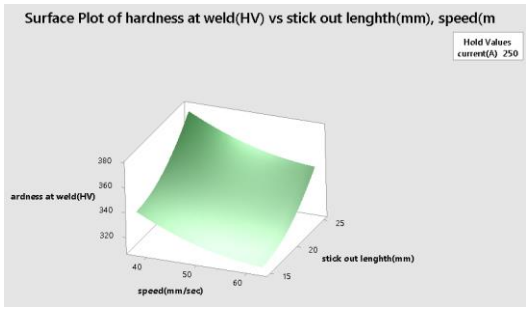

b) At lowest value of current (250 A)

Figure B.13 Response surface plots showing combined effects of S and T on hardness at weld when C is kept constant

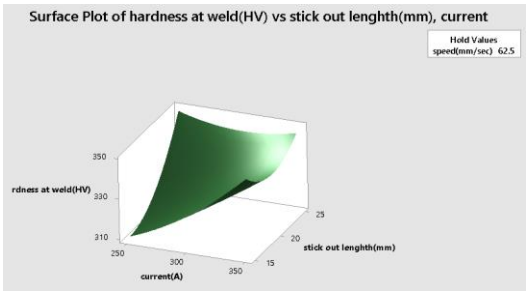

a) At highest value of speed (62.5 mm/sec.)

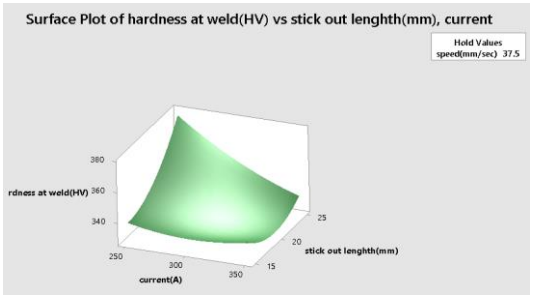

b) At lowest value of speed (37.5 mm/sec.)

Figure B.14 Response surface plots showing combined effects of S and C on hardness at weld when T is kept constant

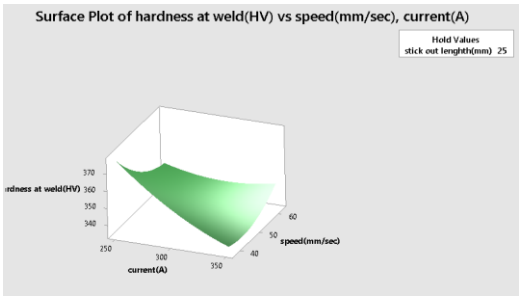

a) At highest value of stick-out length (25 mm)

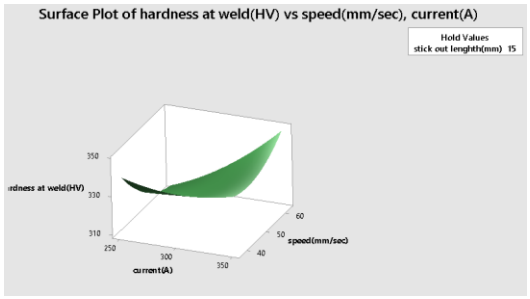

b) At lowest value of stick-out length (15 mm)

Figure B.15 Response surface plots showing combined effects of C and T on hardness at weld when S is kept constant

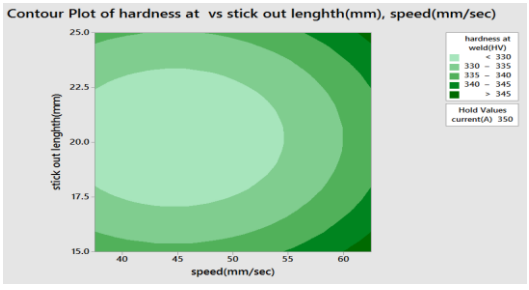

a) At highest value of current (350 A)

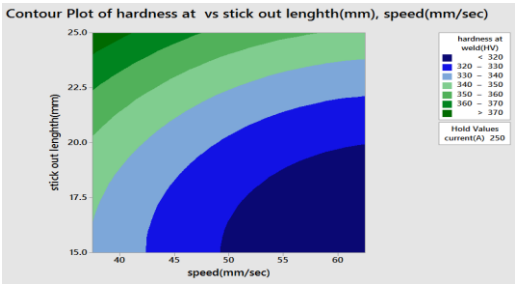

b) At lowest value of current (250 A)

Figure B.16 Contour plots showing combined effects of S and T on hardness at weld when C is constant

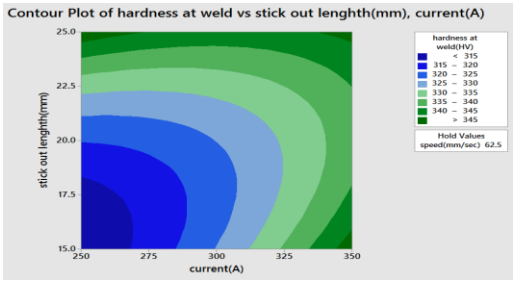

a) At highest value of speed (62.5 mm/sec.)

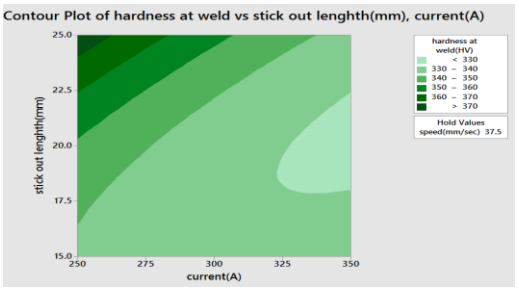

b) At lowest value of speed (37.5 mm/sec.)

Figure B.17 Contour plots showing combined effects of C and S on hardness at weld when T is constant

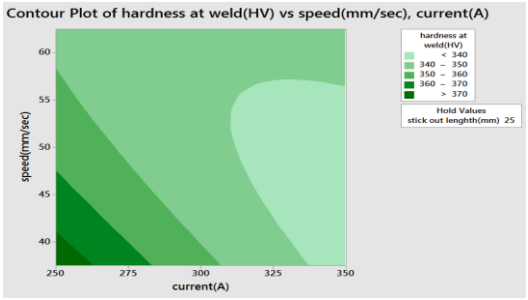

a) At highest value of stick-out length (25 mm)

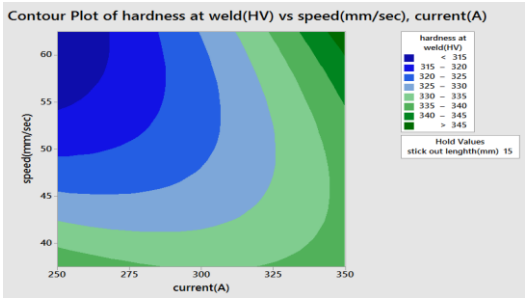

b) At lowest value of stick-out length (15 mm)

Figure B.18 Contour plots showing combined effects of C and T on hardness at weld when S is kept constant

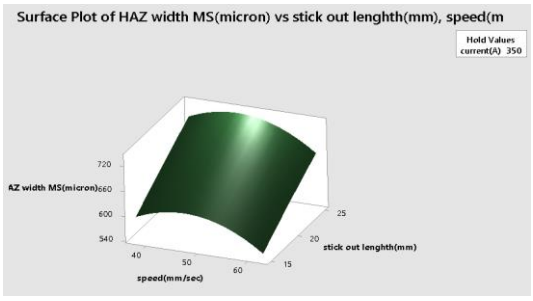

a) At highest value of current (350 A)

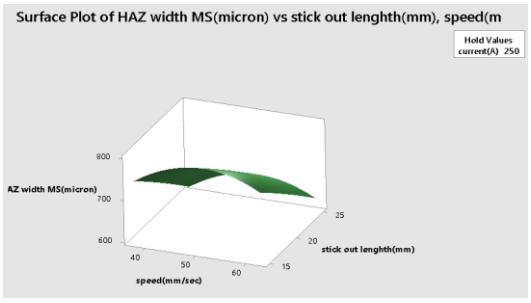

b) At lowest value of current (250 A)

Figure B.19 Response surface plots showing combined effects of S and T on HAZ at MS when C is kept constant

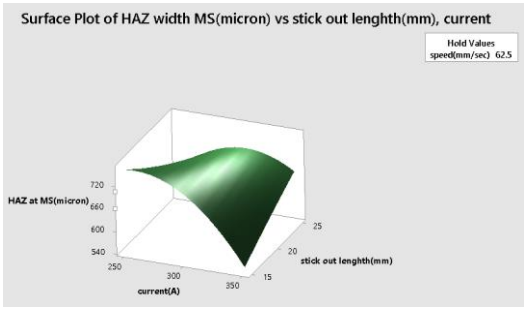

a) At highest value of speed (62.5 mm/sec.)

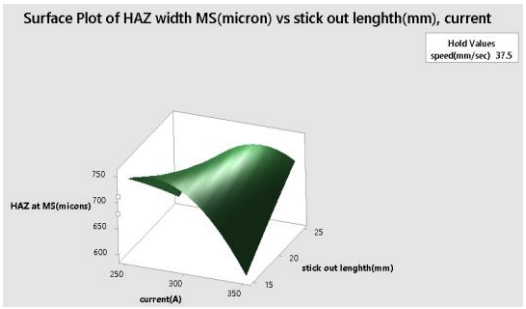

b) At lowest value of speed (37.5 mm/sec.)

Figure B.20 Response surface plots showing combined effects of S and C on HAZ at MS when T is kept constant

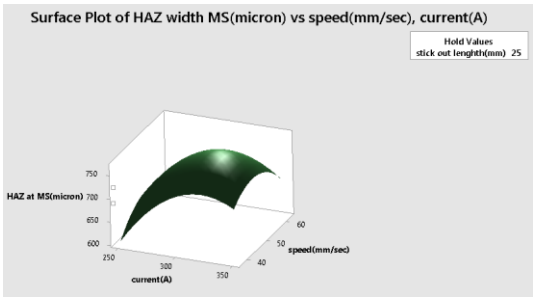

a) At highest value of stick-out length (25 mm)

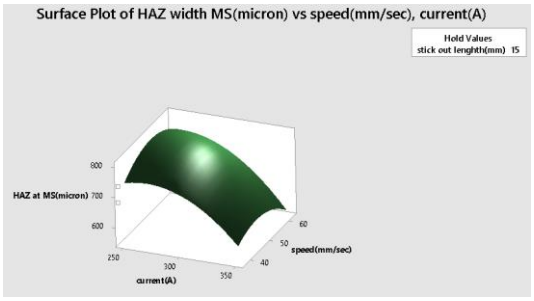

b) At lowest value of stick-out length (15 mm)

Figure B.21 Response surface plots showing combined effects of C and T on HAZ at MS when S is kept constant

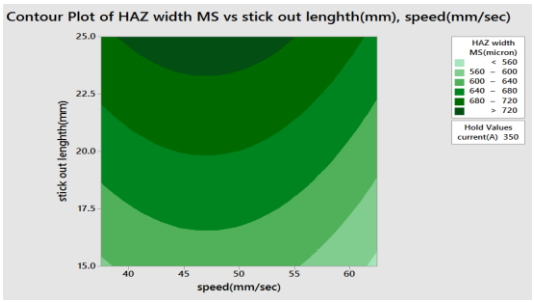

a) At highest value of current (350 A)

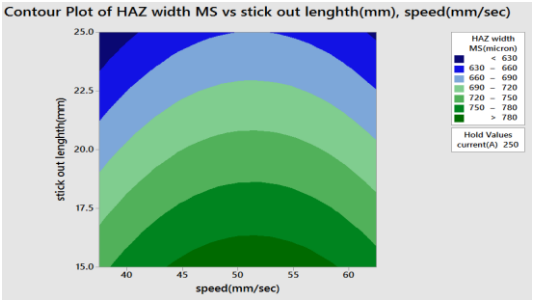

b) At lowest value of current (250 A)

Figure B.22 Contour plots showing combined effects of S and T on HAZ at MS when C is constant

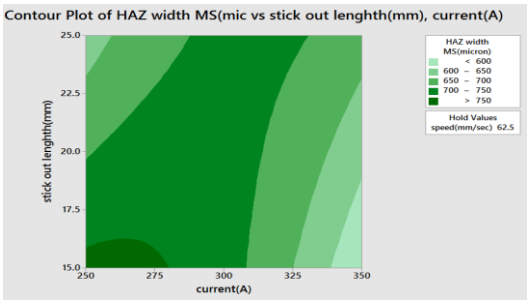

a) At highest value of speed (62.5 mm/sec.)

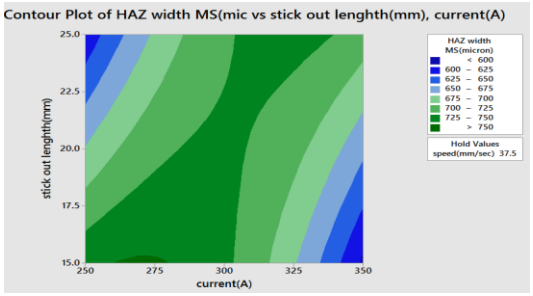

b) At lowest value of speed (37.5 mm/sec.)

Figure B.23 Contour plots showing combined effects of C and S on HAZ at MS when T is kept constant

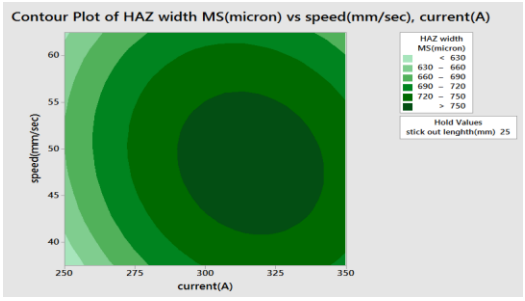

a) At highest value of stick-out length (25 mm)

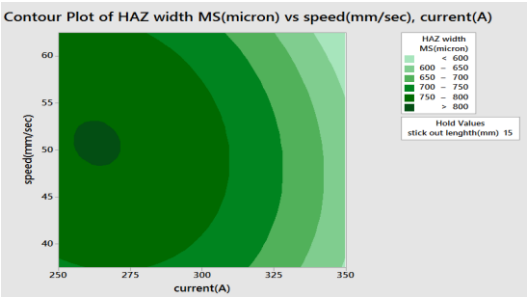

b) At lowest value of stick-out length (15 mm)

Figure B.24 Contour plots showing combined effects of C and T on HAZ at MS when S is kept constant

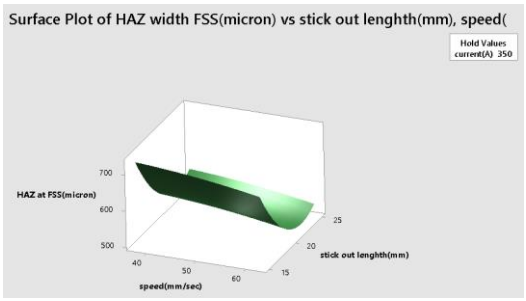

a) At highest value of current (350 A)

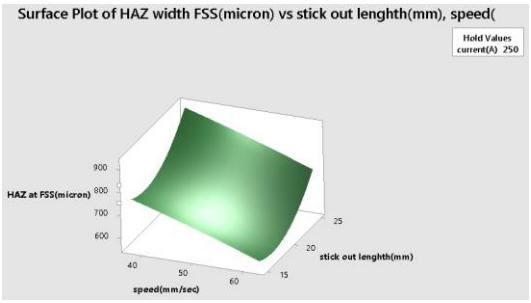

b) At lowest value of current (250 A)

Figure B.25 Response surface plots showing combined effects of S and T on HAZ at FSS when C is kept constant

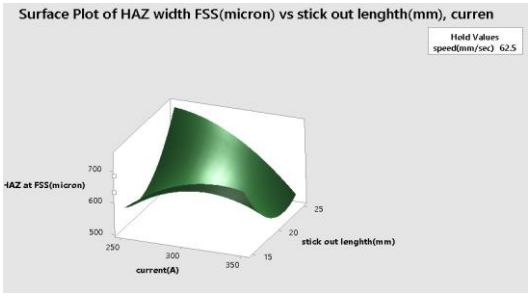

a) At highest value of speed (62.5 mm/sec.)

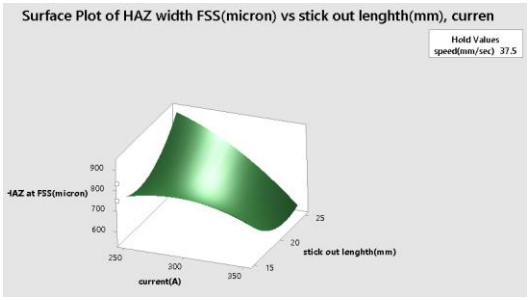

b) At lowest value of speed (37.5 mm/sec.)

Figure B.26 Response surface plots showing combined effects of S and C on HAZ at SS when T is kept constant

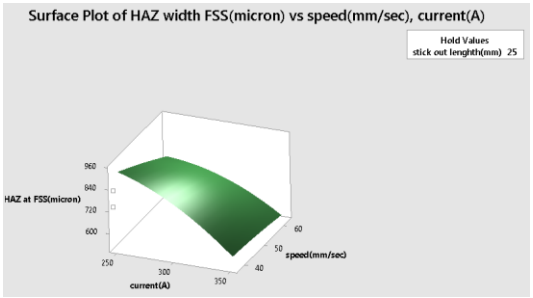

a) At highest value of stick-out length (25 mm)

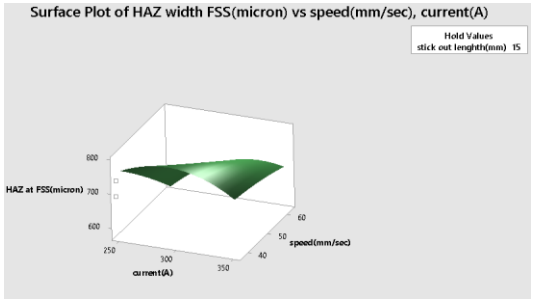

b) At lowest value of stick-out length (15 mm)

Figure B.27 Response surface plots showing combined effects of C and T on HAZ at FSS when S is kept constant

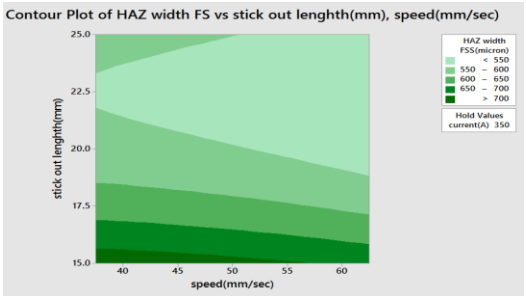

a) At highest value of current (350 A)

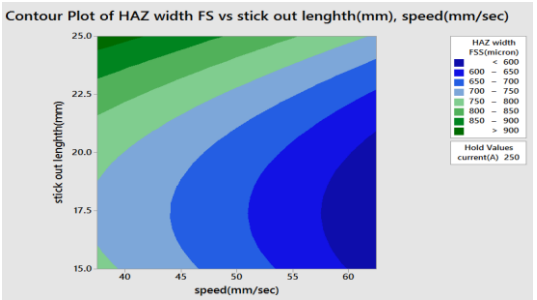

b) At lowest value of current (250 A)

Figure B.28 Contour plots showing combined effects of S and T on HAZ at FSS when C is constant

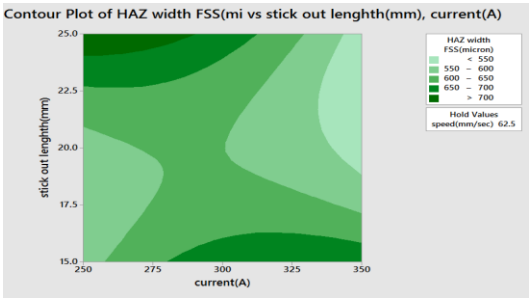

a) At highest value of speed (62.5 mm/sec.)

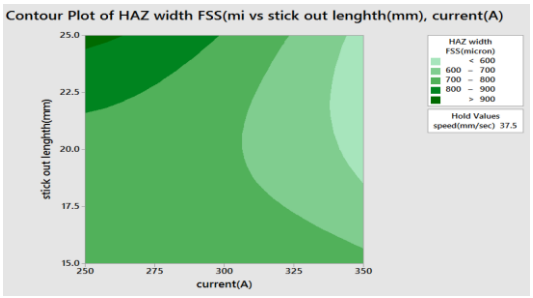

b) At lowest value of speed (37.5 mm/sec.)

Figure B.29 Contour plots showing combined effects of C and S on HAZ at FSS when T is kept constant

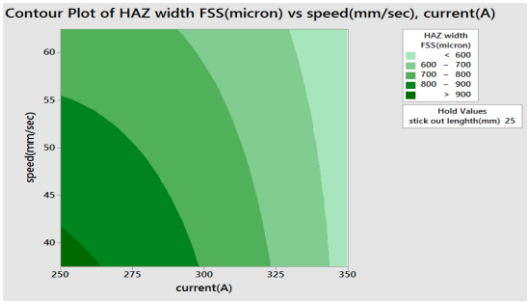

a) At highest value of stick-out length (25 mm)

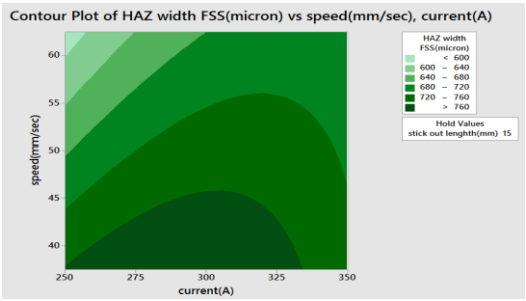

b) At lowest value of stick-out length (15 mm)

Figure B.30 Contour plots showing combined effects of C and T on HAZ at FSS when S is kept constant